Crystallisation Driven Self-Assembly of Polylactide Containing Block Copolymers Synthesised by Combination of ROP and RAFT

Department of Chemistry

Submitted for the degree of Doctor of Philosophy

Nikolaos Petzetakis

September 2012

THE UNIVERSITY OF WARWICK

Declaration of authorship

This thesis is submitted in partial fulfilment of the requirements for the degree of doctor of philosophy. It describes work carried out from January 2009 to May 2012. Unless otherwise indicated, the research described is my own and not the product of a collaboration. No part of this thesis has been submitted to any other university, or as any part of any other submission to the University of Warwick.

Signed, *Date:*

Table of Contents

Acknowledgements I

List of publications II

Summary III

Abbreviations IV

Chapter 1: Introduction 1

1.1 Abstract 1

1.2 Living polymerisations for well-defined building blocks 2

1.2.1 Controlled radical polymerisations (CRPs) 3

1.2.2 Reversible addition fragmentation chain transfer (RAFT) Polymerisation 5

1.2.3 Polylactides and Ring Opening Polymerisation (ROP) of lactides 9

1.2.4 Thiourea/sparteine ring opening polymerisation system 12

1.3 Self-assembly of block copolymers (BCPs) 16

1.4 References 21

Chapter 2: Design and synthesis of reversibly connected block copolymers 25

2.1 Abstract 26

2.2 Introduction 28

2.2.1 Reversibly connected copolymers 28

2.2.2 Maleimide functionalised polymers 33

2.2.3 The Diels–Alder reaction 35

2.2.4 Synthesis of polylactide containing block copolymers 37

2.3 Results and discussion 41

2.3.1 Synthesis of dodecyl 4-(hydroxymethyl) benzyl carbonotrithioate, 2.1 41

2.3.2 Synthesis of 4-(bromomethyl)benzyl dodecyl carbonotrithioate, 2.2 .. 43

2.3.3 Synthesis of furan-3,4-diyldimethanol, 2.3 45

2.3.4 Synthesis of 3,4-bis((methoxymethoxy)methyl)furan, 2.4 45

2.3.5 Synthesis of the Diels Alder adduct, 2.5 47

2.3.6 Synthesis of the protected initiator, 2.6 48

2.3.7 Synthesis of the dual RAFT/ROP initiator, 2.7 49

2.3.8 *L*-Lactide polymerisation using 2.7 to afford a P(*L*-LA) macro–CTA, 2.8. 51

2.3.9 THPA polymerisation using PLA macro CTA, to afford P(*L*-LA)-b-PTHPA, 2.10 54

2.3.10 Deprotection of 2.11 to afford the P(*L*-LA)-b-PAA amphiphilic block copolymer, 2.13. 57

2.3.11 Solution self-assembly of polymer 2.13. 58

2.4 Conclusions 62

2.5 Experimental Section 63

2.5.1 Materials and instrumentation 63

2.5.2 Polymerisation procedures 64

2.5.3 Synthesis of dodecyl 4-(hydroxymethyl) benzyl carbonotrithioate, 2.1 65

2.5.4 Synthesis of 4-(bromomethyl)benzyl dodecyl carbonotrithioate, 2.2 ..65

2.5.5 Synthesis of furan-3, 4-diyldimethanol, 2.3 66

2.5.6 Synthesis of 3,4-bis((methoxymethoxy)methyl)furan, 2.4 67

2.5.7 Synthesis of the DA adduct, 2.5 67

2.5.8 Synthesis of the protected initiator, 2.6 68

2.5.9 Synthesis of the dual RAFT/ROP initiator, 2.7 68

2.5.10 General *L*-lactide polymerisation using 2.7 to afford a polylactide macro–CTA, 2.8 69

2.5.11 General acrylate polymerisation using the polylactide macro–CTA, 2.11 70

2.5.12 Deprotection of 2.11 to give the P(*L*-LA)-b-PAA amphiphilic diblock copolymer, 2.13 71

2.6 References 72

Chapter 3: Synthesis of polylactide containing block copolymers by combination of RAFT and ROP 25

3.1 Abstract 78

3.2 Introduction 79

3.2.1 Protected monomers as precursor for the synthesis of Poly(acrylic acid), PAA 79

3.2.2 Poly(triethyleneglycol acrylate) (PTEGA) 80

3.2.3 End group modification of polymers synthesised by RAFT 82

3.3 Results and discussion 85

3.3.1 ROP of lactide (LA) initiated by the compound 2.1 to prepare PLA macro-CTAs 85

3.3.2 RAFT polymerisation of THPA mediated by PLA macro-CTA to prepare PLA-*b*-PTHPA diblock copolymers 88

3.3.3 RAFT polymerisation of TEGA mediated by 3.1 to prepare P(*L*-LA)-*b*-PTEGA 91

3.3.4 RAFT polymerisation of TEGA mediated by PLA-*b*-PTHPA macro CTA to prepare PLA-*b*-PTHPA-*b*-PTEGA 94

3.3.5 End group modification of polymer 3.7 by a radical addition-fragmentation coupling method 97

3.3.6 End group modification of polymer 3.14 by a radical addition-fragmentation coupling method 98

3.3.7 Synthesis of pyrene functionalised azo initiator, 3.19 100

3.3.8 End group modification of polymer 3.6 by a radical addition-fragmentation coupling method using 3.19 101

3.3.9 End group modification of polymer 3.14 by a radical addition-fragmentation coupling method using 3.19 104

3.4 Conclusions 106

3.5 Experimental Section 107

3.5.1 Materials and instrumentation 107

3.5.2 General polymerisation procedures 108

3.5.3 Representative procedure for the synthesis of PLA macro CTA 108

3.5.4 Representative procedure for the synthesis of PLA-*b*-PTHPA.....109

3.5.5 Representative procedure for the synthesis of PLA-*b*-PTEGA 109

3.5.6 Representative procedure for the synthesis of P(*L*-LA)-*b*-PTHPA-*b*-PTEGA 110

3.5.7 End group modification of polymers 3.6 and 3.14 by a radical addition-fragmentation coupling method 110

3.5.8 Synthesis of the pyrene functionalised azo initiator, 3.19 111

3.5.9 End group modification of polymers 3.6 and 3.14 by a radical addition-fragmentation coupling method using 3.19.....112

3.6 References 113

Chapter 4: Crystallisation driven sphere-to-cylinder transition of polylactide containing block copolymers 116

4.1 Abstract 117

4.2 Introduction 118

4.2.1 Morphology transitions and challenges in block copolymer (BCP) self-assembly.....118

4.2.2 Alternative routes towards 1-dimensional morphologies 121

4.2.3 Crystallisation driven self-assembly (CDSA) of PFS based copolymers 129

4.2.4 Other semicrystalline polymers in CDSA.....135

4.3 Results and discussion.....137

4.3.1 P(THPA) hydrolysis reaction of P(*L*-LA)-*b*-P(THPA) to afford P(*L*-LA)-*b*-P(AA).....137

4.3.2 Self-assembly of P(*L*-LA)-*b*-P(AA) following the THPA hydrolysis reaction. 139

4.3.3 Sphere to cylinder transition of polymer 4.1 141

4.3.4 Study of the effect of concentration and common solvent content 148

4.3.5 Control of the morphology 153

4.3.6 Self-assembly behaviour of P(*DL*-LA)-*b*-P(AA) block copolymers . 155

4.3.7 CDSA with synchronous evaporation of the organic solvent 156

4.3.8 Study of the CDSA of P(*L*-LA)-*b*-PAA with removed end group..... 157

4.3.9 Study of the CDSA of polymer P(*L*-LA)-*b*-PAA with the pyrene end group 159

4.3.10 Study of P(*L*-LA)-*b*-PAA-*b*-PTEGA triblock copolymer in CDSA.. 161

4.3.11 Study of $P(L\text{-LA})_{32}$-*b*-PAA_{264}-*b*-$PTEGA_{32}$ triblock copolymers with transformed end group in CDSA 164

4.4 Conclusions 167

4.5 Experimental Section 169

4.5.1 Materials and instrumentation 169

4.5.2 Particles characterisation 169

4.5.3 General considerations 170

4.5.4 Dynamic light scattering (DLS) 170

4.5.5 Transmission electron microscopy (TEM) 171

4.5.6 Wide angle X-ray diffraction (WAXD) 172

4.5.7 SANS data collection 172

4.5.8 PTHPA hydrolysis reaction to afford PAA followed by the CDSA with constant conditions. 173

4.5.9 PTHPA hydrolysis reaction to afford PAA followed by the CDSA with synchronous solvent evaporation. 174

4.6 References 175

Chapter 5: Living crystallisation driven self-assembly of polylactide-b-poly(acrylic acid) block copolymers towards the synthesis of cylinders of controlled length and dispersity 180

5.1 Abstract 181

5.2 Introduction 182

5.2.1 Living crystallisation driven self-assembly (CDSA) 182

5.3 Results and discussion 190

5.3.1 Preparation of seed micelles solution based on P(*L*-LA)$_{32}$-*b*-PAA$_{265}$ 191

5.3.2 Living crystallisation driven self-assembly (CDSA) under dilute, thermal conditions 193

5.3.3 Solvent switch of P(*L*-LA)$_{32}$-*b*-PTHPA$_{265}$ to afford spherical micelles 196

5.3.4 Study of temperature and assembly time on the living CDSA of P(*L*-LA)$_{32}$-*b*-PAA$_{265}$ 197

5.4 Conclusions 199

5.5 Experimental Section 200

5.5.1 General considerations for this work 200

5.5.2 Materials and instrumentation 200

5.5.3 Preparation of samples for TEM analysis 201

5.5.4 Living crystallisation driven self-assembly of (5.1) to obtain cylinders of different lengths 201

5.5.5 Solvent switch self-assembly of (5.1) to obtain spherical micelles ...201

5.5.6 Self-assembly of (5.1) in different temperatures.....201

5.6 References 202

Chapter 6: Hollow block copolymer nanoparticles through a spontaneous one-step structural reorganisation 203

6.1 Abstract 204

6.2 Introduction 205

6.2.1 Hollow particles from BCP self-assembly.....205

6.2.2 Microscopy in block copolymer (BCP) self-assembly 210

6.2.3 Microscopy on graphene oxide (GO) supports 211

6.3 Results and discussion.....214

6.3.1 Solution state characterisation.....214

6.3.2 Hollow nanoparticle synthesis and characterisation 215

6.3.3 Control over the structural reorganisation.....219

6.3.4 Proposed driving force and mechanism 220

6.4 Conclusions 222

6.5 Experimental Section 223

6.5.1 Materials.....223

6.5.2 Instrumentation 223

6.5.3 Formation of compartmentalised necklace like P(*L*-LA)$_{37}$-*b*-PAA$_{333}$ cylindrical nanoparticles by blotting 224

6.5.4 Formation of solid P(*L*-LA)$_{37}$-*b*-PAA$_{333}$ cylindrical nanoparticles by freeze-drying 224

6.5.5 Self-assembly of P(EO)$_{5k}$-*b*-P(*D*,*L*-LA)$_{4k}$ to give spherical micelles, and subsequent formation of solid nanoparticles 224

6.5.6 Transmission electron microscopy (TEM) 225

6.5.7 Atomic force microscopy (AFM) 225

6.5.8 Small angle neutron scattering (SANS) 226

6.6 References 227

Acknowledgements

My sincere thanks go to my mentor, Prof. Rachel O'Reilly for not only the great opportunity to conduct this research but for her invaluable advice, personal and professional support and continuous encouragement; I feel extremely lucky I had the opportunity to work in her research group. I must also thank Dr. Andrew Dove for his useful advice and discussions especially in the polylactide related matters.

A big thank you goes to all of the O'Reilly and Dove group members who have made my Ph.D a very productive and enjoyable time. In particular, Pepa Cotanda who contributed significantly in my work with experiments, discussions and collaborations during my PhD; also Mathew P. Robin and Joseph P. Patterson for a good collaboration we had on the work presented in Chapter 6 and many useful discussions throughout. I should also thank Cecilia Ieong and Sarah Tempelaar for their useful advice and help.

A very special thank you goes to my mum Nena and my sister Kalliopi for all the support and inspiration they have given along my life.

List of publications

1. Cylindrical micelles from the living crystallization-driven self-assembly of poly(lactide)-containing block copolymers, N. Petzetakis, A. P. Dove, R. K. O'Reilly, *Chem Sci*., **2011**, 2, 955. (Chapter 5)

2. A simple approach to characterizing block copolymer assemblies: graphene oxide supports for high contrast multi-technique imaging, J. P. Patterson, A. M. Sanchez, N. Petzetakis, T. P. Smart, T. H. Epps III, I. Portman, N. R Wilson, R. K. O'Reilly, *Soft Matter.*, **2012**, 8, 3322

3. Functionalized Organocatalytic Nanoreactors: Hydrophobic Pockets for Acylation Reactions in Water, P. Cotanda, A. Lu, J. P. Patterson, N. Petzetakis, R. K. O'Reilly, *Macromolecules*., **2012**, 45, 2277

4. Crystallization-driven sphere-to-rod transition of poly(lactide)-b-poly(acrylic acid) diblock copolymers: mechanism and kinetics, N. Petzetakis, A. P. Dove, R. K. O'Reilly, *Soft Matter*, **2012**, 8, 7408 (Chapter 4)

5. Catalytic polymeric nanoreactors: more than a solid supported catalyst, P. Cotanda, N. Petzetakis, R. K. O'Reilly, *MRS commun*, **2012** (Manuscript accepted for publication)

6. Hollow block copolymer nanoparticles through a one-step structural reorganization, N. Petzetakis, M. P. Robin, J. P. Patterson, E. G. Kelley, P. Cotanda, P. H.H. Boman, N. A. J. M. Sommerdijk, A. P. Dove, T. H. Epps III and R. K. O'Reilly, (Manuscript submitted for publication) (Chapter 6)

7. Functional and adaptive cylindrical micelles deriving from the crystallisation driven self-assembly of P(*L*-LA)-*b*-PAA and P(*L*-LA)-*b*-PAA-*b*-PTEGA block copolymers. N. Petzetakis, A. P. Dove, R. K. O'Reilly, (Manuscript in preparation)

Summary

Chapter 1 is the main introduction of this work and it features the two main concepts of this study. First living polymerisation techniques are introduced with a special focus into RAFT and ROP. Secondly solution self-assembly is briefly discussed.

In **Chapter 2** we describe the synthesis of an amphiphilic block copolymer where the two blocks are connected through a reversible bond. A Diels-Alder (DA) adduct consisted of a maleimide-furan pair was chosen as the reversible linker. The solution self-assembly of this polymer was studied by TEM and DLS giving rise to the unexpected formation of cylindrical micelles.

In **Chapter 3** the main objective was to synthesise new amphiphilic block copolymers without the DA motif in order to investigate their self-assembly behaviour compared to those for DA containing polymers obtained in Chapter 2. To further understand this self-assembly behaviour our method has been extended to the synthesis of other hydrophilic blocks and end group modified polymers. In addition, some key properties of the polymers synthesised have been investigated.

In **Chapter 4** our main goal is to understand the origins of the cylindrical micelle formation seen in Chapter 2. We investigated the aggregation behaviour under the aqueous thermal conditions in which the PTHPA block hydrolysis is performed. Studies at different concentrations and solvent mixtures provide valuable information regarding the self-assembly mechanism. In addition, the polymers with modified end groups and the triblock copolymers synthesised in Chapter 3 are studied and all the results compared.

In **Chapter 5** we explore the living crystallisation driven self-assembly of PLA-*b*-PAA block copolymers in aqueous media towards the formation of cylindrical micelles of controlled length.

Interestingly, in many of the unstained TEM images presented in this work the particles demonstrate a non-uniform contrast along their width. This unexpected result is fully investigated in **Chapter 6**.

.

Abbreviations

°C	degrees Celsius
δ	chemical shift
AFM	atomic force microscopy
AIBN	azo-bis-iso-butyronitrile
ATRP	atom transfer radical polymerisation
br	broad (^{1}H NMR)
CDSA	crystallisation driven self-assembly
cm^{-1}	wavenumbers
CMC	critical micelle concentration
CRP	controlled radical polymerisation
CTA	chain transfer agent
d	days / doublet
Da	Daltons (equivalent to g mol^{-1})
DCM	dichloromethane
D_h	hydrodynamic diameter
DLS	dynamic light scattering
DMF	dimethyl formamide
DMSO	dimethyl sulfoxide
DP	degree of polymerisation
DRI	differential refractive index
DA	Diels-Alder
EDCI	1-ethyl-3-(3-dimethylaminopropyl) carbodiimide

Et	ethyl group
g	grams
GPC	gel permeation chromatography
h	hours
Hz	hertz
IR	infrared
J	coupling constant in Hz
kDa	kiloDaltons
LPO	lauroyl peroxide
m	metres / multiplet
MALDI-TOF	matrix assisted laser desorption ionisation- time of flight
Me	methyl group
MHz	megahertz
min	minutes
mg	milligram
mL	millilitres
mmol	millimoles
M_n	number average molecular weight
M_w	weight average molecular weight
mol	moles
NBS	*N*-bromosuccinimide
nm	nanometres
NMP	nitroxide mediated polymerisation
NMR	nuclear magnetic resonance

o/n	overnight
M_w/M_n	polydispersity index
PAA	poly(acrylic acid)
PLA	polylactide
P(*L*-LA)	poly(L-lactide)
P(*D,L*-LA)	poly(*D, L*- lactide)
ppm	parts per million relative to tetramethylsilane
PS	polystyrene
PDA	photodiode array
PTA	phosphotungstic acid
P*t*BuA	poly(*tert*-butyl acrylate)
PTEGA	poly(triethylene glycol acrylate)
PTHPA	poly(tetrahydropyranyl acrylate)
Py	pyrene
RAFT	reversible addition-fragmentation chain transfer
RI	refractive index
RT	room temperature
SANS	small angle neutron scattering
SEC	size exclusion chromatography
SEM	scanning electron microscopy
s	singlet (NMR)
t	triplet (NMR)
*t*BuA	tertiary-butyl acrylate
t-butyl	tertiary-butyl

T_c	crystallisation temperature
TEM	transmission electron microscopy
T_g	glass transition temperature
T_m	melting temperature
TMS	tetramethylsilane
TFA	trifluoroacetic acid
THF	tetrahydrofuran
UV	ultraviolet
WAXD	wide angle X-ray diffraction
XRD	X-ray diffraction

Chapter 1: Introduction

1.1 Abstract

The present work describes the fabrication and characterisation of functionalised block copolymer (BCP) nanoparticles and is significantly interdisciplinary and impacted by many different fields, such as synthetic chemistry, polymer chemistry, (polymer) physics, biological sciences and more. Therefore, presenting a comprehensive introduction on all the scientific background of the present work would require this chapter to be perhaps much lengthier than the present thesis is in total and such an attempt is beyond the scope of this chapter. However, there are two topics that have a key role in this work; the present study describes the synthesis of range of block copolymers (BCP) *via* the use of controlled/'living' polymerisation techniques. More specifically, a combination of reversible addition fragmentation chain transfer polymerisation (RAFT), employed for the polymerisation of vinyl monomers, and ring opening polymerisation (ROP) of the lactide ring for the synthesis of well-defined polylactides (PLAs). Hence, in the first part of the introduction the topic of living polymerisation techniques is discussed with a special focus on RAFT and ROP processes. Furthermore, large part of the present study focuses on the so-called solution based BCP self-assembly and therefore the main features of BCP self-assembly are also introduced. In addition, each one of the following chapters contains an introduction covering relevant literature to the results they present.

1.2 Living polymerisations for well-defined building blocks

Since the revolutionary work by Szwarc in 1956, a living polymerisation is considered to be a chain polymerisation from which chain transfer and chain termination processes are absent. In many cases, the rate of chain initiation is fast compared with the rate of chain propagation, so that the number of kinetic-chain carriers is essentially constant throughout the polymerisation.[1,2] In order to experimentally confirm if a polymerisation reaction is living, the following experimental criteria have been proposed and utilised as diagnostic characteristics:

1. The polymerisation proceeds until all of the monomer has been consumed.
2. Further addition of monomer results in continued polymerisation.
3. The number average molecular weight, $\overline{M}_n$ (or $\overline{X}_n$, the number average degree of polymerisation), is a linear function of conversion.
4. The number of polymer molecules (and active centres) is a constant, which is sensibly independent of conversion.
5. The molecular weight can be controlled by the stoichiometry of the reaction.
6. Narrow molecular weight distribution polymers are produced.
7. Polymers can be chain-end functionalised

Living ionic polymerisations can give extremely high degree of control. However, the experimental conditions that are required are extremely demanding. Complete exclusion of oxygen and moisture from the reaction in order for these polymerisations to be successful is required. This is the major drawback for the usage of these methods.

1.2.1 Controlled radical polymerisations (CRPs)

In the infancy of this research area, the only viable way to produce polymers with well-defined characteristics was to use living ionic polymerisation techniques, such as anionic or cationic procedures.[1,3] However, due to their synthetically demanding nature and incompatibility with some functional groups, living processes were not readily applicable towards synthesising the wide range of vinyl polymers that were desired. On the other hand, although radical techniques avoid the need for stringent reaction conditions, they lack the high level of control which a living polymerisation offers.

A typical free radical polymerisation consists of three steps; firstly, initiation to create a reactive radical vinyl monomer. Secondly, is propagation resulting in polymer chain growth by successive addition of monomer units to the chain end radical. Lastly is termination between polymer chain ends, or the disproportionation of any remaining reactive radicals. Typically, the reaction rates of these steps are not controlled. The fastest step is termination, which means that many chains terminate before complete conversion to polymer.[4] Furthermore, the propagation step is faster than initiation, so that as the reaction progresses, some chains have grown significantly while others are still initiating. Finally, control is further hindered in free radical polymerisations by chain transfer events (such as disproportionation) that can move growing radical sites between (and even within) polymer chains. A truly living polymerisation does not have any termination events and once all initiated, the number of polymer chains remains constant throughout and after the polymerisation.[2]

The synthesis of a wide range of precisely engineered polymers has been achieved over the last two decades with the development of controlled radical polymerisation (CRP) techniques that share a lot of the features of living polymerisations. Polydispersities obtained for CRPs can approach the values typically obtained for living procedures (*ca*. 1.1) and are often tolerant to trace impurities in the reaction medium. CRPs are based on the establishment of a dynamic equilibrium in solution between active (propagating) and deactivated (dormant) species. The dynamic equilibrium can be achieved by two general mechanistic approaches: the first one involves the reversible deactivation of propagating chains that subsequently can be reactivated, either catalytically as in atom transfer radical polymerisation (ATRP)[5,6] or spontaneously like in nitroxide mediated polymerisation (NMP).[7] The second approach relies on the degenerative transfer between propagating chains and dormant species with a typical example of this kind being reversible addition-fragmentation chain transfer (RAFT) polymerisation.[8] One of the main advantages of CRPs is that they can tolerate a wide range of functionalities while retaining excellent control over the molecular characteristics of the products and hence allowing the synthesis of precisely engineered block copolymer macromolecular architectures.[9] These features give the ability to readily tune the chemical nanoenvironment of a given functionality with excellent precision within the BCP.

For the polymerisation to be controlled (*i.e.* to achieve CRP) the reaction needs to be completely free from oxygen, trace amounts of water however are tolerable, unlike ionic polymerisations. Today, three main types of controlled radical polymerisations are known, ATRP, NMP and RAFT. The latter was used extensively for the preparation of the polymers in this study; hence a thorough description of the method is given.

1.2.2 Reversible addition fragmentation chain transfer (RAFT) Polymerisation

The most recent CRP method to be discovered is reversible addition fragmentation chain transfer (RAFT) polymerisation. It was discovered in 1998 by a team of researchers at the Commonwealth Scientific and Industrial Research Organisation (CSIRO) in Melbourne, Australia.[8] A few months prior, a similar process called MAcromolecular Design *via* the Interchange of Xanthates (MADIX) was reported by a French company, that utilises xanthates as the chain transfer agent (CTA) for the polymerisation, and proceeds through an identical mechanism to the CSIRO-reported RAFT process.[10] Due to this, MADIX is considered a specific type of RAFT polymerisation. RAFT is an extremely useful polymerisation method because it can be used with a vast range of monomers, including, (meth)acrylamides,[11-14] styrenics,[15,16] N-vinyl or O-vinyl species, N-Vinyl carbazoles (NVC)[17] and vinyl acetate (VAc)[18] (under a wide variety of reaction conditions). Until RAFT polymerisation, it had proved difficult to synthesise PVAc with any degree of control using either NMP or ATRP. The RAFT polymerisation process does not depend on a persistent radical effect to establish control, nor does it require a catalytic metal centre. This feature means that polymers synthesised using RAFT polymerisation can potentially be used in biomedical applications without further purification. In addition, high temperatures which are often required for NMP (125 °C) are not necessary for a RAFT polymerisation as a conventional radical initiator is utilised. Of the three CRP, the RAFT technique has been proposed to be the most promising polymerisation technique for the widest range of systems. The accepted mechanism for RAFT polymerisations is shown below (Figure 1.1).[16,19]

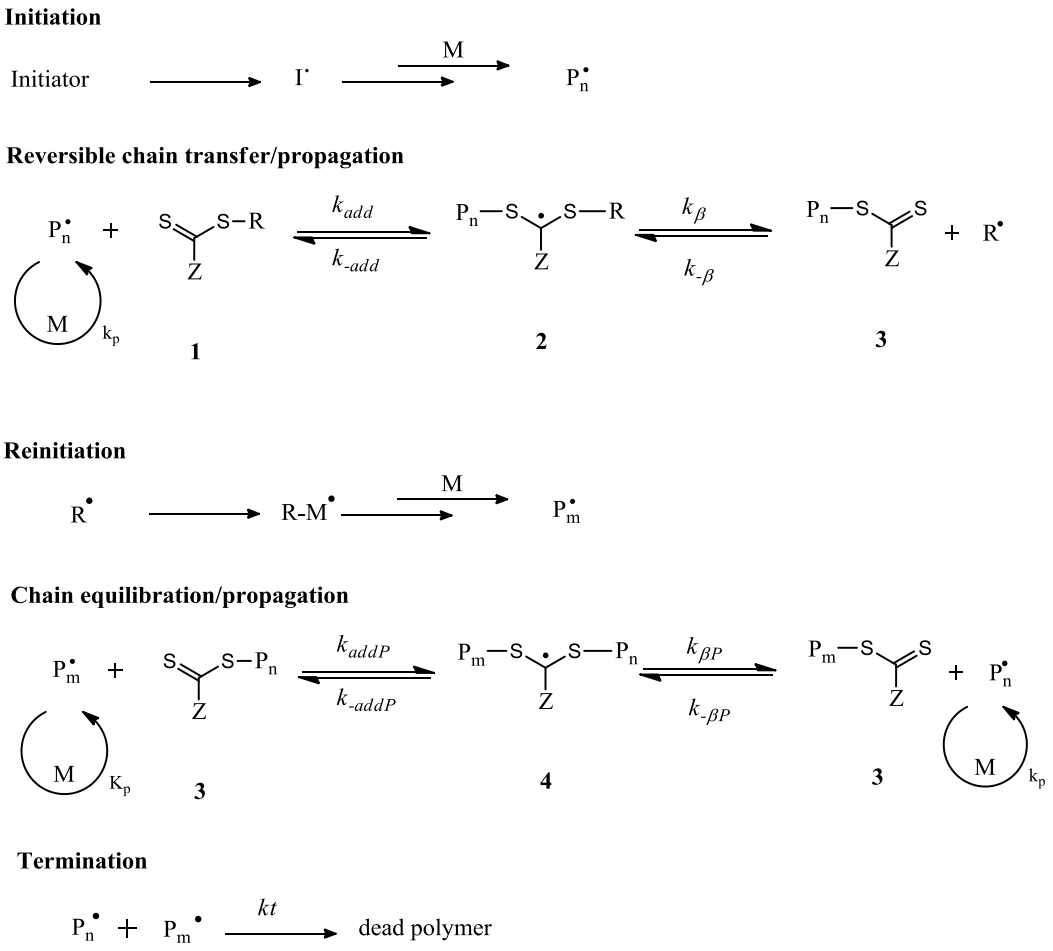

Figure 1.1 Proposed mechanism for the RAFT process.[20]

Step 1, initiation is only necessary when the monomer being polymerised does not self-initiate (such as VAc) and a radical initiator such as azobisisobutyronitrile (AIBN) is needed to form the monomer radical (P_n•). In addition, it is sometimes beneficial to the polymerisation for the Chain Transfer Agent (CTA) to be initiated so that the polymerisation can occur at lower temperatures and/or more quickly. When P_n• associates and dissociates with the CTA (**1**), equilibrium is established. Radical R•, which is released when **2** reversibly transforms into (**3**), reacts with a monomer to form a new propagating radical species (P_m•). The living character of the polymerisation is maintained through the reversible addition-fragmentation

sequence of (**3**) switching from dormant to active (**4**). Some polymerisations have an initial induction period, where little polymerisation occurs. This is due to either delayed fragmentation of (**4**) or slow re-initiation by R• in the reversible chain transfer step. After all monomer has been converted into polymer, R• will recombine with the polymer, which will then be isolatable. The polymer is able to be reactivated and polymerisation can be continued simply using an appropriate solvent with initiator and more monomer.

The choice of CTA is important in the kinetics of RAFT polymerisation, as the polymerisation rate of each monomer depends on which CTA is used. An effectively controlled polymerisation is achieved by correct choice of the free radical leaving group (R) and the Z group.[21] The Z group is important in maintaining the stability of the thiocarbonyl-thio radical intermediate. An effective CTA has a stabilising Z group to aid radical formation but it cannot be too stabilising, otherwise it will not facilitate the fragmentation of the CTA to form the initiating radical R•. When Z is a stabilising group, it will favor the formation of the intermediate and enhance the reactivity of the C=S bond towards the addition of radicals. Rankings for the Z groups for a RAFT CTA are listed below, starting with the most stabilising group (Figure 1.2).[19,21]

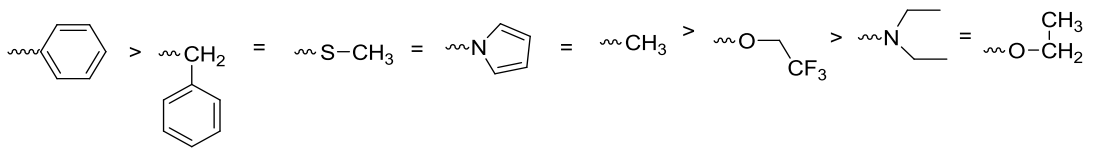

Figure 1.2 A guideline for the selection of RAFT CTA Z group. The addition rate decreases but fragmentation rates increase from left to right.[21]

The R group's main functions are to initiate polymerisation and to stabilise the thiocarbonyl-thio radial. The R group must be a good leaving group, but must also be a good initiating species with respect to the monomer such that it encourages radical formation. Rankings for the R groups for a CTA listed below, starting with the most reactive (Figure 1.3).[19,21]

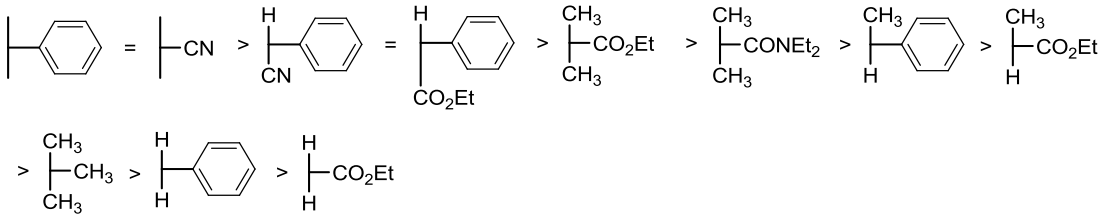

Figure 1.3 Relative stability/ability to re-initiate for RAFT CTA R groups. Fragmentation rates decrease from left to right.[21]

For a controlled RAFT polymerisation.[22] R• must be able to be a persistent radical, and should readily reinitiate polymerisation

1. k_β must be high so that the intermediate radicals fragment rapidly due to weak S-R bonds.
2. Radical intermediate **2** should readily fragment in favor of products.
3. CTAs must have a reactive thiocarbonyl double bond (high k_{add}).
4. R-capped initiators and polymer chains must be unreactive.
5. The equilibrium constant ($k_\beta/k_{-\beta}$) for the fragmentation step must lie far to the left (i.e. much less than one) to keep the steady state concentration of R• low.

There are currently four types of RAFT CTAs, which differ based on the atom which is next to the C=S bond: dithioesters (C), trithiocarbonates (S), xanthates (O), and dithiocarbamates (N). Each of these CTAs is able to polymerise a variety of types of monomers with good control over molecular weight and dispersity (Figure 1.4).[19,21]

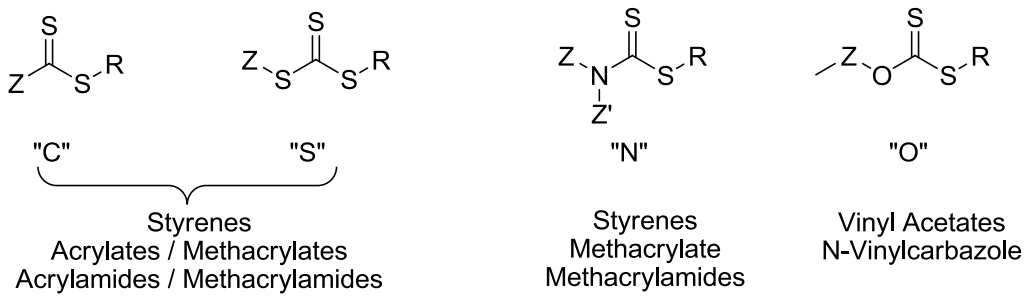

Figure 1.4 Main classes of RAFT CTAs based on the Z group and the monomers they can polymerise in a controlled fashion.

Arguably, RAFT polymerisation is the most versatile and effective in terms of performance compared to ATRP and NMP.[23-26] One of the great advantages of RAFT is that is very tolerant to functional groups and that means that functional polymers can be synthesised without the need of additional protecting groups or tedious synthetic procedures.[14,19]

RAFT also has some disadvantages. One of them is that the synthesis, of the CTA requires the use of toxic starting materials such as carbon disulfide while careful choice of the R and Z groups of the chain transfer agent is required to achieve a controlled polymerisation. Nevertheless, Perrier *et al.* reported an alternative method for the synthesis of CTAs that does not require the use of toxic materials.[27] Another drawback of the RAFT process is that the polymers are typically coloured due to the RAFT end group contained on them. However, this problem has been overcome by using end-group modification chemistries.[28-30]

1.2.3 Polylactides and Ring Opening Polymerisation (ROP) of lactides

Polylactide, PLA, is an aliphatic polyester that derives from 100% renewable resources like corn and sugar beets.[31,32] Due to its great versatility, (bio)degradability and biocompatibility PLA has attracted great interest both in industrial and academic

research. Recently, the synthesis of complex macromolecular architectures containing PLA has been realised which in turn promotes the application of PLA containing polymers in the emerging field of nanotechnology.[33-35]

Although the chemical composition of polylactides is always the same the physical properties can vary significantly depending on the stereochemistry of the polymer.[35,36] The lactide ring exists in the form of four stereoisomers. The enantipopure *L*- and *D*-lactide, the racemic *D,L*-lactide and the *meso*–lactide. The crystallisation properties of polylactides depend to a great extend to the microstructure of the polymer which in turn depends both on the kind of monomer and polymerisation system utilised (Figure 1.5).[36,37]

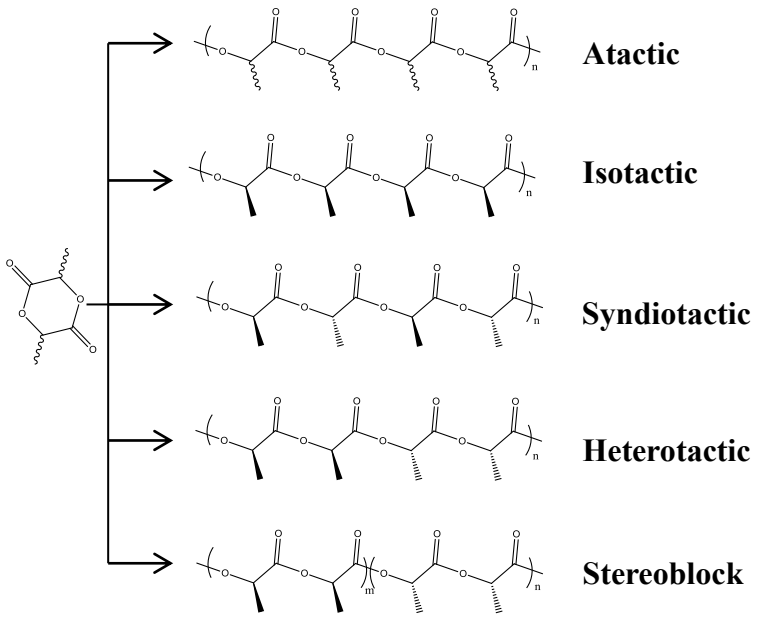

Figure 1.5 Different stereoisomers that can be prepared through the ROP of lactides.[35]

The two enantiopure forms are semicrystalline and exhibit a melting point at ~170 ^{o}C. However, this value can vary significantly depending on the optical purity of the polymer and the molecular characteristics.[35,37] It has been proposed that semicrystalline PLA depending on the crystallisation conditions can obtain three

different crystalline forms, the α, β and γ forms that among them have different helix conformations and cell symmetries. De Santis and Kovacs determined the conformation of the PLA chain in the α form to be left-handed 10_7 helix for P(*L*-LA) and a right handed 10_3 helix for P(*D*-LA).[38] They proposed that two chains are included in an orthorhombic unit-cell of parameters a = 1.06 nm, b = 0.610 nm and c = 2.88 nm. The ratio of a and b was found to be 1.737 which is nearly $\sqrt{3}$, indicating almost hexagonal packing of helices. However, in recent reports they calculated slightly different lattice parameters but no specific crystal form has been proposed.[39] The β form was first identified by Eling *et al.*[40] This crystal structure, which is known to be obtained under mechanical stretching, has not been fully resolved. In 2000, Lotz *et al.* reported the formation of the γ form, this crystal structure is characterised by strict antiparallelism of the two chains which build up in the unit cell and so far it has been formed only through the epitaxial crystallisation of enantiopure PLAs.[41]

Polylactide can be prepared by two techniques; the first is based on the polycondensation reaction of lactic acid,[42-44] while the second is on the ring opening chain reaction of lactides.[35,37] The first is not widely used, especially in state–of–the art applications, because it does not allow controlling the molecular characteristics of the produced polymers therefore, it does not offer the ability to prepare well defined complex architectures. Moreover, polycondensation reactions of lactic acid lack the ability of delivering polymers of high molecular weights, as a consequence of the fact that the water produced through the reaction course is hard to remove.[37] Therefore, ROP (ring opening polymerisation) reactions, that offer good control over

the polymer molecular characteristics are widely used for the preparation of well-defined materials based on PLA.

The lactide ring, from a thermodynamic point of view, is one of the few 6 member ring examples that can undergo ring opening polymerisations. This fact is in agreement with normal polymerisation enthalpy of lactides, which is negative and with a relatively high absolute value (-23 KJ/mol). Crystallographic data, explain the aforementioned unique behavior of lactide, by the fact that the existence of the 2 ester bonds in the same ring, drastically increases the ring strain due to their planar conformation. However, lactides ring strain, which is the driving force of their ring opening polymerisation, is of moderate strength. Thus, an increase in temperature usually promotes the reaction. Practically, optimisation of the polymerisation conditions is crucial to obtain control over the polymerisation. A wide range of polyesters that display different thermal and degradation properties can be synthesised in this manner, controlled by structure and composition of the repeat unit, flexibility of the chain, presence of polar groups, molecular mass and crystallinity. The huge interest in materials based on PLA has triggered ROP investigations with a wide variety of systems with some of them demonstrating a living like character. Catalytic,[37] cationic,[45] anionic,[46] enzymatic[47-49] and more recently organocatalytic pathways have been utilised.[50] In the present work a thiourea/sparteine organocatalytic system was used and is discussed a bit further in the following section

1.2.4 Thiourea/sparteine ring opening polymerisation system

In 2005, Dove *et al.* reported the ring opening polymerisation of lactides using a thiourea based bifunctional organocatalytic system.[50,51] The catalytic behavior of a

thiourea which also contained a tertiary amine centre (**1**) (Figure 1.6) in the polymerisation of lactide was studied in dichloromethane (DCM) (1 M) at 25°C using pyrene butanol as the initiator in the presence of 5 mol % of the organocatalyst.

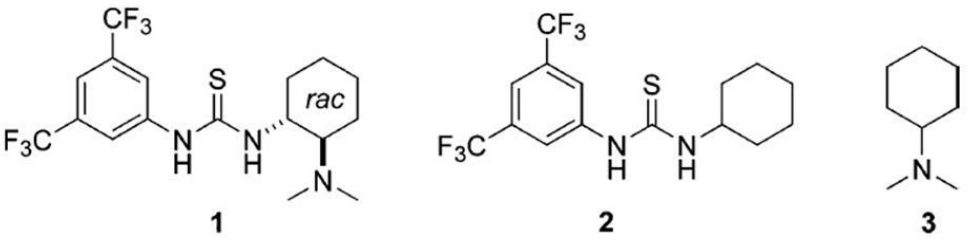

Figure 1.6 Different organacatalysts studied by Dove *et al.*

It was proposed, that the mechanism relies on the activation of the monomer and the initiator by the hydrogen bonding interaction with the thiourea organocatalyst. At a monomer-to-initiator ratio of 100 ([M]/[I]), lactide was converted to polylactide and reached 97% conversion after 48 h. The polylactide produced demonstrated a number average molecular weight M_n 23000 g/mol with a very narrow polydispersity (M_w/M_n=1.05).

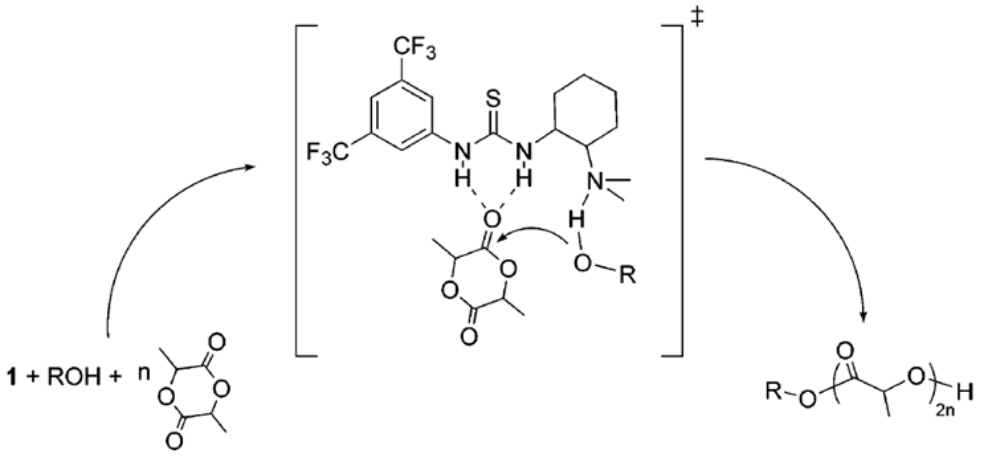

Figure 1.7 Proposed mechanism for the organocatalytic ROP of lactide mediated by compound 1.[51]

The polymerisation exhibited characteristics of a living polymerisation as evidenced by the linear correlation between M_n as confirmed by ^{1}H NMR and monomer conversion, the close correlation between the theoretical and experimental molecular weights and the polydispersities of the produced polymers, through the reaction course. Variation of the [M]/[I] ratio led to narrowly dispersed polylactide and the molecular weight control was very good for a variety of targeted degree of polymerisation (DPs). The polydispersities were extremely low and remained invariant at high monomer conversions (95-100%) For example, when poly(*rac*-lactide) (M_n = 21300 g/mol, M_w/M_n = 1.06 (measured by SEC) was left to react with the catalyst for a further 4 days after complete monomer conversion, analysis of the polylactide revealed a M_n of 20900 g/mol and PDI of 1.07 this result provides strong evidence of the absence of any transesterification reactions. Moreover, analysis of isotactic polylactide (poly(*L*-LA)) by ^{13}C NMR spectroscopy and differential scanning calorimetry (DSC) clearly showed that racemisation does not occur. The extraordinary selectivity of this catalyst system for polymerisation relative to transesterification is unusual. In this work, the reaction between methyl benzoate and either ethanol or 2-propanol in the presence of **1** (5 mol %, 1M CH_2Cl_2) gave no evidence for transesterification (48 h) and resulted in the quantitative recovery of methyl benzoate. These data suggest that the low polydispersities and exceptional control observed are a consequence of selective transesterification of lactide relative to the open chain esters, presumably, the ring strain of lactide provides both a driving force for the polymerisation and a kinetic preference for polymerisation relative to transesterification using catalyst **1**. The same group demonstrated that the usage of a two compound system, consisted of a thiourea (**2**) and *N*, *N*

dimethylcyclohexylamine (**3**) speeds up the reaction. Therefore, DPs of a 100 can be achieved in 2 hours.

Further information regarding the synthesis of block copolymers containing polylactides andother synthetically incompatible polymer blocks can be found in the introduction of Chapter 2.

1.3 Self-assembly of block copolymers (BCPs)

Similar to small molecular weight surfactants, BCPs have the ability to spontaneously coordinate into supramolecular structures. However, structures formed from BCPs are significantly more stable than those formed by lipids due to their larger size and lower solution dynamics.[52,53] It is a balance between strong covalent bonds that hold the polymer blocks together and weak intermolecular forces among the polymer chains, which can be manipulated towards the synthesis of predictable nano-scaled morphologies. Polymer chemists have exploited the wide range of controlled polymerisation techniques now available in order to design macromolecular analogues of nature's simple amphiphiles. In particular, advances in controlled polymerisation methods and especially the development of CRPs have enabled the synthesis of a wide range of well-defined complex macromolecular architectures and incorporation of functional groups that previously was not possible to prepare. Well-defined block copolymer amphiphiles undergo self-assembly in aqueous solution in order to minimise energetically unfavorable interactions of water with hydrophobic groups.

In coil-coil block copolymers the various reported self-assembled morphologies are primarily a result of the inherent molecular curvature and how this influences the packing of the copolymer chains; The morphology obtained is dictated by the aggregates free energy, which in turn depends on three components, the free energy of the core, which relates to the stretching of the core forming block, the free energy of the corona, to which steric or electrostatic interactions of the coronal blocks contribute and the free energy of the interface which depends on the interactions between the core forming block and the solvent. With good knowledge of these parameters a dimensionless 'packing parameter', *p* can be calculated and thereafter

the favourite morphology predicted.[54] Any factor that can influence any of these major contributions will also affect the obtained morphology through the self-assembly process. These can be the copolymer composition, the nature of the selective solvent, the nature and amount of the common solvent, self-assembly temperature, concentration, ionic strength, and presence of homopolymer or other additives. Today, BCP self-assembly in solution has produced more than 20 different morphologies. In some cases their formation is thermodynamically induced, while in other cases it is kinetically controlled.[53,55]

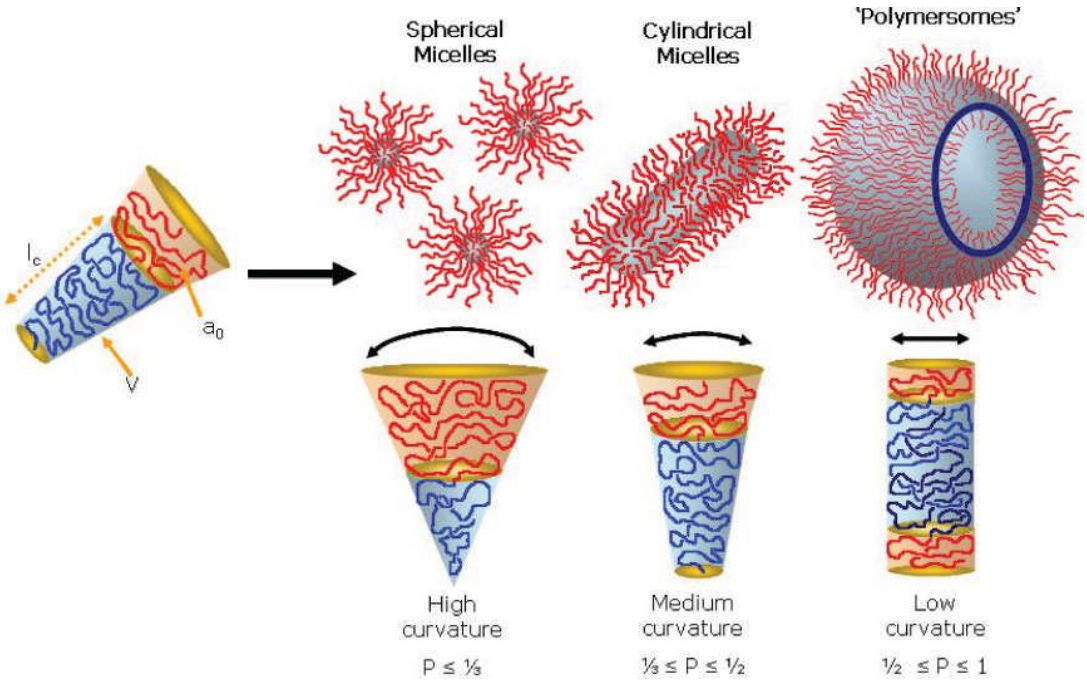

Figure 1.8 Relationship between the curvature of a coil-coil type block copolymer and self-assembled morphology in solution.[56]

The simplest morphology found is that of spherical micelles. In this case a spherical core is surrounded by the soluble corona polymer chains (Figure 1.9A). This morphology is commonly obtained when the weight fraction of the hydrophilic block

is larger than the hydrophobic block. Furthermore, as spherical micelles are formed very frequently at the early stages of self-assembly processes are also considered as the precursors for other morphologies.[53] Importantly, spherical micelles have been studied extensively and developed beyond simple core-corona structures. A few examples of more exotic morphologies based on spherical micelles are Janus micelles with two distinct hemispheres, multi compartment micelles (Figure 1.10), zwitterionic micelles and more.

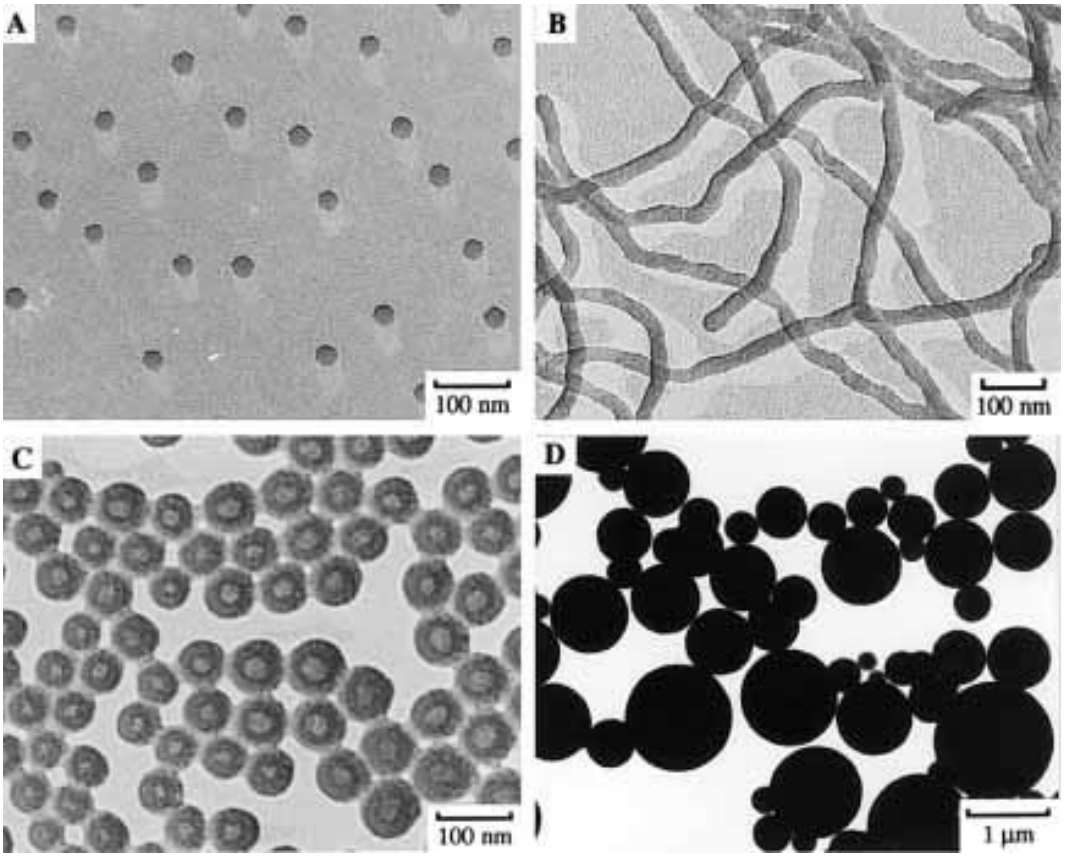

Figure 1.9 Typical morphologies of crew-cut aggregates: (A) small spherical micelles from PS_{500}-*b*-PAA_{58}; (B) rod-like micelles from PS_{190}-*b*-PAA_{20}; (C) vesicles from PS_{410}-*b*-PAA_{20} and (D) large compound micelles from PS_{200}-*b*-PAA_4.[57]

The next major morphology found is this of rod micelles (Figure 1.9B). In this case the core of the aggregates is cylindrical and once more it is surrounded by the

soluble corona polymer chains to give rise to a core-shell type of structure.[53] Cylindrical micelles have great potential for a wide range of applications especially in the biomedical arena where the long circulation periods make them great candidates for drug-delivery applications. Recently, a new method was developed for the formation of cylinders of controlled length by Manners, Winnik and coworkers based on the crystallisation of the core block and as this is of fundamental interest for the present study it will be discussed in more detail in the following chapters.[58]

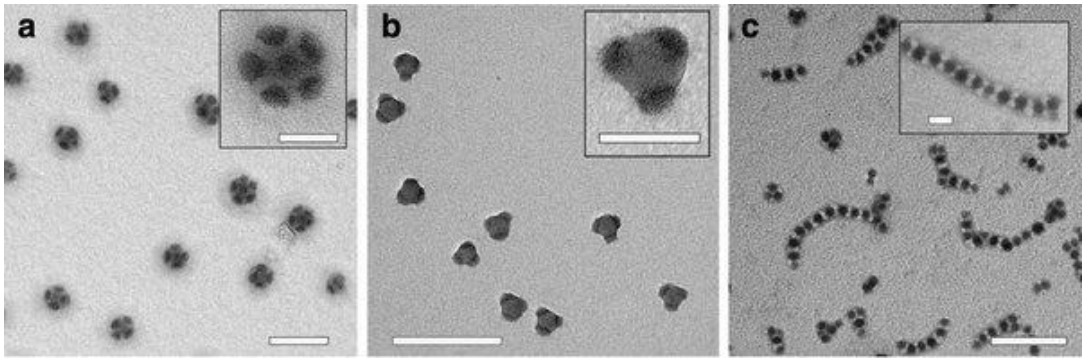

Figure 1.10 A range of multicompartment micelles with spherical or cylindrical morphologies (Scale bars 200 nm and 50 nm in the insets).[55]

Bilayers is the next major morphology obtained from the self-assembly of BCPs. In this case the weight fraction of the hydrophilic block is smaller compared to the hydrophobic. Importantly, bilayers are formed most often by diblock copolymers, while triblock copolymers typically form monolayers or multilayers.[53] This morphology is typically flat or slightly curved, however often closed bilayers are observed which are named vesicles (or polymersomes) (Figure 1.9C).[59] Van Hest and coworkers recently demonstrated a controlled shape transformation in polymer vesicles that resulted in bowl-like bilayers that they named vesicle stomatocytes (Figure 1.11).[60]

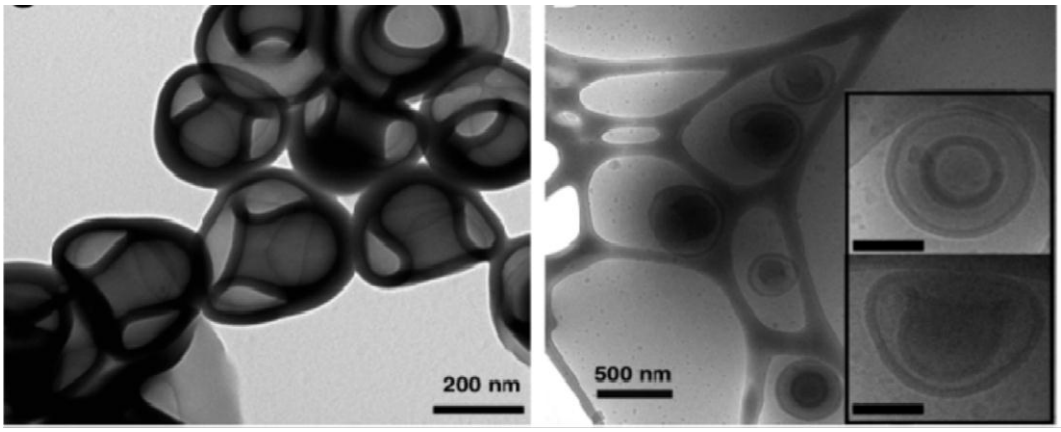

Figure 1.11 Representative TEM images of vesicle stomatocytes in different magnifications.[60]

Another morphology commonly found is large compound micelles. These particles are consisted by inverse micelles aggregates that are stabilised in the outer surface by a thin layer of hydrophilic chains. Typical characteristics of LCMs are that they are highly polydispersed while their size is typically much larger than that seen for normal spherical micelles (Figure 1.9D).[53,57]

BCP self-assembly is of central importance in the present study. However, this work focuses primarily on the self-assembly behaviour of rod-coil (crystalline-coil) block copolymers. In this case all the above self-assembly rules are still valid; however, additional driving forces are introduced in order to direct and get ready access to different morphologies. An introduction on the field of rod-coil polymers self-assembly and the subject of crystallisation driven self-assembly (CDSA) can be found in Chapters 4 and 5.

1.4 References

(1) Szwarc, M. *Nature* **1956**, *178*, 1168.

(2) Szwarc, M.; Levy, M.; Milkovich, R. *J. Am. Chem. Soc.* **1956**, *78*, 2656.

(3) Hadjichristidis, N.; Pispas, S. *Adv. Polym. Sci.* **2006**, *200*, 37.

(4) Russell, G. T.; Napper, D. H.; Gilbert, R. G. *Macromolecules* **1988**, *21*, 2133.

(5) Matyjaszewski, K.; Xia, J. *Chem. Rev.* **2001**, *101*, 2921.

(6) Kato, M.; Kamigaito, M.; Sawamoto, M.; Higashimura, T. *Macromolecules* **1995**, *28*, 1721.

(7) Hawker, C. J.; Bosman, A. W.; Harth, E. *Chem. Rev.* **2001**, *101*, 3661.

(8) Chiefari, J.; Chong, Y. K.; Ercole, F.; Krstina, J.; Jeffery, J.; Le., T. P. T.; Mayadunne, R. T. A.; Meijs, G. F.; Moad, C. L.; Moad, G.; Rizzardo, E.; Thang, S. H. *Macromolecules* **1998**, *31*, 5559.

(9) Matyjaszewski, K. *Macromolecules* **2012**, *45*, 4015.

(10) Charmot, D.; Corpart, P.; Micehlet, D.; Zard, S. Z.; Biadatti, T. *WO 9858974 Priority, June 23 to Rhodia Chimie* **1997**.

(11) Sumerlin, B. S.; Donovan, M. S.; Mitsukami, Y.; Lowe, A. B.; McCormick, C. L. *Macromolecules* **2001**, *34*, 6561.

(12) Sumerlin, B. S.; Lowe, A. B.; Thomas, D. B.; McCormick, C. L. *Macromolecules* **2003**, *36*, 5982.

(13) Thomas, D. B.; Sumerlin, B. S.; Lowe, A. B.; McCormick, C. L. *Macromolecules* **2003**, *36*, 1436.

(14) Vasilieva, Y. A.; Thomas, D. B.; Scales, C. W.; McCormick, C. L. *Macromolecules* **2004**, *37*, 2728.

(15) Barner-Kowollik, C.; Quinn, J. F.; Nguyen, T. L. U.; Heuts, J. P. A.; Davis, T. P. *Macromolecules* **2001**, *34*, 7849.

(16) Mayadunne, R. T. A.; Rizzardo, E.; Chiefari, J.; Chong, Y. K.; Moad, G.; Thang, S. H. *Macromolecules* **1999**, *32*, 6977.

(17) Mori, H.; Nakano, S.; Endo, T. *Macromolecules* **2005**, *38*, 8192.

(18) Fleet, R.; McLeary, J. B.; Grumel, V.; Weber, W. G.; Matahwa, H.; Sanderson, R. D. *Macromol. Symp.* **2007**, *255*, 8.

(19) Barner-Kowollik, C.; Editor *Handbook of RAFT Polymerization*; Wiley-VCH Verlag GmbH & Co. KGaA, 2008.

(20) Moad, G.; Chiefari, J.; Chong, Y. K.; Krstina, J.; Mayadunne, R. T. A.; Postma, A.; Rizzardo, E.; Thang, S. H. *Polymer International* **2000**, *49*, 993.

(21) Perrier, S.; Takolpuckdee, P. *J. Polym. Sci., Part A: Polym. Chem.* **2005**, *43*, 5347.

(22) Moad, G.; Chong, Y. K.; Postma, A.; Rizzardo, E.; Thang, S. H. *Polymer* **2005**, *46*, 8458.

(23) Perrier, S.; Takolpuckdee, P. *J. Polym. Sci., Part A: Polym. Chem.* **2005**, *43*, 5347.

(24) Moad, G.; Rizzardo, E.; Thang, S. H. *Aust. J. Chem.* **2006**, *59*, 669.

(25) Moad, G.; Rizzardo, E.; Thang, S. H. *Aust. J. Chem.***2005**, *58*, 379.

(26) Moad, G.; Rizzardo, E.; Thang, S. H. *Polymer* **2008**, *49*, 1079.

(27) Wood, M. R.; Duncalf, D. J.; Rannard, S. P.; Perrier, S. *Org. Lett.* **2006**, *8*, 553.

(28) Moad, G.; Rizzardo, E.; Thang, S. H. *Polym. Int.* **2011**, *60*, 9.

(29) Chong, B.; Moad, G.; Rizzardo, E.; Skidmore, M.; Thang, S. H. *Aust. J. Chem.* **2006**, *59*, 755.

(30) Willcock, H.; O'Reilly, R. K. *Polym. Chem.* **2010**, *1*, 149.

(31) O'Keefe, B. J.; Hillmyer, M. A.; Tolman, W. B. *J. Chem. Soc., Dalton Trans.* **2001**, 2215.

(32) Anderson, K. S.; Schreck, K. M.; Hillmyer, M. A. *Polym. Rev.* **2008**, *48*, 85.

(33) Ikada, Y.; Tsuji, H. *Macromol. Rapid Commun.* **2000**, *21*, 117.

(34) Vink, E. T. H.; Rabago, R.; Glassner, D. A.; Springs, B.; O'Connor, R. P.; Kolstad, J.; Gruber, P. R. *Macromol. Biosci.* **2004**, *4*, 551.

(35) Dove, A. P. *Chem. Commun.* **2008**, 6446.

(36) Kricheldorf, H. R. *Chemosphere* **2001**, *43*, 49.

(37) Dechy-Cabaret, O.; Martin-Vaca, B.; Bourissou, D. *Chem. Rev.* **2004**, *104*, 6147.

(38) De Santis, P.; Kovacs, A. J. *Biopolymers* **1968**, *6*, 299.

(39) Hoogsteen, W.; Postema, A. R.; Pennings, A. J.; Ten Brinke, G.; Zugenmaier, P. *Macromolecules* **1990**, *23*, 634.

(40) Eling, B.; Gogolewski, S.; Pennings, A. J. *Polymer* **1982**, *23*, 1587.

(41) Cartier, L.; Okihara, T.; Ikada, Y.; Tsuji, H.; Puiggali, J.; Lotz, B. *Polymer* **2000**, *41*, 8909.

(42) Kim, K. W.; Woo, S. I. *Macromol. Chem. Phys.* **2002**, *203*, 2245.

(43) Moon, S. I.; Kimura, Y. *Polym. Int.* **2003**, *52*, 299.

(44) Maharana, T.; Mohanty, B.; Negi, Y. S. *Prog. Polym. Sci.* **2009**, *34*, 99.

(45) Kricheldorf, H. R.; Kreiser, I. *Die Makromolekulare Chemie* **1987**, *188*, 1861.

(46) Kricheldorf, H. R.; Kreiser-Saunders, I. *Die Makromolekulare Chemie* **1990**, *191*, 1057.

(47) Matsumura, S.; Tsukada, K.; Toshima, K. *International Journal of Biological Macromolecules* **1999**, *25*, 161.

(48) Matsumura, S.; Mabuchi, K.; Toshima, K. *Macromol. Rapid Commun.* **1997**, *18*, 477.

(49) Loeker, F. C.; Duxbury, C. J.; Kumar, R.; Gao, W.; Gross, R. A.; Howdle, S. M. *Macromolecules* **2004**, *37*, 2450.

(50) Pratt, R. C.; Lohmeijer, B. G. G.; Long, D. A.; Lundberg, P. N. P.; Dove, A. P.; Li, H.; Wade, C. G.; Waymouth, R. M.; Hedrick, J. L. *Macromolecules* **2006**, *39*, 7863.

(51) Dove, A. P.; Pratt, R. C.; Lohmeijer, B. G. G.; Waymouth, R. M.; Hedrick, J. L. *J. Am. Chem. Soc.* **2005**, *127*, 13798.

(52) Nicolai, T.; Colombani, O.; Chassenieux, C. *Soft Matter* **2010**, *6*, 3111.

(53) Mai, Y.; Eisenberg, A. *Chem. Soc. Rev.* **2012**, *41*, 5969.

(54) Isrelachvili *J. Chem. Soc, Faraday Trans.* **1976**, *72*, 1525.

(55) Gröschel, A. H.; Schacher, F. H.; Schmalz, H.; Borisov, O. V.; Zhulina, E. B.; Walther, A.; Müller, A. H. E. *Nat Commun* **2012**, *3*, 710.

(56) Blanazs, A.; Armes, S. P.; Ryan, A. J. *Macromol. Rapid Commun.* **2009**, *30*, 267.

(57) Zhang, L.; Eisenberg, A. *Polym. Adv. Technol.* **1998**, *9*, 677.

(58) Wang, X.; Guerin, G.; Wang, H.; Wang, Y.; Manners, I.; Winnik, M. A. *Science* **2007**, *317*, 644.

(59) Discher, D. E.; Eisenberg, A. *Science* **2002**, *297*, 967.

(60) Wilson, D. A.; Nolte, R. J. M.; Van Hest, J. C. M. *Nat. Chem.* **2012**, *4*, 268.

Chapter 2: Design and synthesis of reversibly connected block copolymers

2.1 Abstract

The aim of this work is to prepare an amphiphilic block copolymer where the two blocks will be connected through a reversible bond. A Diels-Alder (DA) adduct consisted of a maleimide-furan pair was chosen as the reversible linker. An important feature of this DA pair is that the retro DA delivers a maleimide containing polymer, which can be used for further functionalisation.

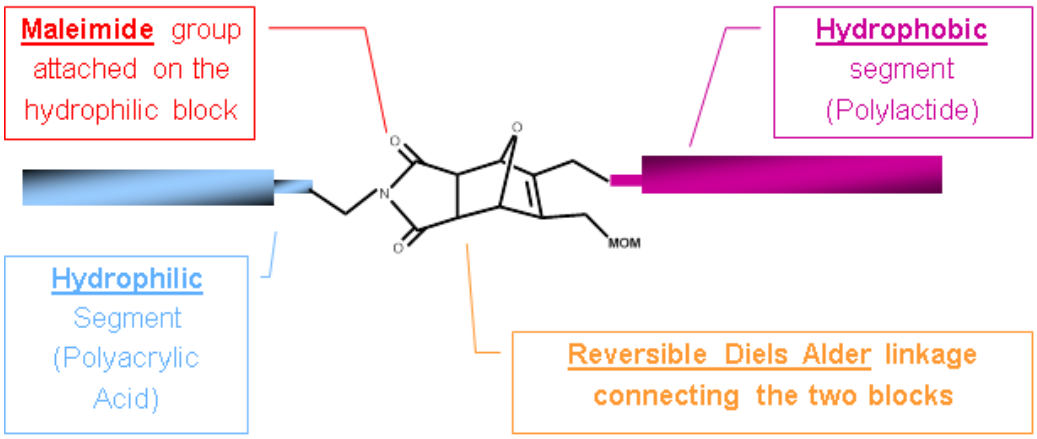

Figure 2.1 Schematic of the target, reversibly connected amphiphilic system

In our target amphiphilic block copolymer the DA linkage bridges a hydrophilic, poly(acrylic acid) (PAA) block that can be prepared from the hydrolysis of poly(tetrahydropyranyl acrylate) (PTHPA) and a polylactide block, which is hydrophobic and readily degradable upon acidic or basic hydrolysis conditions (Figure 2.1). To achieve the preparation of well-defined polymers with predictable molecular weights we used controlled polymerisations techniques. RAFT was employed to polymerise the acrylate monomer while the polylactide block was synthesised by ROP using a thiourea/(-)-sparteine organocatalyst system. The preparation of the aforementioned reversibly connected amphiphilic diblock

copolymer needed the design and synthesis of a dual initiator able to accommodate the variety of different chemistries used in this work.

The ultimate goal of this project is to synthesise internally maleimide functionalised nanocages. This will involve the self-assembly of the DA connected ampihiphilic copolymer in water followed by the cross linking of the shell (particle stabilisation). Subsequently, the retro DA will be induced in order to dissociate the two blocks and unveil the maleimide functionality on the interior surface. The final step will be to degrade-dialyse the polylactide block out of the particles, in order to prepare the desired hollow particles (nanocages).

2.2 Introduction

2.2.1 Reversibly connected copolymers

The concept of non-covalently connected micelles (NCCM) was first reported in 1999 by Jiang *et al.*[1-3] This group developed new routes to prepare polymeric micelles and hollow spheres, using specific intermolecular interactions, especially hydrogen bonding, as the major driving force. In their early work, they used polymer pairs consisting of an oligomer A, with single interaction functionality on one of its ends, and a polymer B, that contained multiple functional sites. Because of the hydrogen bonding between the sites on B and the end of A, a graft like soluble complex was formed with B as the main chain and A as the grafts when a common solvent for both blocks was introduced. In addition, the complex could self-assemble into a core shell structure when a solvent switch to a selective solvent for one of the blocks was performed (Figure 2.2).

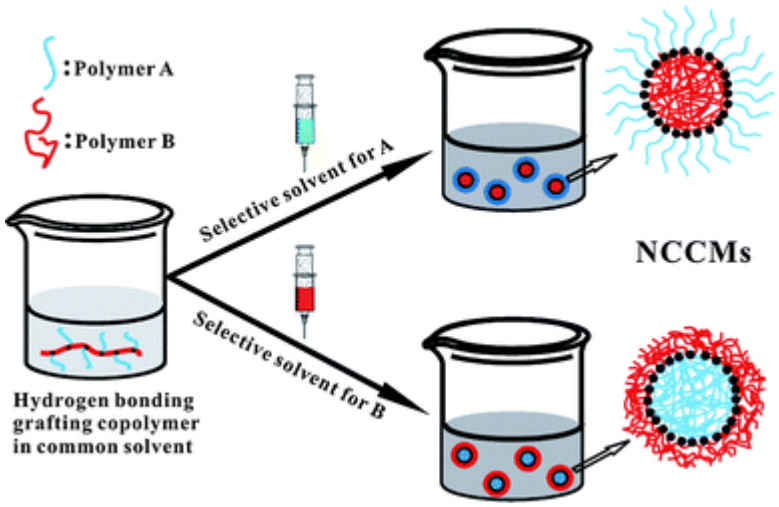

Figure 2.2 Schematic representation of the formation of hydrogen bonding grafting copolymers and their corresponding aggregates.[2]

Host-guest chemistries represent an alternative methodology for the synthesis of reversibly connected copolymers.[4-14] Zou *et al* reported in 2007 on optical switching between self-assembly and disassembly of noncovalently connected amphiphiles based on a cyclodextrin (CD) (host group) and an azo containing amphiphile (guest group).[15] They demonstrated that the complexation of their system can be manipulated by exposing the system to visible or UV irradiation, which in turn causes the isomerisation of the azo-guest groups, thus affecting their complexation ability with the CD host cavities (Figure 2.3).

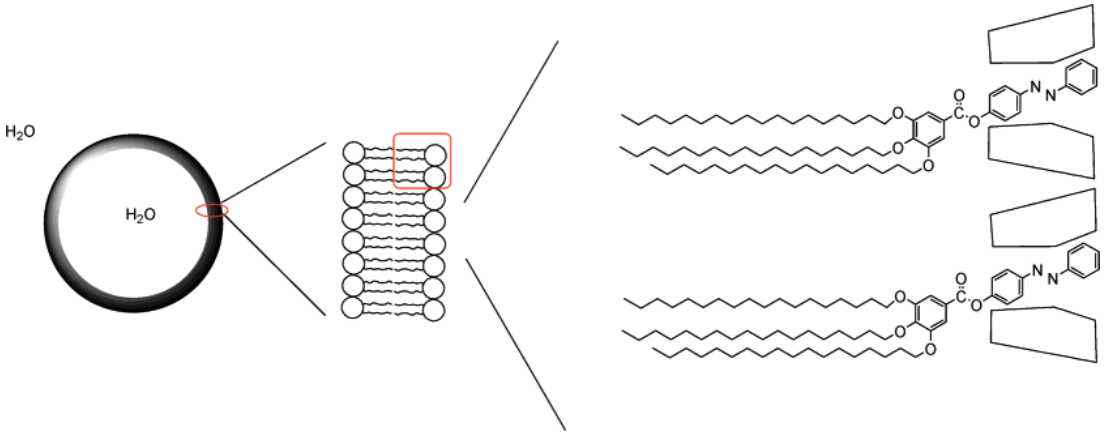

Figure 2.3 Schematic illustrating the host-guest type of interactions between CD and the azo containing amphiphiles.[15]

Curcubit[n]urils (CB[n]) is another class of host molecules in supramolecular systems.[11,12] Jiao *et al* recently reported that the assembly behaviour of aryl/alkyl imidazolium ionic liquid salts in aqueous solution could undergo self-assembly into one-dimensional stacks *via* hydrophobic and π-π interactions upon increasing concentration, which led to a substantial increase in the solution viscosity in water. Addition of the macrocyclic host molecules cucurbit[n]urils (CB[n]) were found to effectively alter the supramolecular assemblies, as evidenced from the dramatic increase (by CB[7]) and decrease (by CB[8]) in solution viscosity and aggregation

size in water, on account of the different binding stoichiometries, 1:1 complexation with CB[7] and 2:1 complexation with CB[8]. Furthermore, the aggregate architectures were controllably modified by competitive guests for the CB[n] hosts.

In parallel with this work, many other research groups focused on developing supramolecular block-copolymers; in which the constituent blocks are connected by specific reversible and tuneable interactions. Among the various interactions used for this purpose, metal-ligand coordination is particularly interesting, given the directional and tuneable nature of these bonds. Schubert *et al* were one of the first groups to report the micellisation behaviour of such metal-supramolecular block copolymers.[16-23] In these studies they used the tridentate 2,2':6',2''-terpyridine ligand. Their most studied block copolymer poly(styrene)-[Ru]-poly(ethyle oxide) (PS-[Ru]-PEO) was prepared from the macro ligands of PEO and PS, both of which had a terpyridine terminal unit (Figure 2.4).[16] Furthermore a library of 13 different metallo-supramolecular block copolymers based on terpyridine functionalised PS and PEO has been synthesised and shown to be useful building blocks for self-assembly.[24]

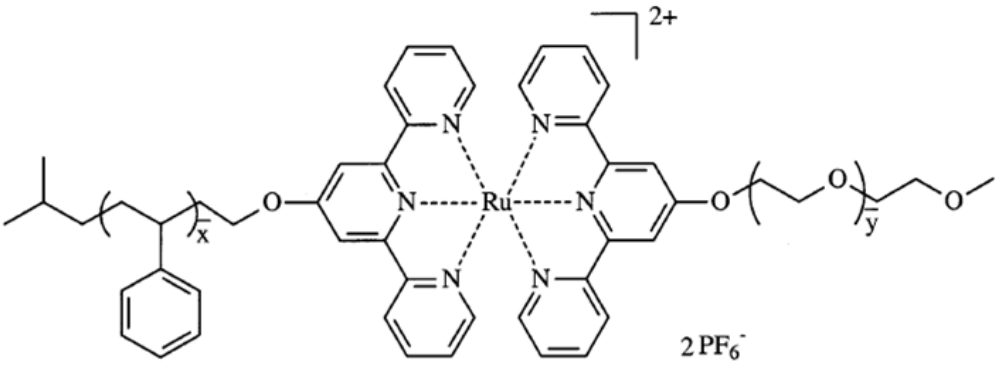

Figure 2.4 Chemical structure of PS-[Ru]-PEO.[16]

O'Reilly *et al.* recently reported a novel supramolecular diblock copolymer, in which the PS block and PAA block have a relatively weak coordinating pyridine ligand and a strong SCS pincer ligand respectively connected to a central Pd(II) metal centre.[25] As expected, this PS-[Pd}-PAA (where [and } refer to different ligands) formed well defined micelles in water with a PS core and a PAA shell. Following cross-linking of the PAA shell, selective cleavage of the pyridine-Pd complex of the PS blocks was easily realised by simply adjusting the acidity of the surrounding medium. Under these acidic conditions, the pyridine ligand was protonated and hence lost its ability to form a complex with Pd(II). Then, the released hydrophobic PS was removed by extensive dialysis against THF/H_2O. Thus, metal functionalised polymeric nanocages of cross-linked PAA were obtained. Compared to the block - copolymers with the terpyridine ligand, this block-copolymer with the unsymmetrical ligand bonds shows a great advantage in its readiness to realise the selective cleavage of the complexes whilst maintaining the metal complex within the structure (Figure 2.5).

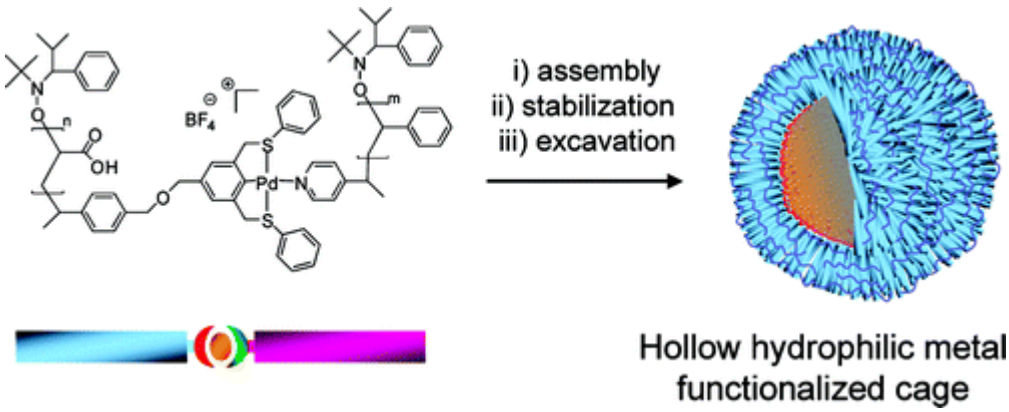

Figure 2.5 Chemical structure and self-assembly of PAA-[Pd}-PS metallo-block copolymer.[25]

One of the most attractive potential uses of such metallo block-copolymers is in the construction of nanoreactors, due to the reversibility of the supramolecular bond that gives rise to the formation of active catalytic sites.[25-27]

Diels-Alder (DA) chemistry has also been explored as a reversible linking group.[28-30] Demirel *et al*. prepared graft copolymers relying on an anthracene–maleimide click reaction. Their work was based on the preparation of random copolymers of polystyrene and 4-chloromethyl styrene. The latter monomeric units were functionalised with an anthracene group in one step by an o-etherification reaction. Subsequently, a DA reaction of this group with a maleimide functionalised PMMA afforded the target graft copolymer (Figure 2.6).[30]

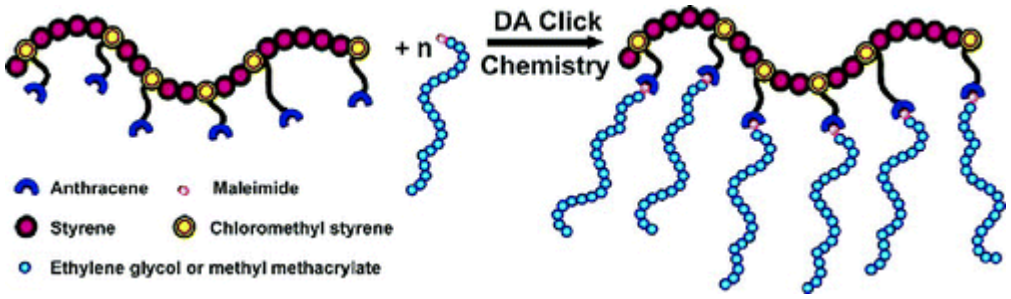

Figure 2.6 General presentation of grafting process by DA Click Chemistry.[30]

Bielawski and co-workers recently demonstrated an alternative route towards DA connected block copolymers. In their example, they first synthesised a DA group that contained two bromine initiating sites. Subsequently, they formed Poly(methyl acrylate) (PMA) polymer blocks by utilising SET–LRP. The resulting PMA polymer contained the DA linker on its middle section. Interestingly the authors managed to mechanically facilitate the retro [4+2] cycloaddition to disassociate the two parts of the polymer (Figure 2.7).[31]

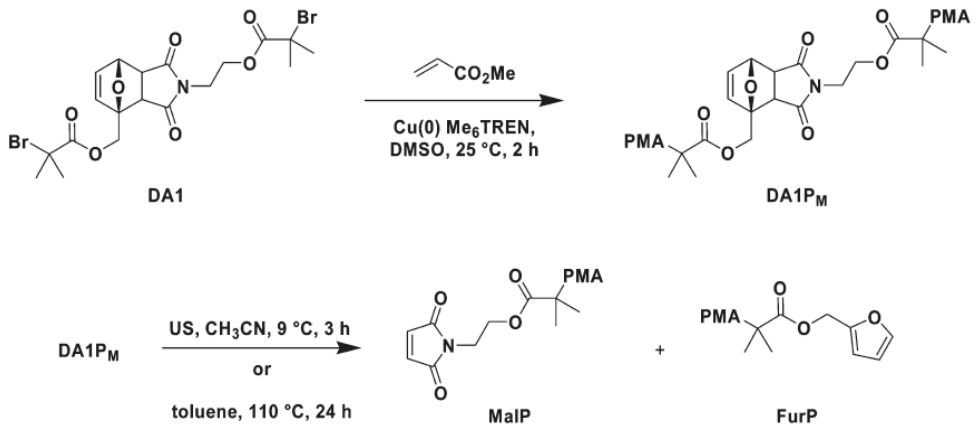

Figure 2.7 Synthetic strategy followed by Bielawski and coworkers to synthesise DA connected polymers.[31]

2.2.2 Maleimide functionalised polymers

Polymers bearing maleimide functionality have been explored recently.[32-35] One of the most interesting examples is that of Sumerlin *et al*, that demonstrated the preparation of a 'smart' polymer–protein conjugate to afford materials which have potential applications in drug delivery, enzymatic catalysis, biosensing or bioseparation, etc. More specifically, in this paper they illustrated the synthesis of a protein-macro CTA by a reaction of a maleimide-functionalised trithiocarbonate with a free sulfhydryl cysteine residue (Cys 34) of bovine serum albumin (BSA). This reaction occurs readily and is specific for the thiol groups at ambient pH (Figure 2.8).[36]

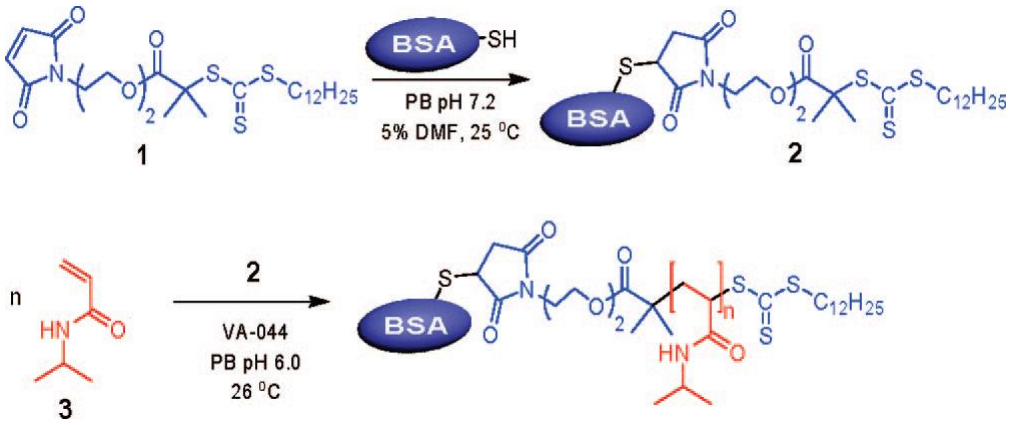

Figure 2.8 Modification of BSA with a maleimide-functionalised CTA and grafting-from *via* RAFT polymerisation of NIPAM.[36]

In 2011 Sanyal and Rotello reported the one-step functionalisation of a surface with a maleimide group. The maleimide functionality was imprinted through the retro DA of nanopatterned polymer surface that contained DA groups. The patterned surfaces were used as scaffolds for the generation of functional and biofunctional structures that could be further functionalised *via* thiol-maleimide click reaction. The biofunctional surface offered a platform for aligning the cells in the direction of patterns, demonstrating the potential for applications in the field of tissue engineering (Figure 2.9).

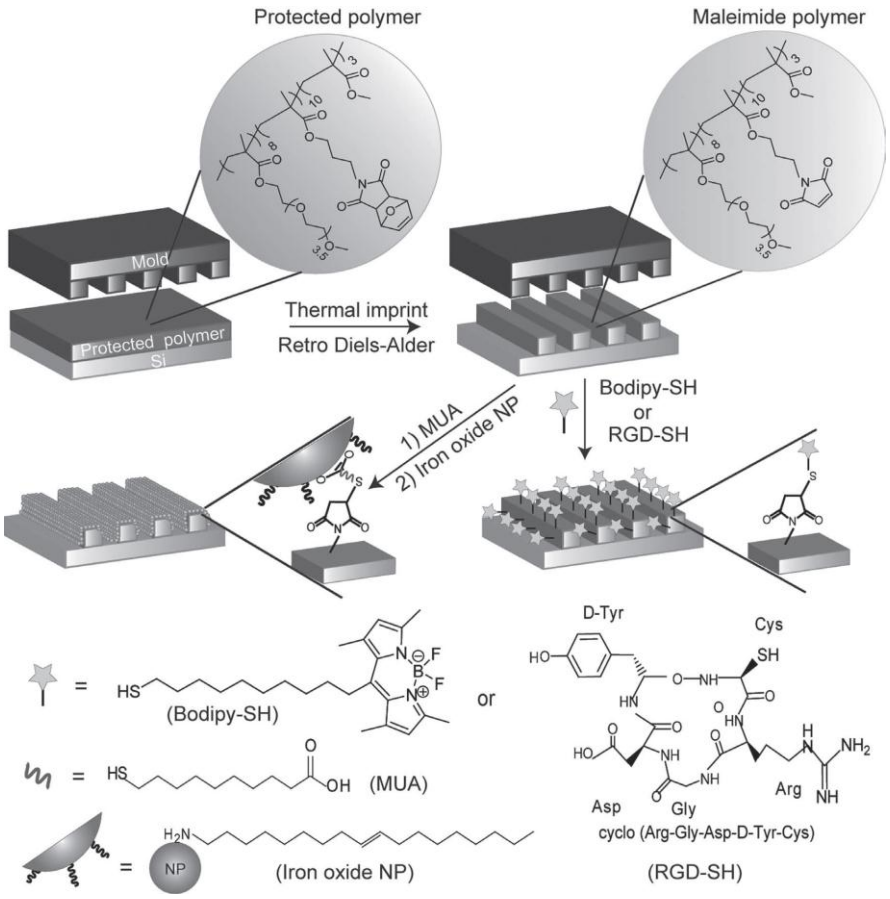

Figure 2.9 Structures of the protected polymer and maleimide formation *via* thermal imprinting, the fabrication of patterned surfaces *via* thermal NIL of protected polymer, immobilisation of iron oxide (Fe_3O_4) nanoparticles (NPs), and arginine-glycine-aspartic acid (RGD) peptide *via* a thiol–maleimide click reaction.[32]

2.2.3 The Diels–Alder reaction

Otto Paul Hermann Diels and Kurt Alder first documented this novel coupling reaction in 1928. For this work they were awarded the Nobel prize in Chemistry in 1950. DA reactions are based on a thermal equilibrium and for a variety of diene–dienophile pairs; it demonstrates a reversible character with the retro DA reaction usually being dominant at higher temperatures.[37] Moreover, the DA reaction is one of the most representative forms of the so called 'click chemistry'. The exact DA

mechanism has been the subject of a lot of debate;[38,39] however, the most widely accepted mechanism describes the cycloaddition as concerted and synchronous.[38,40]

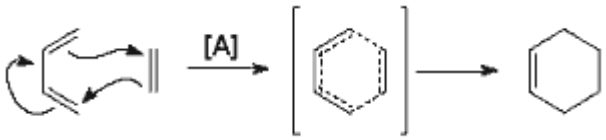

Figure 2.10 General mechanism for the Diels–Alder reaction.[40]

Overlap between the highest occupied molecular orbital (HOMO) of the diene and the lowest unoccupied molecular orbital (LUMO) of the dienophile is thermally allowed in the DA reaction, provided the orbitals are of similar energy (Figure 2.11).[40] The reaction is facilitated by electron-withdrawing groups on the dienophile, since this will lower the energy of the LUMO. Hence, good dienophiles often bear one or two of the following substituents: CHO, COR, COOR, CN, C=C, Ph, or a halogen. The diene component should be as electron rich as possible. There are 'inverse demand' DA reactions that involve the overlap of the dienophile HOMO with the unoccupied MO of the diene. This alternative scenario for the reaction is favoured by electron-donating groups on the dienophile and an electron-poor diene.

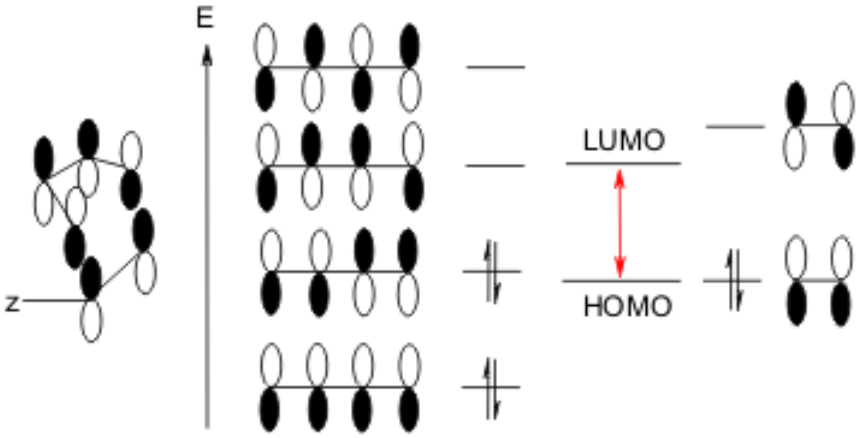

Figure 2.11 HOMO-LUMO energy level representation of the diene-dienophile pair in inverse electron demand DA.

DA reactions can lead to formation of a variety of structural isomers and stereoisomers (enantiomers and diastereoisomers). The identity of the major products can usually be predicted. However, in the reaction of an asymmetrically substituted diene and dienophile, pseudo-ortho and para orientations in products are usually favoured over the meta orientation. A particularly preference in location of substituents in the product can, in some cases, be explained in terms of frontier orbital theory. Most commonly, dienes bear an electron-releasing group and dienophile bears an electron-withdrawing group. The strongest interaction takes place between the HOMO of the diene and the LUMO of the dienophile. Carbons that have the highest coefficients in two frontier orbitals will begin to bond, therefore these carbons will direct the orientation of substituents and thus the identity of major product of the DA reaction. Dealing with the actual frontier orbital coefficients can be avoided since the preferred orientation of the product can be described in terms of partial positive and negative charges that exist in the diene and dienophile. Carbons with a partial negative charge will interact more readily with carbon bearing a partial positive charge. Therefore, those two carbons will start coming together first, dictating the relative orientation of the substituents.

2.2.4 Synthesis of polylactide containing block copolymers

Although CRP techniques allow for the synthesis of well-defined block copolymers, difficulty may arise when complex copolymers are desired. This is the case when synthesising block copolymers containing polylactides. As it was discussed previously well-defined polylactides are prepared through the ROP process. This is the case when the synthesis of polylactides combined with other vinyl monomers is designed. Block copolymers containing polylactide are of particular interest

especially in pharmaceutical and biological applications as it has a biodegradable and biocompatible character, indeed it is one of the few polymers to have been FDA approved. Tandem initiating polymerisation systems have been developed, to incorporate ROP of lactides with otherwise incompatible polymerisation techniques like anionic and controlled radical polymerisation methods. This field of research was comprehensively reviewed by Dove recently and some key examples of his review are highlighted below.[41]

The incorporation of functional and non-degradable blocks allows a greater array of applications for polylactide based systems. Living and controlled polymerisation methodologies such as CRP that include atom transfer radical polymerisation (ATRP),[42] nitroxide mediated polymerisation (NMP)[43] and reversible addition fragmentation chain transfer polymerisation (RAFT)[44] are the three most commonly employed techniques for the controlled polymerisation of vinyl monomers. [41]

Two main methodologies have been applied to combine the mechanistically distinct polymer blocks; a 'grafting from' approach, in which the corresponding polymers are grown from an appropriately designed multi-initiator and a 'grafting to' approach in which the preformed polymer blocks are combined *via* 'click' chemistry.

The 'grafting from' approach performed with the use of dual-headed initiators represents a very versatile methodology and as it is the one we utilised in the present work; it will be discussed in a bit further detail. In this methodology the species, contain initiating sites for both ROP and CRP. Hedrick *et al.* performed both the stepwise and simultaneous ROP of ε-caprolactone following both the NMP of styrene at 125 °C and the ATRP of methyl methacrylate at 80 °C in bulk monomer.[45,46] A wide range of other dual-headed initiating systems have been reported and have been used to synthesise a wide range of mechanistically distinct

di- and triblock copolymers. Howdle and co-workers reported that both sequential and simultaneous enzymatic ROP and Cu catalysed ATRP in supercritical CO_2 of ε-caprolactone and methyl methacrylate or a semifluorinated methacrylate monomer was possible.[47] Interestingly, the authors found that the caprolactone acted as a highly efficient cosolvent for the methacrylate monomers preventing precipitation of the polymers. Furthermore, the authors suggest that the application of $scCO_2$ provided an increased level of control over the copolymerisation by comparison to synthesis in standard organic solvents. Meijer, Palmans and co-workers demonstrated a one-pot cascade approach to the synthesis of poly(4-methyl-ε-caprolactone)-*b*-poly(methyl methacrylate) was possible. In this study the authors first used Novozym 435 to effect the enzymatic enantioselective ROP.[48] In the second step, ATRP of MMA was carried out by injection of $[NiBr_2(PPh_3)_2]$ to both effect ATRP and inhibit the enzyme activity to further prevent polymerisation or transesterification side reactions. NMP and RAFT polymerisations have also been applied in dual-headed polymerisation strategies. Wooley and coworkers utilised a dual headed initiator/chain transfer agent (CTA) where the ROP initiating site was incorporated on the Z group of the CTA. Well defined polymers of the type poly(N-(acryloyloxy)succinimide-*co*-N-acryloylmorpholine)-*b*-poly(*L*-lactic acid) (P(NAS-*co*-NAM)-*b*-P(*L*-LA)) were synthesised and their self-assembly properties were explored.[49] Jerome *et al.* showed that both sequential and simultaneous polymerisation of ε-caprolactone and styrene was possible. Again, the sequential polymerisation strategy yielded polymers with narrower dispersities.[45,46] More recently, the hydroxymethyl functional alkoxyamine initially reported by Hawker *et al.* was applied as a dual-headed initiator for NMP and metal-free ROP.[50-53] Heise

and co-workers reported the sequential and one pot sequential polymerisation of ε-caprolactone/4-methyl-ε-caprolactone with styrene.[53]

2.3 Results and discussion

The first step was to synthesise a dual initiator that would connect RAFT and ROP polymerisation sites through a DA linkage (see Scheme 2.1). This system was designed in such a way that, (**2.7**) would be stable under the various chemistries that were used on the following steps of this project.

The second step was to investigate the performance of the aforementioned initiator, (**2.7**), for the polymerisations and sequentially explore the synthetic possibilities of this tandem polymerisation system.

2.3.1 Synthesis of dodecyl 4-(hydroxymethyl) benzyl carbonotrithioate, 2.1

Dodecyl 4-(hydroxymethyl) benzyl carbonotrithicarbonate, (**2.1**) was the first compound prepared. Dodecanethiol was activated by potassium carbonate (lewis base) to subsequently 'attack' carbon disulfide, to form the trithiocarbonate anion, the addition of 4-(chloromethyl) benzyl alcohol produced the desired trithiocarbonate through a S_N2 mechanism. The yield of the reaction was strongly influenced by the solvent used and specifically favoured by acetone that led to 81% conversion after 4 days while the conversion was less than 50% after the same period when the reaction was carried out in THF. The product was characterised by ^{1}H and ^{13}C NMR, MS and IR spectroscopy (Figure 2.12 and Figure 2.14).

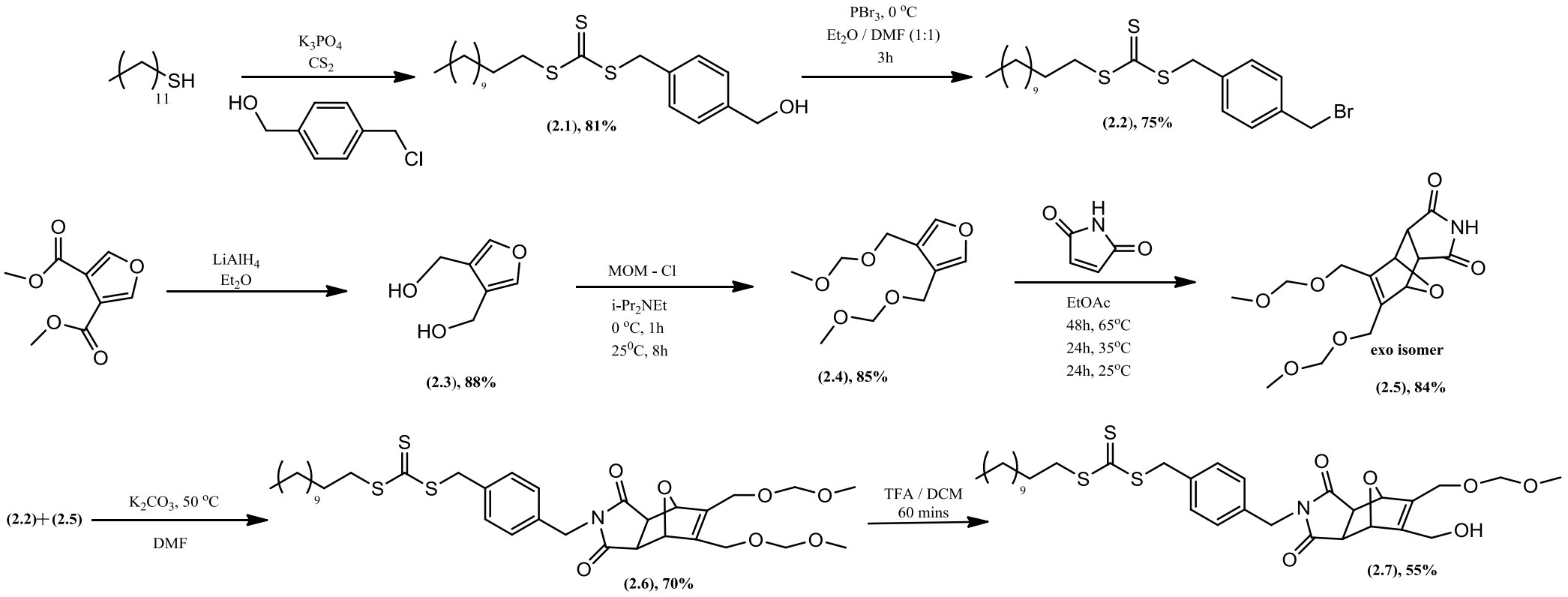

Scheme 2.1 Synthetic strategy for the synthesis of the DA connected dual headed RAFT CTA/ROP initiator, **2.7**.

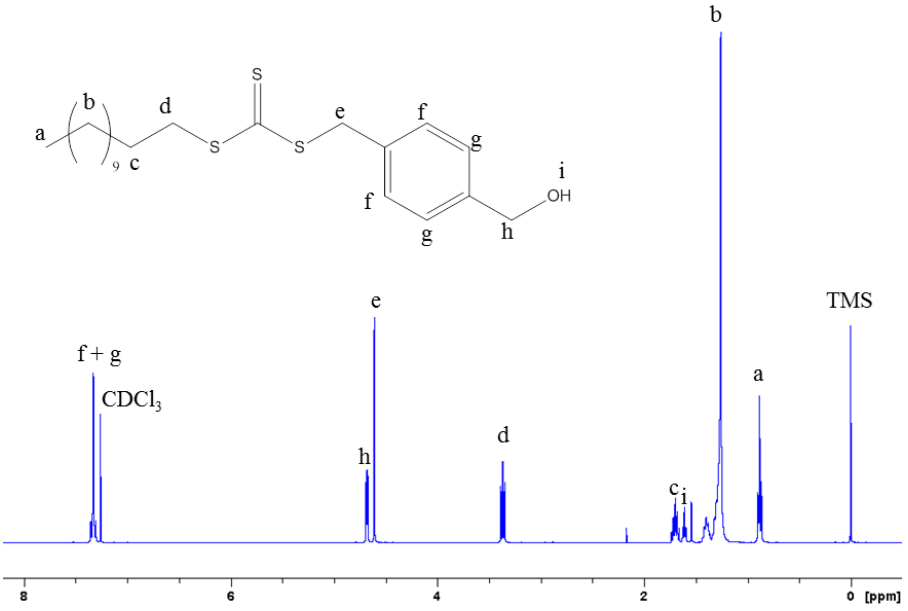

Figure 2.12 ^{1}H NMR spectrum of compound **2.1** after purification in $CDCl_3$ (400 MHz, 293K).

2.3.2 Synthesis of 4-(bromomethyl)benzyl dodecyl carbonotrithioate, 2.2

The next step was the bromination of the hydroxyl group to afford 4-(bromomethyl) benzyl dodecyl carbonotrithioate (**2.2**) this was achieved by treating **2.1** with PBr_3 for 3 hours in a Et_2O/DMF 1:1 mixture. Compound **2.2** was not very soluble in diethyl ether, therefore, the addition of DMF optimised solubility and as a consequence it significantly increased the reaction yield, which was around 60% for a 4:1 Et_2O/DMF ratio and rose to 75% yield when a 1:1 ratio of the two solvents was used. The conversion from an alcohol to a halide was clearly illustrated by ^{1}H NMR spectrum where the characteristic signal at 1.62-1.68 ppm of the hydroxyl group proton completely disappeared and was also confirmed by IR spectroscopy where the characteristic broad peak for the O-H stretch at 3492-3293cm^{-1} also disappeared on the products (Figure 2.13 and Figure 2.14).

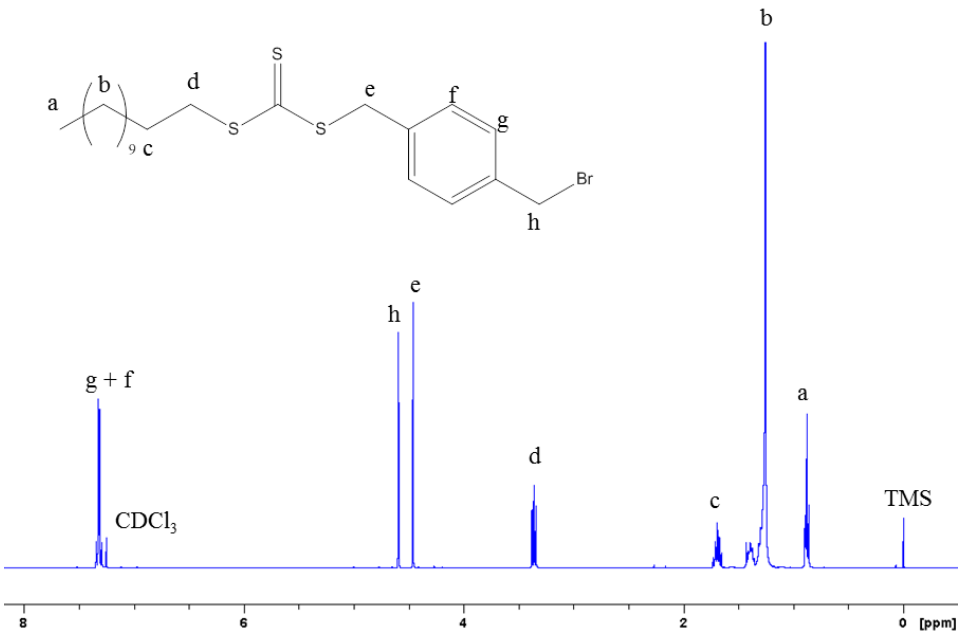

Figure 2.13 ^{1}H NMR spectroscopy of compound **2.2** after purification in $CDCl_3$ (400 MHz, 293K).

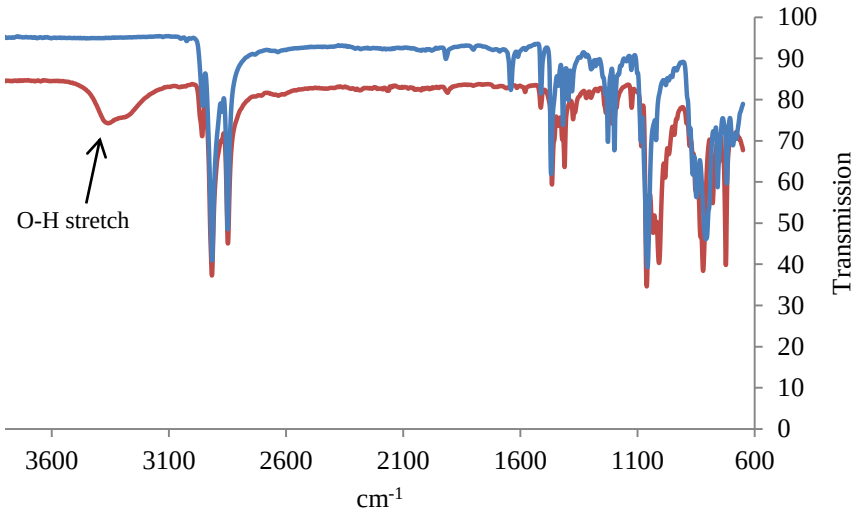

Figure 2.14 Overlay of the IR spectra of compound **2.1** (red line) and **2.2 (**blue line).

2.3.3 Synthesis of furan-3,4-diyldimethanol, 2.3

Furan-3, 4-diyldimethanol (**2.3**) was synthesised by the reduction of dimethyl-3, 4-furan dicarboxylate by lithium aluminum hydride based on a literature report.[54] The reaction was left for 1 hour and subsequently it was quenched with the slow addition of 4.5 mL of water, 4.5 mL of NaOH 15%, followed by 13.5 mL of water. The dry, granular precipitate was filtered and washed using an excess of diethyl ether. The successful synthesis was confirmed by a combination of NMR, MS and IR spectroscopy (see Figure 2.15 and experimental section).

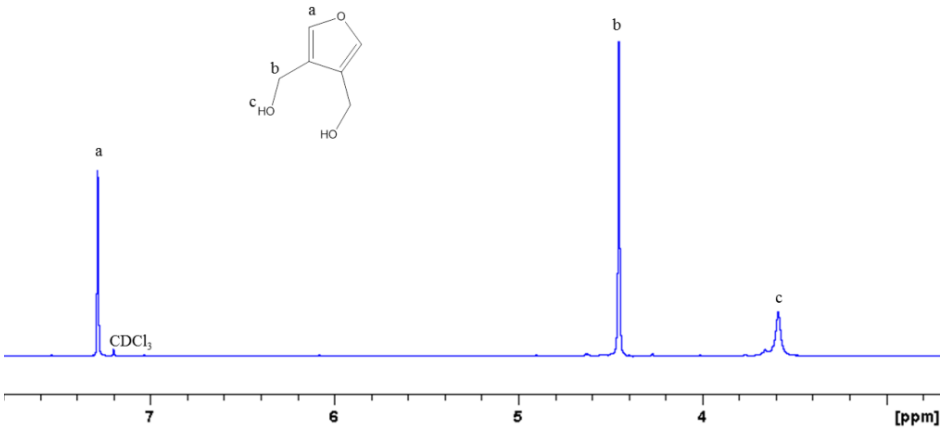

Figure 2.15 ^{1}H NMR spectrum of compound **2.3** after purification in $CDCl_3$ (400 MHz, 293K).

2.3.4 Synthesis of 3,4-bis((methoxymethoxy)methyl)furan, 2.4

Our first trial to prepare the DA adduct was based on the reaction of **2.3** with the maleimide group, the product of this reaction came out of solution after a few hours as a white solid, which was insoluble in all common solvents. The uncharacterised material we hypothesised to be the product of the secondary amine reacting with the

OH groups that could possibly lead to an uncontrolled 'step polymerisation' scheme resulting to an insoluble product, the aforementioned result illustrated the need to protect the hydroxyl groups prior to the DA reaction. The choice of the protection group was key as the deprotection would have to be performed in the presence of the trithiocarbonate which is labile to Lewis acid/base hydrolysis conditions that are commonly used in deprotection chemistries. Chloro methoxy methane (MOM-Cl) was used as the protection group, which can be removed using TFA/DCM 1:1 mixture, in which trithiocarbonates are relatively stable.[55,56] The protection reaction that proceeds through an S_N2 mechanism proved to be clean and high yielding, the protection of both hydroxyl groups was confirmed by ^{1}H NMR spectroscopy where we observed the complete elimination of the broad peak at 3.6 ppm that corresponded to the OH group protons. In addition, the characteristic signals of the MOM group appeared in the product (Figure 2.15 and Figure 2.16).

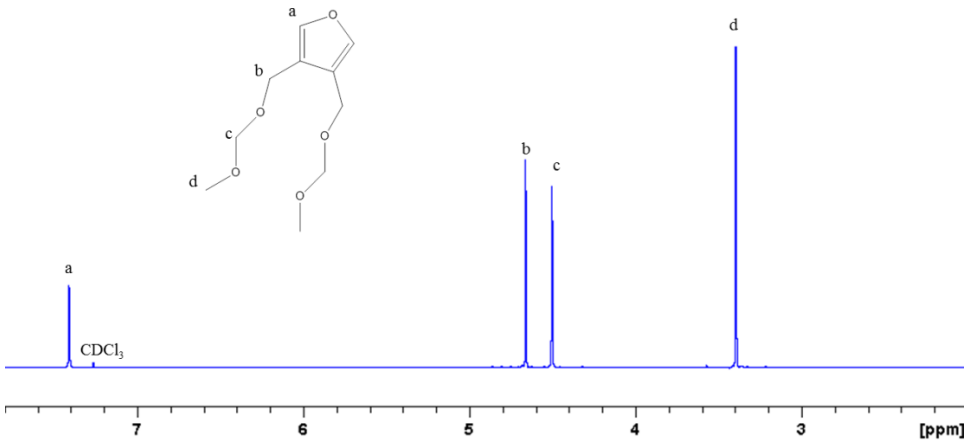

Figure 2.16 ^{1}H NMR spectrum of compound **2.4** after purification in $CDCl_3$ (400 MHz, 293K).

2.3.5 Synthesis of the Diels Alder adduct, 2.5

Next step of the synthesis was the DA reaction of the protected furan compound **2.4** with the maleimide group. The DA reaction was initially performed at 90 ^{o}C in EtOAc and the reaction was monitored by HPLC, the conversion was 25% in less than 24 hours and it did not increase during the following 2 days, indicating that the reaction equilibrium had been reached. To optimise the reaction conditions we decreased the temperature to 65^{o}C. HPLC analysis revealed 65% conversion over the following 2 days. Furthermore, leaving the reaction for an additional 24 hours at 50 ^{o}C increased the conversion of **2.5** to 75% while decreasing the temprature at 25 ^{o}C for further 24 hours increased the overall conversion to 84%. Interestingly, the *endo* and *exo* isomers were both formed; however, more than 90% corresponded to the exo isomer which is the thermodynamic product.

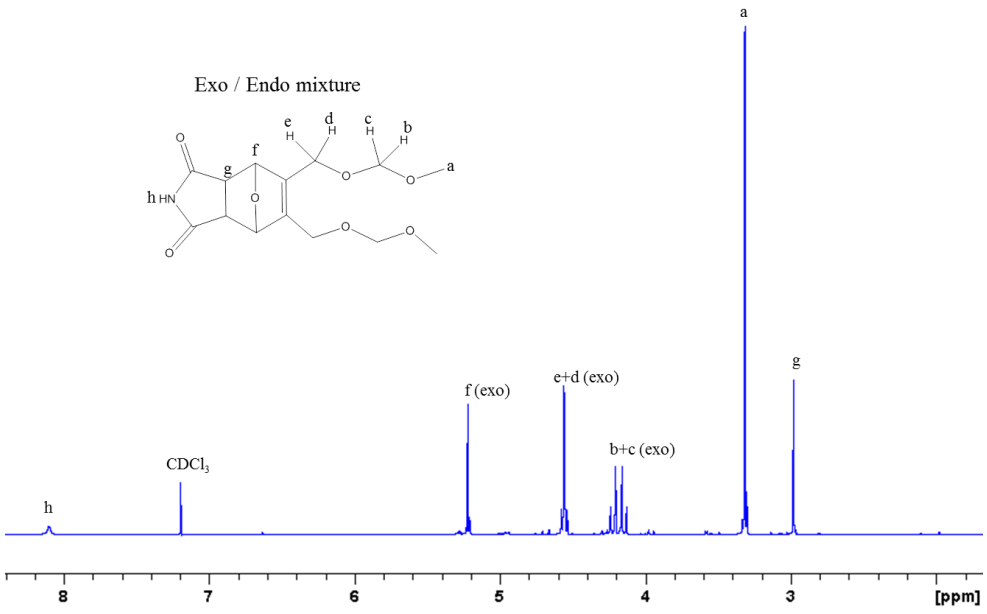

Figure 2.17 ^{1}H NMR spectrum of compound **2.5** after purification in $CDCl_3$ (400 MHz, 293K).

2.3.6 Synthesis of the protected initiator, 2.6

The next reaction was a coupling reaction between **2.2** and **2.5**. It is important to highlight that the most common methodology reported in literature to introduce functionalities on a RAFT agent is based on an esterification reaction of the CTA with the desired group. While this route is adaptable in some cases, it wasn't applicable in our work, as the ester bond would be prone to degradation and hence the maleimide functionality would be lost under the acidic hydrolysis conditions, that we intended to use on some of the following steps. Moreover, it was crucial to attach the functional group with a robust linker over a wide range of conditions. The first alternative was an amide bond, which is more stable. However, the restrictions introduced by the presence of the trithio group, which is sensitive to nucleophiles and especially on primary amines neglected this method. In this work we carried out a halide to amine coupling at 50 ^{o}C in the presence of K_2CO_3, the reaction was monitored initially by TLC and stopped after 3 ½ hours, when a byproduct started appearing. The final yield of the pure product was 70 %. The successful synthesis of **2.6** was confirmed by a fully assigned ^{1}H NMR spectrum and mass spectroscopy (Figure 2.18 and experimental section). Interestingly, both the *exo* and *endo* starting materials (contained in **2.5**) reacted, however the major product was the *exo* DA isomer and was isolated successfully by column chromatography.

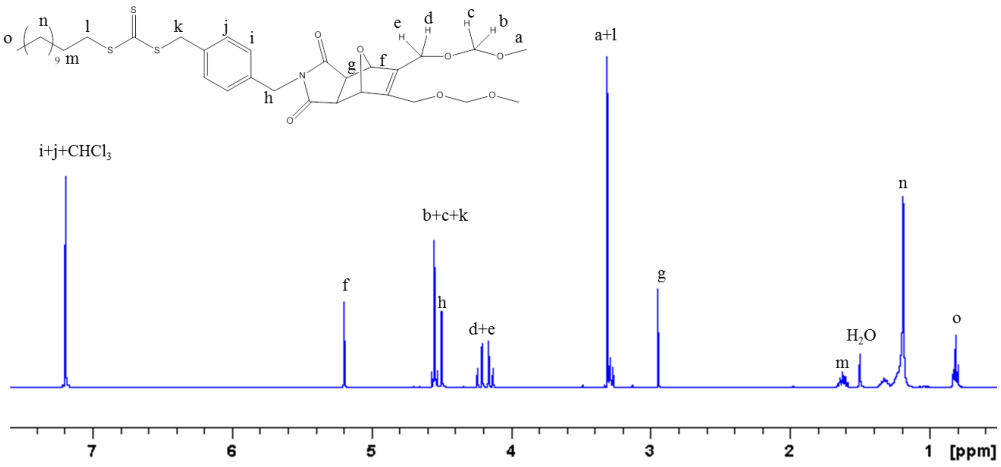

Figure 2.18 ^{1}H NMR spectrum of compound **2.6** after purification in $CDCl_3$ (400 MHz, 293K).

2.3.7 Synthesis of the dual RAFT/ROP initiator, 2.7

The last step towards the synthesis of the dual initiator was the deprotection reaction of the hydroxyl groups by using an excess of TFA. Initially, we were aiming for the deprotection of both hydroxyl groups. On our first trial, HPLC indicated the appearance of several by products, isolation of these fractions and characterisation by ^{1}H NMR and MS spectroscopy revealed that none of the major peaks were corresponding to our desired product. We monitored the reaction progress by stopping it over shorter periods of time. TLC and LC-MS monitoring of the reaction revealed that after 30 minutes the reaction was still 'clean' and the mono deprotected derivative was the major product. For the following 30 minutes the yield of the mono deprotected product was increasing. A number of unidentified side products appeared after 70-80 minutes, while the mono deprotected compound progressively started to decompose. The reaction was repeated several times, and the results were

reproducible, giving 55% maximum yield of the mono-deprotected product after 60 minutes. The fact that one hydroxyl group gets deprotected first, can be attributed to the relative selectivity of this reaction over more sterically hindered centres. The successful transformation was confirmed with several characterisation methods. IR spectroscopy clearly indicated the appearance of a broad signal in the region of the O-H stretch 3550-3000 cm^{-1} (Figure 2.19).

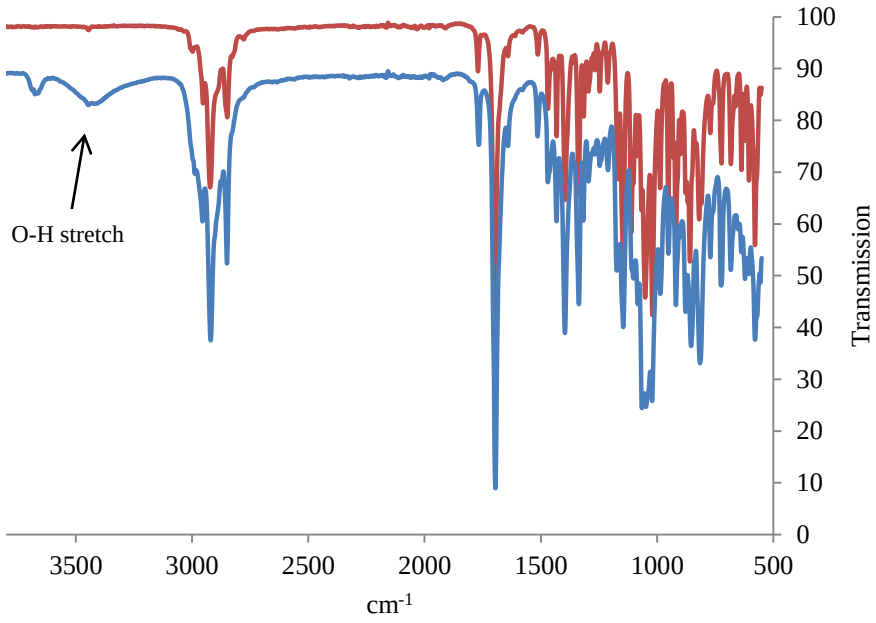

Figure 2.19 Overlay of the IR spectra of compound **2.6**, red line and **2.7**, blue line.

^{1}H NMR spectroscopy illustrated that all the other groups of our initiator were stable while elemental analysis supported the successful preparation of the mono hydroxyl derivative (Figure 2.20 and experimental section).

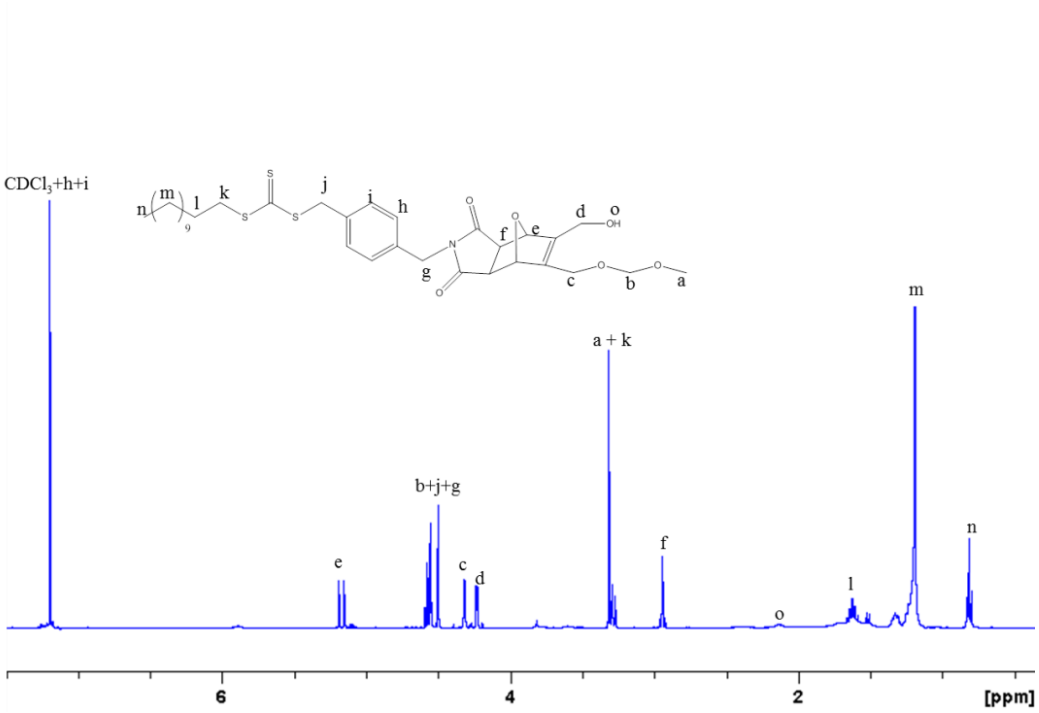

Figure 2.20 ^{1}H NMR spectrum of compound **2.7** after purification in $CDCl_3$ (400 MHz, 293K).

After the successful preparation of the dual initiator, we explored the utility of compound **2.7** for the synthesis of block copolymers by a combination of ROP and RAFT polymerisations. Two routes were possible; ROP of lactide could be employed first, followed by RAFT of tetrahydropyran acrylate monomer and vice versa. The second route proved to be not applicable with this system, due to the fact that the PTHPA block poisons, through hydrogen bonding, the thiourea organocatalyst. That was evidenced by the fact that no conversion was observed over the course of 30 days under our standard ROP conditions.

2.3.8 *L*-Lactide polymerisation using 2.7 to afford a P(*L*-LA) macro–CTA, 2.8.

The ROP step was carried out with the thiourea/(-)-sparteine system (Figure 2.21). This polymerisations demonstrated living characteristics by producing polymers with predictable molecular weights, narrow polydispersities and high end group

fidelity. Importantly, these polymerisations were conducted at room temperature, this was crucial in order not to facilitate the retro DA reaction. Polymers with DP's ranging from 25 to 50 were prepared. The produced polymers had an excellent agreement with the theoretical molecular weights, as revealed by ^{1}H NMR spectroscopy end group analysis; while the PDIs were always around 1.1 as illustrated by SEC analysis.

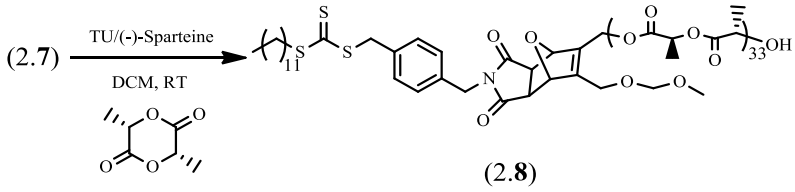

Figure 2.21 ROP for the synthesis of the PLA macro CTA with the thiourea/(-)-sparteine organocatalytic system initiated by compound **2.7**.

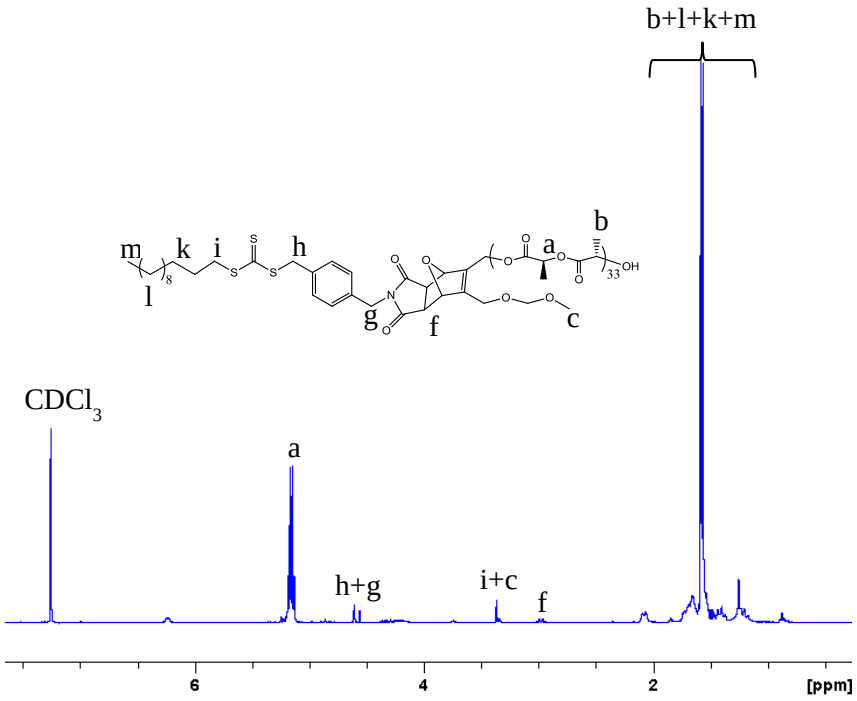

Figure 2.22. ^{1}H NMR spectrum of the crude P(*L*-LA) sample of the macro CTA with DP = 33 (**2.8)** in $CDCl_3$, (400 MHz, 293K).

Additionally, the end group fidelity was worked out by a combination of ^{1}H NMR spectroscopy and MALDI ToF MS, illustrating very good end group retention (Figure 2.23). ^{1}H NMR showed good integrations of the two sides of the DA group, as it was illustrated by careful integration of protons i, c, h, g and f (Figure 2.22). By MALDI ToF MS we could confirm that all the polymer chains had the furan group attached. The DA counterpart wasn't present because it was undergoing the retro DA under the relatively harsh experimental conditions utilised during the MALDI ToF MS experiment.

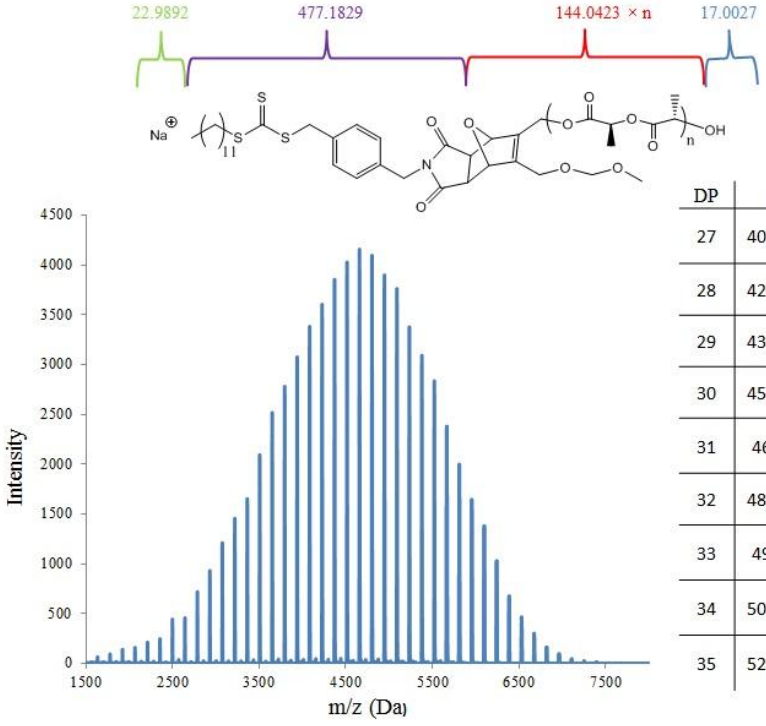

DP	Found	Furan only Na
27	4084.300044	4084.2043136
28	4228.371455	4228.2465724
29	4372.440808	4372.2888311
30	4516.514596	4516.3310899
31	4660.59152	4660.3733487
32	4804.678222	4804.4156075
33	4948.75917	4948.4578662
34	5092.847783	5092.5001250
35	5236.942351	5236.5423838

Figure 2.23 MALDI-ToF mass spectrum of P(*L*-LA)$_{33}$, **2.8**. Spectrum collected in linear mode, with high resolution masses obtained in reflector mode. Average difference between calculated and found m/z = 0.3264 Da.

2.3.9 THPA polymerisation using PLA macro CTA, to afford P(*L*-LA)-b-PTHPA, 2.10

The PLA macro CTA's bearing a trithiocarbonate group at the chain end were employed to polymerise tetrahydropyran acrylate (THPA) through the RAFT process in order to prepare DA connected diblock copolymers.

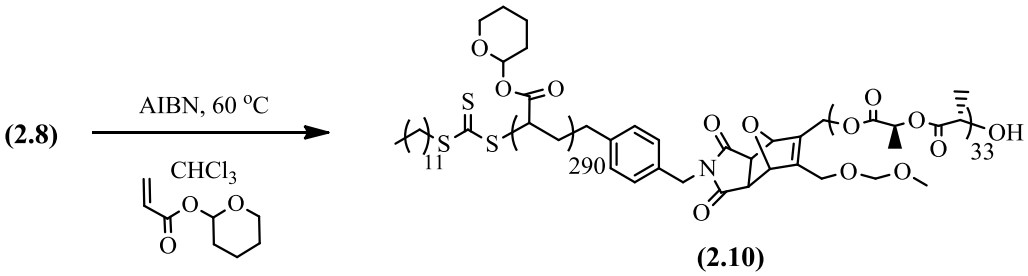

Figure 2.24 RAFT of THPA mediated by the P(*L*-LA) macro CTA for the synthesis of the corresponding DA connected block copolymer.

The choice of PTHPA as a reactive poly(acrylic acid) precursor allowed full characterisation of the diblock copolymers before the formation of the amphiphilic P(*L*-LA)-*b*-PAA under mild aqueous hydrolysis conditions. The temperature had to be as low as possible, due to the presence of the thermally labile DA group. Therefore the polymerisations were conducted at 60 °C which is the lowest possible to facilitate the efficient initiation with AIBN. It was observed that careful choice of solvent for chain extension of the PLA macro-RAFT agents was needed to avoid the formation of products that contained significant amounts of unreacted homopolymer, resulting from incomplete initiation from the polymeric precursor. It was found that chloroform gave optimum results, being a good solvent for both PLA, and the trithiocarbonate end-group (see Table 2.1 and Figure 2.26). However, when the polymerisation was conducted in DMF or dioxane incomplete initiation was

observed (Table 2.1 and Figure 2.26). We speculate that the uncontrolled fashion of these polymerisations was a result of the poor solubility of the trithiocarbonate end group in these solvents, which facilitated the formation of aggregates with the RAFT end group in the core, reducing that way its accessibility.

Table 2.1 Molecular characteristics of the polymers synthesised.

Polymer	M_n^{NMR} (kDa)	M_n^{DRI} (kDa)	M_w/M_n^{DRI}	M_w/M_n^{UV}
P(*L*-LA)$_{33}$, **2.8**	5.1	10.3	1.09	-
P(*L*-LA)$_{25}$, **2.9**	3.9	8.3	1.11	-
P(*L*-LA)$_{33}$-*b*-PTHPA$_{290}$, **2.10**	51.2	46.2	1.15	1.15
P(*L*-LA)$_{25}$-*b*-PTHPA$_{235}$, **2.11**	40.6	30.3	1.52	1.78
P(*L*-LA)$_{33}$-*b*-PTHPA$_{120}$, **2.12**	23.2	20.2	1.61	1.85

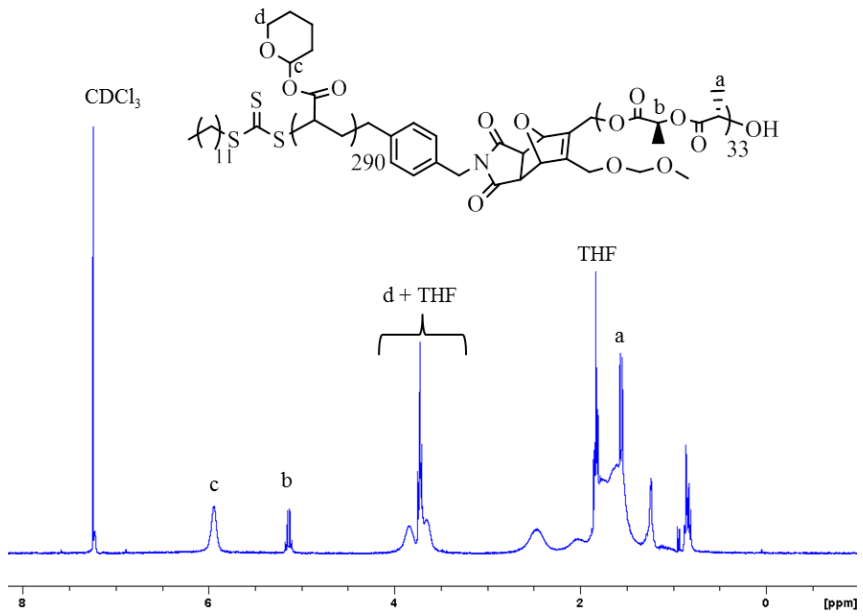

Figure 2.25 ^{1}H NMR spectrum of the P(*L*-LA)-*b*-PTHPA block copolymer **2.10** in $CDCl_3$, (400 MHz, 293K).

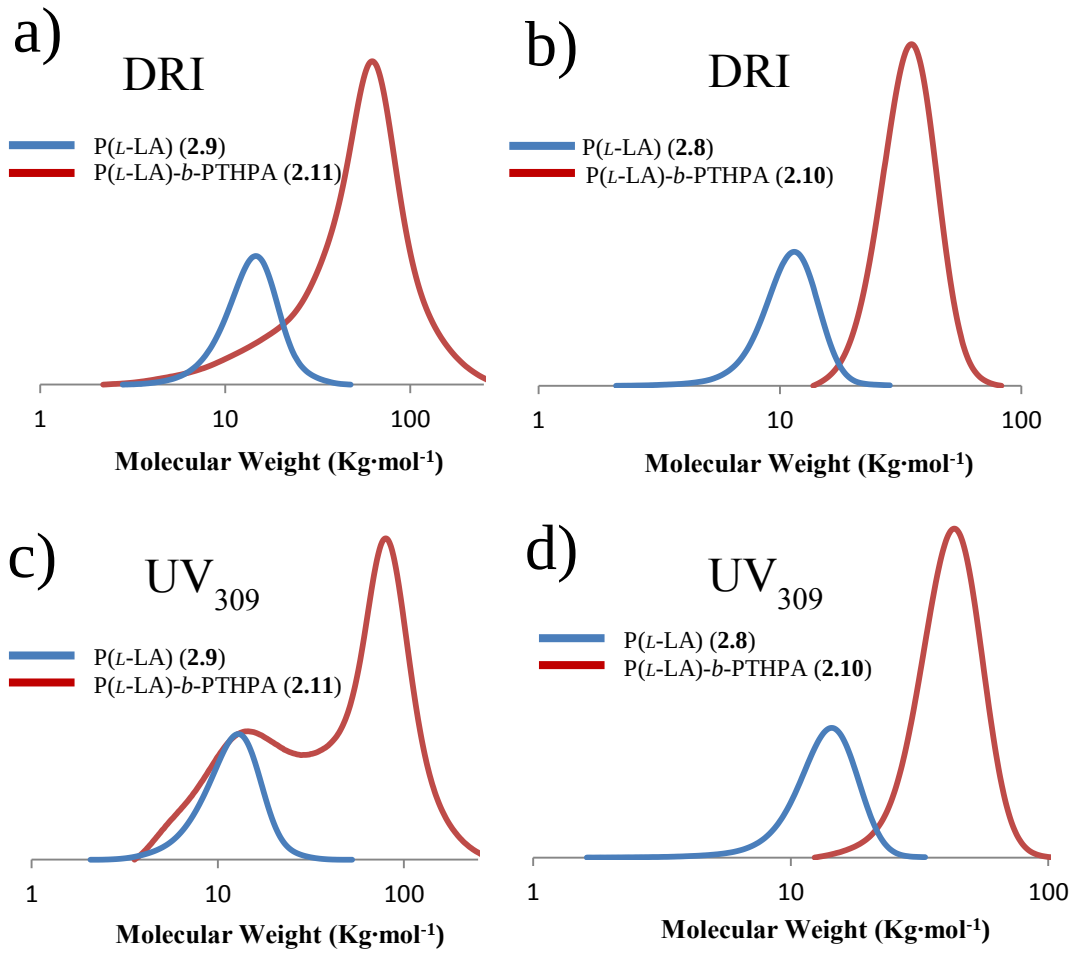

Figure 2.26 Molecular weight distribution obtained by SEC with DRI detector for a) chain extension in DMF; b) chain extension in $CHCl_3$; and weight distribution obtained by SEC with UV 309 detector for c) chain extension in DMF; d) chain extension in $CHCl_3$.

Importantly, when analysing the resultant polymers by size exclusion chromatography with THF as the eluent it was essential to use both a DRI and UV detector to determine homopolymer content. As PLA is near isorefractive with all the commonly employed solvents ($CHCl_3$, DMF, THF), it has a low refractive index increment (*dn/dc*) and hence a very weak response is observed by DRI detectors, compared to the response observed for acrylate polymers such as PTHPA. This can lead to an underestimation of PLA homopolymer present in the sample. For

example; if the chain extension of P(*L*-LA) (**2.8** and **2.9**) was carried out in DMF (**2.10**), this led to products with significant amount of P(*L*-LA) contaminants due to poor initiation from the macro–CTA, however when the chain extension was carried out in chloroform (**2.11**) this facilitated excellent initiation from the macro-CTA leading to complete chain extensions with minimum amount of residual P(*L*-LA) precursor. When both chain extended polymers (**2.10** and **2.11**) were initially analysed by SEC utilizing DRI detection (commonly the only possibility due to lack of UV activity on PLA), the molecular weight distributions of both polymers appeared to be unimodal with a slight low molecular weight 'tailing', being more pronounced in the case of (**2.10**) (see Figure 2.26a and Figure 2.26b). However, the UV detector set to 309 nm (λ_{max} for the trithiocarbonate end-group) revealed significant bimodality for (**2.11**), resulting from unreacted PLA homopolymer, in the resultant weight distribution (Figure 2.26c), while no such bimodality was seen for (**2.11**) (Figure 2.26d). These results highlight the fact that due to the large different in *dn/dc* values for these two blocks, use of a DRI detector alone is insufficient to analyse the entire content of the polymer sample. ^{1}H NMR spectroscopy was used to determine the molecular weight by comparing the integration of the PTHPA characteristic signals with the P(*L*-LA) signal. IR spectroscopy in combination with ^{1}H NMR spectroscopy confirmed that no THPA deprotection took place during the reaction course.

2.3.10 Deprotection of 2.11 to afford the P(*L*-LA)-b-PAA amphiphilic block copolymer, 2.13.

Last step of the synthesis was the deprotection of the PTHPA block by selective hydrolysis. PTHPA can be deprotected in relatively mild acidic hydrolysis

conditions. This was very important as the reaction, in our system, had to take place in the presence of the thermally labile DA group and the polylactide block which is degradable under acidic conditions. After experimenting with a variety of different conditions we found that upon heating at 65 ^{o}C in the presence of a catalytic amount of acetic acid, the desired deprotection was taking place, while the conditions were mild enough to avoid any side reactions. IR spectroscopy gave us a strong handle to monitor the deprotection. PTHPA gave the C=O stretch at 1738 cm^{-1} and it shifted at 1709 cm^{-1} after the deprotection. ^{1}H NMR analysis also confirmed that the PTHPA deprotection to PAA is complete by the complete disappearance of the PTHPA signals (Figure 2.27).

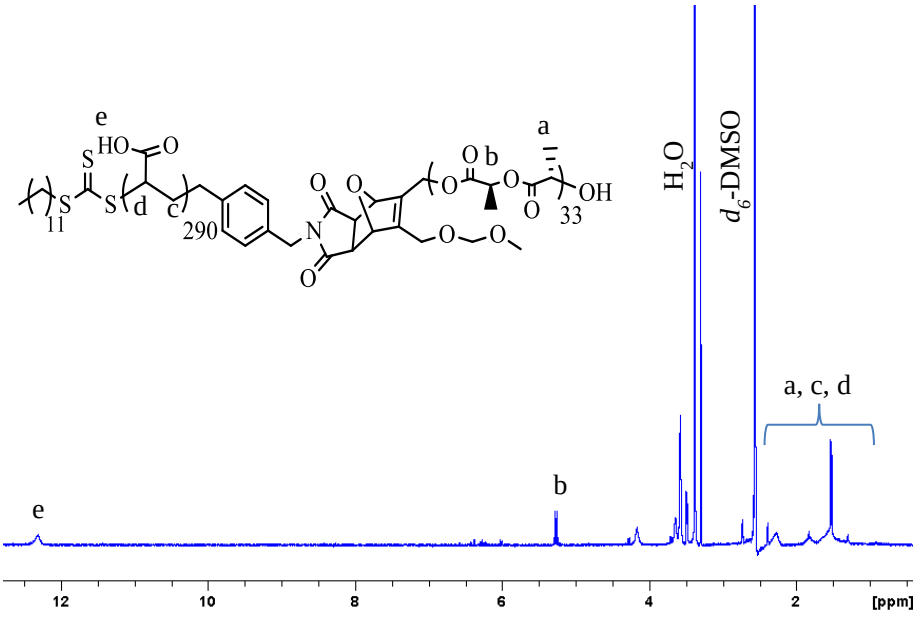

Figure 2.27 ^{1}H NMR spectrum of the P(*L*-LA)-*b*-PAA block copolymer **2.13** in $CDCl_3$, (400 MHz, 293K).

2.3.11 Solution self-assembly of polymer 2.13

The DA connected block copolymer **2.13** synthesised in the previous section was used for self-assembly studies. Initially the sample was prepared by direct

dissolution of **2.13** in nanopure water fixing a final concentration of 0.25 mg/mL **2.14**. The solution was left to stir overnight and subsequently characterised by DLS. The analysis illustrated the presence of two distinct populations of 55 and 130 nm. The overall distribution of sizes was broad and the overall quality of the sample poor (Figure 2.28).

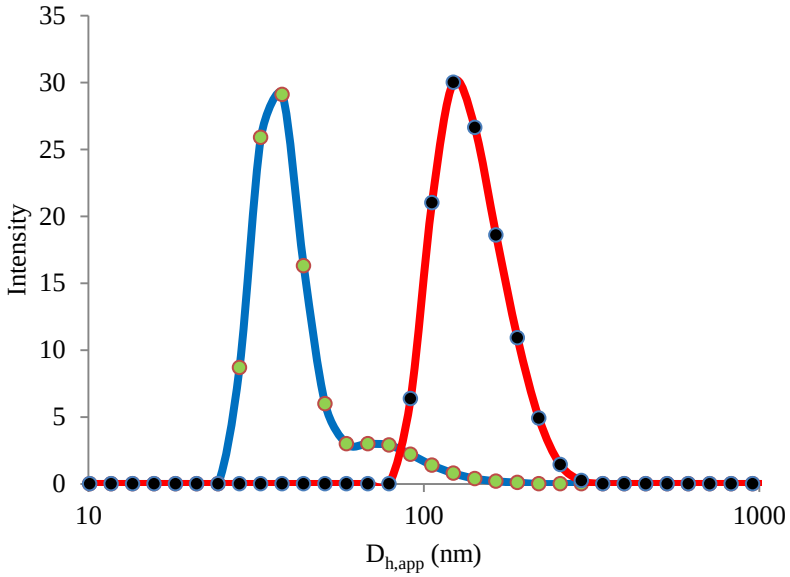

Figure 2.28 DLS results of sample **2.14** prepared by direct dissolution in nanopure water before heating (blue line) and after heating at 65 ^{0}C for 60 minutes (red line).

TEM characterisation showed the presence of two morphologies, spherical micelles with a diameter of 25 nm and short cylinders with average length of approximately 60 nm. Our initial interpretation of these results was that due to the relatively high T_g (*ca* 50-60 ^{o}C) and hydrophobicity of the polylactide core block, unimer exchange was restricted and hence the particles were kinetically trapped in non-equilibrium states. To solve this problem the solution was heated at 65 ^{o}C, which is above the T_g of polylactide, with this we intended to increase core mobility and aid unimer exchange between aggregates. The solution was monitored by DLS. Interestingly,

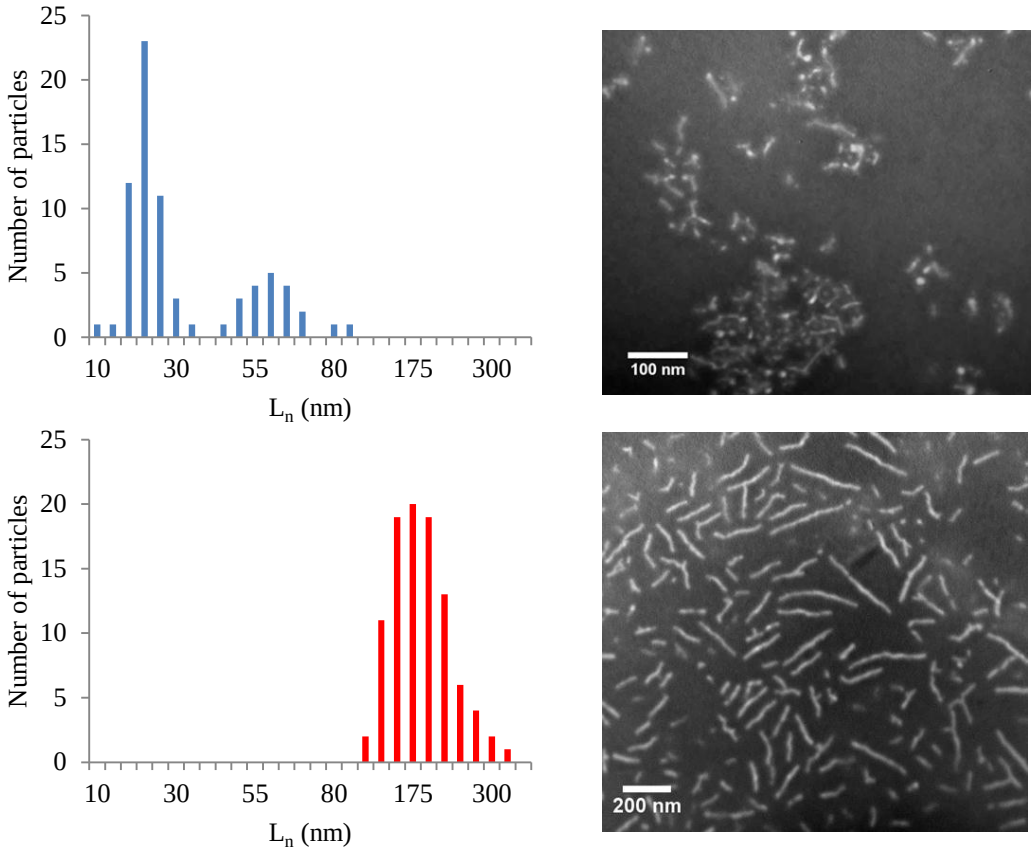

Figure 2.29 On the top: TEM image and corresponding histogram of sample **2.14** prepared by direct dissolution in nanopure water before heating; at the bottom: TEM image and corresponding histogram of sample **2.14** prepared by direct dissolution in nanopure water after heating at 65 ^{o}C for 60 minutes.

after 60 minutes of heating, the population with the smaller hydrodynamic diameter disappeared by DLS and the results indicated one population with a hydrodynamic diameter of 150 nm. TEM analysis of the sample illustrated the complete disappearance of the population with the smaller hydrodynamic diameter (Figure 2.29). Although the quality of the solution after the period of heating was improved (in terms of polydispersity), this result was not in agreement with what we expected. Importantly, the block ratio of **2.13** strongly favours the hydrophilic block, therefore spherical micelles were expected to form through its aqueous self-assembly.

To explain this result we had to consider the presence of other driving forces than the solvophobic effects. Two scenarios were likely to be the case; either the self-assembly process was directed by mid-block interactions based on the DA group that was incorporated on the interphase of the two blocks[57] or the polylactide core crystallised during the self-assembly process which in turn could influence the produced morphology.[58]

This result was extremely interesting as the ready synthesis of cylindrical micelles by BCP self-assembly remains until today a challenging task. These results warranted further investigations so that full understanding would be achieved. For this reason, our work focused on these self-assembly studies.

2.4 Conclusions

Herein, we illustrate the successful multistep synthesis of a dual headed chain transfer agent (CTA)/ROP initiator where the two active sites are connected through a DA bond. The product was obtained in 7 synthetic steps in overall yield of 18 %.

This bifunctional compound was utilised for the synthesis of well–defined block copolymers. First, well–defined polylactide blocks were synthesised *via* the ROP of *L*-La monomer under ambient conditions. The thoroughly characterised products were found to have narrow polydispersities and quantitative end group fidelities. Furthermore, the polylactide macro CTA's were used to mediate the RAFT polymerisation of THPA monomer. The reaction proceeded in a controlled fashion in $CHCl_3$, however, incomplete chain extensions due to poor initiation were observed in DMF and dioxane. In addition, the importance of using multiple detectors on the SEC analysis of these copolymers was illustrated.

The successful synthesis of DA connected P(*L*-LA)-*b*-PAA amphiphilic block copolymers was achieved *via* the selective hydrolysis of the PTHPA units under mild acid/thermal conditions. Finally, the aqueous self-assembly of this amphiphilic polymer was explored. Interestingly, well defined cylindrical micelles were found to form after heating the corresponding solutions at 65 ^{o}C for 60 minutes, the origins of this result will be studied in greater depth in the following chapters.

2.5 Experimental Section

2.5.1 Materials and instrumentation

Chemicals were used as received from Aldrich, Fluka and Acros. *L*-lactide was donated by Purac and further purified/dried over 4 Å molecular sieves in dichloromethane solution before being dried under vacuum and sublimed. Lactides were stored in a nitrogen-filled glove box. Tetrahydropyran acrylate (THPA) was prepared as described previously and stored below 4 °C.[59] AIBN (2,2'-azo-bis(isobutyronitrile)) was recrystallised twice from methanol and stored in the dark at 4 °C. Dry dichloromethane was obtained by passing over a column of activated alumina using an Innovative Technologies solvent purification system. (-)-Sparteine was dried over CaH_2 and distilled prior to use and 1-(3,5-bis(trifluoromethyl)phenyl)-3-cyclohexyl-thiourea was prepared and dried as previously reported.[60]

^{1}H NMR and ^{13}C NMR spectra were recorded on a Bruker DPX-400 spectrometer in $CDCl_3$ unless otherwise stated. Chemical shifts are given in ppm downfield from TMS. Size exclusion chromatography (SEC) measurements were conducted using a Varian 390-LC-Multi detector suite fitted with differential refractive index (DRI) and photodiode array (PDA) detectors equipped with a guard column (Varian Polymer Laboratories PLGel 5 μm, 50×7.5 mm) and two mixed D columns (Varian Polymer Laboratories PLGel 5 μm, 300×7.5 mm). The mobile phase was tetrahydrofuran with 2% triethylamine eluent at a flow rate of 1.0 mL·min^{-1} and samples were calibrated against Varian Polymer laboratories Easi-Vials linear poly(styrene) standards (162-2.4 × 10^5 g·mol^{-1}) using Cirrus v3.3 software. Infrared spectroscopy was recorded on a Perkin Elmer Spectrum 100 FT-IR Spectrometer.

Mass Spectrometry (HR-MS) was conducted on a Bruker UHR-Q-TOF MaXis with electrospray ionisation.

2.5.2 Polymerisation procedures

In all RAFT polymerisations three freeze-pump-thaw cycles were applied to the reaction vessel for the removal of oxygen and were released and sealed in an ampoule under nitrogen before being immersed in an oil bath at the required temperature. ROP polymerisations were carried out in a glove box under a well-defined atmosphere. polydispersity indices were measured by GPC measurements, whereas ^{1}H NMR spectroscopy was used for the determination of end group functionality and molecular weight by careful integration of the polymer backbone to the end group signals. MALDI ToF MS was used for end group analysis.

2.5.3 Synthesis of dodecyl 4-(hydroxymethyl) benzyl carbonotrithioate, 2.1

Dodecanethiol (1.53 mL, 6.4 mmol) was dissolved in acetone, potassium phosphate (1.5 g, 7.0 mmol) and carbon disulfide (1.15 mL, 20 mmol) were added and the solution mixture was stirred at room temprature for 2 hours. Subsequently, 4-(chloromethyl)benzyl alcohol (1 g, 6.4 mmol) was added to the yellow solution and the reaction was left for 72 hours. Afterwards the solvent was evaporated and the remaining solid was dissolved in dichloromethane. The organic layers were then washed with HCL (100 mL), 3 × water (100 mL) and then a saturated brine solution (100 mL). The organic phase was dried over magnesium sulphate, filtered and concentrated under vacuo. The crude product was purified by flash chromatography eluting with 3:2 hexane: ethyl acetate to give the product. (R_f = 0.55 in 3:2 hexane/ethyl acetate) as a yellow solid, (2.1 g, 81%). ^{1}H NMR ($CDCl_3$, ppm, 400 MHz): δ = 7.30-7.20 (m, 4H, ArH), 4.61 (s, 2H, SCH_2Ph), 4.51 (s, 2H, $PhCH_2OH$), 3.32-3.25 (t, 2H, CH_2SCS), 1.72-1.68 (m, 2H, CH_2CH_2SCS), 1.62-1.68 (s, 1H, -OH), 1.38-1.27 (m, 2H CH_3CH_2), 1.27-1.08 (s, 16H, $CH_3CH_2(CH_2)_8CH_2CH_2$), 0.85-0.75 (t, 3H, CH_3); ^{13}C NMR ($CDCl_3$, ppm, 400 MHz): δ = 129.5, 129.3, 65.0, 41.0, 37.1, 31.9, 29.6, 29.5, 29.1, 28.9, 28.0. ν_{max}/cm^{-1} 3492-3293 (O-H), 1583 (aromatic), 1469 (aromatic); LC-MS gave m/z 421.2 (M^+, 100 %)

2.5.4 Synthesis of 4-(bromomethyl)benzyl dodecyl carbonotrithioate, 2.2

2.1 (1.8 g, 4.6 mmol), was dissolved in a 1:1 mixture of dichloromethane/dimethylformamide and the reaction mixture was cooled down to 0 ^oC with an ice bath. phosphorus tribromide (0.42 g, 4.6 mmol) was added dropwise. The reaction was left at 0 ^oC for 3 hours. Sequentially, diethyl ether (100 mL) was added and the organic layers were washed twice with sodium hydrocarbonate (100

mL), twice with water (100 mL), and then a saturated brine solution (100 mL). The organic phase was dried over magnesium sulphate, filtered and concentrated under vacuo. The crude product was purified by flash chromatography eluting with 9:1 hexane/ethyl acetate to give the product (1.58 g, 75%) as a yellow solid. (R_f = 0.85 in 3:2 hexane/ethyl acetate). ^{1}H NMR ($CDCl_3$, ppm, 400 MHz): δ = 7.30-7.20 (m, 4H, ArH), 4.65 (s, 2H, SCH_2Ph), 4.45 (s, 2H, $PhCH_2OH$), 3.32-3.25 (t, 2H, CH_2SCS), 1.68-1.55 (m, 2H, CH_2CH_2SCS), 1.38-1.27 (m, 2H CH_3CH_2), 1.27-1.08 (s, 16H, $CH_3CH_2(CH_2)_8CH_2CH_2$), 0.85-0.75 (t, 3H, CH_3); ^{13}C NMR ($CDCl_3$, ppm, 400 MHz): δ = 129.7, 129.4, 40.1, 37.1, 31.9, 29.5, 29.4, 29.1, 22.7, 28.0. ν_{max}/cm^{-1}, 1583 (aromatic), 1469 (aromatic); LC-MS gave m/z 448.2 (M^+, 100 %).

2.5.5 Synthesis of furan-3, 4-diyldimethanol, 2.3

This compound was prepared according to an already published procedure.[54] Lithium aluminum hydride (4.46 g, 11.6 mmol) was suspended in anhydrous diethyl ether and cooled down to 0 ^oC with an ice bath. Dimethyl-3,4-furan dicarboxylate (5 g, 2.3 mmol) was added in the stirring solution dropwise in such a manner that the addition lasted for 30 minutes. The reaction was left for 1 hour further after the addition was completed. Subsequently, the reaction was quenched with the slow addition of 4.5 mL of water, 4.5 mL of NaOH 15%, followed by 13.5 mL of water. The dry, granular precipitate was filtered and washed using an excess of diethyl ether. The diethyl ether solution was dried over magnesium sulphate, filtered and dried *in vacuo*, affording the pure product as a colourless liquid (88%, 2.61 g). (R_f = 0.15 in 1:1 dichloromethane/ethyl acetate). ^{1}H NMR ($CDCl_3$, ppm, 400 MHz): δ = 7.25 (s, 2H, =CH), 4.45 (s, 4H, CH_2OH), 2.05 (broad s 2H, -OH); ^{13}C NMR ($CDCl_3$, ppm, 400 MHz): δ = 140.9, 124.4, 55.0.

2.5.6 Synthesis of 3,4-bis((methoxymethoxy)methyl)furan, 2.4

2.3 (0.5 g, 3.9 mmol) was dissolved in dichloromethane and diisopropylethyl amine (2.02 mL, 11.6 mmol) was added. The solution mixture was cooled down to 0^{o}C with an ice bath and chloro methoxy methane (0.88 mL, 11.6 mmol) was added dropwise, after the addition the reaction was left for 8 additional hours, the organic layers were washed twice with water (100 mL), and then a saturated brine solution (100 mL). The organic phase was dried over magnesium sulphate, filtered and concentrated under vacuo to afford the pure product as a light yellow liquid (85%, 0.71 g). ^{1}H NMR ($CDCl_3$, ppm, 400 MHz): δ = 7.45 (s, 2H, =CH), 4.68 (s, 4H, CH_2O), 4.48 (s, 4H, OCH_2O), 3.42 (s, 6H, OCH_3); ^{13}C NMR ($CDCl_3$, ppm, 400 MHz): δ = 142.0, 121.4, 95.4, 59.4, 55.4; LC-MS gave m/z 216.12 (M^+, 100 %).

2.5.7 Synthesis of the DA adduct, 2.5

2.4 (1.55 g, 7.2 mmol) was dissolved in 20 mL of ethyl acetate, maleimide (0.85 g, 8.6 mmol) was then added and the reaction mixture was heated at 65^{o}C with an oil bath. The reaction was left at this temperature for 48 hours and then it was lowered at 35^{o}C where it was left for 24 hours and finally set to 25^{o}C to be left for another 24 hours. Subsequently, the solvent was evaporated and the crude product was subjected to flash chromatography eluting with ethyl acetate to give the product (1.8 g, 81%) as a white solid. (R_f = 0.33 in ethyl acetate) ^{1}H NMR ($CDCl_3$, ppm, 400 MHz): δ = 8.23-8.18 (broad s, 1H, NH), 5.21 (s, 2H, OCH), 4.62-4.55 (q, 4H, OCH_2O), 4.25-4.11 (q, 4H, CH_2O), 3.37-3.32 (t, 6H, OCH_3), 2.98 (s, 2H CH); ^{13}C NMR ($CDCl_3$, ppm, 400 MHz): δ = 142.1, 83.3, 60.2, 55.6, 49.5; LC-MS gave m/z 336.1 (M^+, 20 %).

2.5.8 Synthesis of the protected initiator, 2.6

2.2 (2.5 g, 5.4 mmol) and **2.5** (1.7 g, 5.4 mmol) were dissolved in dimethylformamide (anhydrous) and potassium carbonate (3.73 g, 27 mmol) was added, the entire reaction mixture was stirred for 3.5 hours at 50 ^{o}C. Sequentially, ethyl acetate (100 mL) was added and the organic layers were washed twice with water (100 mL) and then a saturated brine solution (100 mL). the organic phase was dried over magnesium sulphate, filtered and concentrated under vacuo (70%, 2.6 g). The crude product was purified by flash chromatography eluting with 3:2 ethyl acetate/hexane to give the pure product,. (R_f = 0.65 in 3:2 ethyl acetate/hexane) as a light yellow solid (70%, 2.6 g). ^{1}H NMR ($CDCl_3$, ppm, 400 MHz): δ = 7.19 (s 4H, ArH), 5.23 (s, 2H, OCH), 4.59-4.52 (q, 4H, CH_2O), 4.54 (s, 2H, CH_2Ph), 4.50 (s, 2H, $PhCH_2$), 4.25-4.12 (q, 4H, OCH_2O), 3.30 (s, 6H, OCH_3), 3.29-3.24 (t, 2H, CH_2SCS), 2.95 (s, 2H CH_2), 1.68-1.55 (m, 2H, CH_2CH_2SCS), 1.38-1.27 (m, 2H CH_3CH_2), 1.27-1.08 (s, 16H, $CH_3CH_2(CH_2)_8CH_2CH_2$), 0.85-0.75 (t, 3H, CH_3); ^{13}C NMR ($CDCl_3$, ppm, 400 MHz): δ = 142.2, 129.5, 128.5, 83.2, 60.2, 55.5, 48.3, 42.1, 40.9, 37.1, 31.9, 29.5, 29.4, 29.1, 22.7, 28.0. ν_{max}/cm^{-1}. 2954 (C-C stretch), 2920 (C-C stretch), 2850 (C-C stretch), 1695 (C-O stretch of ether); LC-MS gave m/z 716.2 $[M+Na]^+$ (73%), 732.1 $[M+K]^+$ (27 %).

2.5.9 Synthesis of the dual RAFT/ROP initiator, 2.7

Compound **2.6** (0.95 g, 1.4 mmol) was dissolved in dichloromethane (5 mL) and then trifluoroacetic acid (5 mL) was added in the stirring solution. The reaction was left to stir for 1 hour. Subsequently, dichloromethane (100 mL) was added and the organic layers were washed with NaOH 1M (100 mL), twice with water (100 mL) and then a saturated brine solution (100 mL). the organic phase was dried over

magnesium sulphate, filtered and concentrated *in vacuo*. The crude product was purified by flash chromatography eluting with 1:1 ethyl acetate:dichloromethane to give the pure product. (R_f = 0.3 in 1:1 ethyl acetate/dichloromethane) as a light yellow solid (0.5 g, 55%), this product was dried under a P_2O_5 atmosphere in a dessicator for 2 days and stored under a N_2 atmosphere. ^{1}H NMR ($CDCl_3$, ppm, 400 MHz): δ = 7.19 (s 4H, ArH), 5.23 (s, 2H, OCH), 4.59-4.52 (q, 4H, CH_2O), 4.54 (s, 2H, CH_2Ph), 4.50 (s, 2H, $PhCH_2$), 4.25-4.12 (q, 4H, OCH_2O), 3.30 (s, 6H, OCH_3), 3.29-3.24 (t, 2H, CH_2SCS), 2.95 (s, 2H CH_2), 1.68-1.55 (m, 2H, CH_2CH_2SCS), 1.38-1.27 (m, 2H CH_3CH_2), 1.27-1.08 (s, 16H, $CH_3CH_2(CH_2)_8CH_2CH_2$), 0.85-0.75 (t, 3H, CH_3); ^{13}C NMR ($CDCl_3$, ppm, 400 MHz): δ = 142.2, 129.5, 128.5, 83.2, 60.2, 55.5, 48.3, 42.1, 40.9, 37.1, 31.9, 29.5, 29.4, 29.1, 22.7, 28.0. ν_{max}/cm^{-1}; LC-MS gave m/z 672.1 (M+, 100 %). Elemental analysis found (in the brackets are the theoretical values) % wt/wt C : 60.44 (60.98), % H wt/wt : 7.21 (7.29), % N wt/wt : 2.23 (2.16), % S wt/wt : 14.66 (14.80); ν_{max}/cm^{-1}, 3732-3142 (O-H strech), 2954 (C-C stretch), 2920 (C-C stretch), 2850 (C-C stretch), 1695 (C-O stretch of ether), 1061 (C-O stretch of the alcohol).

2.5.10 General *L*-lactide polymerisation using 2.7 to afford a polylactide macro–CTA, 2.8

In a 20 mL scintillation vial equipped with a stir bar, a solution of the thiourea organocatalyst (14.3 mg, 34.5 μmol), sparteine (0.17 μmol, 0.039 mg) and **2.7** (10 mg, 0.15 μmol) in $CHCl_3$ (0.2 mL) was added to a solution of L-lactide (140 mg, 0.97 mmol) in $CHCl_3$ (0.8 mL). The reaction mixture was stirred for 1 h (for DP =15-70) before the solution was reduced under vacuum to yield a light yellow solid. The conversion was determined by ^{1}H NMR spectroscopy. The polymer was

precipitated from $CHCl_3$ into petroleum ether and dried to a constant weight to afford an end functionalised polylactide. The degree of polymerisation and end group retention were determined by ^{1}H NMR spectroscopy and MALDI ToF MS while the molecular weight and PDI = 1.08 were determined by SEC. ^{1}H NMR ($CDCl_3$, ppm, 400 MHz): δ = 5.18-5.05 (q, 1H, backbone), 4.56-4.53 (t, 4H, end group), 4.51-4.48 (s, 2H, end group), 3.31-3.30 (s, 3H, end group), 3.32-3.26 (t, 2H, end group), 2.95-2.88 (m, 2H, end group), 1.53-1.49 (d, 3H, backbone).

2.5.11 General acrylate polymerisation using the polylactide macro–CTA, 2.11

The THPA monomer (150 eq), the polylactide macro CTA (1 eq) and AIBN (0.1 equiv) were disolved in 0.5 mL of DMF and transferred in an oven dried vial with a stirrer bar. The vial was degassed (three times) and sealed under nitrogen, and the polymerisations were heated at 60 °C for 15h. Aliquots were removed from the reaction mixture to follow the reaction kinetics with ^{1}H NMR spectroscopy. The polymer was then dissolved in a minimum amount of tetrahydrofuran and purified by precipitation into ice cold hexane (three times) to afford a pure DA linked diblock copolymer P(*L*-LA)-*b*-PTHPA. The degree of polymerisation and end group retention were determined by 1H NMR spectroscopy and MALDI TOF MS while the molecular weight and PDI=1.12 were determined by SEC. ^{1}H NMR ($CDCl_3$, ppm, 400 MHz): δ = 6.02-5.90 (br, 1H, PTHPA backbone) 5.18-5.05 (q, 1H, PLLA backbone), 2.10-1.48 (d, 8H, backbone of both blocks). ν_{max}/cm^{-1}. 2954 (C-C stretch), 2920 (C-C stretch), 2850 (C-C stretch), 1758 (C=O stretch of PLLA backbone), 1736 (C=O stretch of PTHPA)

2.5.12 Deprotection of 2.11 to give the P(*L*-LA)-b-PAA amphiphilic diblock copolymer, 2.13

P(*L*-LA)-*b*-PTHPA (0.2 mg) was added to a round-bottom flask equipped with a stirrer bar and a needle on top, followed by tetrahydrofuran (3 mL). Deionised water was added (1 mL), followed by glacial acetic acid in a catalytic amount (20 μL). The mixture was allowed to stir at 65 ^{o}C for 15h. The polymer was freeze dried for 2 days. And it was characterised by ^{1}H NMR and IR spectroscopy. ^{1}H NMR (*d*^{6} DMSO, ppm, 400 MHz): δ = 12.50-11.98 (br, O-H), 5.22-5.04 (q, 1H, PLLA backbone), 1.53-1.49 (d, 3H, PLLA backbone), $\nu_{max/}cm^{-1}$. 3630-2840 (O-H stretch + C-O strech), 2954 (C-C stretch), 2920 (C-C stretch), 2850 (C-C stretch), 1758 (C=O stretch of PLLA backbone), 1707 (C=O stretch of PAA acid groups).

2.6 References

(1) Jiang, M.; Li, M.; Xiang, M.; Zhou, H. *Adv. Polym. Sci.* **1999**, *146*, 121.

(2) Guo, M.; Jiang, M. *Soft Matter* **2009**, *5*, 495.

(3) Liu, S.; Zhang, G.; Jiang, M. *Polymer* **1999**, *40*, 5449.

(4) Huan, X.; Wang, D.; Dong, R.; Tu, C.; Zhu, B.; Yan, D.; Zhu, X. *Macromolecules*, Ahead of Print.

(5) Kohut, A.; Dai, X.; Pinnick, D.; Schulz, D. L.; Voronov, A. *Soft Matter* **2011**, *7*, 3717.

(6) Zhang, Z.-X.; Liu, K. L.; Li, J. *Macromolecules* **2011**, *44*, 1182.

(7) Pessego, M.; Basilio, N.; Moreira, J. A.; Garcia-Rio, L. *ChemPhysChem* **2011**, *12*, 1342.

(8) Chen, C.-J.; Liu, G.-Y.; Liu, X.-S.; Li, D.-D.; Ji, J. *New J. Chem.* **2012**, *36*, 694.

(9) Quan, C.-Y.; Chen, J.-X.; Wang, H.-Y.; Li, C.; Chang, C.; Zhang, X.-Z.; Zhuo, R.-X. *ACS Nano* **2010**, *4*, 4211.

(10) Li, L.; Nachtergaele, S.; Seddon, A. M.; Tereshko, V.; Ponomarenko, N.; Ismagilov, R. F. *J. Am. Chem. Soc.* **2008**, *130*, 14324.

(11) Appel, E. A.; Biedermann, F.; Rauwald, U.; Jones, S. T.; Zayed, J. M.; Scherman, O. A. *J. Am. Chem. Soc.* **2010**, *132*, 14251.

(12) Jiao, D.; Biedermann, F.; Tian, F.; Scherman, O. A. *J. Am. Chem. Soc.* **2010**, *132*, 15734.

(13) Ligthart, G. B. W. L.; Scherman, O. A.; Sijbesma, R. P.; Meijer, E. W.; Wiley-VCH Verlag GmbH & Co. KGaA: 2007; Vol. 1, p 351.

(14) Zayed, J. M.; Nouvel, N.; Rauwald, U.; Scherman, O. A. *Chem. Soc. Rev.* **2010**, *39*, 2806.

(15) Zou, J.; Tao, F.; Jiang, M. *Langmuir* **2007**, *23*, 12791.

(16) Lohmeijer, B. G. G.; Schubert, U. S. *Angew. Chem., Int. Ed.* **2002**, *41*, 3825.

(17) Fustin, C.-A.; Guillet, P.; Schubert, U. S.; Gohy, J.-F. *Adv. Mater.* **2007**, *19*, 1665.

(18) Andres, P. R.; Schubert, U. S. *Adv. Mater.* **2004**, *16*, 1043.

(19) Gohy, J.-F.; Lohmeijer, B. G. G.; Decamps, B.; Leroy, E.; Boileau, S.; van, d. B. J. A.; Schubert, D.; Haase, W.; Schubert, U. S. *Polym. Int.* **2003**, *52*, 1611.

(20) Gohy, J.-F.; Lohmeijer, B. G. G.; Schubert, U. S. *Macromol. Rapid Commun.* **2002**, *23*, 555.

(21) Hofmeier, H.; Schmatloch, S.; Wouters, D.; Schubert, *Macromol. Chem. Phys.* **2003**, *204*, 2197.

(22) Lohmeijer, B. G. G.; Schubert, U. S. *J. Polym. Sci., Part A: Polym. Chem.* **2003**, *41*, 1413.

(23) Marin, V.; Holder, E.; Meier, M. A. R.; Hoogenboom, R.; Schubert, U. S. *Macromol. Rapid Commun.* **2004**, *25*, 793.

(24) Lohmeijer, B. G. G.; Wouters, D.; Yin, Z.; Schubert, U. S. *Chem. Commun.* **2004**, 2886.

(25) Moughton, A. O.; O'Reilly, R. K. *J. Am. Chem. Soc.* **2008**, *130*, 8714.

(26) Ievins, A. D.; Moughton, A. O.; O'Reilly, R. K. *Macromolecules* **2008**, *41*, 3571.

(27) Moughton, A. O.; Stubenrauch, K.; O'Reilly, R. K. *Soft Matter* **2009**, *5*, 2361.

(28) Dag, A.; Aydin, M.; Durmaz, H.; Hizal, G.; Tunca, U. *J. Polym. Sci., Part A: Polym. Chem.*, Ahead of Print.

(29) Durmaz, H.; Dag, A.; Cerit, N.; Sirkecioglu, O.; Hizal, G.; Tunca, U. *J. Polym. Sci., Part A: Polym. Chem.* **2010**, *48*, 5982.

(30) Gacal, B.; Durmaz, H.; Tasdelen, M. A.; Hizal, G.; Tunca, U.; Yagci, Y.; Demirel, A. L. *Macromolecules* **2006**, *39*, 5330.

(31) Wiggins, K. M.; Syrett, J. A.; Haddleton, D. M.; Bielawski, C. W. *J. Am. Chem. Soc.* **2011**, *133*, 7180.

(32) Subramani, C.; Cengiz, N.; Saha, K.; Gevrek, T. N.; Yu, X.; Jeong, Y.-D.; Bajaj, A.; Sanyal, A.; Rotello, V. M. *Adv. Mater.* **2011**, *23*, 3165.

(33) Sumerlin, B. S. *ACS Macro Lett.* **2011**, *1*, 141.

(34) Robin, M. P.; Jones, M. W.; Haddleton, D. M.; O'Reilly, R. K. *ACS Macro Lett.* **2012**, *1*, 222.

(35) Thomas, C. S.; Glassman, M. J.; Olsen, B. D. *ACS Nano* **2011**, *5*, 5697.

(36) De, P.; Li, M.; Gondi, S. R.; Sumerlin, B. S. *J. Am. Chem. Soc.* **2008**, *130*, 11288.

(37) Nicolaou, K. C.; Snyder, S. A.; Montagnon, T.; Vassilikogiannakis, G. *Angew. Chem., Int. Ed.* **2002**, *41*, 1668.

(38) Goldstein, E.; Beno, B.; Houk, K. N. *J. Am. Chem. Soc.***1996**, *118*, 6036.

(39) Li, Y.; Houk, K. N. *J. Am. Chem. Soc.* **1993**, *115*, 7478.

(40) Sauer, J. *Angew. Chem., Int. Ed.* **1967**, *6*, 16.

(41) Dove, A. P. *Chem. Commun.* **2008**, 6446.

(42) Matyjaszewski, K.; Xia, J. *Chem. Rev.* **2001**, *101*, 2921.

(43) Hawker, C. J.; Bosman, A. W.; Harth, E. *Chem. Rev.* **2001**, *101*, 3661.

(44) Perrier, S.; Takolpuckdee, P. *J. Polym. Sci., Part A: Polym. Chem.* **2005**, *43*, 5347.

(45) Hawker, C. J.; Hedrick, J. L.; Malmström, E. E.; Trollsås, M.; Mecerreyes, D.; Moineau, G.; Dubois, P.; Jérôme, R. *Macromolecules* **1998**, *31*, 213.

(46) Mecerreyes, D.; Moineau, G.; Dubois, P.; Jérôme, R.; Hedrick, J. L.; Hawker, C. J.; Malmström, E. E.; Trollsas, M. *Angew. Chem., Int. Ed.* **1998**, *37*, 1274.

(47) Duxbury, C. J.; Wang, W.; de Geus, M.; Heise, A.; Howdle, S. M. *J. Am. Chem. Soc.* **2005**, *127*, 2384.

(48) Peeters, J.; Palmans, A. R. A.; Veld, M.; Scheijen, F.; Heise, A.; Meijer, E. W. *Biomacromolecules* **2004**, *5*, 1862.

(49) Samarajeewa, S.; Shrestha, R.; Li, Y.; Wooley, K. L. *J. Am. Chem. Soc.* **2012**, *134*, 1235.

(50) Pratt, R. C.; Lohmeijer, B. G. G.; Long, D. A.; Lundberg, P. N. P.; Dove, A. P.; Li, H.; Wade, C. G.; Waymouth, R. M.; Hedrick, J. L. *Macromolecules* **2006**, *39*, 7863.

(51) Lohmeijer, B. G. G.; Pratt, R. C.; Leibfarth, F.; Logan, J. W.; Long, D. A.; Dove, A. P.; Nederberg, F.; Choi, J.; Wade, C.; Waymouth, R. M.; Hedrick, J. L. *Macromolecules* **2006**, *39*, 8574.

(52) Zhang, L.; Nederberg, F.; Pratt, R. C.; Waymouth, R. M.; Hedrick, J. L.; Wade, C. G. *Macromolecules* **2007**, *40*, 4154.

(53) van As, B. A. C.; Thomassen, P.; Kalra, B.; Gross, R. A.; Meijer, E. W.; Palmans, A. R. A.; Heise, A. *Macromolecules* **2004**, *37*, 8973.

(54) McElhanon, J. R.; Wheeler, D. R. *Org. Lett.* **2001**, *3*, 2681.

(55) Ladavière, C.; Lacroix-Desmazes, P.; Delolme, F. d. r. *Macromolecules* **2008**, *42*, 70.

(56) Strube, O. I.; Nothdurft, L.; Drache, M.; Schmidt-Naake, G. *Macromol. Chem. and Phys.* **2011**, *212*, 574.

(57) Kim, S. H.; Nederberg, F.; Jakobs, R.; Tan, J. P. K.; Fukushima, K.; Nelson, A.; Meijer, E. W.; Yang, Y. Y.; Hedrick, J. L. *Angew. Chem., Int. Ed.* **2009**, *48*, 4508.

(58) Wang, X.; Guerin, G.; Wang, H.; Wang, Y.; Manners, I.; Winnik, M. A. *Science* **2007**, *317*, 644.

(59) O'Reilly, R. K.; Joralemon, M. J.; Hawker, C. J.; Wooley, K. L. *Chem.--Eur. J.* **2006**, *12*, 6776.

(60) Pratt, R. C.; Lohmeijer, B. G. G.; Long, D. A.; Lundberg, P. N. P.; Dove, A. P.; Li, H.; Wade, C. G.; Waymouth, R. M.; Hedrick, J. L. *Macromolecules* **2006**, *39*, 7863.

Chapter 3: Synthesis of polylactide containing block copolymers by combination of RAFT and ROP

3.1 Abstract

In this chapter the synthesis of block copolymers containing a polylactide block are reported. The synthetic approach presented is analogous with the one used in Chapter 2; however, the dual headed initiator does not contain the Diels-Alder (DA) linker. The main objective was to synthesise new amphiphilic block copolymers without the DA motif in order to investigate their self-assembly behaviour compared to those for DA containing polymers obtained in Chapter 2. To further understand this self-assembly behaviour our method has been extended to the synthesis of other hydrophilic blocks and end group modified polymers. In addition, some key properties of the polymers synthesised have been investigated.

3.2 Introduction

In this chapter we present the synthesis of polylactide (PLA) macro-CTAs and their chain extension with a range of different polymer blocks synthesised by RAFT polymerisation. The polymer blocks we synthesised by RAFT were poly(tetrahydropyranyl acrylate) (PTHPA) and poly(triethyleneglycol acrylate) PTEGA. Furthermore, (the residual from the RAFT process dodecane end group) was modified based on a recently reported method which we further optimised.[1] The main features of the polymer blocks prepared by RAFT as well as the end group modification chemistry we used in this work are briefly discussed in the following sections.

3.2.1 Protected monomers as precursor for the synthesis of poly(acrylic acid), PAA

The main hydrophilic block studied in this work is poly(acrylic acid) (PAA). With the exception of RAFT, no other CRP technique can directly polymerise acrylic acid (AA).[2] Rizzardo *et al.* reported a direct synthesis of PAA with relatively narrow molecular weight distribution (M_w/M_n = 1.23) *via* the RAFT polymerisation of AA with 1-phenylethyl dithiobenzoate as a chain transfer agent and AIBN as the initiator at 60 °C.[3] Controlled polymerisation of AA has been also performed with dibenzyl trithiocarbonate and bis(1-phenylethyl) trithiocarbonate as a CTA[2] and under γ-irradiation in the presence of dibenzyl trithiocarbonate at ambient temperature.[4] However, PAA characterisation (especially by SEC) is overall challenging because of its polyelectrolyte character. Therefore, for the preparation of well-defined polymers that can be thoroughly characterised CRPs of protected monomers has often been used.[5-7] Typical examples of protected molecules that have been used as

masked acrylic acid monomers are *tert*-butyl acrylate (*t*BuA),[8,9] *tert*-butyl methacrylate (*t*-BuMA),[10] trimethylsilyl methacrylate (TMSMA),[11] 2-tetrahydropyranyl methacrylate (THPMA),[12] p-nitrophenyl methacrylate (p-NPMA)[13] as well as N-(acryloyloxy)succinimide (NAS).[14]

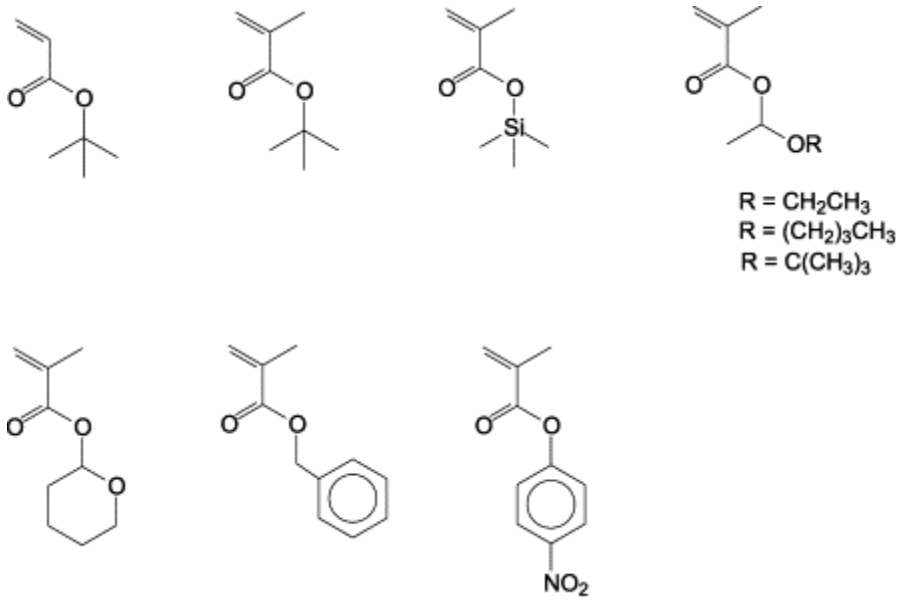

Figure 3.1 Example of protected acrylate and merthacrylate monomers utilised for the synthesis of well-defined polymer-precursors of poly(acrylic acid).[2]

In the present work we used tetrahydropyranyl acrylate (THPA). This is a hydrophobic acrylate monomer that can be polymerised with remarkable control by CRP techniques.[15] and undergoes hydrolysis under very mild acidic/thermal conditions.[16] This characteristic makes it extremely suitable when its deprotection is desired in the presence of other functionalities susceptible to hydrolysis.

3.2.2 Poly(triethyleneglycol acrylate) (PTEGA)

In 2006 Lutz *et al* illustrated that random copolymers of oligo(ethyleneglycol methacrylate) (OEGMA) with different side-chain lengths displayed an LCST, which could be tuned by changing the molar ratio of the different OEGMAs.[17] This

group of polymers is attractive as it appears to show high biocompatibility, blocks protein /cell absorption,[18] can be prepared readily with a wide range of polymerisation methods and also shows limited hysteresis while cycling above/below its LCST.[19] Furthermore the degree of polymerisation of the POEGMA does not strongly influence the LCST, giving more predictable properties than commonly used PNIPAM.[20]

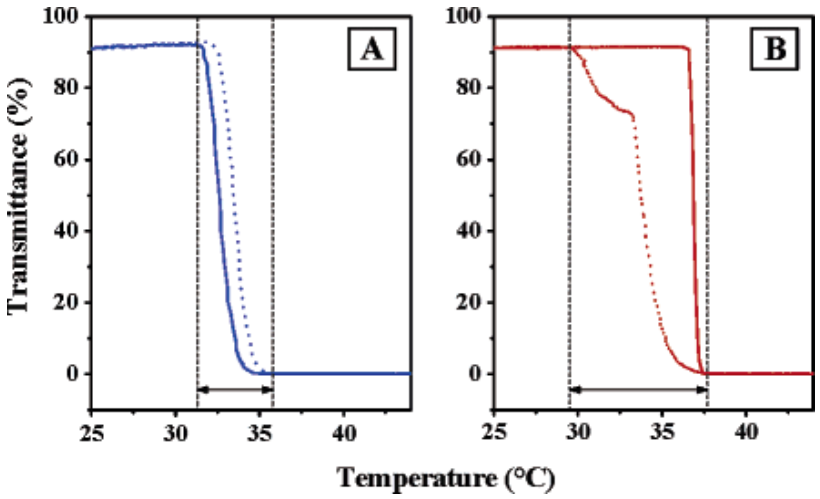

Figure 3.2 Plots of transmittance as a function of temperature measured for aqueous solutions of either (A) a copolymer P(MEO_2-MA-*co*-OEGMA) containing 5 mol % of OEGMA per chain or (B) a homopolymer of NIPAM.[19]

The acrylate analogues exhibit similar thermoresponsive properties, however due to the slightly more hydrophilic character of the backbone the LCST values are slightly higher compared to the methacrylate counterparts. In the present work we use PTEGA which is the analogue with three ethylene glycol side units and exhibits an LCST at 52 ^{o}C and thus is suitable for the present work in which the self-assembly process is performed under mild thermal conditions.

3.2.3 End group modification of polymers synthesised by RAFT

A key feature of the RAFT process is the thiocarbonyl thio compound which is used to control the polymerisation is also retained in the polymer products as an end group. That means that the polymer products are macro–CTA agents that exist in their dormant state. This feature is key as it enables us to readily form block copolymers by a further RAFT polymerisation mediated this time by the macro–CTA. In addition, the incorporation of functionalities on the CTA can also be used to introduce functional groups at the end of the produced polymers. Furthermore, the thicarbonyl thio terminal unit constitutes a chemical moiety that can be modified with a wide range of chemistries, therefore allowing for post polymerisation functionalisation of the RAFT polymers.[1,21]

Many processes for end group removal/modification have been demonstrated in the recent literature. Reactions with nucleophiles,[22-24] reactions with oxidising agents,[25,26] radical induced reductions,[27,28] radical addition fragmentation coupling reactions,[29] thermolysis,[30,31] hetero Diels-Alder chemistries[32] have all been successfully utilised to remove or transform the RAFT functionality. In the present work the radical addition fragmentation coupling method was used and therefore will be discussed a bit further.

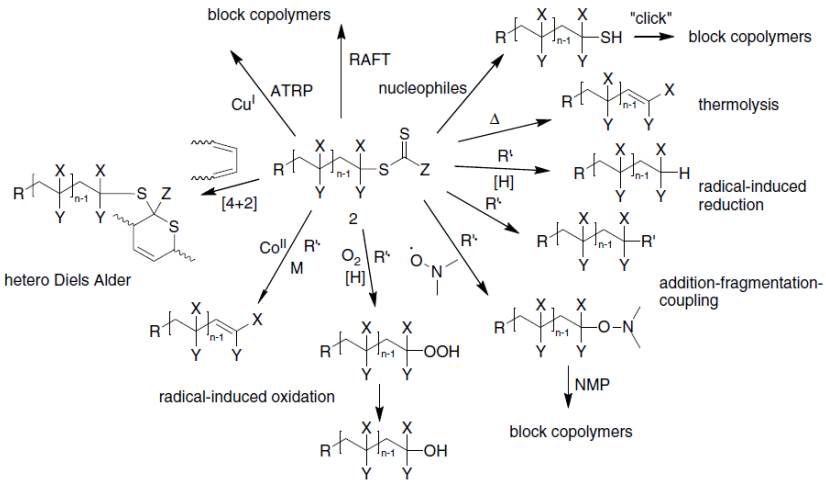

Figure 3.3 Processes for RAFT end-group transformation (R = radical; [H] = hydrogen donor; M = monomer).[1]

In 2005, Perrier *et al.* reported a process that can conveniently modify thiocarbonylthio end-groups from polymers synthesised through the RAFT process.[33] The reaction typically involves heating the polymer in the presence of a large excess of a radical initiator (AIBN). This process has been reported to be efficient with dithiobenzoates and trithiocarbonates, while it was found not to be effective for the end group modification of xanthate end-groups. Another factor that affects the efficiency of this method relates to the monomeric unit attached to the end group. Groups that form stable radicals and hence are good radical leaving groups (methacrylates) undergo this reaction very efficiently. However, when the same conditions are used with polystyrene or poly(acrylate) polymers the end group removal is incomplete even for very large molar excess (up to 100 fold) of the radical initiator (AIBN). Moad *et al.* demonstrated a variation of this method that is effective for polymers that form less stable radicals. In their method an additional amount of lauroyl peroxide (LPO) is added in the reaction mixture.[27] This radical initiator forms a very unstable radical and therefore its addition to the RAFT end

group is irreversible. The large excess of AIBN is still required as an ‘end capping’ agent in order to prevent polymer coupling under the end group removal conditions.

3.3 Results and discussion

All the polymer syntheses described in this chapter were carried out using compound **2.1** as a dual headed initiator/chain transfer agent (CTA) (Figure 3.4). As it was shown previously this compound can be synthesised in a one pot synthesis in high yield from relatively cheap and readily available starting materials. Importantly, this compound can be used as a dual headed initiator/CTA in an analogous manner to compound **2.7**. However, in this case the polymerisation sites are not connected with the DA functionality. This allows for a simpler synthetic approach and very importantly, for the present work, will enable us to assess if the presence of the DA functionality was important for the formation of the cylindrical micelles reported in Chapter 2.

3.3.1 ROP of lactide (LA) initiated by the compound 2.1 to prepare PLA macro-CTAs

The ROP reactions were conducted in an exactly analogous manner as described in the previous chapter (Figure 3.4). It was found that the different initiator used herein did not affect the kinetics or overall efficiency of the lactide polymerisation compared to our DA containing system achieving quantitative conversion of the monomer in about 2 hours (DP ~35). The ROP products were characterised by a combination of SEC (with RI and UV detectors inline) and ^{1}H NMR spectroscopy.

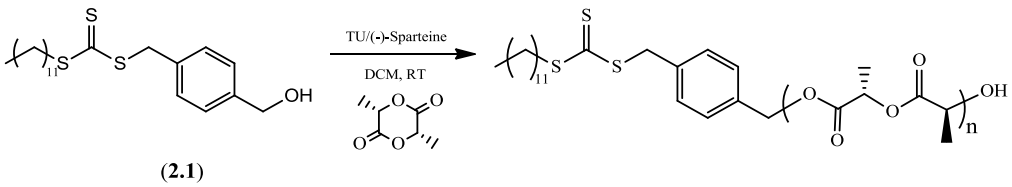

(**2.1**)

Figure 3.4 ROP reaction step for the synthesis of polylactides bearing a trithiocarbonate end group functionality.

With end group analysis by ^{1}H NMR spectroscopy we could calculate the degree of polymerisation of the resultant polymer (Figure 3.5). The experimental values were always in excellent agreement with the theoretical values (Table 3.1). Furthermore, SEC characterisation of the products revealed narrow molecular weight dispersity and the good overlay of the SEC traces as recorded by the RI and UV detectors (collecting at 309 nm) suggested good end group retention in all cases (Figure 3.6).

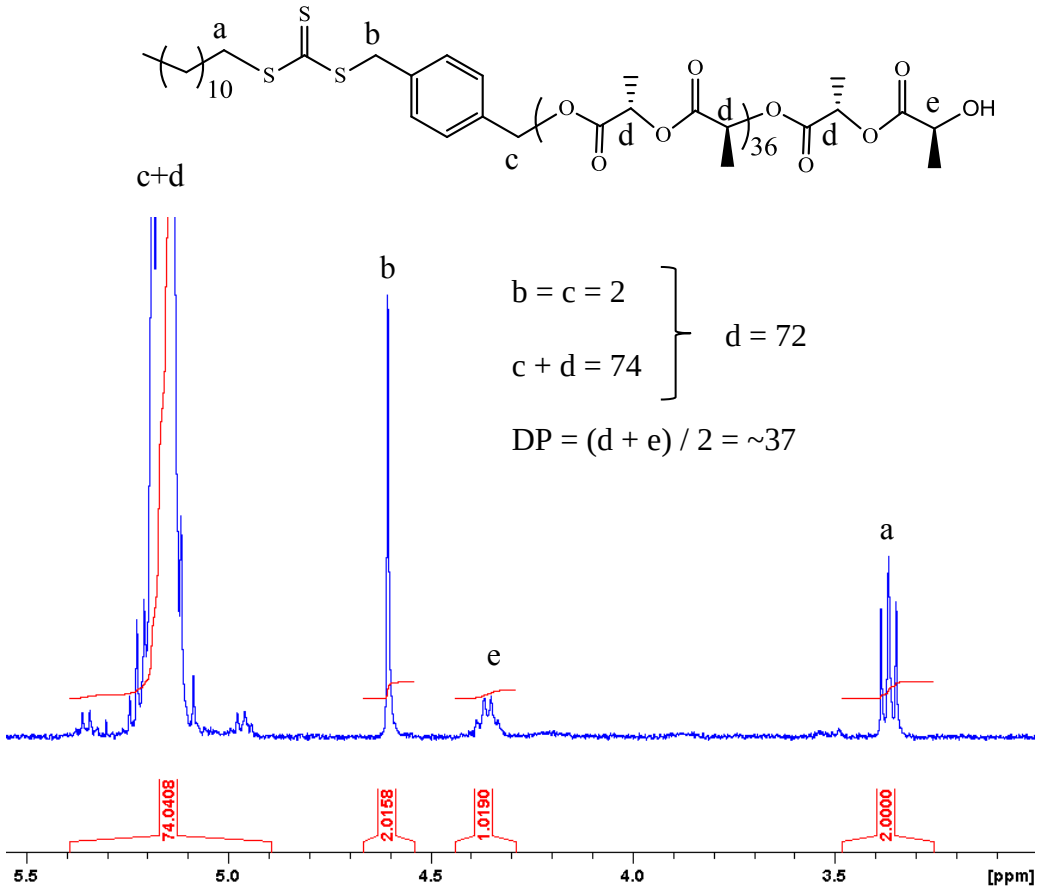

Figure 3.5 Example of end group analysis by ^{1}H NMR spectroscopy for the calculation of the degree of polymerisation of **3.1** in $CDCl_3$ (400 MHz, 293K).

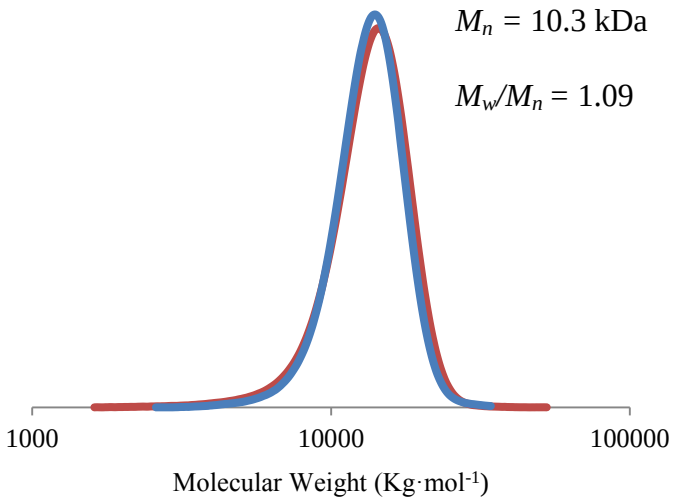

Figure 3.6 Example of the overlay of the RI (blue trace) and UV (red trace) SEC chromatograms for polymer **3.1**.

Table 3.1 Molecular characteristics of the PLA polymers prepared.

polymer	DP_{theor} [a]	DP_{exp} [b]	M_n^{SEC}(kDa) [c]	M_w/M_n [d]
P(*L*-LA), 3.1	35	37	10.3	1.09
P(*L*-LA), 3.2	35	35	9.9	1.11
P(*L*-LA), 3.3	35	32	9.4	1.08
P(*D*-LA), 3.4	35	33	9.5	1.06
P(*D,L*-LA), 3.5	35	33	8.4	1.09

[a] *Theoretical degree of polymerisation as calculated by the initiator and monomer feed for the obtained conversion.* [b] *Degree of polymerisation as calculated by ^{1}H NMR spectroscopy end group analysis.* [c] *Molecular weights as calculated by SEC analysis calibrated with polystyrene standards.* [d] *Molecular weight dispersity index as calculated by SEC analysis.*

Furthermore, the thermal properties of polymer **3.1** were measured by differential scanning calorimetry (DSC). We confirmed the presence of a glass transition temperature (T_g) at 47.5 ^oC, crystallisation point (T_c) at 95.3 ^oC and a melting point (T_m) at 148.2 ^oC (Figure 3.7).

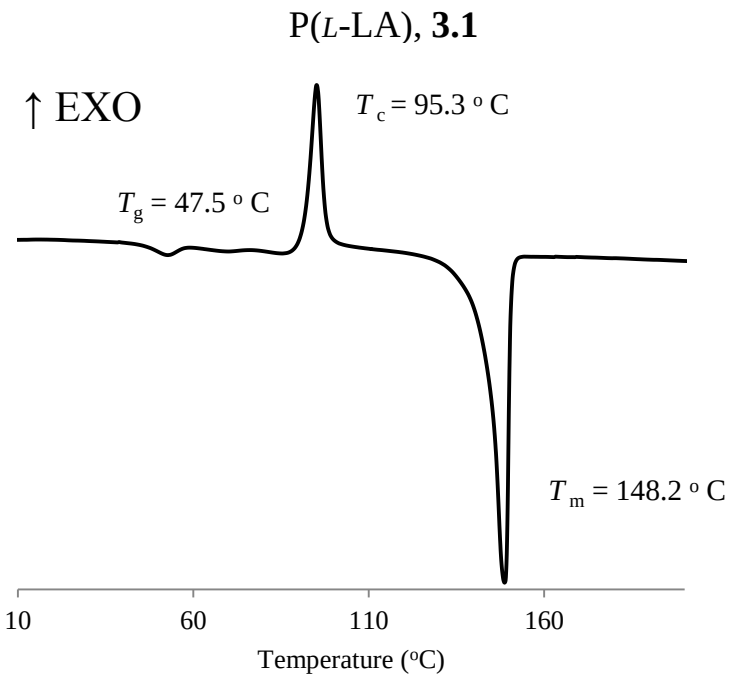

Figure 3.7 Differential scanning calorimetry thermogram for polymer **3.1** (2nd scan); Scan rate: 0.5 ^oC/min.

3.3.2 RAFT polymerisation of THPA mediated by PLA macro-CTA to prepare PLA-*b*-PTHPA diblock copolymers

The polylactide macro-CTAs prepared in the previous section were chain extended with the THPA monomer (Figure 3.8). We were targeting for degrees of polymerisation in the range of 250-350 and thus similar hydrophilic weight fraction to the polymers with the DA functionality synthesised in the previous chapter (Table 3.2).

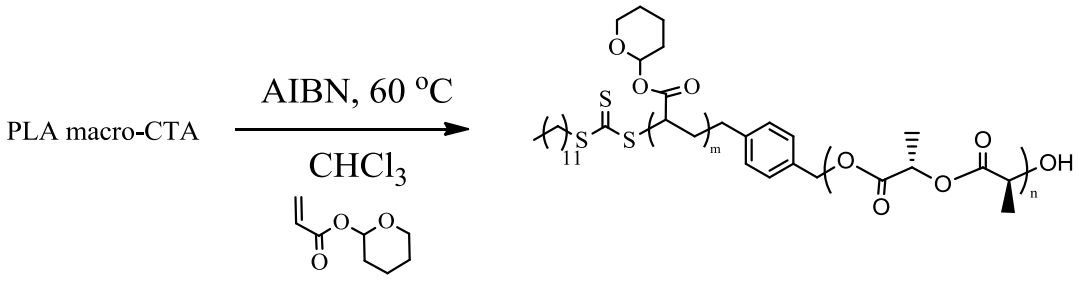

Figure 3.8 RAFT polymerisation of THPA mediated by a PLA macro-CTA for the synthesis of PLA-*b*-PTHPA

The polymerisations were conducted under the optimised conditions found in Chapter 2 (60 ^{o}C, $CHCl_3$, AIBN). The monomer conversions were calculated by ^{1}H NMR spectroscopy. Overall, SEC analysis revealed unimodal MW distributions and narrow molecular weight dispersities for conversions up to 60% (achieved in 5 hours of reaction) (Figure 3.9).When the reaction was left for longer additional high and low molecular weight populations were appearing on the SEC traces. The high molecular weight tailing could be attributed to termination reactions occurring through bimolecular coupling, while the low molecular weight tail was attributed to initiation by the AIBN initiator (although further work would be required to confirm this hypothesis). The block ratio of the resultant polymers was calculated by ^{1}H NMR spectroscopy (Figure 3.10). Once more good overlay of the SEC traces produced by the UV and RI detector suggested good end group retention in all cases.

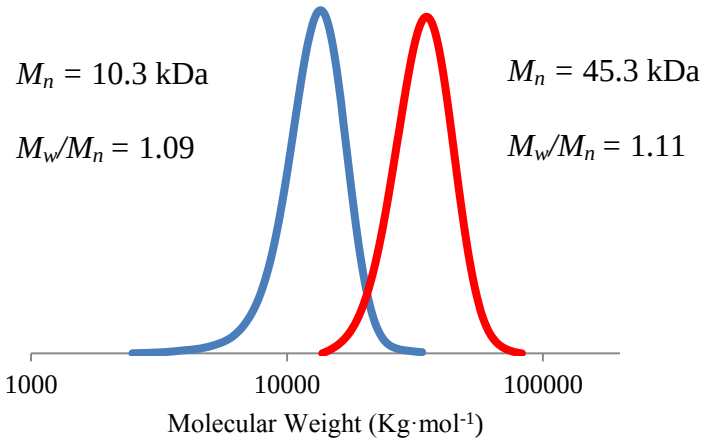

Figure 3.9 SEC chromatograms of **3.1** (blue trace) and **3.6** (red trace) as collected from the RI detector.

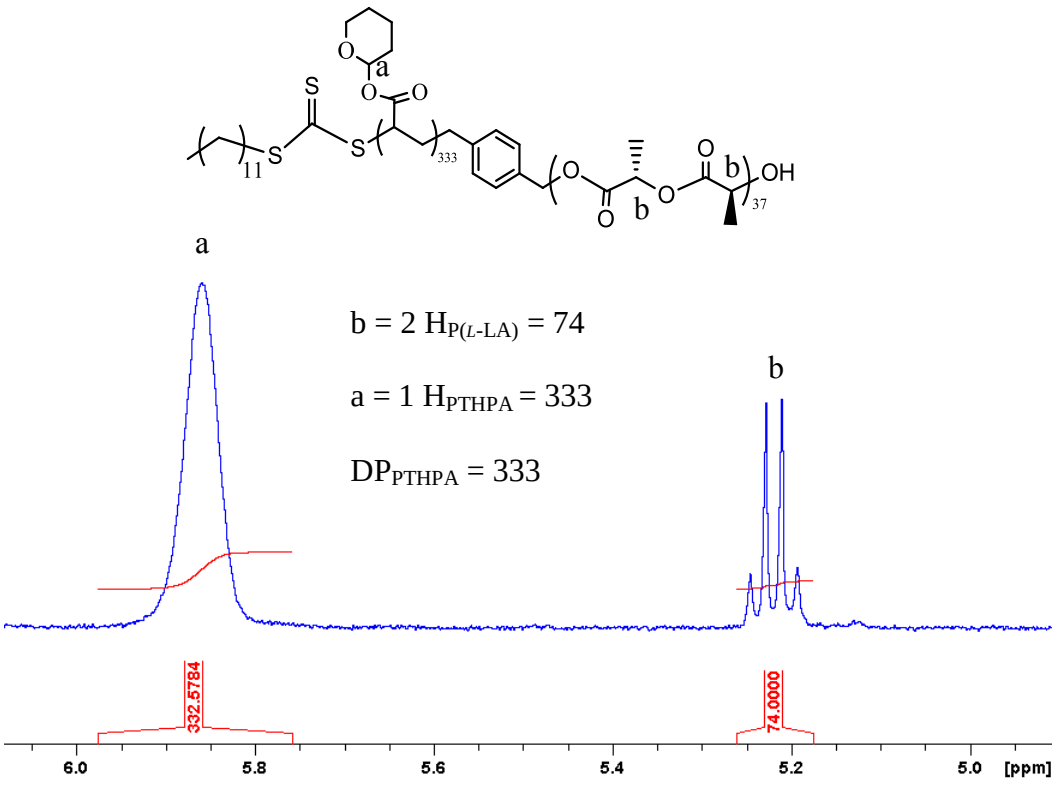

Figure 3.10 Calculation of the experimental degree of polymerisation of PTHPA by ^{1}H NMR spectroscopy block analysis for **3.6** in $CDCl_3$ (400 MHz, 293K).

Table 3.2 Molecular characteristics of the PLA-*b*-PTHPA diblock copolymers prepared

Polymer	PLA macro-CTA[a]	% Conv[b]	DP_{theor}[c]	DP_{exp}[d]	M_w/M_n[e]
3.6	**3.1**	63	315	333	1.11
3.7	**3.1**	65	292	264	1.13
3.8	**3.2**	54	162	164	1.07
3.9	**3.3**	87	261	265	1.42
3.10	**3.4**	75	225	220	1.38
3.11	**3.5**	77	231	240	1.31

[a] PLA macro CTA utilised for the chain extension with THPA [b]% monomer conversion achieved. [c] Theoretical degree of polymerisation as calculated by the macro-CTA and monomer feed for the achieved conversion. [d] Degree of polymerisation of the PTHPA block as calculated by ^{1}H NMR spectroscopy block analysis [e] Molecular weight dispersity index as calculated by SEC analysis.

3.3.3 RAFT polymerisation of TEGA mediated by 3.1 to prepare P(*L*-LA)-*b*-PTEGA

Poly(triethyleneglycol acrylate) (PTEGA) which is hydrophilic and thermoresponsive was synthesised by RAFT polymerisation of triethyleneglycol monomethyl acrylate (TEGA) mediated by **3.1** under our standard conditions (60 ^{o}C, $CHCl_3$, AIBN) (Figure 3.11). The reaction was found to be slightly faster than the THPA polymerisation under the same conditions as 64% conversion was reached in only 3 hours (Figure 3.12). Moreover, SEC characterisation suggested that the diblock copolymers were well-defined (Figure 3.13) and ^{1}H NMR spectroscopy provided a reliable handle to calculate the degree of polymerisation of the PTEGA block.

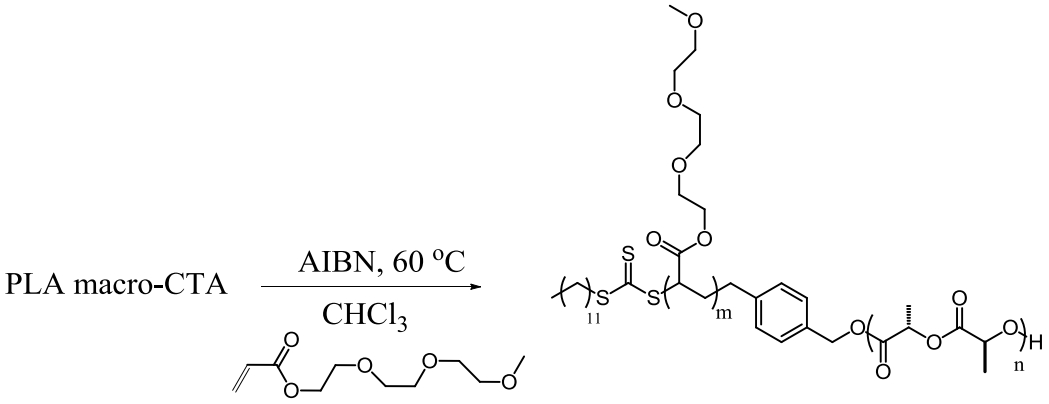

Figure 3.11 RAFT polymerisation of TEGA mediated by a PLA macro-CTA for the synthesis of PLA-*b*-PTEGA.

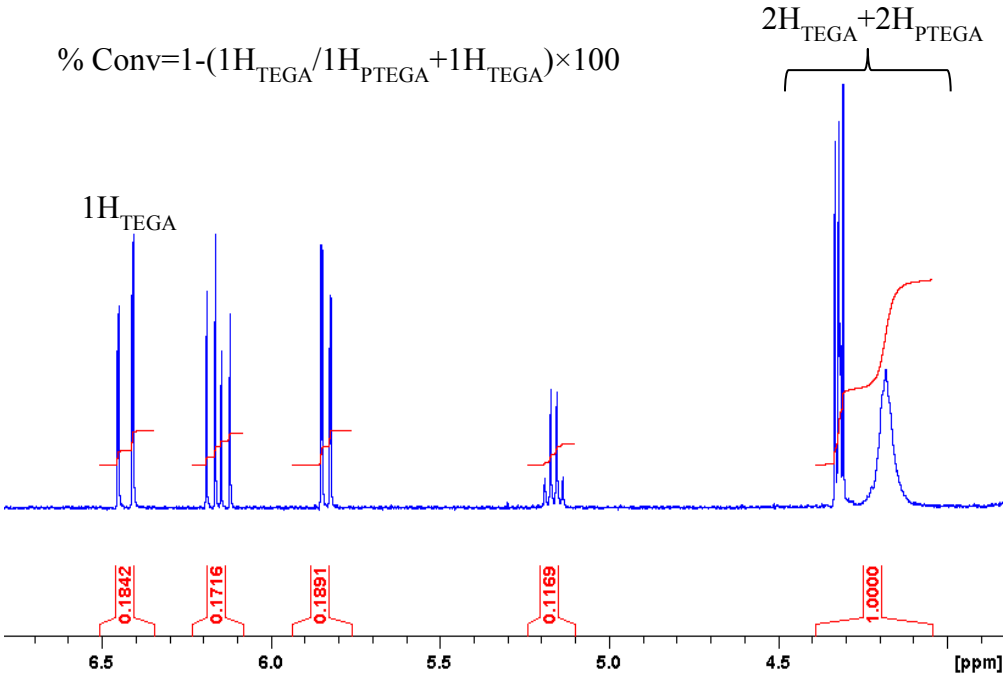

Figure 3.12 Example of calculation of monomer conversion by ^{1}H NMR spectroscopy in this case after 3 hours of reaction for **3.12** in $CDCl_3$ (400 MHz, 293K).

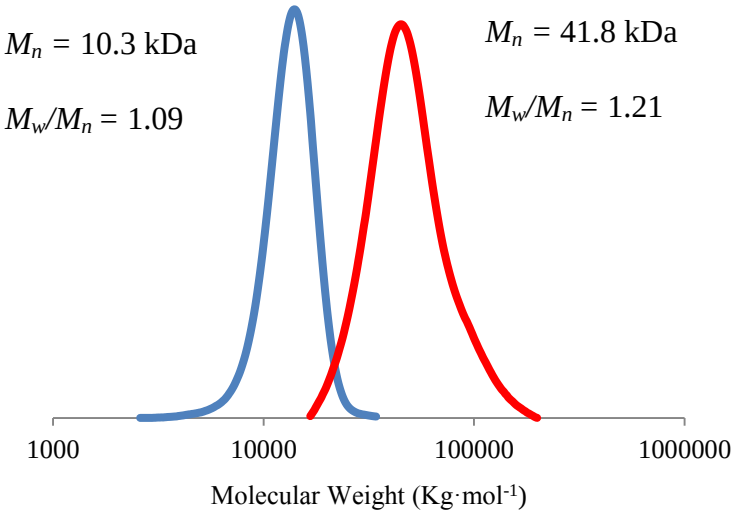

Figure 3.13 SEC chromatograms of **3.1** (blue trace) and **3.12** (red trace) as collected from the RI detector.

Table 3.3 Molecular characteristics of the PLA-*b*-PTEGA diblock copolymers prepared

Polymer	PLA macro-CTA[a]	%Conv[b]	DP_{theor}[c]	DP_{exp}[d]	M_w/M_n[e]
3.12	**3.1**	64	224	212	1.21
3.13	**3.1**	52	130	141	1.18

[a] *PLA macro CTA utilised for the chain extension with TEGA.* [b] *% monomer conversion achieved.* [c] *Theoretical degree of polymerisation as calculated by the macro-CTA and monomer feed for the achieved conversion.* [d] *Degree of polymerisation of the PTEGA block as calculated by* ^{1}*H NMR block analysis.* [e] *Molecular weight dispersity index as calculated by SEC analysis.*

In order to briefly investigate the aggregation and thermoresponsive properties of polymer **3.12** we directly dissolved it in nanopure water at a concentration of 1 $g \cdot L^{-1}$ and subsequently we analysed the solution by DLS and TEM. DLS revealed the presence of structures with a hydrodynamic radius of 54 nm (PD = 0.124) and TEM confirmed the presence of spherical particles (Figure 3.14a). Further studies by UV-

Vis spectroscopy illustrated a cloud point at 52 ^{o}C while a small degree of hysteresis was present on the cooling cycle (Figure 3.14b). PTEGA homopolymers are known not to have hysteresis and this effect was attributed on the fact that the polymer was on the micelle state.

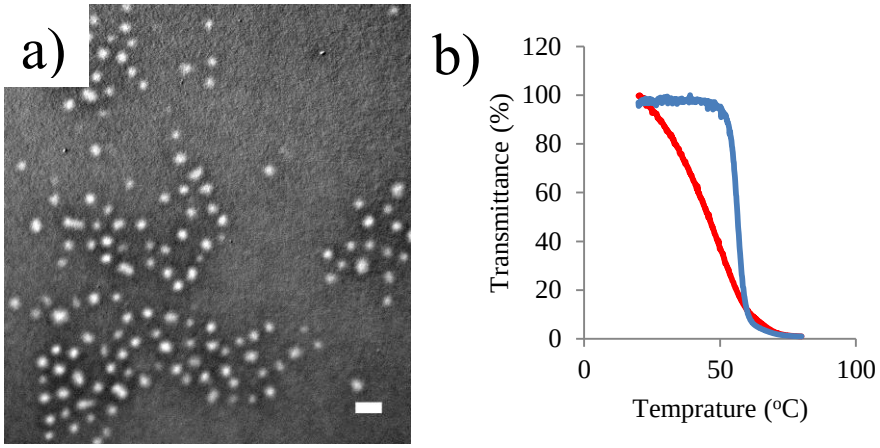

Figure 3.14 a) Representative TEM image of particles formed by **3.12** (PTA stained) (Scale bar = 100 nm); b) Cloud point data collected by a UV/vis Spectrometer equipped with a temperature controller at 500 nm. Heating cycle (blue trace)/cooling cycle (red trace).

3.3.4 RAFT polymerisation of TEGA mediated by PLA-*b*-PTHPA macro CTA to prepare PLA-*b*-PTHPA-*b*-PTEGA

Triblock copolymers of the type poly(*L*-LA)-*b*-PTHPA-*b*-PTEGA were synthesised by chain extending the PLA-*b*-PTHPA macro CTAs **3.6** and **3.7** synthesised in the previous section (Figure 3.15). In our initial experiments the reaction was left for 3 hours, however, it was revealed by SEC analysis that the polymer had a higher tendency to undergo bimolecular coupling as was indicated by the high molecular weight shoulder. This problem was eliminated by stopping the polymerisation reaction at lower conversion (~50%), achieved in 150 min of reaction time. Indeed, in this case the polymerisation produced well defined products as revealed by SEC

(Figure 3.16). ^{1}H NMR spectra of the produced polymer enabled us once more to calculate the degree of polymerisation of the PTEGA block (Figure 3.17).

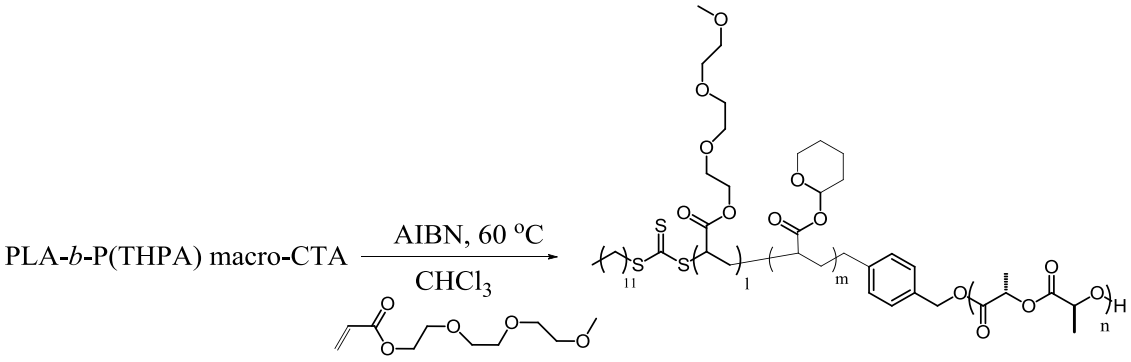

Figure 3.15 RAFT polymerisation of TEGA mediated by PLA-*b*-PTHPA macro-CTA for the synthesis of PLA-*b*-PTHPA-*b*-PTEGA.

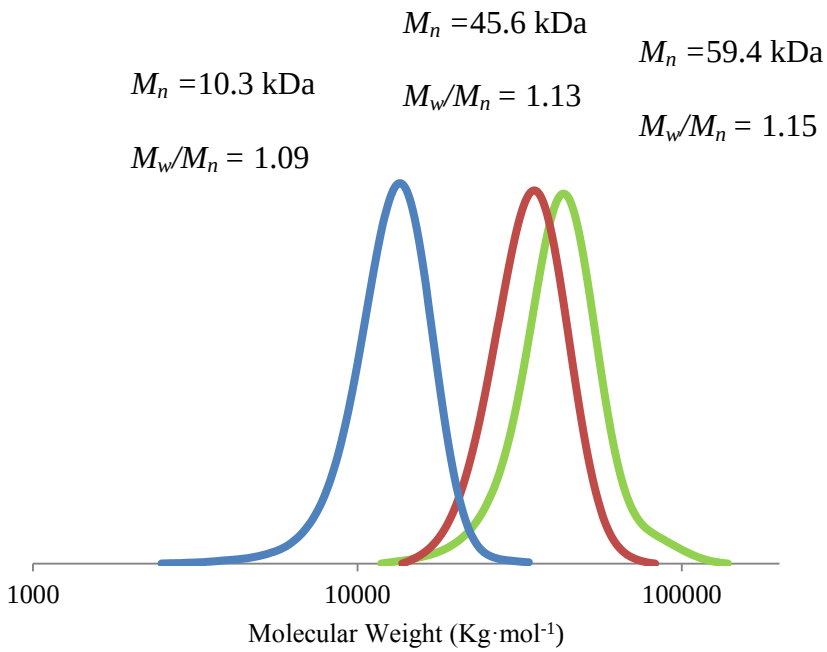

Figure 3.16 SEC chromatograms illustrating the traces for the poly(*L*-LA) macro CTA (**3.1**) (blue trace); the poly(*L*-LA)-*b*-PTHPA (**3.7**) diblock copolymer (red trace); the poly(*L*-LA)-*b*-PTHPA-*b*-PTEGA triblock copolymer (**3.16**) (green trace), all on the RI detector.

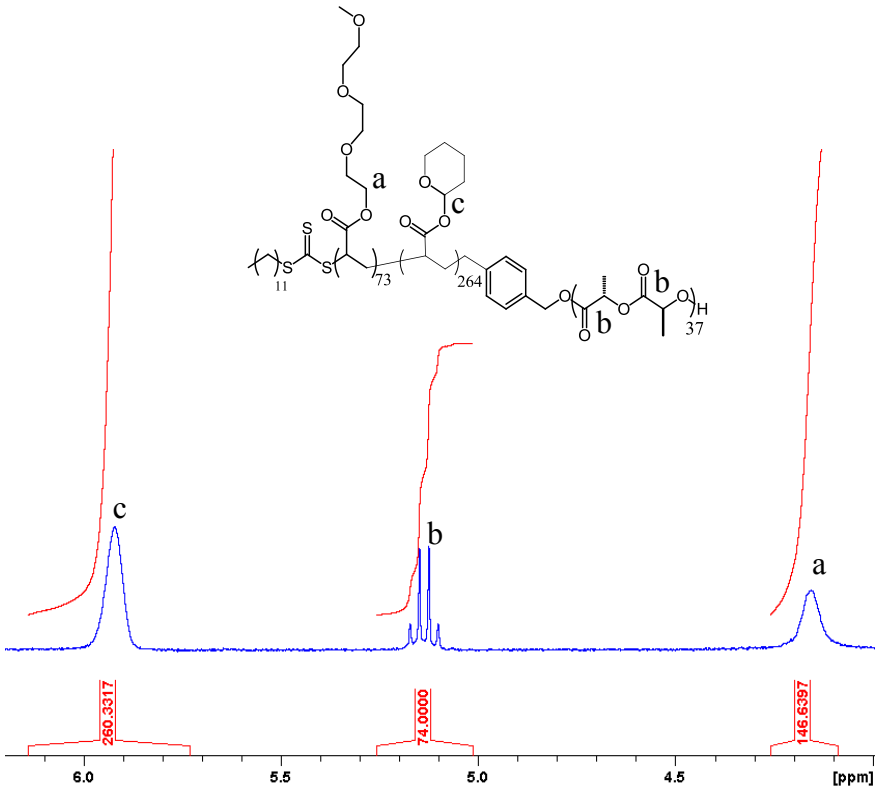

Figure 3.17 ^{1}H NMR spectrum of **3.15** illustrating the signals from which we calculate the degree of polymerisation in $CDCl_3$ (400 MHz, 293K).

Table 3.4 Molecular characteristics of the PLA-*b*-PTHPA-*b*-PTEGA triblock copolymers prepared

Polymer	macro-CTA[a]	%Conv[b]	DP_{theor}[c]	DP_{exp}[d]	M_w/M_n[e]
3.14	**3.7**	32.3	40	32	1.11
3.15	**3.6**	85	85	73	1.34
3.16	**3.7**	51	51	48	1.15

[a] Macro-CTA utilised for the chain extension with TEGA [b] % monomer conversion achieved. [c] Theoretical degree of polymerisation as calculated by the macro-CTA and monomer feed for the achieved conversion. [d] Degree of polymerisation of the PTEGA block as calculated by ^{1}H NMR block analysis. [e] Molecular weight dispersity index as calculated by SEC analysis.

3.3.5 End group modification of polymer 3.7 by a radical addition-fragmentation coupling method

In the present work, we took advantage of the end group modification reaction as reported by Moad and coworkers.[34] In this case the strong absorbance of the trithiocarbonate end-group at 309 nm gave us a good handle to monitor the reaction efficiency by SEC analysis. By monitoring the suppression of the signal at 309 nm (UV detector) we could observe the reaction conversion while from the corresponding RI trace we could check if any side reactions had occurred (especially dimerisation reactions) during the end group modification. Initially, polymer **3.7** was exposed under exactly the same conditions as reported by Moad *et al.*(4 eq LPO, 20 eq AIBN, 80 ^{o}C) We found that under these conditions, although full end group removal was achieved, bimolecular coupling was significant as it was indicated by the high molecular weight shoulder present on the SEC trace recorded by the RI detector. Following this result a larger excess of AIBN was added (100 eq) in order to decrease the side reaction and increase the efficiency of the reaction, the polymer coupling was slightly reduced but still evident by SEC analysis (RI detector). Complete inhibition of the dimerisation was given by a combination of increasing the amount of AIBN and significantly diluting the solution. SEC analysis of the product under these conditions showed complete end group removal and no dimerisation at all (Figure 3.19).

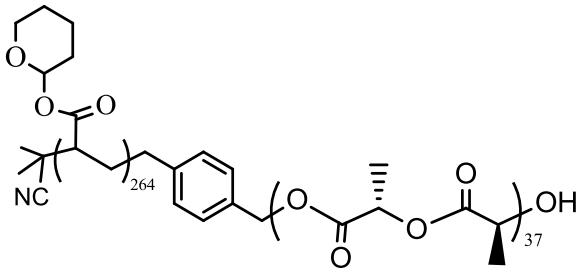

(**3.17**)

Figure 3.18 Chemical structure of **3.17** illustrating the modified end group.

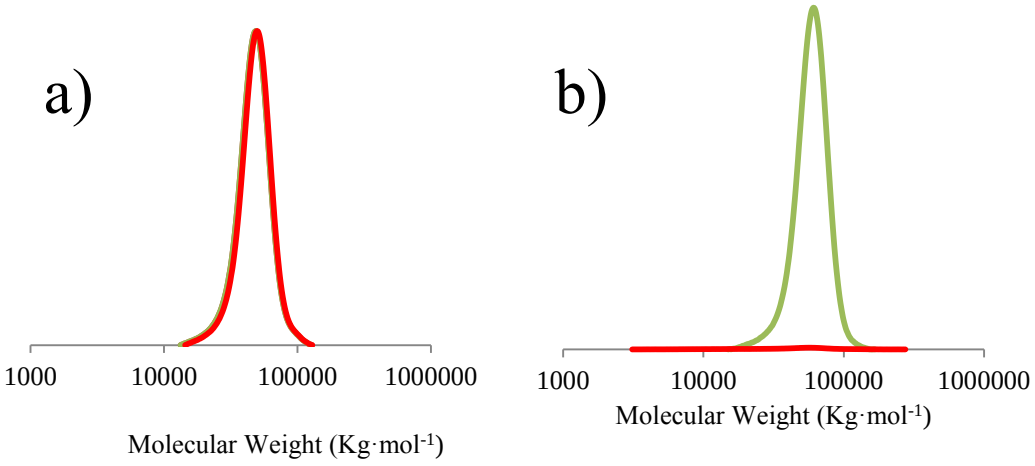

Figure 3.19 a) SEC traces of polymer **3.17** before (green trace) and after the end group removal (red trace) on the RI detector confirming retention of the well-defined characteristics of the polymer through the good overlay of the two traces; b) SEC traces of polymer **3.17** before (green trace) and after the end group removal (red trace) on the UV detector illustrating quantitative efficiency.

3.3.6 End group modification of polymer 3.14 by a radical addition-fragmentation coupling method

The same method was also utilised in order to modify the end group from the poly(*L*-LA)-*b*-PTHPA-*b*-PTEGA triblock copolymer **3.14** (Figure 3.20). The reaction was carried out under the previously optimised conditions found for the synthesis of **3.17**

and the reaction was found to be highly efficient as it was revealed once more by SEC characterisation (Figure 3.21).

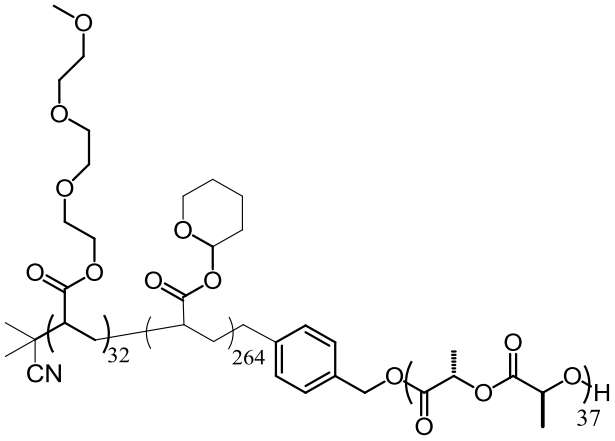

(**3.18**)

Figure 3.20 Chemical structure of **3.18** illustrating the modified end group

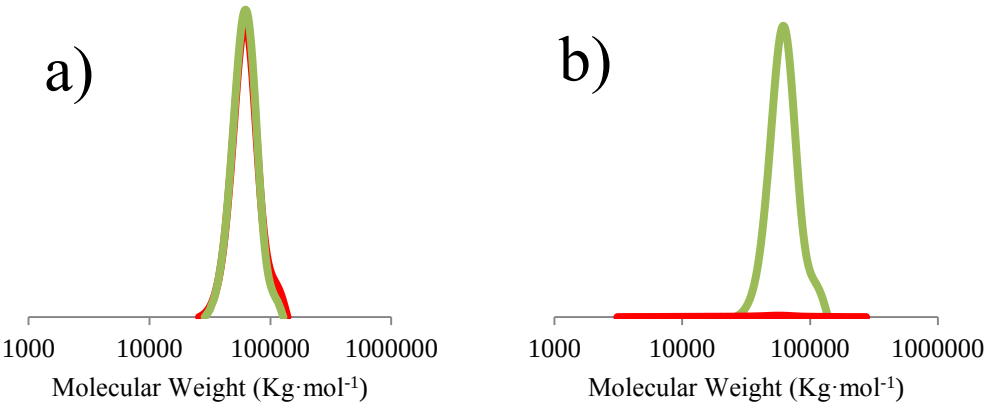

Figure 3.21 a) SEC traces of polymer **3.18** before (green trace) and after the end group modification (red trace) on the RI detector confirming retention of the well-defined characteristics of the polymer through the good overlay of the two traces; b) SEC traces of polymer **3.18** before (green trace) and after the end group modification (red trace) on the UV detector illustrating quantitative efficiency.

3.3.7 Synthesis of pyrene functionalised azo initiator, 3.19

The end group modification strategy we used in the previous sections could also provide a facile method to add different functionalities at the end of our polymers. Our approach was to incorporate a fluorescent label that would provide an additional handle to characterise our polymers and their corresponding assemblies. First step towards this end group functionalisation was to incorporate the desired fluorescent molecule on an azo initiator. For this reason we used 4,4-azobis-4-cyanovaleric acid as the azo initiator that bears two acid group on the two sides and therefore can be readily functionalised through amidation coupling reactions. In order to incorporate a fluorescent functionality we coupled pyrene methyl amine (Figure 3.22). The reaction was carried out in DMF at room temperature. Initially, 4,4-azobis-4-cyanovaleric acid was dissolved in DMF followed by the addition of EDCI and then DMAP. Subsequently, a DMF solution of pyrene methyl amine was added in the activated acid solution, for the amidation reaction to proceed. The reaction was monitored by HPLC, which revealed that product formation was increasing for up to 48 hours. The overall reaction yield after purification was 28%, and the successful synthesis was confirmed by NMR and MS spectroscopy (Figure 3.23).

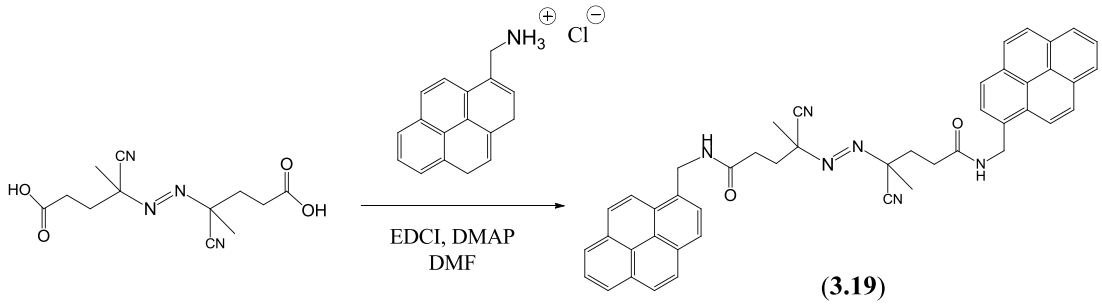

(**3.19**)

Figure 3.22 Amidation reaction for the synthesis of compound **3.19**.

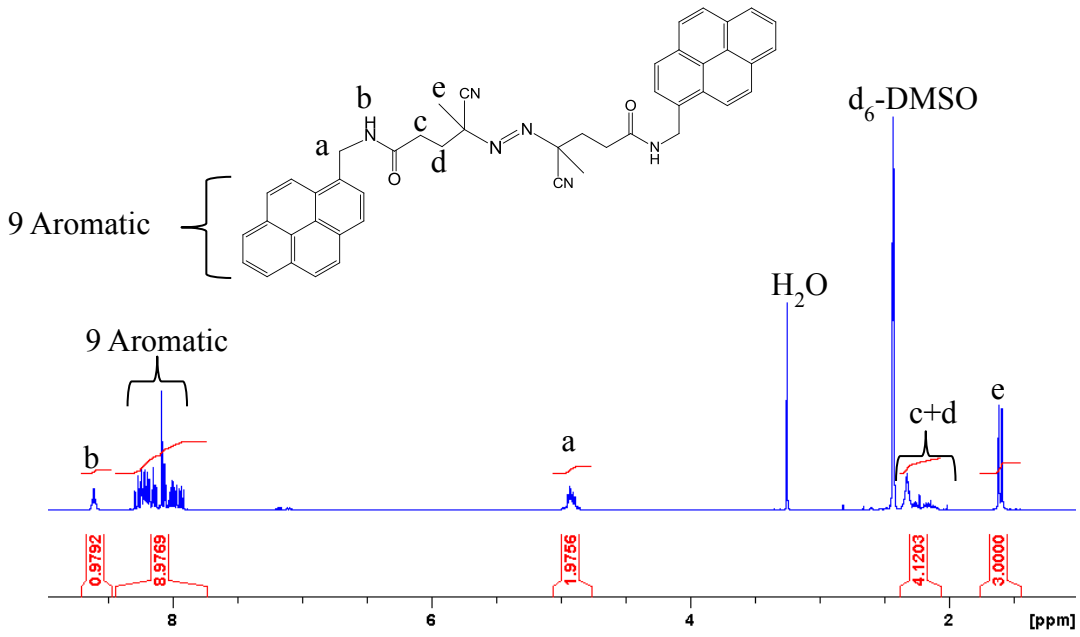

Figure 3.23 ^{1}H NMR spectrum of compound (**3.19**) after purification in d_6-DMSO (400 MHz, 293K)

3.3.8 End group modification of polymer 3.6 by a radical addition-fragmentation coupling method using 3.19

In a completely analogous fashion as described previously polymer **3.6** was readily functionalised with a pyrene group (Figure 3.24). The reaction was conducted initially in toluene. However, compound **3.19** was poorly soluble in this medium. This difficulty was overcome by using benzene as the reaction solvent which was a good solvent for all of the starting materials and products. Importantly, the characterisation of the reaction in this case was more challenging as the resulting polymer still bears a chromophore that absorbs at 309 nm therefore confirmation of successful modification by collecting data in a single wavelength is not possible. This problem was overcome by analysing the SEC traces on a PDA (photodiode array) detector. In this case simultaneous collection of the whole UV spectrum is performed and therefore the total absorbance profile of the end group can be

visualised. Indeed this analysis confirmed complete conversion of the polymer signal from a trithiocarbonate to a pyrene absorbance profile (Figure 3.25). Once more additional analysis of the SEC trace using the RI detector provided additional evidence of the efficiency of the reaction (Figure 3.26). An additional challenge in this end group modification was that due to the poor solubility of **3.19** it was not readily removable from the resulting polymer by selective precipitation. Therefore, in order to purify the polymer, gel permeation chromatography with polystyrene biobeads was utilised. The separation, which could be readily monitored by UV analysis of the chromatographic fractions collected, successfully separated the functionalised polymer from the fluorescent starting material and by products of the reaction. The reaction and purification led to quantitative conversion and recovery of the polymer.

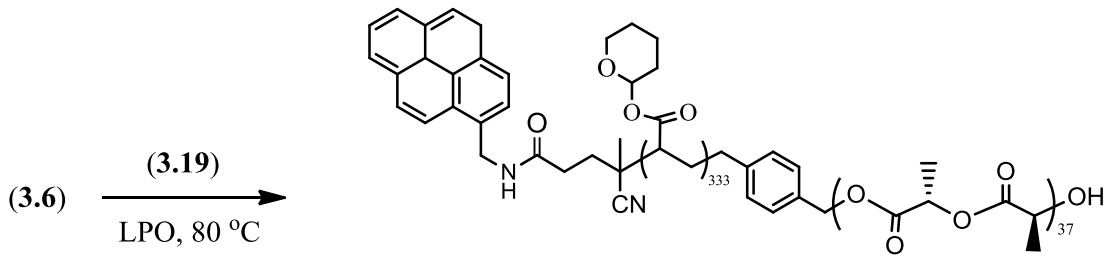

(**3.20**)

Figure 3.24 End group modification of **3.6** by **3.19** in order to introduce a pyrene functionality as an end group of **3.20**.

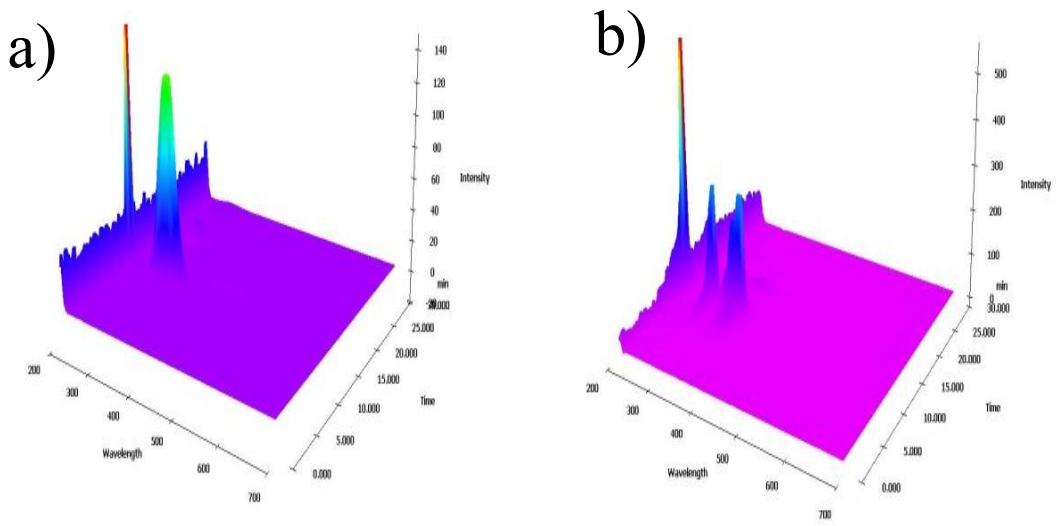

Figure 3.25 a) SEC of polymer **3.6** on the PDA detector illustrating a trithiocarbonate absorbance profile; b) SEC trace of **3.20** on the PDA detector illustrating a pyrene absorbance profile confirming the efficient end group modification.

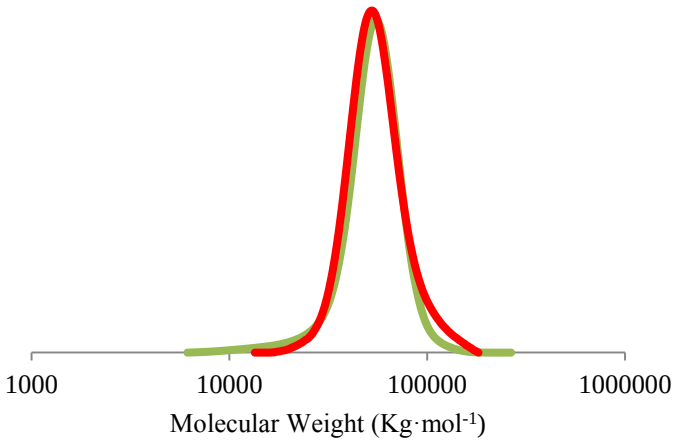

Figure 3.26 SEC traces of polymer **3.20** before (green trace) and after the end group removal (red trace) on the RI detector confirming retention of the well-defined characteristics of the polymer through the good overlay of the two traces.

3.3.9 End group modification of polymer 3.14 by a radical addition-fragmentation coupling method using 3.19

The same reaction conditions, characterisation and purification method was utilised in the case of the triblock copolymer **3.14** (Figure 3.27). The successful synthesis was once more confirmed by SEC couple to a PDA detector (Figure 3.28). The overlay of the RI traces before and after revealed the presence of a high molecular weight shoulder which is an indication that bimolecular coupling took place to an extent. We hypothesise that this behaviour is a result of the poor compatibility between the hydrophobic pyrene group of **3.19** and the hydrophilic PTEGA block which perhaps led to a slightly lower 'capping' ability of **3.19**.

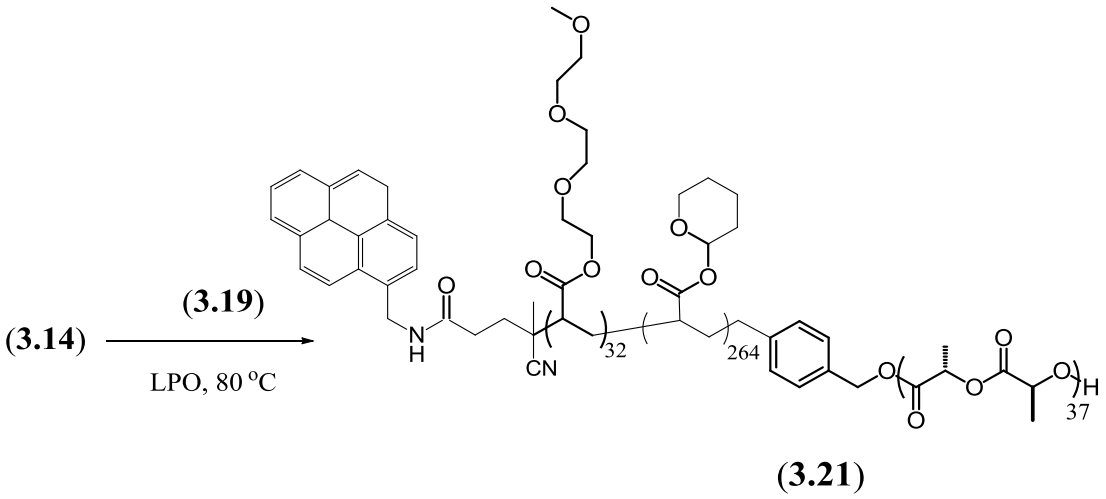

Figure 3.27 End group modification of **3.14** by **3.19** in order to introduce a pyrene functionality as an end group of **3.21**.

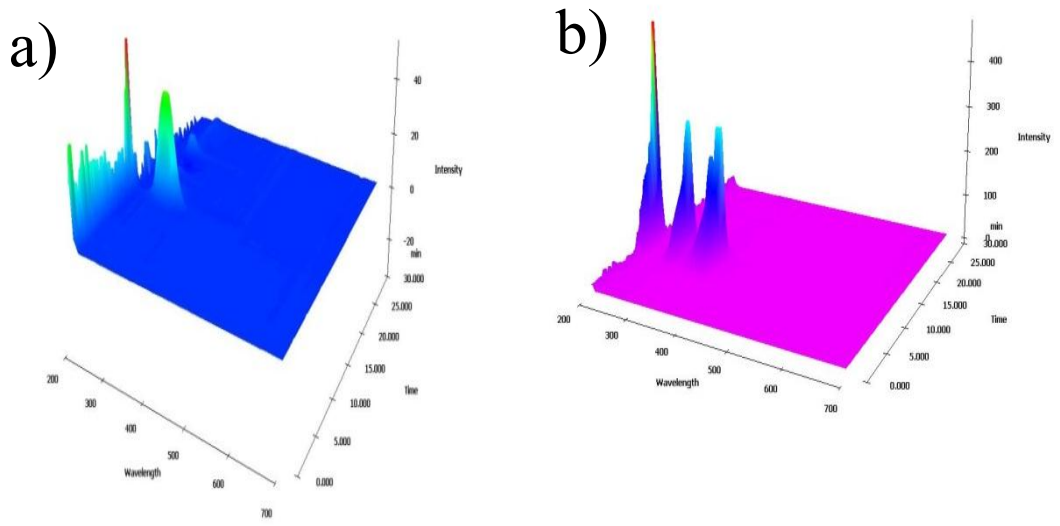

Figure 3.28 a) SEC of polymer **3.14** on the PDA detector illustrating a trithiocarbonate absorbance profile; b) SEC trace of **3.21** on the PDA detector illustrating a pyrene absorbance profile confirming the efficient end group modification.

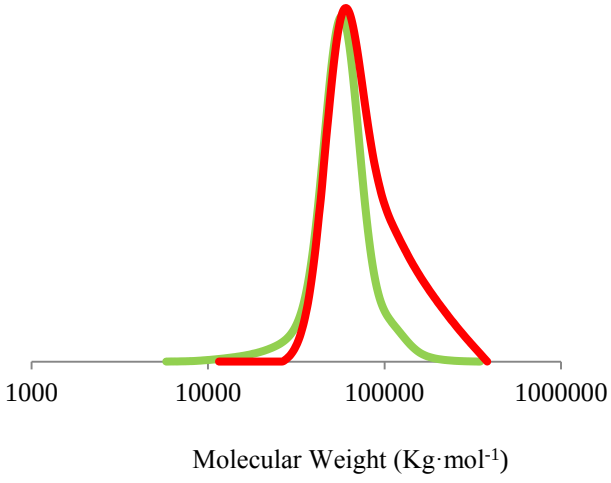

Figure 3.29 SEC traces of polymer **3.21** before (green trace) and after the end group removal (red trace) on the RI detector.

3.4 Conclusions

In this chapter we achieved the synthesis of well-defined block copolymers combining a polylactide block. Although the synthetic methodology is analogous to the one we introduced in the previous chapter, a simpler, alternative dual headed initiator/CTA was used herein. The synthesis of a range of hydrophilic blocks was successfully performed and the synthetic method was expanded to triblock copolymers while a very facile end group modification reaction was utilised to change the functionality at the end of our polymers. The products were thoroughly characterised by NMR, SEC with multiple detectors, MS and FT-IR spectroscopy. The self-assembly behaviour of these polymers will be investigated in the next chapters.

3.5 Experimental Section

3.5.1 Materials and instrumentation

Chemicals were used as received from Aldrich, Fluka and Acros. *L*-lactide was donated by Purac and further purified/dried over 4 Å molecular sieves in dichloromethane solution before being dried under vacuum and sublimed. Lactides were stored in a nitrogen-filled glove box. Tetrahydropyran acrylate (THPA) was prepared as described previously and stored below 4 °C.[35] Triethyleneglycol monomethyl ether acrylate (TEGA) was prepared as reported previously and stored below 4 ^{o}C.[36] AIBN (2,2'-azo-bis(isobutyronitrile)) was recrystallised twice from methanol and stored in the dark at 4 °C. Dry dichloromethane was obtained by passing over a column of activated alumina using an Innovative Technologies solvent purification system. (-)-Sparteine was dried over CaH_2 and distilled prior to use and 1-(3,5-bis(trifluoromethyl)phenyl)-3-cyclohexyl-thiourea was prepared and dried as previously reported.[37]

^{1}H NMR and ^{13}C NMR spectra were recorded on a Bruker DPX-400 spectrometer in $CDCl_3$ unless otherwise stated. Chemical shifts are given in ppm downfield from TMS. Size exclusion chromatography (SEC) measurements were conducted using a Varian 390-LC-Multi detector suite fitted with differential refractive index (DRI) and photodiode array (PDA) detectors equipped with a guard column (Varian Polymer Laboratories PLGel 5 μm, 50×7.5 mm) and two mixed D columns (Varian Polymer Laboratories PLGel 5 μm, 300×7.5 mm). The mobile phase was tetrahydrofuran with 2% triethylamine eluent at a flow rate of 1.0 mL·min^{-1} and samples were calibrated against Varian Polymer laboratories Easi-Vials linear poly(styrene) standards (162-2.4 × 10^5 g·mol^{-1}) using Cirrus v3.3 software. Infrared

spectroscopy was recorded on a Perkin Elmer Spectrum 100 FT-IR Spectrometer. Mass Spectrometry (HR-MS) was conducted on a Bruker UHR-Q-TOF MaXis with electrospray ionisation. Cloud point measurements were analysed using a Perkin-Elmer UV/vis Spectrometer (Lambda 35) equipped with a Peltier temperature controller at 500 nm with a heating/cooling rate of 1 °C/min.

3.5.2 General polymerisation procedures

In all RAFT polymerisations and end group modifications three freeze-pump-thaw cycles were performed on the reaction vessel for the removal of oxygen and were then sealed in an ampoule under nitrogen before being immersed in an oil bath at the required temperature. ROP polymerisations were carried out in a glove box under an inert nitrogen atmosphere at ambient temperature.

3.5.3 Representative procedure for the synthesis of PLA macro CTA

In a 20 mL scintillation vial equipped with a stir bar, a solution of the thiourea organocatalyst (14.3 mg, 34.5 μmol), (-)-sparteine (0.039 mg, 0.17 μmol) and **2.1** (10 mg, 0.15 μmol) in dry CH_2Cl_2 (0.2 mL) was added to a solution of *L*-lactide (140 mg, 0.97 mmol) in dry CH_2Cl_2 (0.8 mL). The reaction mixture was stirred for 2 h (for DP=15-70) before the solution was reduced under vacuum to yield a light yellow solid. The conversion was determined by ^{1}H NMR spectroscopy. The polymer was precipitated from $CHCl_3$ into hexane and dried to a constant weight to afford a triothiocarbonate end functionalised poly(lactide). The degree of polymerisation were determined by ^{1}H NMR spectroscopy while the PDI was determined by SEC. ^{1}H NMR ($CDCl_3$, ppm, 400 MHz): δ = 5.18- 5.05 (q, 1H, backbone), 4.56-4.53 (t, 4H, end group), 4.51-4.48 (s, 2H, end group), 3.31-3.30 (s,

3H, end group), 3.32-3.26 (t, 2H, end group), 2.95-2.88 (m, 2H, end group), 1.53-1.49 (d, 3H, backbone).

3.5.4 Representative procedure for the synthesis of PLA-*b*-PTHPA

The THPA monomer (500 eq), the poly(lactide) macro CTA, **2.1** (1 eq) and AIBN (0.1 equiv) were disolved in 0.5 mL of $CHCl_3$ and transferred in an oven dried ampoule with a stirrer bar. The ampoule was degassed (three times) and sealed under nitrogen, and the polymerisations were heated at 60 °C for 5 h. The polymer was then dissolved in a minimum amount of tetrahydrofuran and purified by precipitation twice into ice cold hexane to afford a pure diblock copolymer PLA-*b*-PTHPA. The degree of polymerisation was determined by ^{1}H NMR spectroscopy while the polydispersity was determined by SEC. ^{1}H NMR ($CDCl_3$, ppm, 400 MHz): δ = 6.02-5.90 (br, 1H, PTHPA backbone) 5.18-5.05 (q, 1H, PLLA backbone), 2.10-1.48 (d, 8H, backbone of both blocks). ν_{max}/cm^{-1} 2954 (C-C stretch), 2920 (C-C stretch), 2850 (C-C stretch), 1758 (C=O stretch of PLA backbone), 1736 (C=O stretch of PTHPA).

3.5.5 Representative procedure for the synthesis of PLA-*b*-PTEGA

The TEGA monomer (300 eq), the poly(lactide) macro CTA, **2.1** (1 eq) and AIBN (0.1 eq) were disolved in 0.5 mL of $CHCl_3$ and transferred in an oven dried ampoule with a stirrer bar. The ampoule was degassed (three times) and sealed under nitrogen, and the polymerisations were heated at 60 °C for 3 h. The polymer was then dissolved in a minimum amount of tetrahydrofuran and purified by precipitation twice into ice cold hexane to afford a pure diblock copolymer PLA-*b*-PTEGA. The degree of polymerisation was determined by ^{1}H NMR spectroscopy while the polydispersity was determined by SEC. ^{1}H NMR ($CDCl_3$, ppm, 400 MHz): δ = 5.18-

5.05 (q, 1H, P(*L*-LA backbone), 4.25-4.08 (br, 2H, PTEGA side group), 3.71-3.28 (d, 13H, PTEGA side group), 2.10-1.48 (d, 6H, backbone of both blocks). ν_{max}/cm^{-1} 2954 (C-C stretch), 2920 (C-C stretch), 2850 (C-C stretch), 1758 (C=O stretch of PLA backbone), 1732 (C=O stretch of PTEGA).

3.5.6 Representative procedure for the synthesis of P(*L*-LA)-*b*-PTHPA-*b*-PTEGA

The TEGA monomer (150 eq), the poly(lactide) macro CTA, **3.7** (1 eq) and AIBN (0.1 eq) were dissolved in 0.5 ml of $CHCl_3$ and transferred in an oven dried vial with a stirrer bar. The vial was degassed (three times) and sealed under nitrogen, and the polymerisations were heated at 60 °C for 150 minutes. The polymer was then dissolved in a minimum amount of tetrahydrofuran and purified by precipitation twice into ice cold hexane to afford a pure triblock copolymer PLA-*b*-PTHPA-*b*-PTEGA. The degree of polymerisation was determined by ^{1}H NMR spectroscopy while the polydispersity was determined by SEC. ^{1}H NMR ($CDCl_3$, ppm, 400 MHz): δ = 6.02-5.90 (br, 1H, PTHPA side group), 5.18-5.05 (q, 1H, P(*L*-LA) backbone), 4.25-4.08 (br, 2H, PTEGA side group), 3.71-3.28 (d, 13H, PTEGA side group), 2.10-1.48 (d, 11H, backbone of both blocks). ν_{max}/cm^{-1} 2954 (C-C stretch), 2920 (C-C stretch), 2850 (C-C stretch), 1758 (C=O stretch of PLA backbone), 1736 (C=O stretch of PTHPA+PTEGA).

3.5.7 End group modification of polymers 3.6 and 3.14 by a radical addition-fragmentation coupling method

Polymer **3.6** (0.250 g,, 1 eq), AIBN (0.088 g, 100 eq) and LPO (0.0084 g, 4 eq) were dissolved in 13.25 mL of toluene and transferred in an oven dried ampoule with a

stirrer bar. The ampoule was degassed (three times) and sealed under nitrogen, and the polymerisations were heated at 80 °C for 5 h. Subsequently, the mixture was dissolved in a minimum amount of THF and precipitated three times into hexane to afford a pure diblock copolymer PLA-*b*-PTHPA with modified end group. The successful end group modification was confirmed by SEC analysis both using an RI and UV detector. ^{1}H NMR ($CDCl_3$, ppm, 400 MHz): δ = 6.02-5.90 (br, 1H, PTHPA backbone) 5.18-5.05 (q, 1H, PLLA backbone), 2.10-1.48 (d, 8H, backbone of both blocks)

3.5.8 Synthesis of the pyrene functionalised azo initiator, 3.19

4, 4 Azobis 4-cyanovaleric acid (0.5 g, 1 eq) and EDCI·HCl (0.75 g, 2 eq) were added in a round bottom flask and dissolved in DMF (30 mL). Subsequently, DMAP (0.3 g, 1 eq) was added and the mixture was stirred for 30 minutes, followed by pyrene methyl amine and the reaction mixture was stirred at ambient temperature for 48 hours. To isolate the product the solution was initially passed through a silica column with 100% ethyl acetate as the eluent solvent in order to remove the reaction salts and then the desired product **3.19** was isolated by selective precipitation and filtration from toluene. ^{1}H NMR (d_6-DMSO, 400 MHz): δ = 8.64-8.57 (t, 2H, 2NH), 8.30-7.89 (m, 18H, Ar), 5.01-4.83 (m, 2H, CH_2Py), 2.37-1.98 (m, 4H, CH_2CH_2C(CH_3)CN), 1.68-1.49 (d, 3H, $CH_2CH_2C(CH_3)CN$), ^{13}C NMR (d_6-DMSO, 400 MHz): δ = 164.2, 127.6, 127.3, 127.0, 126.8, 126.7, 126.2, 125.2, 125.1, 124.7, 123.1, 40.5, 39.9, 39.7, 39.3, 39.1, 38.9. LC-MS gave m/z 729.3 $[M+Na]^+$ (68%), 745.8 $[M+K]^+$ (32 %).

3.5.9 End group modification of polymers 3.6 and 3.14 by a radical addition-fragmentation coupling method using 3.19

Polymer **3.6** (0.035 g, 1 eq), **3.19** (0.025 g, 50 eq) and LPO (0.0011 g, 4 eq) were dissolved in 1.76 mL of benzene and transferred in an oven dried ampoule with a stirrer bar. The ampoule was degassed (three times) and sealed under nitrogen, and the reactions were heated at 80 °C for 5 h. Subsequently, the mixture was dissolved in a minimum amount of THF and purified with a column of polystyrene beads to afford a pure diblock copolymer PLA-*b*-PTHPA with pyrene functionalised end group. The successful end group modification and purification were confirmed by SEC analysis of the data collected using both a PDA and a RI detector. (^{1}H NMR spectroscopy results same as with precursor)

3.6 References

(1) Moad, G.; Rizzardo, E.; Thang, S. H. *Polym. Int.* **2011**, *60*, 9.

(2) Mori, H.; Müller, A. H. E. *Progress in Polymer Science* **2003**, *28*, 1403.

(3) Chiefari, J.; Chong, Y. K.; Ercole, F.; Krstina, J.; Jeffery, J.; Le, T. P. T.; Mayadunne, R. T. A.; Meijs, G. F.; Moad, C. L.; Moad, G.; Rizzardo, E.; Thang, S. H. *Macromolecules* **1998**, *31*, 5559.

(4) Hong, C.-Y.; You, Y.-Z.; Bai, R.-K.; Pan, C.-Y.; Borjihan, G. *J. Polym. Sci., Part A: Polym. Chem.* **2001**, *39*, 3934.

(5) Davis, K. A.; Matyjaszewski, K. *Macromolecules* **2000**, *33*, 4039.

(6) Davis, K. A.; Charleux, B.; Matyjaszewski, K. *J. Polym. Sci., Part A: Polym. Chem.* **2000**, *38*, 2274.

(7) Hawker, C. J.; Bosman, A. W.; Harth, E. *Chemical Reviews* **2001**, *101*, 3661.

(8) Zhang, L.; Shen, H.; Eisenberg, A. *Macromolecules* **1997**, *30*, 1001.

(9) Burguière, C.; Pascual, S.; Bui, C.; Vairon, J.-P.; Charleux, B.; Davis, K. A.; Matyjaszewski, K.; Bétremieux, I. *Macromolecules* **2001**, *34*, 4439.

(10) Lowe, A. B.; Billingham, N. C.; Armes, S. P. *Macromolecules* **1998**, *31*, 5991.

(11) Sanji, T.; Nakatsuka, Y.; Kitayama, F.; Sakurai, H. *Chem. Commun.* **1999**, 2201.

(12) Lu, S.; Fan, Q.-L.; Liu, S.-Y.; Chua, S.-J.; Huang, W. *Macromolecules* **2002**, *35*, 9875.

(13) Liu, Y.; Wang, L.; Pan, C. *Macromolecules* **1999**, *32*, 8301.

(14) Samarajeewa, S.; Shrestha, R.; Li, Y.; Wooley, K. L. *J. Am. Chem. Soc.* **2012**, *134*, 1235.

(15) Bütün, V.; Vamvakaki, M.; Billingham, N. C.; Armes, S. P. *Polymer* **2000**, *41*, 3173.

(16) Patrickios, C. S.; Hertler, W. R.; Abbott, N. L.; Hatton, T. A. *Macromolecules* **1994**, *27*, 2364.

(17) Lutz, J.-F.; Hoth, A. *Macromolecules* **2005**, *39*, 893.

(18) Fan, X.; Lin, L.; Messersmith, P. B. *Biomacromolecules* **2006**, *7*, 2443.

(19) Lutz, J.-F.; Akdemir, Ö.; Hoth, A. *J. Am. Chem. Soc.* **2006**, *128*, 13046.

(20) Becer, C. R.; Hahn, S.; Fijten, M. W. M.; Thijs, H. M. L.; Hoogenboom, R.; Schubert, U. S. *J. Polym. Sci., Part A: Polym. Chem.* **2008**, *46*, 7138.

(21) Willcock, H.; O'Reilly, R. K. *Polym. Chem.* **2010**, *1*, 149.

(22) Moad, G.; Chong, Y. K.; Postma, A.; Rizzardo, E.; Thang, S. H. *Polymer* **2005**, *46*, 8458.

(23) Harrisson, S. *Macromolecules* **2009**, *42*, 897.

(24) Plummer, R.; Hill, D. J. T.; Whittaker, A. K. *Macromolecules* **2006**, *39*, 8379.

(25) De, B. H.; Schellekens, M. A. J.; Klumperman, B.; Monteiro, M. J.; German, A. L. *J. Polym. Sci., Part A: Polym. Chem.* **2000**, *38*, 3596.

(26) Vana, P.; Albertin, L.; Barner, L.; Davis, T. P.; Barner-Kowollik, C. *J. Polym. Sci., Part A: Polym. Chem.* **2002**, *40*, 4032.

(27) Chong, Y. K.; Moad, G.; Rizzardo, E.; Thang, S. *Macromolecules* **2007**, *40*, 4446.

(28) Destarac, M.; Charmot, D.; Franck, X.; Zard, S. Z. *Macromol. Rapid Commun.* **2000**, *21*, 1035.

(29) Chong, Y. K.; Krstina, J.; Le, T. P. T.; Moad, G.; Postma, A.; Rizzardo, E.; Thang, S. H. *Macromolecules* **2003**, *36*, 2256.

(30) Tanaka, S.; Nishida, H.; Endo, T. *Macromolecules* **2009**, *42*, 293.

(31) Chong, B.; Moad, G.; Rizzardo, E.; Skidmore, M.; Thang, S. H. *Aust. J. Chem.* **2006**, *59*, 755.

(32) Sinnwell, S.; Synatschke, C. V.; Junkers, T.; Stenzel, M. H.; Barner-Kowollik, C. *Macromolecules* **2008**, *41*, 7904.

(33) Perrier, S.; Takolpuckdee, P.; Mars, C. A. *Macromolecules* **2005**, *38*, 2033.

(34) Chen, M.; Moad, G.; Rizzardo, E. *J. Polym. Sci., Part A: Polym. Chem.* **2009**, *47*, 6704.

(35) O'Reilly, R. K.; Joralemon, M. J.; Hawker, C. J.; Wooley, K. L. *Chem.--Eur. J.* **2006**, *12*, 6776.

(36) Ryu, J.-H.; Roy, R.; Ventura, J.; Thayumanavan, S. *Langmuir* **2010**, *26*, 7086.

(37) Pratt, R. C.; Lohmeijer, B. G. G.; Long, D. A.; Lundberg, P. N. P.; Dove, A. P.; Li, H.; Wade, C. G.; Waymouth, R. M.; Hedrick, J. L. *Macromolecules* **2006**, *39*, 7863.

Chapter 4: Crystallisation driven sphere-to-cylinder transition of polylactide containing block copolymers

4.1 Abstract

One-dimensional morphologies have enhanced properties in a range of applications compared to their spherical counterparts. However, their formation remains challenging. To this end, the unexpected formation of cylindrical particles that we reported in Chapter 2 warranted further studies. Herein, our main goal is to understand the origins of the cylindrical micelle formation. We investigated the aggregation behaviour under the aqueous thermal conditions in which the PTHPA block hydrolysis is performed.

Transmission electron microscopy (TEM) and dynamic light scattering (DLS) is utilised to follow the kinetics of the morphological transition and wide angle X-ray diffraction (WAXD) to evaluate the degree and role of crystallinity. Studies at different concentrations and solvent mixtures provide valuable information regarding the self-assembly mechanism. We demonstrate that the micelle morphology can be readily switched between cylinders and spheres, demonstrating a simple method to control the morphology of the resultant assembly. In addition, the polymers with modified end groups and the triblock copolymers synthesised in Chapter 3 are studied and all the results compared.

4.2 Introduction

4.2.1 Morphology transitions and challenges in block copolymer (BCP) self-assembly

The self-assembly of block copolymers in solution is governed both by thermodynamic[1,2] and kinetic factors.[3,4] Under conditions that allow a rapid unimer exchange, thermodynamics dominate and the energetically most favoured state is obtained. In a wide range of self-assembly systems however, most commonly in polymers that contain long insoluble blocks, the dynamics of the system are restricted and hence much slower unimer exchange rates are observed.[5] Under these conditions a system is considered to be under kinetic control and the products are either kinetically trapped in non-equilibrium states, or rearrange extremely slowly towards energetically more favoured structures. Thermodynamics and kinetics have been used to control block copolymer self-assembly and fabricate various supramolecular morphologies ranging from spheres,[6] cylinders[7,8] and vesicles[9] to a range of more exotic morphologies.[10,11] These morphologies are being investigated for a range of applications such as drug delivery vehicles,[12] catalytic supports,[13] nanoreactors,[14] and nanolithography templates.[15] Spherical micelle morphologies are the most accessible and therefore most studied and understood. However, access to nanostructured assemblies with other morphologies can allow for altered function in a range of applications. Vesicles, for example, can act as vehicles for the high loadings of both hydrophobic and hydrophilic drugs,[16] while cylindrical micelles can function as carriers of hydrophobic therapeutics and dyes with long circulation lifetimes in the blood.[17] Furthermore, cylindrical micelles can be used as templates for nanowires and have potential as doping agents.[18]

The morphology obtained through polymer self-assembly is generally dictated by the free energy of the aggregates, which in turn depends on three components; the free energy of the core, which relates to the stretching of the core forming block; the free energy of the corona, to which steric or electrostatic interactions of the coronal blocks contribute; and the free energy of the interface which depends on the interactions between the core forming block and the solvent.[2,19] Based on good knowledge of these parameters a dimensionless packing parameter can be calculated and thereafter the favoured morphology predicted.[19]

Sphere-to-rod,[20,21] sphere-to-vesicle[22-24] and rod-to-vesicle[25] transitions using solvent switching methods and/or external stimuli have been explored recently. Hadjichristidis and coworkers utilised light scattering and atomic force microscopy to study the sphere-to-cylinder transition of polystyrene-*b*-polyisoprene, PS-*b*-PI polymers in heptane, a selective solvent for the PI block. The polymer was found to form cylindrical micelles at room temperature, while the cylinders were converted to spheres upon heating at 35 ^{o}C. Importantly, they found that the transition was reversible as cylinders were reformed upon cooling down at 25 ^{o}C. They also reported that the cylinder-to-sphere transition upon heating was much faster than the sphere-to-cylinder transition upon cooling (Figure 4.1).[21]

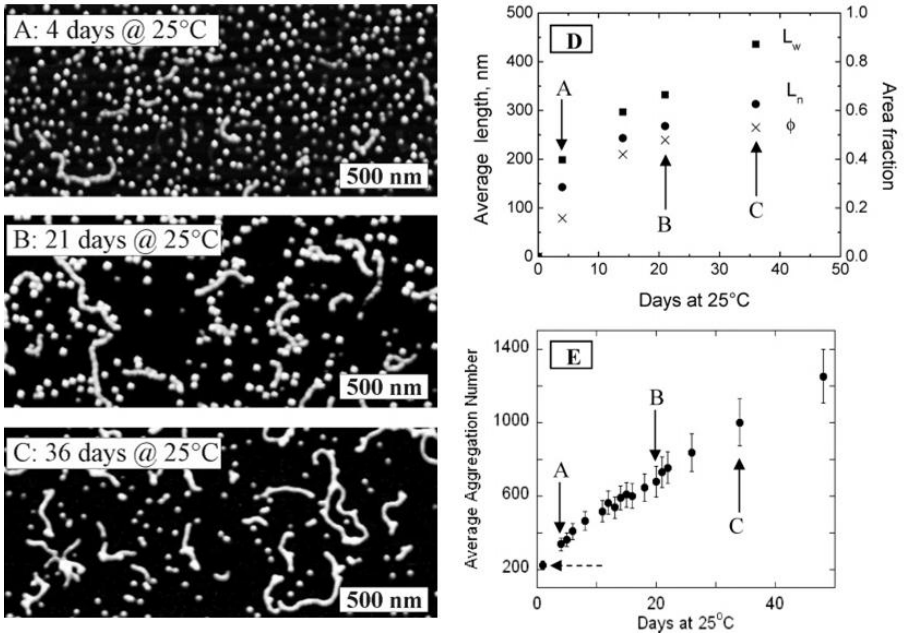

Figure 4.1 Sphere-to-cylinder transition upon heating of PS-*b*-PI micelles in heptane.[21]

Eisenberg and Burke have studied the relaxation kinetics and transition mechanisms of the sphere-to-rod and rod-to-sphere transitions occurring in polystyrene-*b*-poly(acrylic acid), PS-*b*-P(AA) aggregates by solution turbidity measurements and transmission electron microscopy. The copolymer PS_{310}-*b*-$P(AA)_{52}$ was found to self-assemble into aggregates with spherical, rod like or vesicular shapes in various dioxane-water mixtures. Notably, they proposed that the transformation of spherical micelles to rod like aggregates occurred through a two-step mechanism; where initially adhesive collisions of spheres occurred resulting in the formation of irregular "pearl necklace" intermediate structures. According to the authors, this was followed by the reorganisation of the necklace intermediates to form smooth rods. They claimed the rod-to-sphere transition also involved two steps. They demonstrated that a bulb developed quickly on one or both ends of the rod, and then the bulbs were slowly pinched off to release free spheres in solution. In their work,

the sphere-to-rod transition occurred at comparable rates to the reverse process (Figure 4.2).[20]

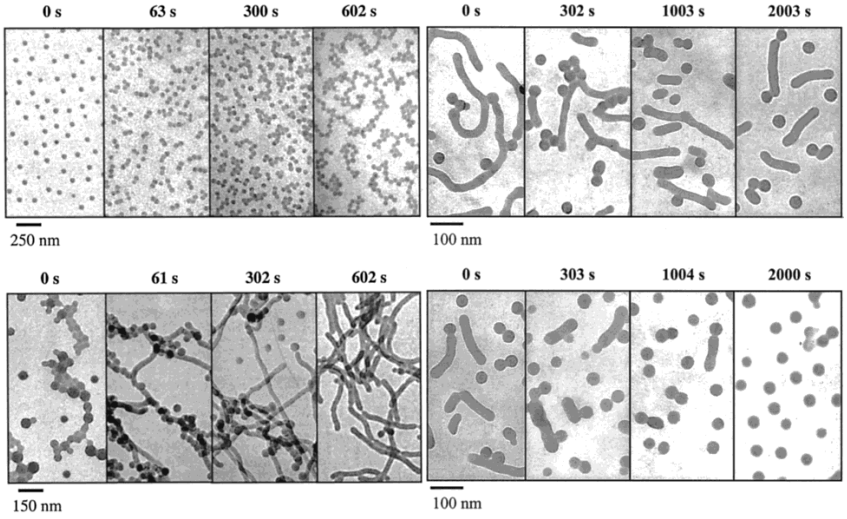

Figure 4.2 TEM images of the aggregates at different time points during the sphere-to-rod and rod-to-sphere transition occurring in solutions of 1.0 wt % PS_{310}-*b*-$P(AA)_{52}$ in dioxane-water mixtures.[20]

All the above references represent examples of morphological transitions resulting to cylindrical micelles based on solvophobic effects. However, according to this method cylinders are only formed by polymers with an insoluble block comparable or bigger than the corona-forming block. Furthermore, cylindrical micelles are only formed in a very narrow window of conditions and frequently coexist with other morphologies.[21,26] Several methods have been introduced to 'alter' the conventional self-assembly rules and thus allow the ready access to cylindrical particles. Some of the most notable efforts will be discussed in the next section.

4.2.2 Alternative routes towards 1-dimensional morphologies

Hedrick and coworkers recently reported a range of hydrogen-bonding motifs that, when were placed at the interface of an amphiphilic block copolymer, had a pronounced effect upon the assembly morphology.[27] Both the urea–benzamide and

thiourea–benzamide motifs proved to be simple building blocks capable of inducing anisotropic hydrogen-bonding interactions. In their work the block copolymer assemblies were prepared by membrane dialysis with subsequent sonication and equilibration of the micelle solution. Once the dialysis was complete, cotton-like aggregates of cylindrical micelles were formed. The solution was then sonicated to facilitate an aqueous dispersion of the block copolymer micelles and maintained at ambient condition to equilibrate the micelle formation. Importantly, it was shown that these hydrogen bonding motifs transformed the morphology of PEG–PLA diblock copolymers from spherical to nanotubular. The authors highlighted that block copolymer nanotubes can easily enhance the solubility and mechanical/thermal stabilities of the supramolecular architectures, compared to well-studied examples of low-molecular-weight amphiphiles. (Figure 4.3).[27]

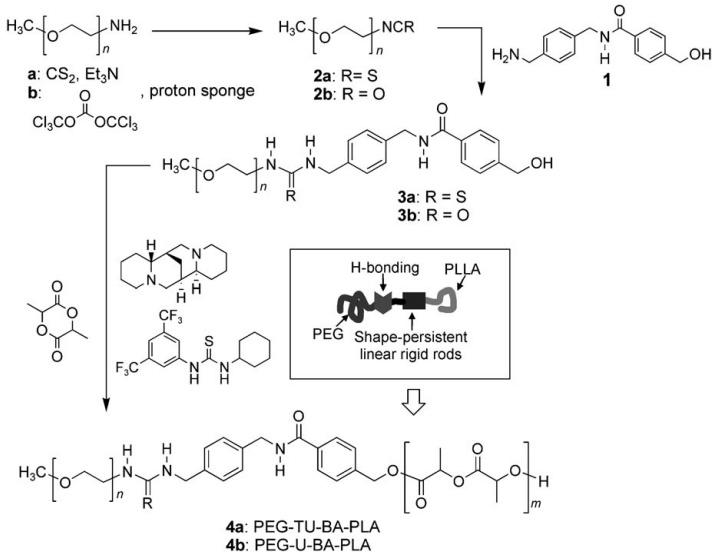

Figure 4.3 Example of the system Hedrick *et al* utilised to induce anisotropy into their self-assembly system.[27]

A different approach towards the synthesis of cylindrical nanoparticles is that of brush copolymers.[28-33] In this case the formed particles are not supramolecular

assemblies, however, as the particles contain anisotropy perhaps share some of the useful properties of cylindrical micelles. Mueller and coworkers reported the synthesis of copolymer brushes with a poly(tert-butyl acrylate) (PtBA) core, a poly(3-(trimethoxysilyl)propyl acrylate) (PAPTS) shell, and a poly(oligo(ethylene glycol) methacrylate) (POEGMA) corona that were prepared *via* the "grafting from" strategy by the combination of anionic polymerisation and ATRP. The as synthesised polymeric brushes were applied as a unimolecular cylindrical template for the *in situ* fabrication of water-soluble organo-silica hybrid nanotubes *via* condensation of the PAPTS shell middle block to form a silsesquioxane network. With different monomer feed ratios, it was possible to change the dimensions of the formed nanotubes. Not only could the lengths of the nanotubes be controlled rather uniformly by the length of the backbone, but also the actual diameter (PtBA and PAPTS) as well as the shell thickness (PAPTS) were easy to adjust. They confirmed the formation of their tubular nanostructures by transmission electron microscopy (TEM), cryogenic TEM, and atomic force microscopy (AFM) (Figure 4.4).[29]

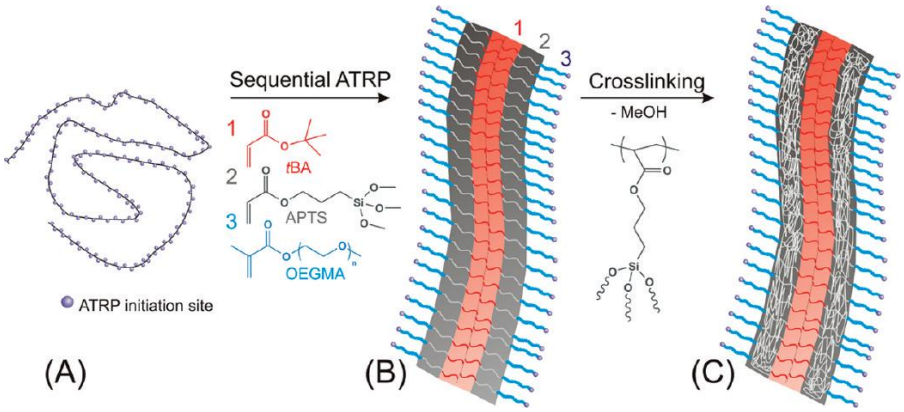

Figure 4.4 'Grafting from' synthetic methodology applied by Muller and coworkers for the preparation of hybrid organo-silica polymeric brushes.[29]

Furthermore, the introduction of specific interactions in the core domain of aggregates has attracted a lot of interest in recent years. Namely, hydrogen bonding, π-π stacking and crystallisation are some of the effects that have been systematically employed as additional thermodynamic driving forces.

Stupp, Hartgerink and Beniash reported in 2001 that peptide amphiphiles (PA) could self-assemble into nanofibres through a pH induced self-assembly method. The formation of the fibres was found to be concentration-independent over more than three orders of magnitude (0.01 mg/mL to 50 mg/mL); however, a second level of hierarchy was observed that was concentration-dependent. As the concentration of the PA was increased, a larger number of the fibres were observed to pack into flat ribbons of fibres. Examination of the self-assembled material by Fourier transform infrared spectroscopy (FT-IR) revealed a bimodal amide peak with maxima at 1658 cm^{-1} (α helix) and 1632 cm^{-1} (β sheet) along with a N-H stretching peak at 3287 cm^{-1}, indicating the formation of a hydrogen bonded structure, possibly using a combination of β sheet and α helical secondary structure in the fibres. On the basis of the above data, the nanofibres were modelled as cylindrical micelles in which the alkyl tails pack on the inside of the fibre and peptide segments are displayed on the outside in the form of both β sheet and α helical secondary structures. This model resulted in a fibre with a diameter of 8.5 nm (Figure 4.5).[34-36]

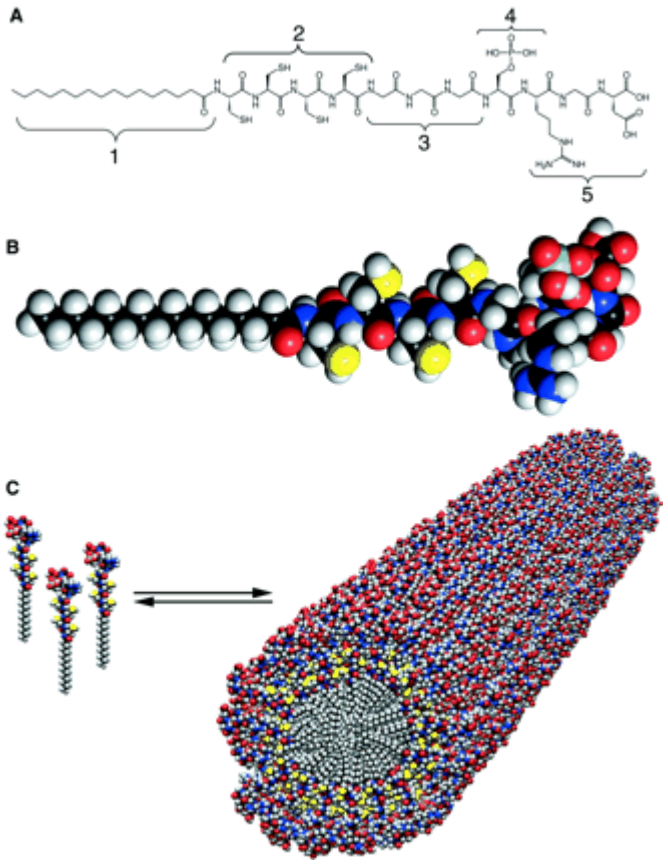

Figure 4.5 (**A**) Chemical structure of the peptide amphiphile; (**B**) Molecular model of the PA showing the overall conical shape of the molecule going from the narrow hydrophobic tail to the bulkier peptide region; (**C**) Schematic showing the self-assembly of PA molecules into a cylindrical micelle.[34]

Strong complimentary interactions, like hydrogen bonding and π-π stacking have also been utilised. A characteristic example is this reported by Kilbinger and coworkers in 2006. They utilised rod-coil polymers based on polyaramide (Kevlar) oligomers as the rod, and PEG as the coil section.[37-41] They demonstrated that strong hydrogen bonding and π-π interactions developed in the polyaramide oligomer core drive the formation of cylindrical particles. The 1-dimensional assemblies were formed in chloroform and toluene, as well as in aqueous solutions (Figure 4.6).[41]

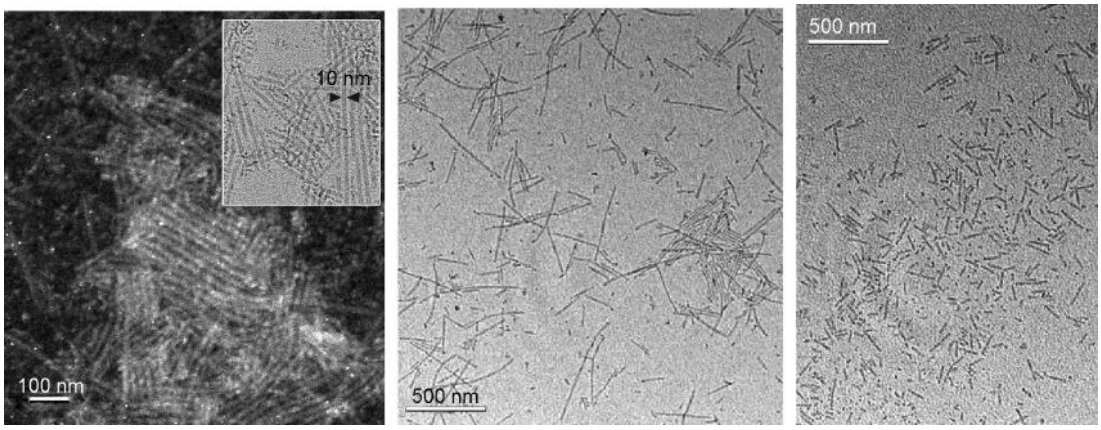

Figure 4.6 Left: scanning TEM image of cylindrical particles deposited from chloroform solution onto carbon-coated copper grids; Middle: TEM image of cylindrical particles deposited from toluene solution onto carbon-coated copper grids; Right: TEM image of cylindrical particles deposited from aqueous solution onto carbon-coated copper grids.[41]

Likewise, Borner *et al.* studied the assembly behaviour of a rod-coil amphiphile based on peptide oligomers and butyl acrylate. The amphiphile was self-assembled by direct dissolution into a mixture of diethyl ether and methanol and found to afford helical elongated tape-like structures. A β-sheet formation of the peptide core was argued by the authors to be the main driving force of this assembly (Figure 4.7). [42,43]

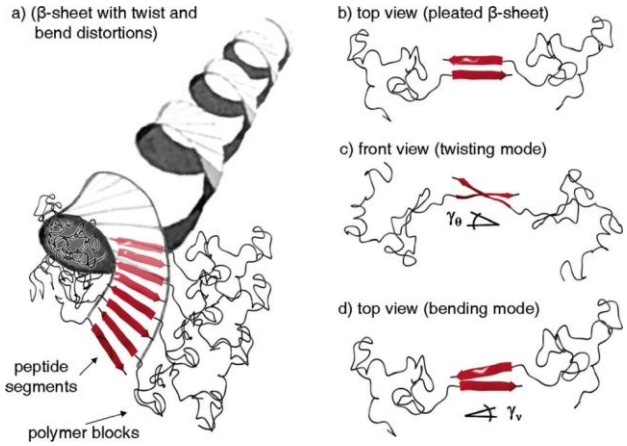

Figure 4.7 Helical structures formed by peptide-polymer amphiphiles in organic solvent mixtures.[42]

While these examples demonstrate how specific interactions in the core of aggregates can be utilised to fabricate 1-dimensional structures they all deal with oligomeric rod-like segments that have a perfectly monodispersed character. The crystallisation of conventional polymers in the restricted environment of a micellar core is non-trivial and can have profound effects both on the crystallisation event as well as on the self-assembly products. The first studies regarding the self-assembly of coil crystalline polymers in dilute solutions were carried out by Lotz and coworkers in 1966. In their work poly(ethyleneoxide)-*b*-polystyrene, PEO-*b*-PS were assembled in a selective solvent for PS and platelet like micelles with a crystalline PEO core were found to form.[44]

Vilgis and Halperin were amongst the first to conduct a theoretical study based on a scaling analysis to investigate the effect of the crystallisation of the core forming block in BCP micelles in dilute solutions.

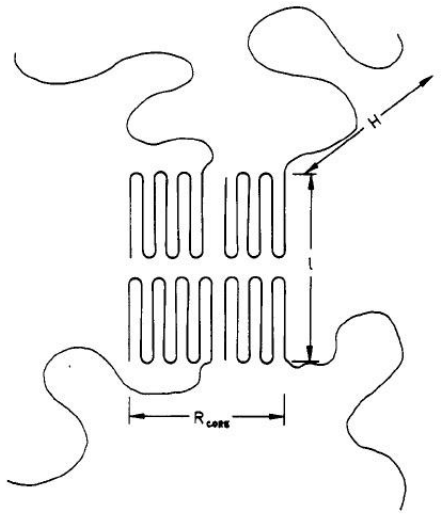

Figure 4.8 Chain folded morphology attained by the crystallised core block as predicted by Vilgis and Halperin.[45]

According to their work the core crystallinity can affect the equilibrium state *via* the following two routes. Firstly the chain fold crystallisation can determine the packing mode of the core blocks, and this sets the relationship between the grafting density and the core's geometry. Secondly, the chain fold crystallisation gives rise to two different surface tensions. One is associated with the fold's plane, while the other characterises the lateral surface which incorporates "unkinked'' chain segments. In this work they predict that the two surface tensions associated with fold crystals cause significant core anisotropy which in turn will give rise to lamellar or cylindrical morphologies (Figure 4.8).[45]

A range of semi crystalline polymers has been explored in recent years for the formation of cylinders including polyethylene, polyacrylonitrile, polyesters and polythiophenes. However the field tremendously benefitted by the revolutionary research of Manners, Winnik and coworkers that focused mainly on the self-assembly behaviour of poly(ferrocenyldimethylsilane), PFS based copolymers. PFS is semicrystalline and when copolymers of PFS are assembled in a non-polar organic solvent they readily form cylindrical particles with a crystalline PFS core. Here the morphology of the formed nanoparticles is not primarily dependent on the hydrophobic:hydrophilic block ratio, with cylinders resulting from the self-assembly process even when polymers with a large hydrophilic block compared to the hydrophobic block are employed. In depth experimental evidence has shown that the main driving force for this behaviour is the crystallisation of the core block. Because of the model behaviour that this system demonstrates it has been a benchmark in this field and as so it will be analysed in greater detail in the following section.

4.2.3 Crystallisation driven self-assembly (CDSA) of PFS based copolymers

In 1998, Massey *et al*. reported that PFS-*b*-polydimethylsiloxane (PFS-*b*-PDMS) based thin films were self-assembled to form PFS cylinders into a hexagonal array within a PDMS matrix as it was expected for diblock copolymers whose components had a volume ratio in the range of 18±40 %. Interestingly, they documented that when the bulk sample was dissolved into n-hexane in a sealed vial and heated at 80 ^{o}C cylindrical particles were observed by TEM. No evidence for the presence of crystallinity was shown at this point and the authors speculated that this was effectively the redispersion of the already formed cylinders from the bulk state (Figure 4.9).[46,47]

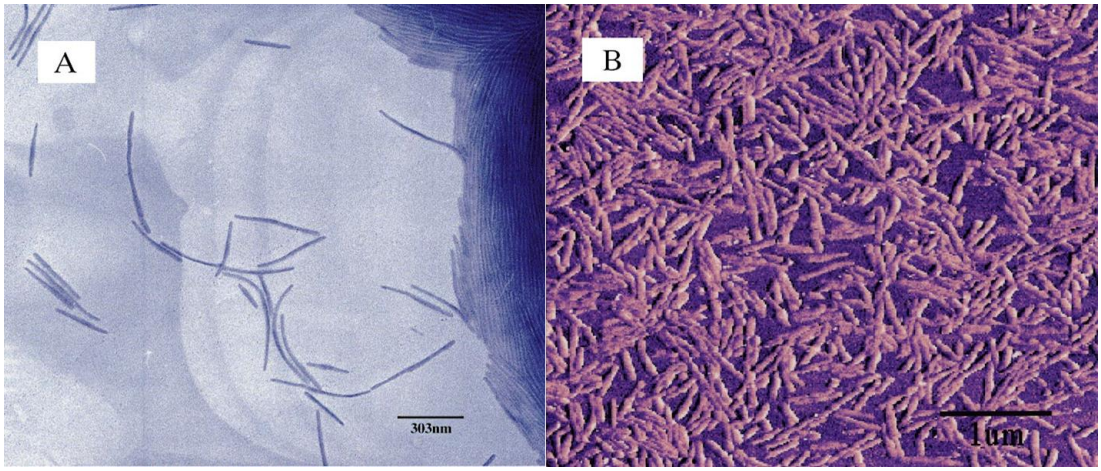

Figure 4.9 (A)Transmission electron micrograph and (B) atomic force micrograph (tapping mode, phase image) of cylindrical micelles of PFS-b-PDMS (Mn = 35 100, PDI = 1.10) aerosol-sprayed from hexane solution.[47]

Following on, the same group in 2000 reported for the first time on the role of crystallisation of the PFS block on the formation of otherwise unexpected worm-like micelles of PFS-*b*-PDMS copolymers in alkane solvents (Figure 4.10).[48] The authors also demonstrated control over the length and width of the resulting cylinders by

altering the self-assembly methodology and block ratio of the block copolymer utilised

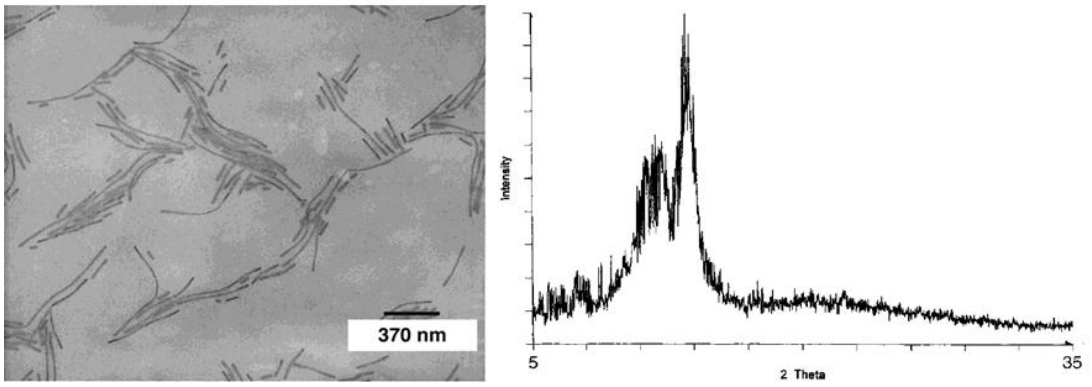

Figure 4.10 TEM image of cylindrical micelles and WAXD pattern illustrating the presence of a crystalline PFS domain.[48]

In this paper they demonstrated that crystallisation during the self-assembly of coil crystalline BCP's can be utilised as a major driving force for the formation of cylindrical micelles. They found that the crystallisation of the core block can override the so-called solvophobic effects resulting in 1-dimensional particles for a broad window of block ratios and self-assembly conditions. These results had a significant impact in the self-assembly community and set the foundations for the new concept of crystallisation driven self-assembly (CDSA).[48]

This strategy has been extended to enable cylinder formation with a variety of different diblock and triblock copolymers based on PFS including PFS-*b*-poly(aminoalkyl methacrylate), PFS-*b*-PDMAEMA, PFS-*b*-polyisoprene, PFS-*b*-PI, PFS-*b*-PEO and PFS-*b*-poly(2-vinylpyridine), PFS-*b*-P2VP.

Work by Wang *et al* demonstrated the aqueous self-assembly of a polyferrocenylsilane-*b*-poly(aminoalkyl methacrylate) that produced cylindrical micelles of highly monodispersed width but rather polydispersed length. The

experiments were performed by direct dissolution in water and the dispersion required 20 days to stabilise.[49] The same year the group also reported the self-assembly results of a poly(ferrocenylphosphine)-*b*-poly(ferrocenylsilane)-*b*-polysiloxane (PFP-*b*-PFS-*b*-PDMS) coil-crystalline-coil triblock copolymer. In this case the self-assembly of the ABC triblock copolymers was studied in hexane. Hexane is a non-solvent for both PFP and PFS but a good solvent for PDMS. All micelle samples were prepared by slow addition of hexane to solutions of the polymer (1% w/v) in THF, a good solvent for all three blocks. THF was removed by slow dialysis against hexane. They found that the crystallisation of the core block played a key role in the formation of cylindrical particles while they concluded that the amorphous and solvophobic PFP block was, to an extent disrupting PFS from crystallising.[50]

In another report in 2003, they formed cylindrical micelles with a polyisoprene-*b*-ferrocenyldimethylsilane (PI-*b*-PFS) block copolymer in THF/hexane mixtures. Shell cross-linking was performed by derivatising the pendent vinyl groups on the coronal PI chains by means of Pt-catalysed hydrosilylation chemistry. The cross-linker used was tetramethyldisiloxane, and the reaction was carried out in the presence of Karstedt's catalyst. The stabilisation of the cylinders was demonstrated by transferring the cross-linked micelles from hexane to THF, a common solvent for both blocks. DLS analysis in THF gave an R_h value of 59 nm which suggested the preservation of the cylindrical structure rather than dissociation to yield unimers, a conclusion confirmed by TEM analysis (Figure 4.11).[51]

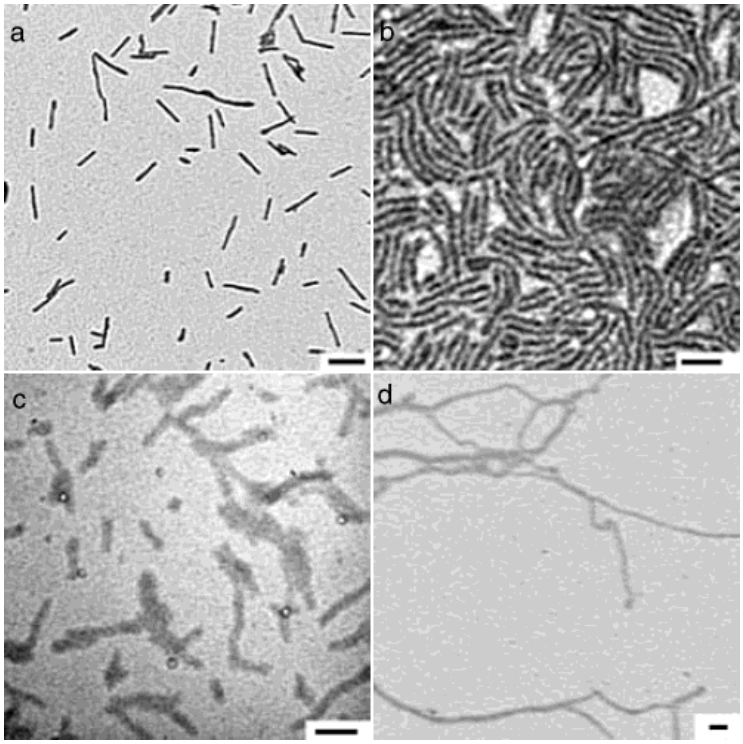

Figure 4.11 TEM images of Cylindrical micelles and shell-cross linked particles based on PI-*b*-PFS block copolymers.[51]

Schubert, Winnik and Manners documented the aqueous self-assembly of a Poly(ethylene oxide)-*b*-Poly(ferrocenylsilane) (PEO-*b*-PFS) block copolymer with a metallo-supramolecular linker at the block junction. Cylindrical micelles were formed and the role of crystallisation was once more highlighted.[52]

Diblock copolymers, PFS-*b*-P2VP (poly(2-vinylpyridine)), were synthesised *via* 1,1-dimethylsilacyclobutane (DMSB)-mediated sequential anionic polymerisation. A significant change in the morphology of the observed micelles was found depending on the nature of selective solvent. Simply by using different alcohols as solvents either spherical or cylindrical micelles could be selectively formed from the same copolymer. WAXD experiments indicated that the crystallisation of the core had a key role in the morphologies observed (Figure 4.12).[53]

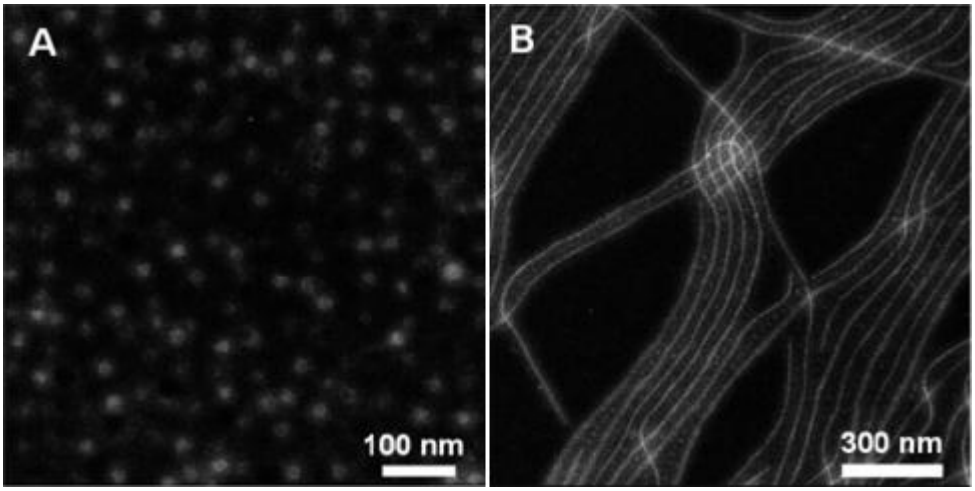

Figure 4.12 Dark-field TEM images of PFS_{17}-*b*-$P2VP_{170}$ micelles prepared from (A) methanol and (B) isopropanol.[53]

Impressively, in a following report they demonstrated a thorough kinetic study on the aforementioned polymer system. They monitored the sphere-to-cylinder transition over the period of 1 year in ethanol. An important observation was the growth in intensity of the characteristic crystalline PFS WAXD peak domains as the number and uniformity of the cylindrical micelles increased. This result provided strong evidence that the crystallisation of the core segment was the key driving force of this morphological transition (Figure 4.13).[54] It has been suggested that this is a result of a two-step process, where the initially formed spherical micelles undergo a nucleation event to form semicrystalline micelle nuclei, followed by a bidirectional epitaxial crystal growth resulting in a crystallisation driven sphere-to-rod transition (Figure 4.14).

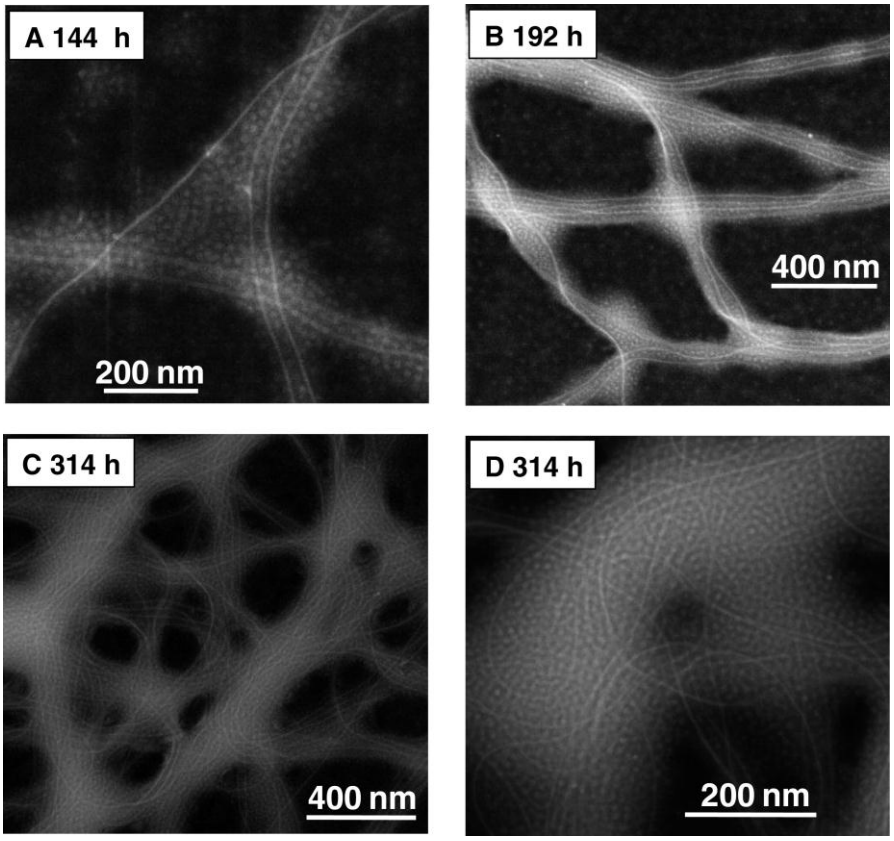

Figure 4.13 Dark-field TEM micrographs depicting structure evolution for a sample of PFS_{23}-b-$P2VP_{230}$ diblock copolymer in ethanol (1.0×10^{-4}g/mL) aged for different times at 20 °C: (A) 144 h; (B) 192 h; (C, D) 314 h at two different levels of magnification.[8]

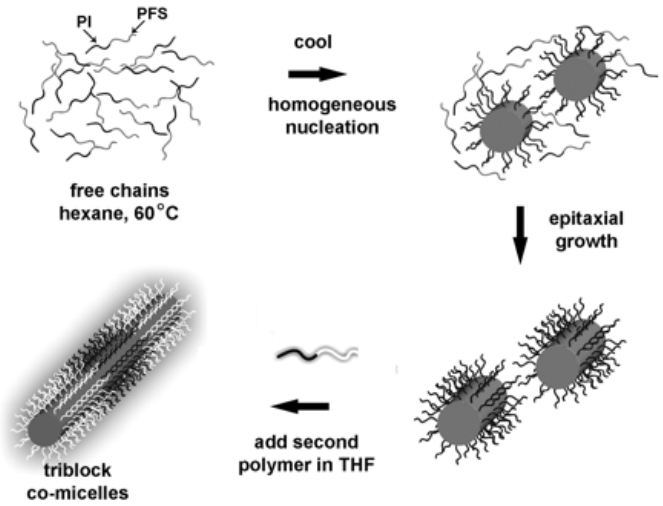

Figure 4.14 Manners and coworkers proposed a two-step process involving a homogeneous nucleation and an epitaxial crystal growth step.[55]

4.2.4 Other semicrystalline polymers in CDSA

A range of other studies regarding the crystallisation-driven self-assembly (CDSA) of various semicrystalline polymers have also yielded cylindrical micelles. Lazzari and Quintela reported the CDSA of polyacrylonitrile-*b*-polystyrene, PAN-*b*-PS, and polyacrylonitrile-*b*-poly(methyl methacrylate), PAN-*b*-PMMA, in non-polar selective solvents, where they found that cylinders were formed independently of the block ratio (Figure 4.15).[56]

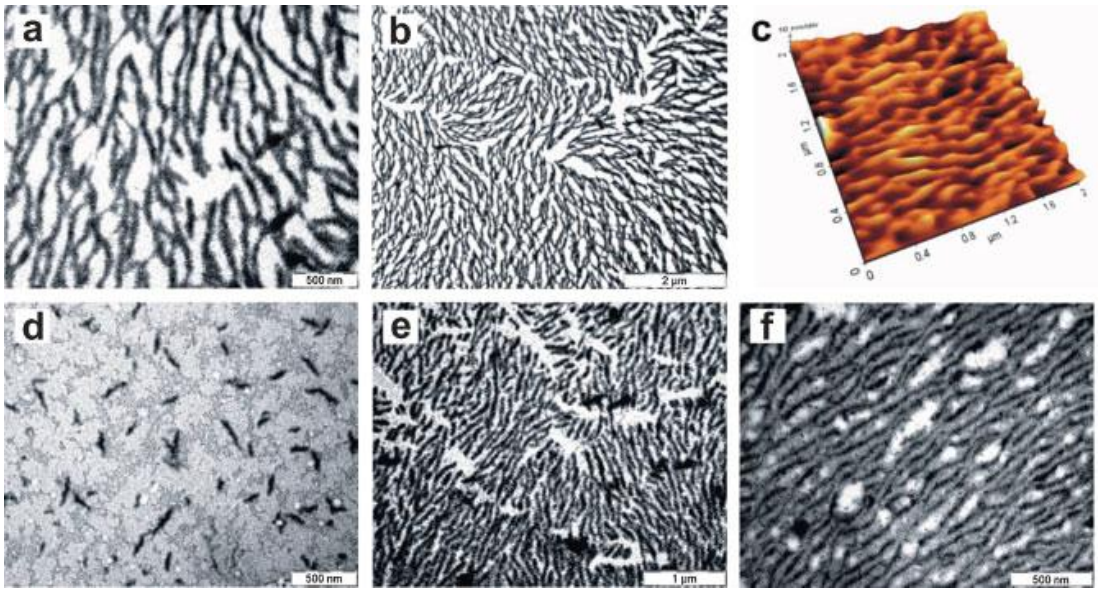

Figure 4.15 Cylinders and nanofibers observed for PAN-*b*-PS copolymers in chloroform/DMF mixtures.[56]

The micellisation phenomena of semicrystalline polylactide containing polymers have only recently been studied. Wang and coworkers found that cylinders were formed by a series of poly(3-caprolactone)-b-poly(L-lactide)-b-methoxy poly(ethylene glycol), PCL-b-P(L-LA)-b-mPEG, terpolymers. In this case the core of the micelle consists of dually crystalline PCL-b-PLLA segment. In this case the authors restricted their studies to polymers with longer hydrophobic than hydrophilic

blocks and only utilised a solvent switch based-micelle preparation methodology (Figure 4.16).[57]

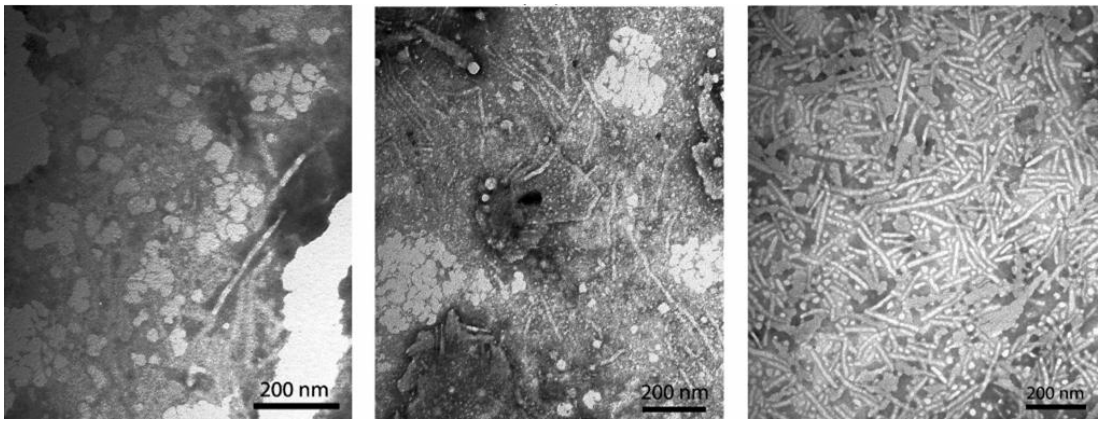

Figure 4.16 Different morphologies observed by Wang et al for a range of PCL-b-PLLA-b-mPEG block copolymers.[57]

In another report by Iwata *et al*. a poly(lactide)-*b*-poly(ethylene glycol), PLLA-*b*-PEG, diblock and a poly(lactide)-*b*-poly(ethylene glycol)-*b*-poly(lactide), PLLA-*b*-PEG-*b*-PLLA, triblock copolymers were studied. Nanobands were formed during the annealing of the polymer at 60 ^{o}C on a mica substrate.[58] No solution based assemblies were demonstrated in this case, while again the effect was studied for polymers with a longer hydrophobic than hydrophilic blocks. Bouteiller *et al.* studied the dually hydrophobic PLA-*b*-PCL and their assemblies in THF, and the authors managed to form cylinders by inducing the stereocomplex formation of two homochiral PLA block copolymer analogues.[59]

4.3 Results and discussion

4.3.1 P(THPA) hydrolysis reaction of P(*L*-LA)-*b*-P(THPA) to afford P(*L*-LA)-*b*-P(AA)

Poly(*L*-LA)$_{37}$-*b*-P(THPA)$_{333}$ (**3.6**) block copolymer synthesis was achieved using a combination of ring-opening polymerisation (ROP) of *L*-lactide and the reversible-addition fragmentation chain transfer polymerisation (RAFT) of THPA monomer that allows the preparation of well-defined polymers as reported in the previous chapter. The target block ratio of the polymer was around 1:10 thus strongly favouring the hydrophilic block (>70% wt) such that spherical micelles would be expected to result from their self-assembly in water under conventional conditions. We were interested in exploring the deprotection step of polymer **3.6** to form the P(*L*-LA)$_{37}$-*b*-P(AA)$_{333}$ (**4.1**) amphiphile. Our initial studies focused on the hydrolysis of P(THPA) esters to form the hydrophilic P(AA) block at 20 g·L^{-1}, 65 ^{o}C, 20% THF. By monitoring the signal disappearance by ^{1}H NMR spectroscopy at ~5.95 ppm in d_6-DMSO it was found that under our standard reaction conditions more than 98% of the P(THPA) monomeric units were converted to P(AA) within the first hour, while after 2 h complete conversion to P(AA) was observed (Figure 4.17). The conversion of poly(*L*-LA)$_{37}$-*b*-P(THPA))$_{333}$ (**3.6**) to poly(*L*-LA)$_{37}$-*b*-P(AA)$_{333}$ (**4.1**) was also followed by FT-IR where the characteristic signal of the carbonyl stretch at 1736 cm^{-1} shifted to 1708 cm^{-1} which corresponds to the carbonyl stretch of the resulting acid group (Figure 4.18).

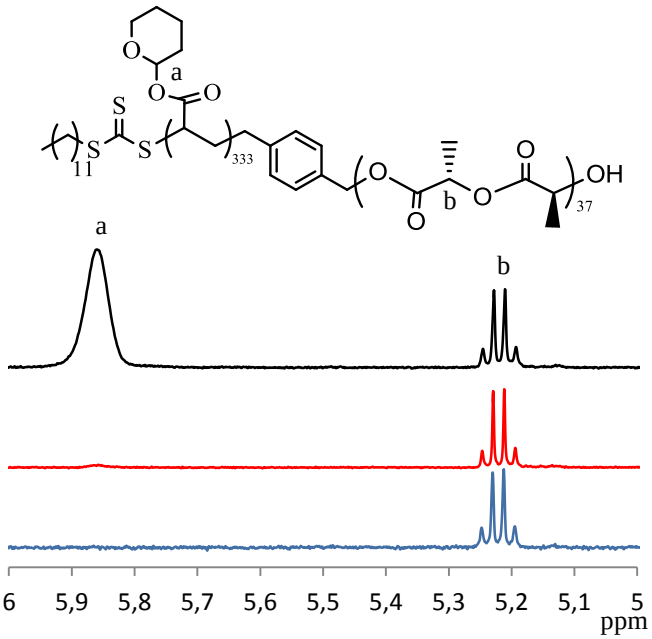

Figure 4.17 ^{1}H NMR spectrum of the poly(*L*-LA)$_{37}$-*b*-P(THPA)$_{333}$, **3.6**, before the THPA hydrolysis (top spectrum); 1 hour after the reaction commenced (middle spectrum); 2 hours after the reaction commenced (bottom spectrum). All spectra in d_6-DMSO, (400 MHz, 293 K).

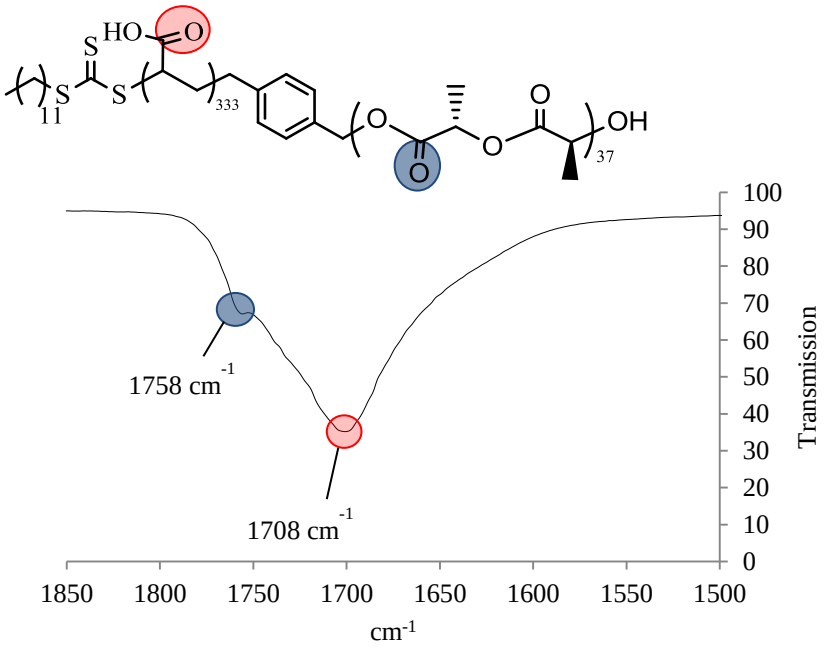

Figure 4.18 FT-IR spectrum of the P(*L*-LA)$_{37}$-*b*-P(AA)$_{333}$, **4.1** showing the carbonyl group stretch region.

Importantly, retention of the polylactide block stereoregularity under the PTHPA hydrolysis conditions was confirmed by comparison of the homonuclear decoupled ^{1}H NMR spectra before and after the exposure of the polymer under these conditions (Figure 4.19).

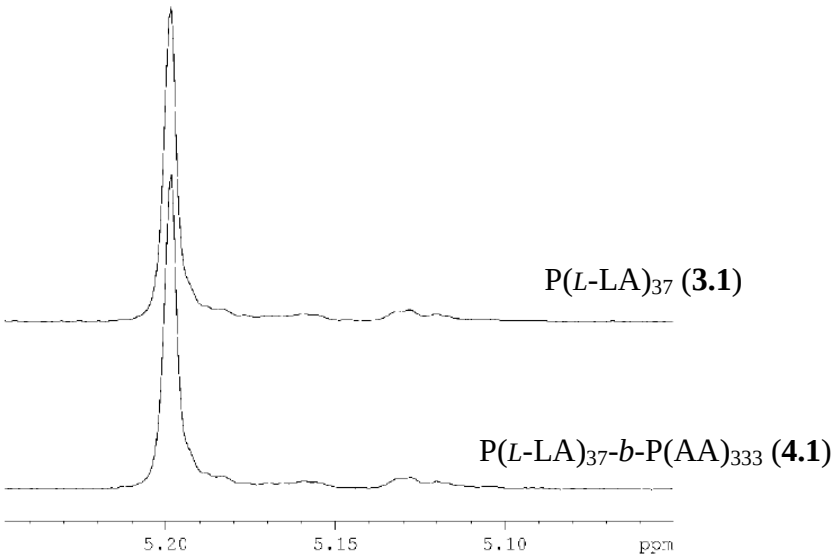

Figure 4.19 Homonuclear decoupled ^{1}H NMR spectrum of (a) P(***L***-LA) (**3.1**) and (b) P(***L***-LA)-*b*-P(AA) (**4.1**) in *d*6-DMSO (500 MHz, 293 K).

4.3.2 Self-assembly of P(*L*-LA)-*b*-P(AA) following the THPA hydrolysis reaction.

To more fully understand the self-assembly process, the behaviour of the P(*L*-LA)$_{37}$-*b*-P(AA)$_{333}$ (**4.1**) amphiphile under these deprotection reaction conditions was further investigated. It is noted however, that as a consequence of the high concentration under which these deprotection reaction was conducted, this solution was not directly suitable for characterisation by scattering or microscopy techniques and therefore samples were freeze dried and the polymers dispersed in a dilute aqueous solution (0.5 g L^{-1}) and kept at room temperature at all times. Importantly, under

these conditions the poly(lactide) core is glassy and therefore the particles are non ergodic (kinetically trapped). To demonstrate this, different dilutions were prepared and their stability was studied over 4 weeks. Virtually no differences were observed by DLS and TEM amongst the fresh solutions of different concentrations as well in the corresponding aged solutions, providing strong evidence that molecular exchange is restricted under these conditions and thus the particles present in the dilute solutions are representative of the particles formed at higher concentrations. Interestingly, analysis of the polymer solutions immediately post-deprotection and dilution by DLS and TEM analyses revealed the presence of spherical micelles. Dynamic light scattering (DLS) measurements of the solution after 2 hours showed the presence of structures with a hydrodynamic radius of (R_{av}=35 nm, PD=0.244) as it was revealed by CONTIN analysis while further studies by transmission electron microscopy (TEM) showed that there was only one population of particles in solution with a spherical morphology (Figure 4.20).

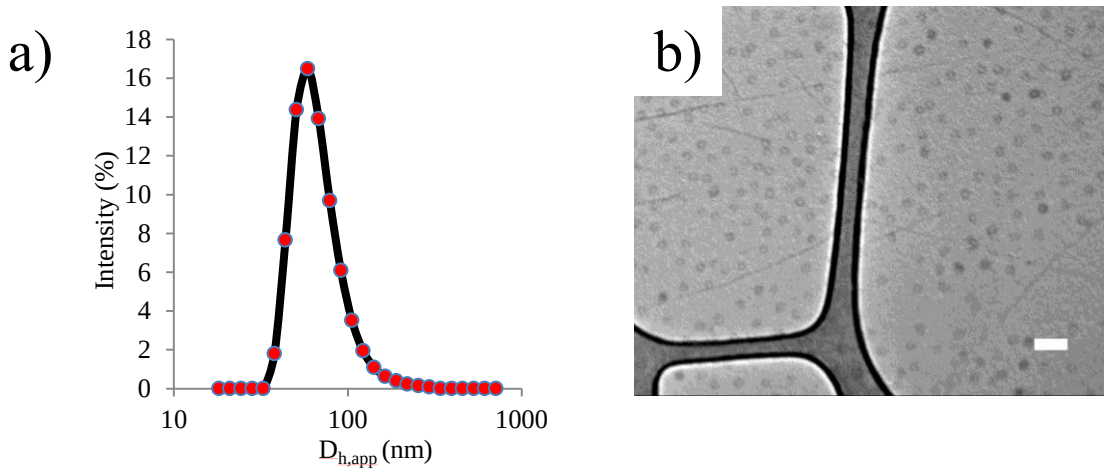

Figure 4.20 (a) DLS trace of the micelle solution 2 hours after starting the THPA hydrolysis reaction; (b) Representative TEM image of the spherical micelles 2 hours after starting the THPA hydrolysis reaction (Scale bar = 100 nm).

4.3.3 Sphere to cylinder transition of polymer 4.1

We speculated that the conditions utilised in the P(THPA) hydrolysis step could be controlled to enhance the core chain mobility aiding the polylactide block crystallisation. To further explore this scenario the solution was exposed under these conditions (at 20 $g \cdot L^{-1}$, 65 ^{o}C, 20% THF) for 30 hours and samples were removed after regular time intervals. By following the same protocol as before we could trap the formed particles in dilute solutions and subsequently follow the aggregation behaviour by DLS and TEM characterisation. After a total of 3 hours the aggregation state of the solution looked almost identical by DLS (R_{av}=36 nm, PD=0.258) and TEM however, after 5 hours (total) a second population in the particle size distribution, towards higher hydrodynamic diameter, appeared by DLS producing a bimodal distribution in CONTIN analysis. Further analysis of this sample by TEM illustrated the presence of some cylindrical particles in addition to spherical particles showing an onset of a sphere-to-cylinder transition. Importantly, the solution also contained significant amounts of nanoparticles that had a slightly anisotropic character as it was observed by TEM (Figure 4.21). These particles (that had very similar size with the spherical particles in solution) we speculate that could be micelles with a semicrystalline core. The crystallisation in the restricted environment of these particles could slightly deform them, introducing the degree of anisotropy observed. These particles could be a direct observation of the semicrystalline micelle nuclei that act as seed micelles for further growth of cylinders. Unfortunately it was impossible to obtain reliable information regarding the amount of these particles in solution. However, their presence in solution was notable in all stages of the transition. These observations suggested that after around 5 hours of heating

nucleation had already started to occur and cylinders begin to form. Given that spheres coexist with cylinders and the cylinders are observed to grow with time, a unimer growth mechanism similar to that observed previously by Manners and Winnik *et al*, is implied.

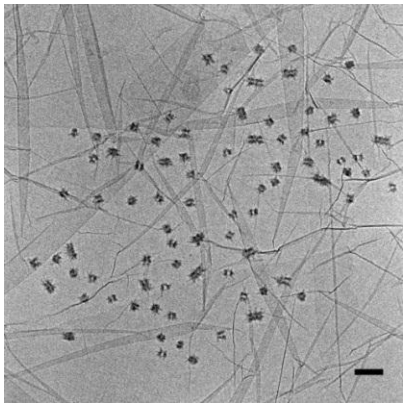

Figure 4.21 TEM image of the solution 5 hours after the THPA hydrolysis reaction commenced illustrating the presence of 'deformed' spherical micelles (Scale bar =100 nm).

Further aliquots were removed after 10, 15, 20 and 30 hours. Both TEM and DLS analyses showed that with the progress of time the amount of cylindrical particles gradually increased. After 20 hours TEM confirmed that ultimately a complete transition from spheres to cylindrical micelles was observed with average length of 346 nm, while DLS analysis showed only one population in solution with a size of (R_{av}=125 nm, PD=0.180). Importantly, in polarised dynamic light scattering conducted at a single angle both the translational and the rotational Brownian motion will contribute on the observed decay rates of the autocorrelation function. The rotational motion is not 'detectable' in the case of spherical particles due to symmetry. However, the rotational motion is of particular importance in samples that contain anisotropy as it will contribute in the observed decay rate and thus on the apparent diffusion coefficient calculated thereafter.

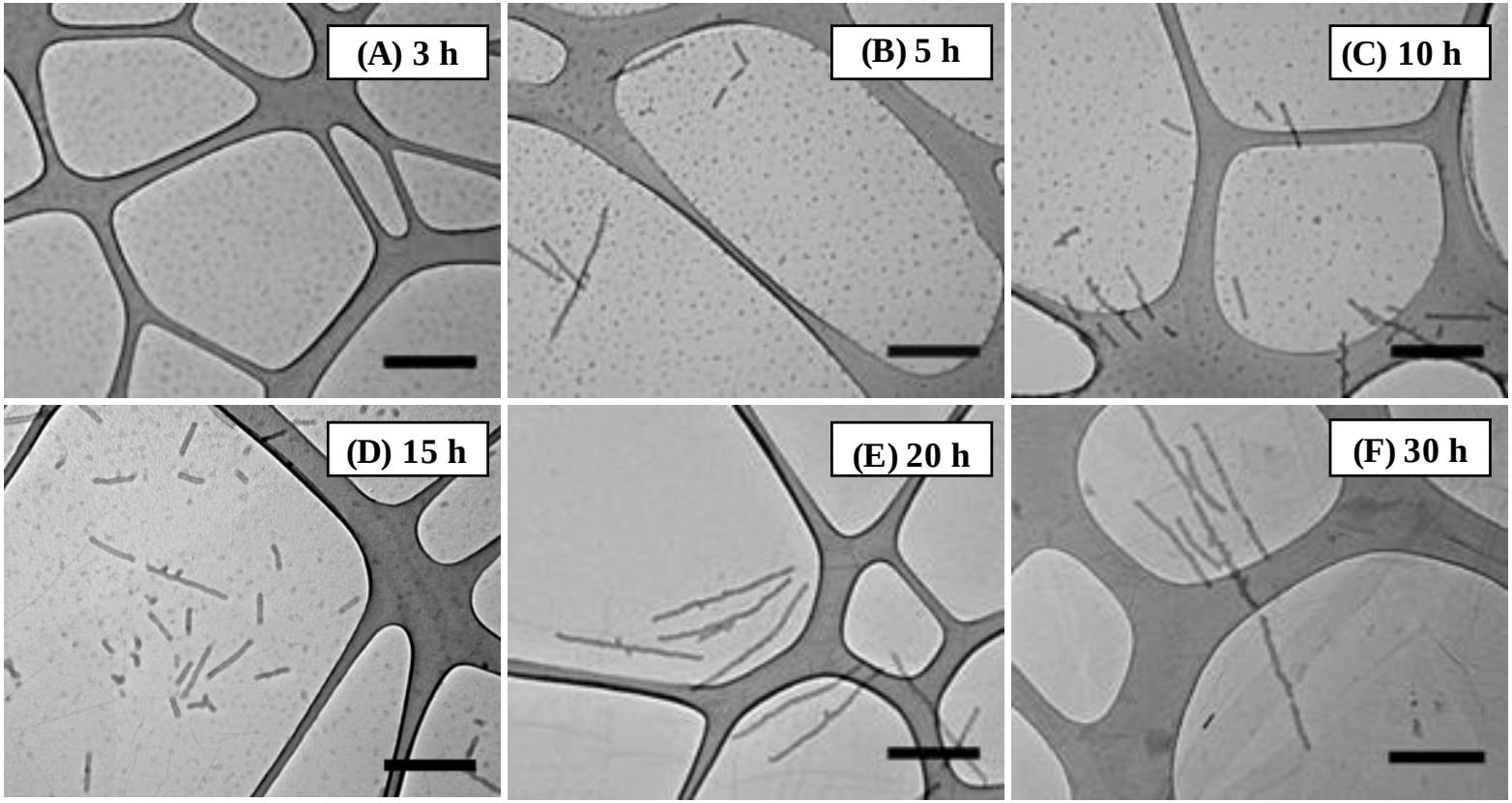

Figure 4.22 Representative TEM images of different time points of the *in situ* transition from spheres to cylinders following the THPA block hydrolysis: (A) 3 hours after starting the reaction; (B) after 5 hours ; (C) after 10 hours; (D) after 15 hours; (E) after 20 hours; (F) and finally after 30 hours Scale bars = 0.5μm.

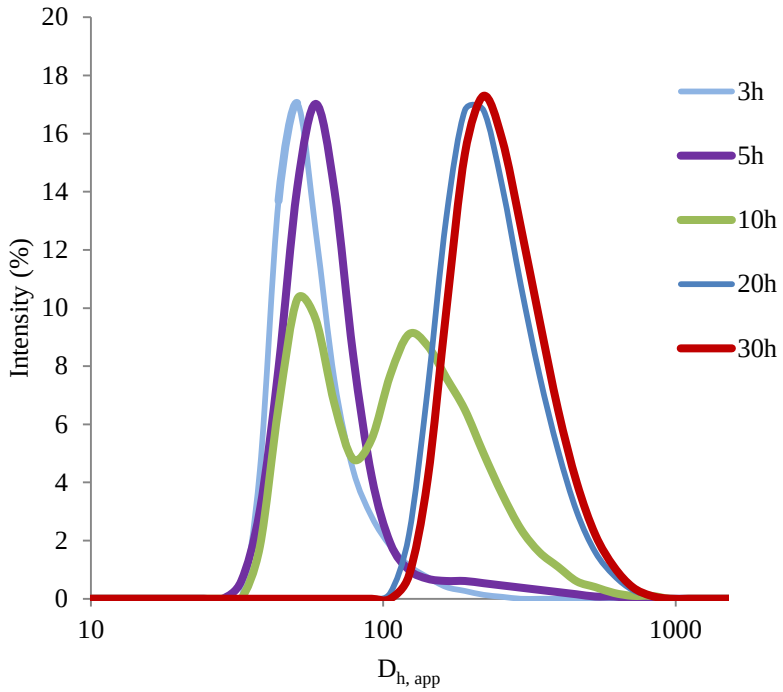

Figure 4.23 Size distributions obtained by dynamic light scattering illustrating the morphological transformation from spheres to cylinders.

Therefore, technically is not correct to introduce these diffusion coefficient values in the Stokes-Einstein equation because the latter deals exclusively with the translational Brownian motion. Furthermore, the conversion from an intensity distribution to a volume and number distributions performed by CONTIN analysis is based on the assumption that all the populations analysed have a spherical morphology. If this assumption is not satisfied then these conversions are subjected to potentially significant errors. Based on the above considerations the DLS data (number distributions) presented in Figure 4.23 potentially contain errors both on the x and y axis. However, these data are still valuable as unarguably the observed trend of shifting from the original population to a second population is based on a real change in the detected decay rates and in these terms DLS can provide important

semi-quantitative information regarding the amount and kind of populations in solution. Furthermore, we used a second alternative method to analyse our data that was perhaps more consistent with the underlying theory. In this case analysis of the correleograms based on the empirical Kohrausch-Williams-Watts (KWW) stretched exponential equation was carried out (Figure 4.24).[60] This gave evidence of the presence of a single relaxation time, thereby avoiding inconsistencies with the theory regarding the processing of the data.

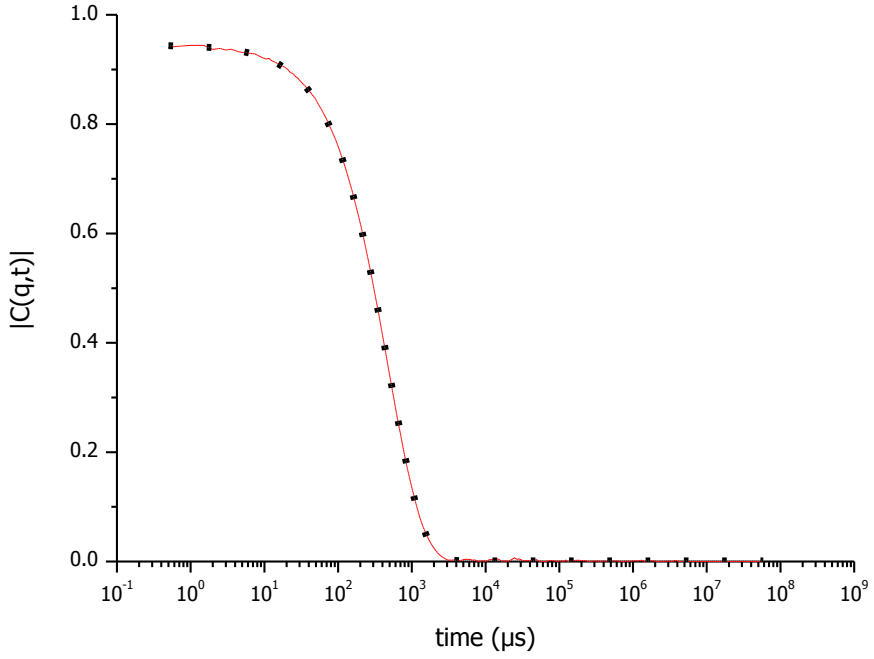

Figure 4.24 DLS correleogram of the cylinders solution obtained after 20 hours of heating polymer **4.1** at 65 ^{o}C in H2O/THF (8/2 v/v) (red line) indicating the presence of a single relaxation time as suggested by the good fitting in the corresponding KWW stretched exponential expression (black points).

To probe the role of crystallinity in this morphological transformation, WAXD analysis was performed for each of the previously studied time points. Observation

of the characteristic Bragg peak at ~16.6^{o} 2θ angle that corresponds at the (110)/(200) reflections of the semicrystalline poly(*L*-LA) domains provided a handle with which we could monitor the evolution of crystallinity within the poly(*L*-LA) core (see Figure 4.25).

The WAXD results revealed an excellent correlation between the degree of core crystallinity contained and the percentage of cylindrical particles in solution giving strong evidence of the key role of crystallisation in the self-assembly process. The first sample, measured after 3 hours contained no crystallinity and its WAXD spectrum produced a very broad peak in the spectra, characteristic for an amorphous material, in good agreement with the DLS and TEM analyses in which only spherical particles were observed. The sample taken after 5 hours showed a very weak peak at the expected characteristic 2θ angle for semicrystalline PLA, showing that the formation of cylinders occurred upon the crystallisation event. Analysis of the subsequent samples revealed a gradual increase in the crystalline content. After 20 hours, the point that we observed complete transition to cylinders, the crystallinity content reached a maximum. The broad character of the peaks observed is typical of small crystals, which is consistent with the fact that the crystal growth takes place in the restricted environment of micelle cores.

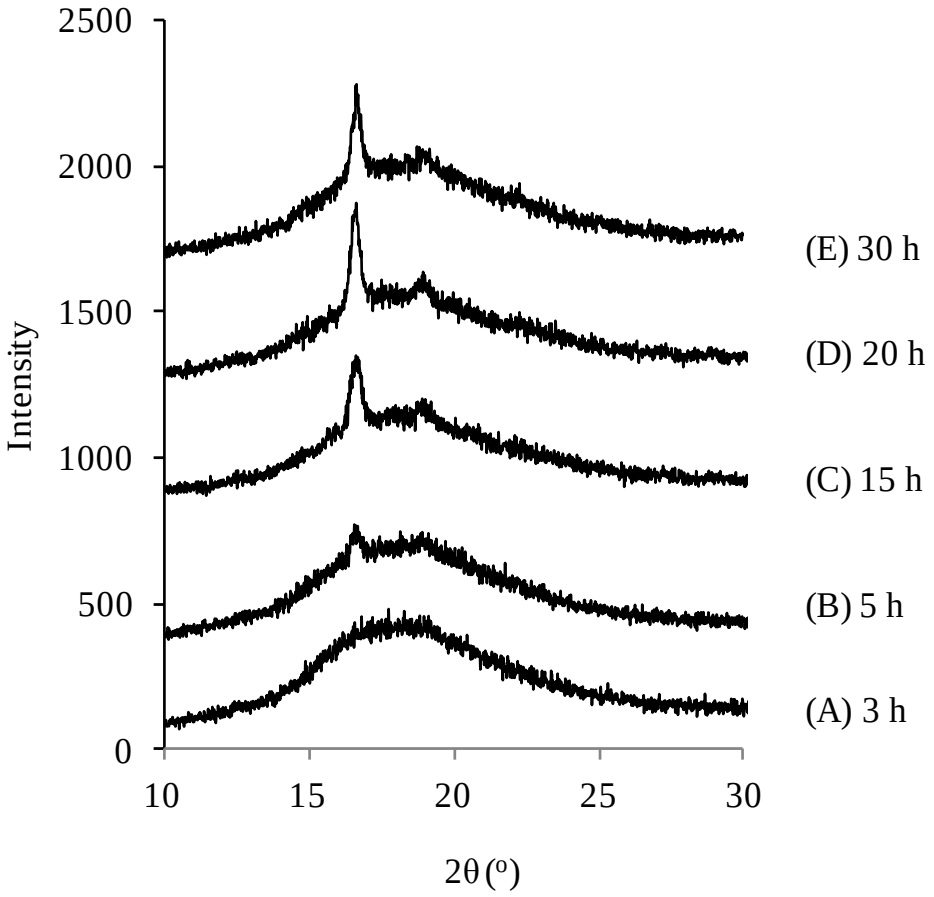

Figure 4.25 Offset WAXD spectra showing the increase of crystalline content during the cylinder formation (A) 3 hours after starting the reaction; (B) after 5 hours; (C) after 15 hours; (D) after 20 hours; (E) and finally after 30 hours.

In addition, samples were analysed by small angle neutron scattering (SANS). The SANS pattern for the sample after 3 hours was consistent with the presence of spherical morphology in solution. In the following samples the scattering pattern gradually changed, giving an indication of a change in morphology while the SANS pattern of the sample after 20 hours had a better fit on a model of rod-like particles. These results further suggested that a sphere-to-cylinders transition took place during heating of the sample at 65 ^{o}C in H_2O/THF (8/2 v/v) for 20 hours (Figure 4.26).

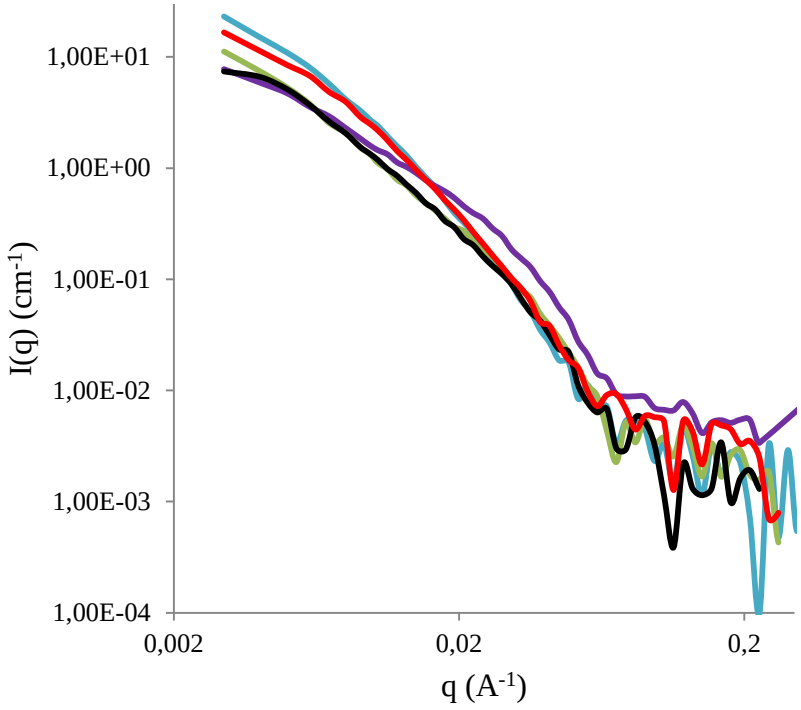

Figure 4.26 Small angle neutron scattering (SANS) data for 3 hours after starting the reaction (black pattern); after 5 hours (purple pattern); after 10 hours (green pattern); after 15 hours (red pattern) and after 20 hours (blue pattern) illustrating the transition from spherical to cylindrical morphology.

4.3.4 Study of the effect of concentration and common solvent content

To date, only a few reports regarding concentration and solvent effects on the self-assembly of crystalline-coil polymers exist. Winnik, Manners and coworkers studied the influence of different solvents on the crystallisation-driven self-assembly of a PFS-PI diblock copolymer. Interestingly, they found that by increasing the quality of the solvent for the PFS block the transition to cylinders was slower while the formed cylinders were significantly longer.[8] The authors demonstrated that in a better solvent for PFS, the micelle nucleation was disturbed resulting in a slower formation of fewer semicrystalline nuclei. This effect directly correlates to the kinetics and size of the cylinders. In another report by Lazzari *et al*. a PAN-*b*-PS copolymer was

shown to yield longer cylinders in solvent mixtures with a better quality for the semicrystalline PAN block.[56] In this case the authors suggested that the increased length was a result of faster crystal growth due to the increased core mobility. To study the effect of polymer concentration and solvent quality in our system we systematically varied these two parameters and analysed the samples after 20 hours, always following the same work up procedures. Interplay between the semicrystalline micelle nucleation and micelle growth seemed to affect in each case the length and quality of the cylinders. Sufficient core mobility for the required chain rearrangements is essential, however exceeding a critical point can disturb the crystallisation process, resulting in slower kinetics or complete inhibition of the crystallisation event. The self-assembly temperature, concentration of the polymer and the quality of the solvent are all means with which to fine tune the dynamics of the formed micelles and thereby their ability to crystallise. A range of THF contents (5, 10, 20 and 40 vol%) for the assembly process was studied. A trend of increased cylinder length was observed as the ability of the solvent mixture to solvate the hydrophobic PLA block increased (Figure 4.27 - Figure 4.30). Interestingly, this is the opposite of that expected when solvophobic forces dictate that smaller micelles would be expected due to reduced surface tension in the core solvent interface. The effect observed herein can be related to the disturbance of the nucleation and/or faster crystal growth rates based on a unimer growth mechanism due to enhanced polymer chain mobility as the ability of the solvent to solvate the core block increases.

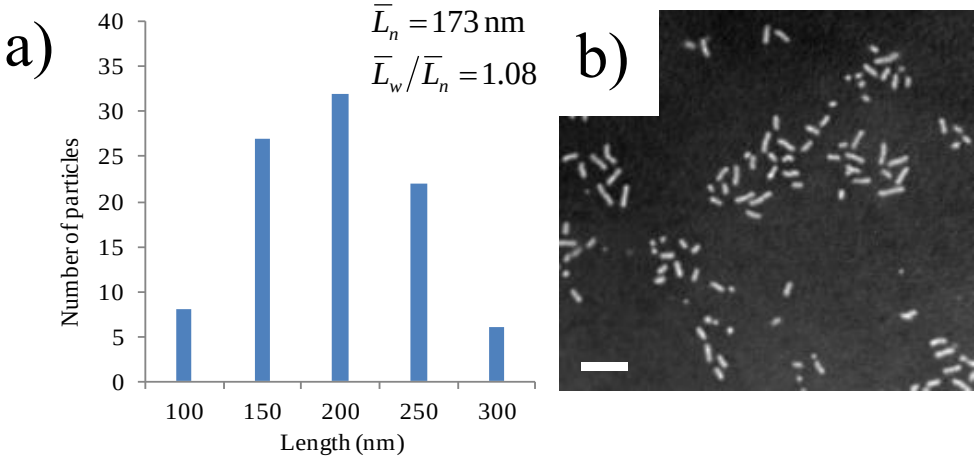

Figure 4.27 a) Histogram of the cylinders length produced from the self-assembly at 20 g·L^{-1} 5% THF; b) representative TEM image of the micelle solution produced from the same solution stained with PTA (Scale bar=200 nm).

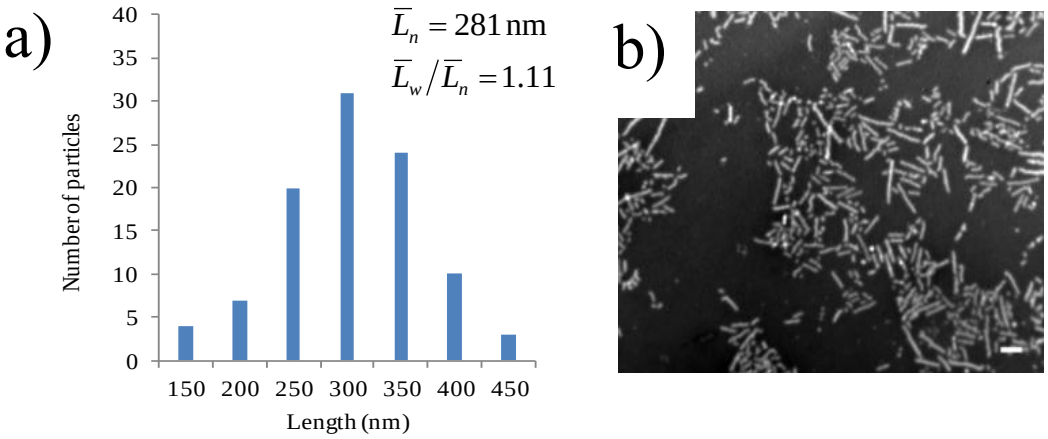

Figure 4.28 a) Histogram of the cylinders length produced from the self-assembly at 20 g·L^{-1} 10% THF; b) representative TEM image of the micelle solution produced from the same solution stained with PTA (Scale bar=200 nm).

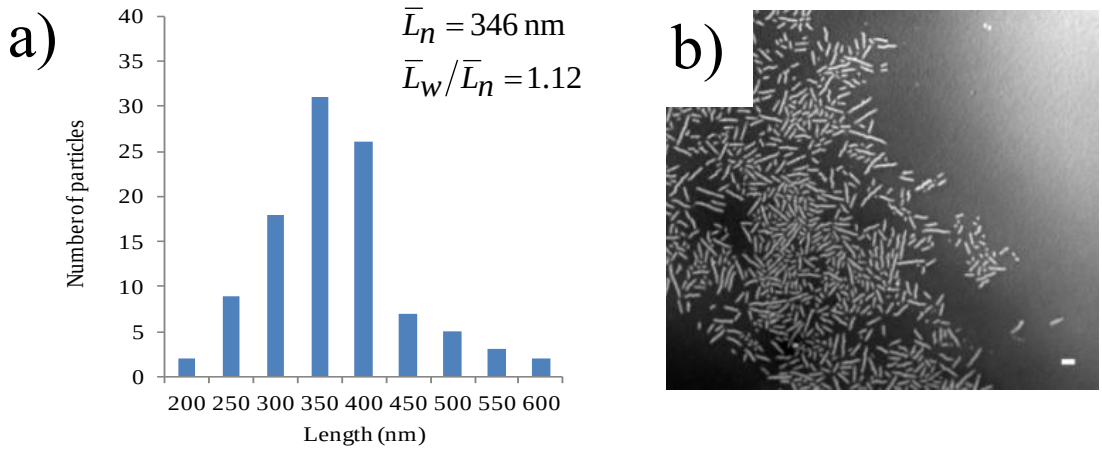

Figure 4.29 a) Histogram of the cylinders length produced from the self-assembly at 20 g·L^{-1} 20% THF; b) representative TEM image of the micelle solution produced from the same solution stained with PTA (Scale bar=200 nm).

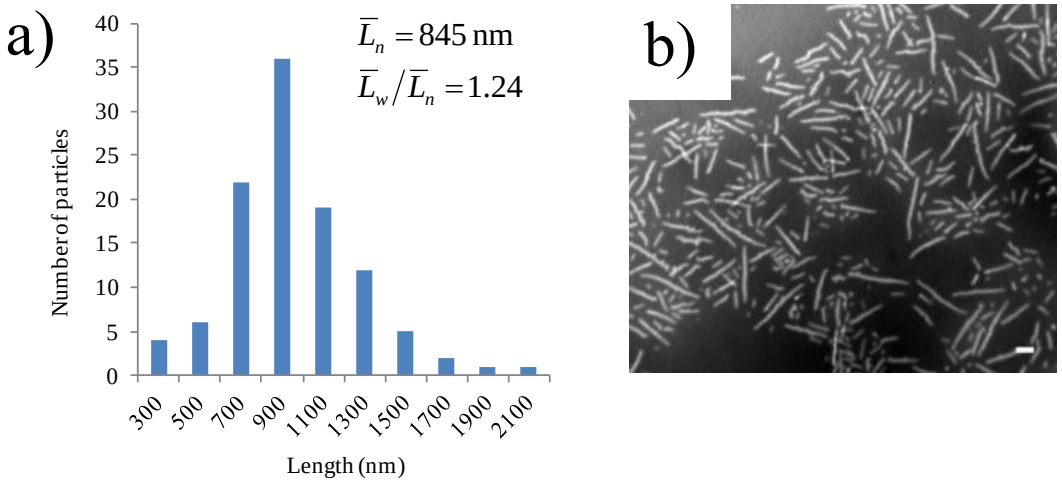

Figure 4.30 a) Histogram of the cylinders length produced from the self-assembly at 20 g·L^{-1} 40% THF; b) representative TEM image of the micelle solution produced from the same solution stained with PTA (Scale bar=200 nm).

Furthermore, the length could be affected by the colloidal stability of the particles, which in turn could be affected by a number of parameters such as the length of the hydrophilic block, the end groups present, the quality of the solvent and the concentration of polymer in solution. In order to compare the dispersities of the cylinders length produced under different conditions $\overline{L}_w/\overline{L}_n$ values were calculated (see experimental part for more details). A trend of increased dispersity was found for the cylinders synthesised with higher THF amounts.

To study the effect of concentration on the sphere-to-cylinder transition, solutions of different concentrations were studied ranging from 0.5 to 50 g L^{-1}. The concentration effects can be divided in two concentration regimes. The first regime includes concentrations lower than 1 g L^{-1}. In these solutions only spherical micelles were formed as determined by TEM studies, while the resulting materials did not contain any crystallinity as was evidenced by WAXD analysis, demonstrating that such low concentrations are not sufficient to induce nucleation and therefore no cylinders are formed.

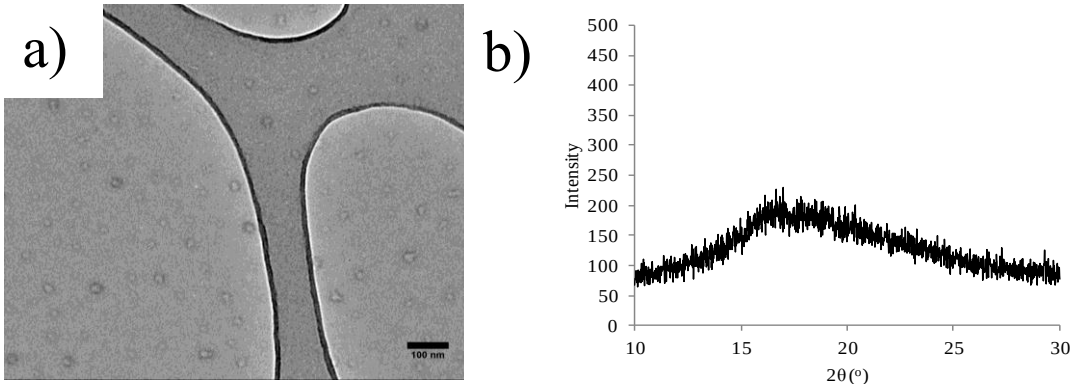

Figure 4.31 a) Representative TEM image of the micelle solution produced from the self-assembly of **4.1** at 0.5 g·L^{-1} (20% THF); (b) WAXD pattern of the sample that was self-assembled at 0.5 g·L^{-1}.

The present studies focus in the high concentration regime (typically c >5 g L^{-1}), where we found that the micelle core nucleation is more favoured (compared to more dilute solutions at 65 ^{o}C). The micelle dynamics, the unimer concentration in solution and the intermicelle interactions are all important micelle characteristics and may all contribute to the enhanced nucleation rates at higher concentrations. However, based on the concentration data it would appear that there is a critical nucleation concentration that produces sufficiently stable nuclei for the crystal growth to initiate. From our kinetic studies it is revealed that new semicrystalline micelle nuclei are formed continuously in the whole course of the transition and hence no linear relationship between the cylinder length and time is observed in a process exhibiting similarities with a free radical polymerisation (slow initiation relative to propagation). Clearly, the extended deprotection reactions at high concentration lead to the formation of some crystalline and some amorphous material. The crystalline material can act as 'seed' for cylinders growth through non-crystalline unimer addition.

4.3.5 Control of the morphology

Following these results, we investigated if switching between the two morphologies based on cycles of erasing and recycling the micelle crystallinity was possible. For these studies a solution of cylindrical micelles with a crystalline core of polymer **4.1** was freeze dried and subsequently stirred in THF overnight to dissolve the previously formed aggregates and destroy crystallinity. The polymer was then dried under vacuum and resuspended into an aqueous solution by directly dissolving in nanopure water (0.5 g L^{-1}) at ambient temperature. Under these conditions, nucleation and growth of P(*L*-LA) crystals cannot take place and therefore

solvophobic effects dominate the self-assembly process. The product was characterised by TEM to confirm the formation of spherical particles (Figure 4.32). This solution was freeze dried and analysed by WAXD, where no Bragg peaks were observed thus indicating that the self-assembled structures were indeed noncrystalline. The solution of spheres was then exposed to the same conditions that first introduced the crystallinity (65 ^{o}C, 20 g L^{-1}, 20% THF). Reformation of cylinders with very similar size and quality was achieved (L_n = 315 nm, L_w/L_n = 1.10), illustrating that recycling the crystallinity as confirmed by WAXD and morphology of the assembled polymer can be readily performed, with no effects on the quality of the self-assembled products.

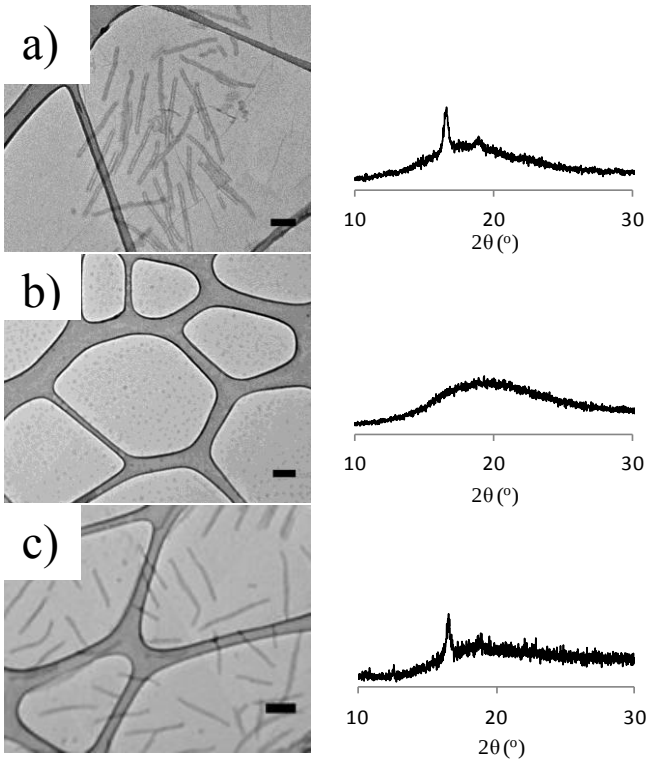

Figure 4.32 On the left column: Representative TEM images of the P(*L*-LA)$_{37}$-*b*-P(AA)$_{333}$, **4.1** morphology in water: (a) following the first crystallisation cycle; (b) after erasing crystallinity; (c) after recycling crystallinity. Scale bars = 200 nm. On the right column: the corresponding WAXD patterns.

4.3.6 Self-assembly behaviour of P(*DL*-LA)-*b*-P(AA) block copolymers

To further highlight the role of crystallisation in this system and demonstrate that is not a concentration or solvent quality effect alone that alters the morphology in solution, P(*DL*-LA)$_{33}$-*b*-P(THPA)$_{240}$ (**3.11**) that was synthesised in the previous chapter was utilised. In this case the PLA block is atactic and therefore is amorphous. The polymer was exposed to the same conditions and work up protocols as previously described in section 4.3.3 in order to form P(*DL*-LA)$_{33}$-*b*-P(AA)$_{240}$ (**4.2**) and undergo the sphere-to-cylinder transition. At all time points, DLS and TEM analyses (Figure 4.33) confirmed the presence of one population with a spherical morphology and WAXD analysis confirmed the absence of crystallinity (Figure 4.33). The hydrodynamic radius of the spheres was 32 nm; which is very similar value to the one obtained from the spheres at the initial stages of the sphere-to-cylinder transition. This result gives further evidence that the cylinder formation is the result of the crystal growth taking place in the core of the micelles which is present when a crystalline PLA is used.

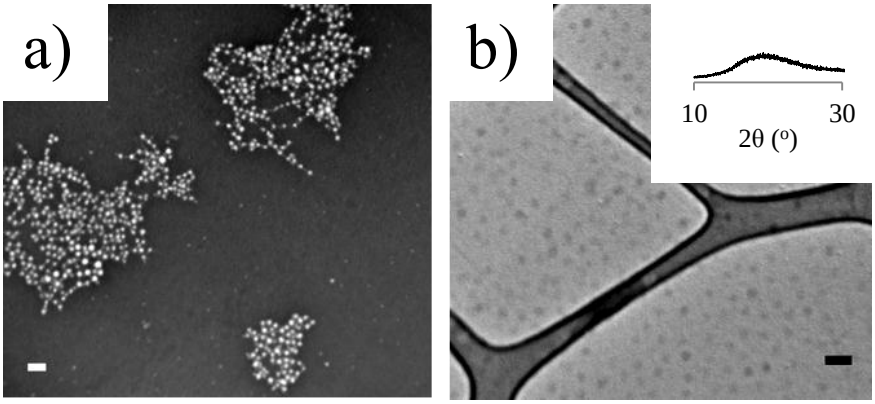

Figure 4.33 a) Representative TEM image of the micelle solution produced from the self-assembly of poly(*DL*-LA)-P(AA), (**4.2**) at 20 g/L 20 hours after starting the THPA hydrolysis reaction (with PTA staining). b) and on a GO support (Scale bars = 100 nm). Inset: WAXD pattern of polymer **4.2** self-assembled at 65 ^{o}C for 30 hours H_2O/THF (8/2 v/v).

4.3.7 CDSA with synchronous evaporation of the organic solvent

The crystallisation driven self-assembly of polymer **4.1** was also performed with a different experimental set-up. In this case the organic solvent was evaporated during the self-assembly step by introducing an outlet in the reaction vessel (see experimental part for set-up details) ($B.P_{THF} = 66\ ^oC$).

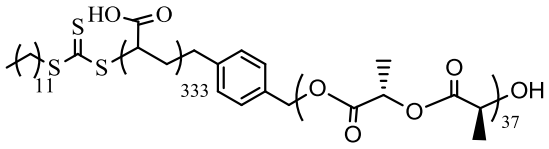

Figure 4.34 Chemical structure of polymer **4.1**

Obviously, this experimental approach introduced a new variable in the system of which we did not have precise control. Important drawbacks of this methodology were the lack of exact knowledge of the composition of our self-assembly solution in each stage of the CDSA but also the fact that the exact composition of the solution as a function of time depended on the scale in which the self-assembly experiment was performed. Nevertheless, this methodology produced good results comparable with those of our standard methodology. Interestingly, a broad variation of the attained length was found from batch to batch that was perhaps related to the inconsistency of the exact experimental set-up which in turn could affect the evaporation rate. Importantly, the evaporation of the 'good' solvent for the PLA block could promote the crystallisation of PLA through its supersaturation. It is remarkable that with the means of this method we got access to by far the longest cylinders ($L_n > 3$ μm) we have formed so far with this self-assembly system (Figure 4.35b). However, due to the aforementioned barriers the self-assembly conditions were not easily reproducible and in many cases shorter cylinders were formed. Figure 4.35a and

Figure 4.35b illustrate an example where the same polymer formed particles of very different characteristics.

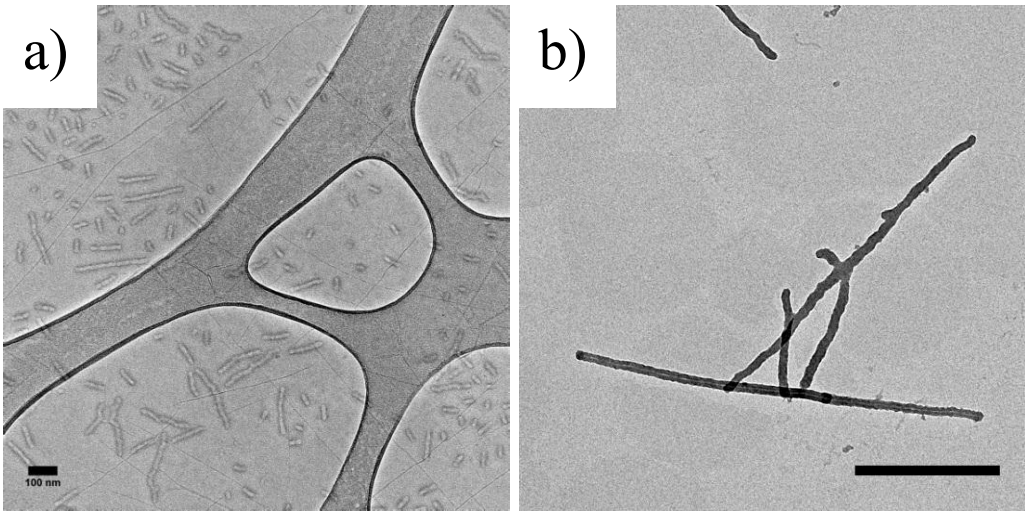

Figure 4.35 Example of cylinders formed by polymer **4.1** with the solvent evaporation method; in both cases the starting self-assembly conditions were 20g·L^{-1}, 65 ^{o}C, 20% THF; a) Scale bar = 100nm; b) Scale bar = 1000nm

4.3.8 Study of the CDSA of P(*L*-LA)-*b*-PAA with removed end group

Interestingly, the RAFT end group at the end of the hydrophilic block of the polymers that we studied so far has a strong hydrophobic character. It was proposed recently by Manners *et al*[61] and also by Park and coworkers[62] that the colloidal stability of the particles can have a significant effect on the crystallisation process of systems based on polythiophenes. In their case they found an inverse relationship between the length of the corona and the length of the cylinders. In addition, interactions of the end group with the hydrophobic core could potentially affect the crystal growth taking place in the core. We were interested to investigate if the RAFT end group had an effect on the CDSA process of our system. For this reason we repeated the same self-assembly experiments with the polymer that had been end group modified as prepared in Chapter 3. The polymer **3.17** was exposed under the

same conditions as previously to hydrolyse P(THPA) and form P(*L*-LA)$_{37}$-*b*-PAA$_{264}$ (**4.3**) (65 ^{o}C, 20 g L^{-1}, 20% THF).

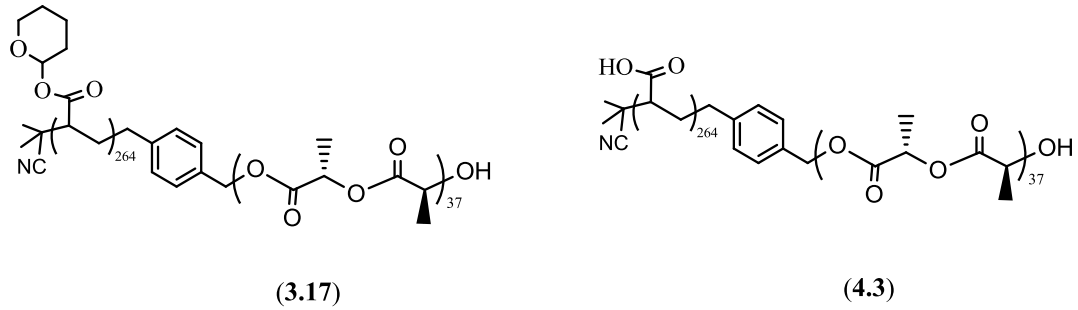

(**3.17**) (**4.3**)

Figure 4.36 Chemical structure of diblock copolymer before PTHPA hydrolysis (**3.17**) and after PTHPA hydrolysis (**4.3**)

The TEM results illustrated cylindrical particles with slightly shorter average length (288 *versus* 346 nm) and very similar disperisty characteristics compared to polymers containing the RAFT end group. These results led us to the conclusion that although the end group did not have a key effect on the process, it can influence the cylinder length to a certain extent.

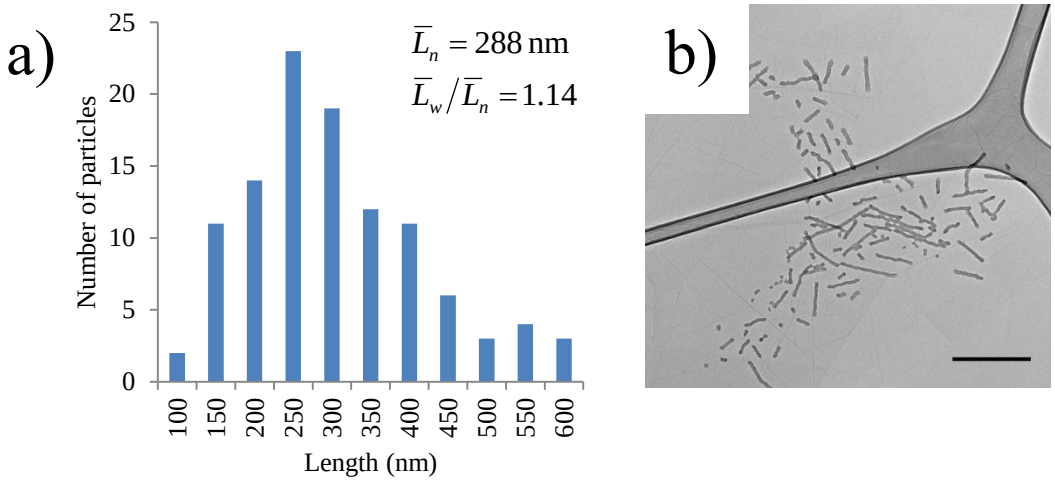

Figure 4.37 TEM image of cylindrical particles observed for polymer self-assembled at 20 g L^{-1}, 20% THF with removed end group (**4.3**) (Scale bar = 500 nm).

4.3.9 Study of the CDSA of polymer P(*L*-LA)-*b*-PAA with the pyrene end group

Furthermore, we also studied the self-assembly behaviour of a polymer containing the pyrene (Py) end-group, poly(L-LA)$_{37}$-*b*-PAA$_{264}$ (**4.4**). In this case cylinders of similar length and dispersity were observed by TEM characterisation, and WAXD analysis of this sample illustrated the presence of crystallinity. Interestingly, a curvy surface was identified by TEM examination (Figure 4.38). A possible explanation was that, due to the strong hydrophobic character of Py; the latter could 'back-bite' in the hydrophobic core of the cylinder giving rise to the formation of a flower-like coronal morphology. It is well known that the fluorescence behaviour of Py strongly depends on the environment and different bands on the emission and excitation spectra are observed depending on whether the Py is located in a hydrophilic or hydrophobic environment.[63] In order to test our hypothesis, we used this property of Py as a `means to probe the location of our end group. Specifically, we examined the red shift in the excitation spectrum that accompanies the transfer of Py from a hydrophilic to a hydrophobic environment. By comparing the fluorescent excitation spectra for our AIBN-Py initiator with the cylindrical micelles containing Py as an end group we found a shift to a higher wavelength for the latter, indicating that Py was not dispersed in water but it was instead situated in a hydrophobic environment (Figure 4.39b). Furthermore, CONTIN analysis of the DLS data showed one population with a hydrodynamic diameter in the range of 250 nm, suggesting that no intermicellar aggregation was present in solution (Figure 4.39a). Interestingly, the fact that Py interacts with the polylactide core did not affect the crystallisation of the

core during the CDSA process as revealed by WAXD analysis (Figure 4.40) and thus well-defined cylinders could be obtained.

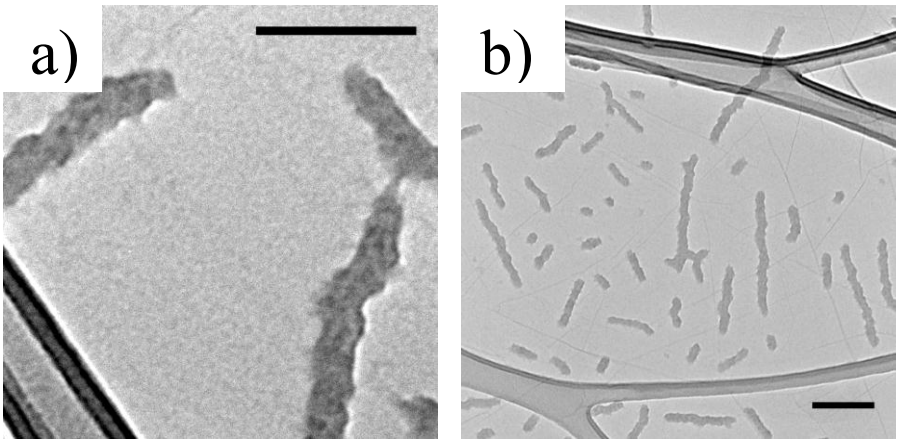

Figure 4.38 (a) TEM image of the cylinder solution with a pyrene end group (Scale bar = 100 nm); (b) Representative TEM image of the cylinders with pyrene end group in lower magnification (Scale bar = 200 nm).

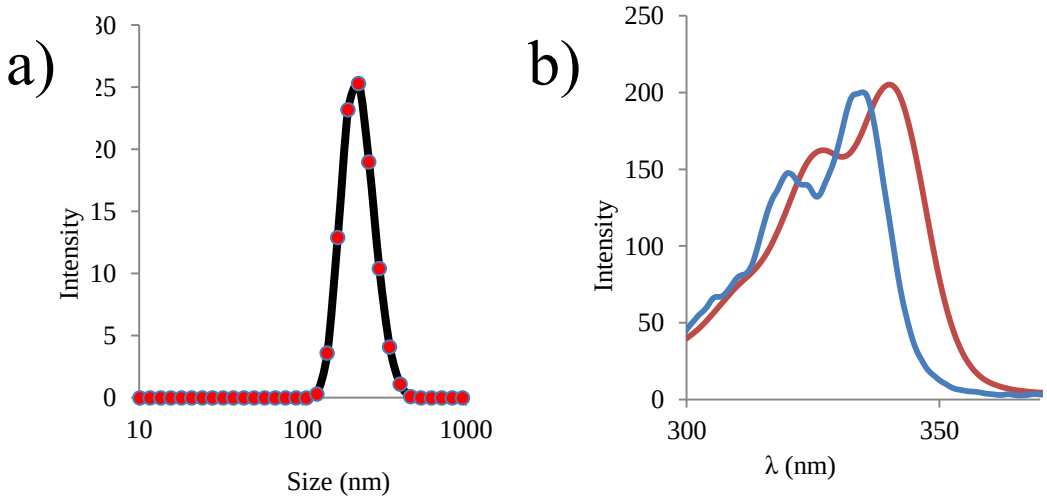

Figure 4.39 (a) DLS data for the cylindes containing Py as the end group; (b) Excitation spectrum of the pyrene initiator in water (**3.19**) (blue graph) and of the cylinders solution with the pyrene end group (**4.4**) (red graph).

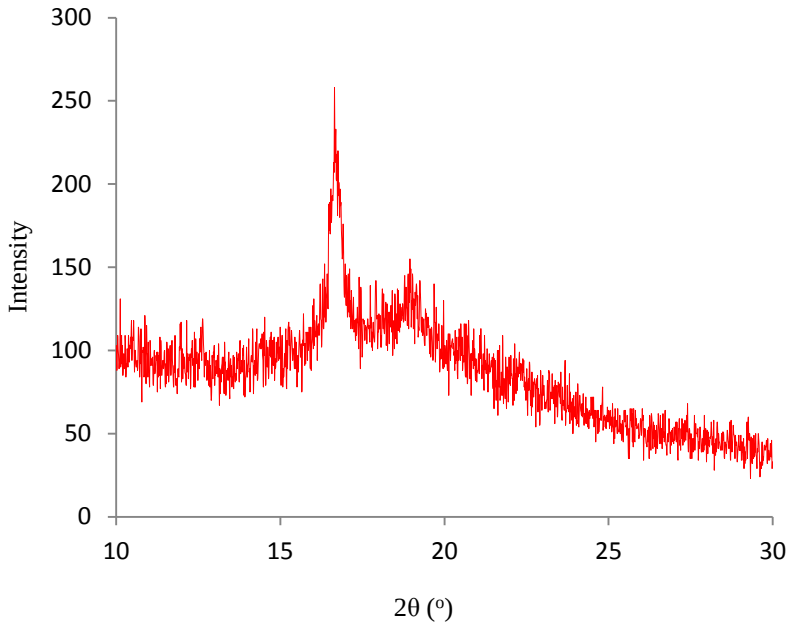

Figure 4.40 WAXD pattern of the cylinders generated by polymer **4.4** illustrating the presence of crystallinity.

4.3.10 Study of P(*L*-LA)-*b*-PAA-*b*-PTEGA triblock copolymer in CDSA

In Chapter 3 we described the synthesis of P(*L*-LA)$_{37}$-*b*-PTHPA$_{264}$-*b*-PTEGA$_{32}$ triblock copolymers. Herein we explore the self-assembly behaviour of the corresponding P(*L*-LA)$_{37}$-*b*-PAA$_{264}$-*b*-PTEGA$_{32}$ copolymers under our CDSA conditions. The methodology we followed was the same as the one we used with the diblock copolymers. Polymer **3.14** was exposed to our standard PTHPA hydrolysis/CDSA conditions (20 g·L^{-1}, 65 ^{o}C, 20% THF) for 30 hours in order to facilitate the PTHPA hydrolysis to afford the corresponding P(*L*-LA)$_{37}$-*b*-PAA$_{264}$-*b*-PTEGA$_{32}$ (**4.5**) and sequentially undergo CDSA in a one pot scheme. Interestingly, this polymer exhibited poor solubility during the CDSA and precipitated out of solution. That was perhaps a consequence of the LCST behaviour of the PTEGA block. For this reason these assemblies were conducted under more dilute conditions

(5 g·L^{-1}, 65 ^{o}C, 20% THF). Once the self-assembly was complete (30 h) the product was freeze dried and dissolved in a 0.5 g·L^{-1} aqueous solution that was suitable for characterisation by scattering and microscopy techniques. Initially the particles were characterised by DLS, which confirmed that only one population was present in solution ($D_{h,app}$ = 396 nm, PD = 0.064) (Figure 4.41). Furthermore the samples were analysed by TEM; first in the presence of a heavy metal staining agent (phosphotungstic acid) from which we found that well defined particles of an average length of 370 nm had been formed. Interestingly, the cylinders had a distinct appearance on their two sides (see Figure 4.42b). Further characterisation on graphene oxide supports (without the addition of a heavy metal stain) revealed a characteristic 'hairy' appearance on the two sides of the cylinders, which we speculate to be due to the low T_g of the P(TEGA) blocks (Figure 4.43b).

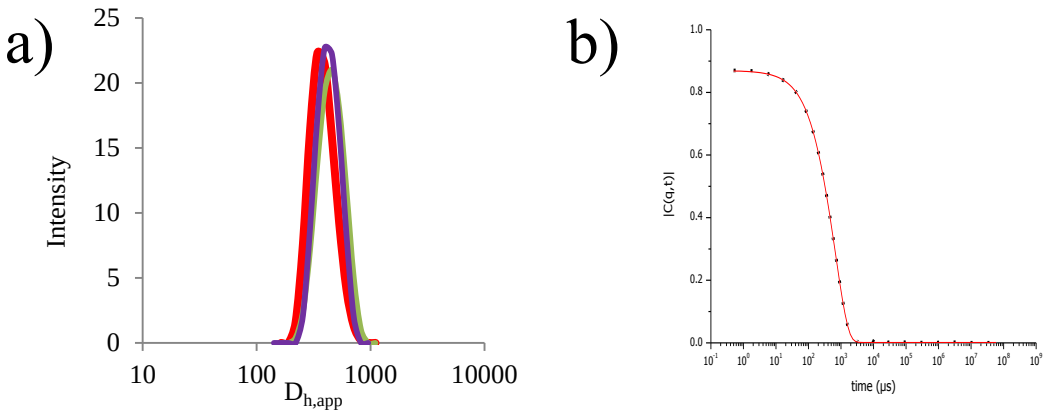

Figure 4.41 (a) Intensity, volume and number distributions by Dynamic light scattering (DLS) CONTIN analysis of the P(*L*-LA)$_{32}$-*b*-PAA$_{264}$-*b*-PTEGA$_{32}$ (**4.5**) triblock copolymer cylinders self-assembled at 5 g·L^{-1}, 20% THF; (b) DLS correleogram (red line) of the same cylindrical micelles and the fitting in the KWW stretched exponential expression (black points) which illustrates the presence of a single relaxation time.

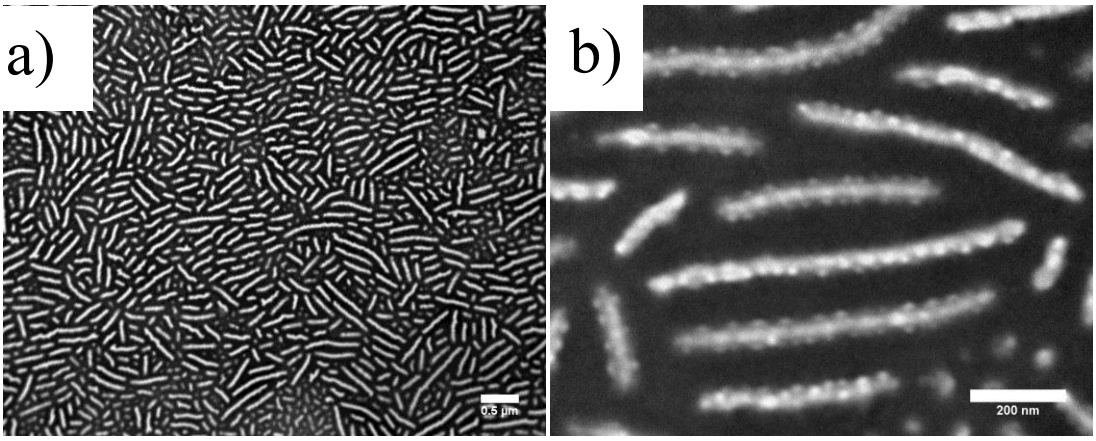

Figure 4.42 Representative TEM images of cylindrical micelles produced by the P(*L*-LA)-*b*-PAA-*b*-PTEGA (**4.5**) triblock copolymer after the CDSA process in different magnifications (images stained with PTA). (a) Scale bar = 500 nm; (b) Scale bar = 200 nm.

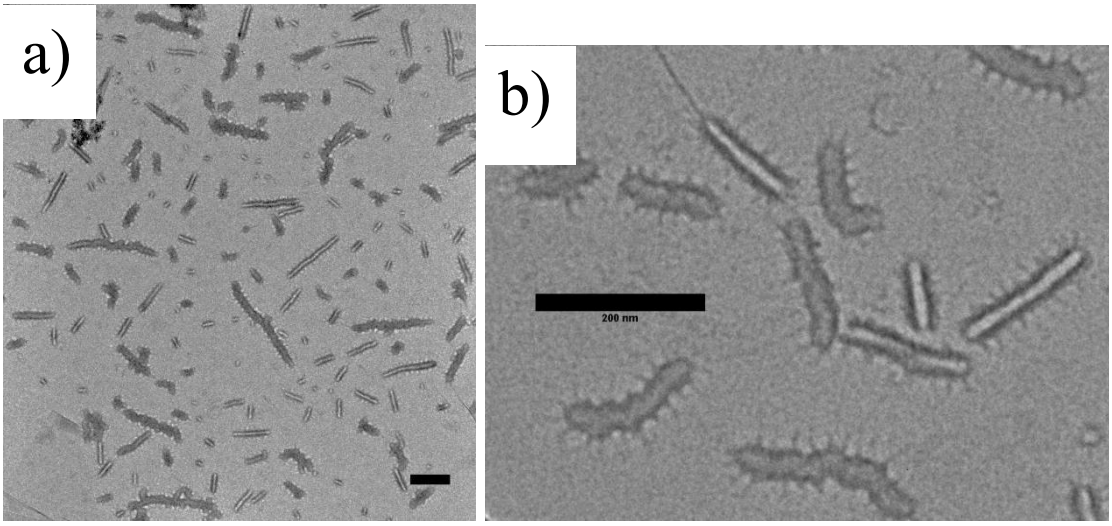

Figure 4.43 Representative TEM images of cylindrical micelles produced by the P(*L*-LA)-*b*-PAA-*b*-PTEGA (**4.5**) triblock copolymer after the CDSA process in different magnifications (images obtained on a graphene oxide support without staining). (Scale bars = 200 nm).

4.3.11 Study of P(*L*-LA)$_{32}$-*b*-PAA$_{264}$-*b*-PTEGA$_{32}$ triblock copolymers with transformed end group in CDSA

The P(*L*-LA)$_{32}$-*b*-PTHPA$_{264}$-*b*-PTEGA$_{32}$ triblock copolymers with the modified end groups (**3.18** and **3.21**) were also exposed to our optimised CDSA conditions (5 g·L^{-1}, 65 ^{o}C, 20% THF) in order to hydrolyse the P(THPA) block and form cylindrical micelles.

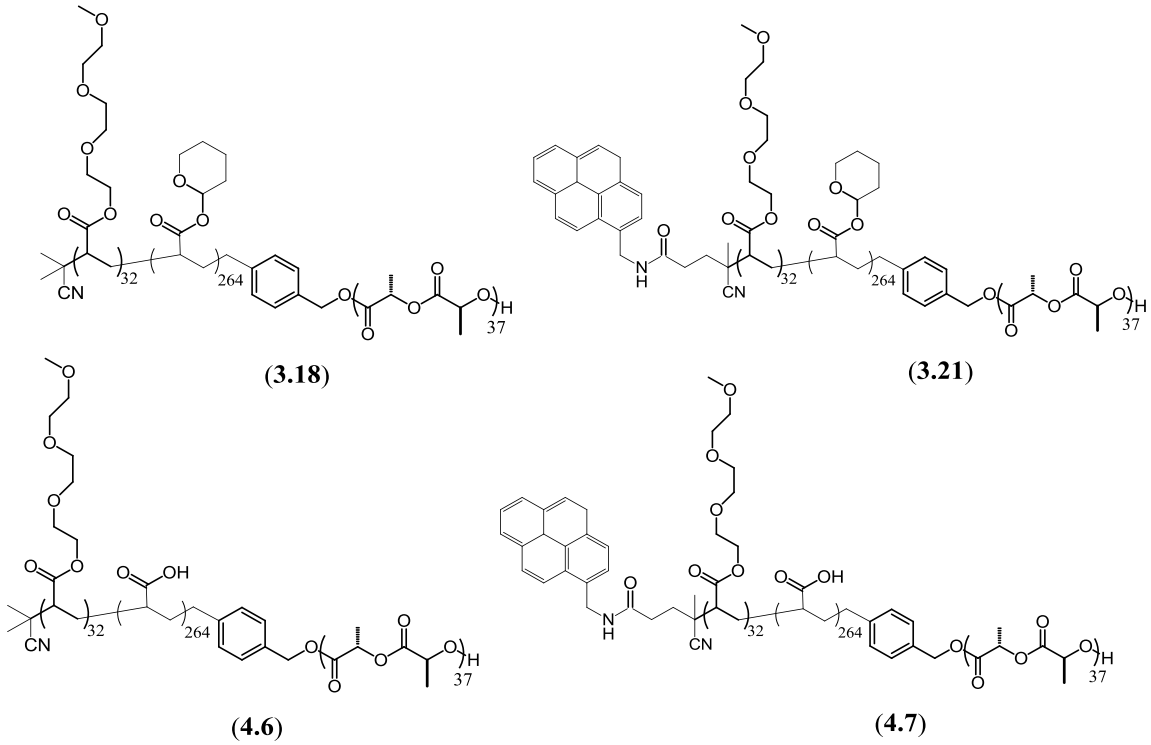

Figure 4.44 Chemical structures of triblock copolymers before the PTHPA hydrolysis (**3.18** and **3.21**) and after the PTHPA hydrolysis (**4.6** and **4.7**)

In both cases relatively well-defined cylinders were realised as it was confirmed by TEM and DLS characterisation. The polymer **4.6** that contained the isobutyronitrile functionality produced slightly shorter cylinders (L_n = 179 nm) than **4.5**. The triblock copolymers that contained the pyrene end group **4.7** formed well-defined cylinders with very similar lengths compared to the polymers containing the dodecane RAFT

end group. Importantly by WAXD characterisation all the cylinder samples based on triblock polymers were found to contain crystalline polylactide domains. These data once more support that the formation of cylinders is based on a crystallisation driven process which in this case was not disturbed by the presence of the PTEGA block or the different end group functionalities (Figure 4.47).

DLS in both cases revealed one population present in solution consistent with our TEM results. In both cases the particles exhibited the same visual effect on TEM as polymer **4.5** in the previous section. The sample containing the pyrene end group was once more analysed by fluorometry and similar results with those observed for polymer **4.4** were found supporting once more the existence of the pyrene end group in a hydrophobic environment. No conclusive evidence was observed by the corresponding TEM images.

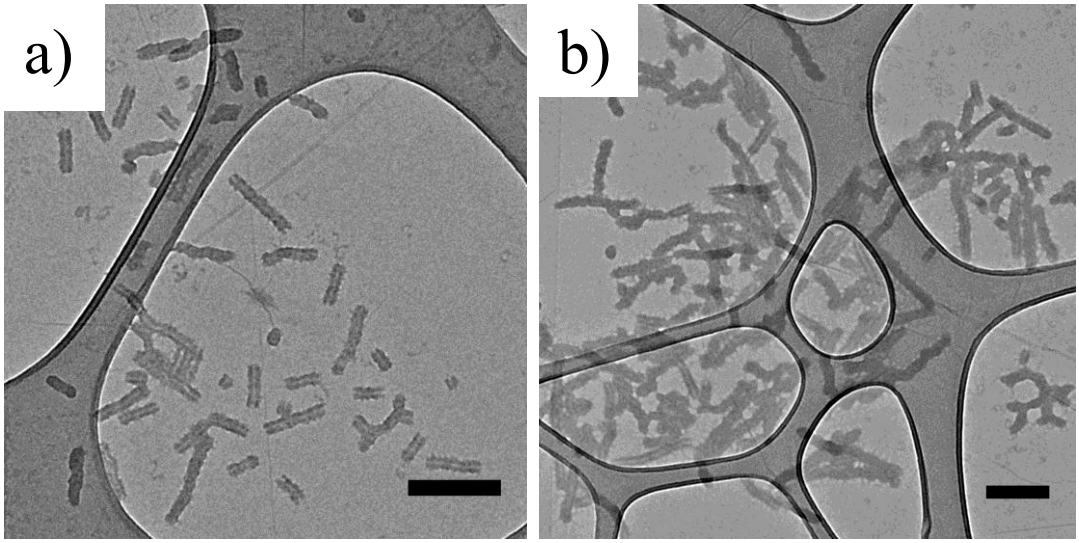

Figure 4.45 (a) Representative TEM images of cylindrical micelles produced by the P(*L*-LA)-*b*-PAA-*b*-PTEGA triblock copolymer with removed end group (**4.6**) after the CDSA process; (b) Representative TEM images of cylindrical micelles produced by the P(*L*-LA)-*b*-PAA-*b*-PTEGA triblock copolymer with the pyrene end group (**4.7**) after the CDSA process. (Scale bars = 200nm)

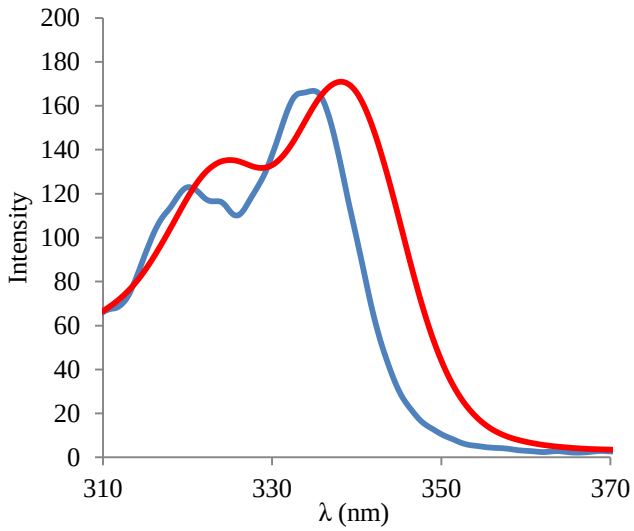

Figure 4.46 Fluorescence spectroscopy data of the pyrene initiator in water (**3.19**) (blue line) and of the cylinders solution with the pyrene end group (**4.7**) (red line).

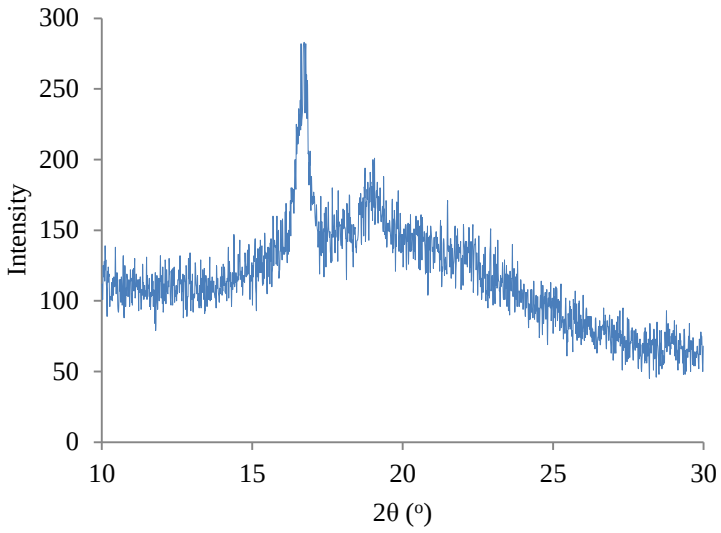

Figure 4.47 WAXD pattern of the cylinders generated by polymer **4.6** illustrating the presence of crystallinity.

4.4 Conclusions

The present work provided details about the mechanism and the kinetics of the crystallisation driven sphere-to-rod transition of P(*L*-LA)-*b*-PAA diblock and P(*L*-LA)-*b*-PAA-*b*-PTEGA triblock copolymers. It was found that the transformation can occur *in situ*, following the THP acrylate hydrolysis reaction under thermal conditions. Spherical micelles are shown to form upon deprotection, which upon prolonged heating slowly undergo crystallisation to afford seeds that can initiate cylinder growth. Furthermore, this study indicates that assembly under conditions with increasing good solvent content for both blocks allows for the preparation of longer cylinders. This suggests that the growth mechanism is unimer based and the higher unimer concentration with increasing THF content allows for the formation of longer cylinders. The kinetics of the morphological transformation were found to correlate with the crystallinity as revealed by WAXD analysis through the assembly process. The on-demand production of either spherical or cylindrical morphologies could also be achieved by facilitating or blocking the poly(*L*-LA) core crystallisation accordingly.

Furthermore, it was found that removal of the dodecane end group did not have a significant effect on the CDSA process and the resultant cylinders had similar size characteristics with those formed from polymers containing the RAFT end group. However, when the end group was transformed to a pyrene moiety our data supported the existence of pyrene in a hydrophobic environment, indicating the interaction of the end group with the hydrophobic core.

In addition the P(*L*-LA)-*b*-P(AA)-*b*-P(TEGA) triblock copolymers formed well defined cylindrical micelles through the CDSA process. Interestingly, the P(TEGA)

shell block could be identified on the dried state due to its characteristic appearance relating to its low $T_{g..}$

Importantly, all the employed polymers were synthesised without the Diels-Alder (DA) functionality and therefore all the above results prove that its presence was not key for the formation of the cylinders we observed in Chapter 2. However, the results in Chapter 2 demonstrate that the DA functionality can be incorporated in the polymers without any affects to the CDSA process.

4.5 Experimental Section

4.5.1 Materials and instrumentation

Chemicals were used as received from Aldrich, Fluka and Acros. *L*-lactide was recrystallised twice in acetone prior to use and stored in a glove box. ^{1}H NMR and ^{13}C NMR spectra were recorded on a Bruker DPX-400 spectrometer. Size exclusion chromatography (SEC) measurements were performed using a Viscotek VE1122 solvent delivery system with a Viscotek VE3580 RI detection system with THF as an eluent and 2% TEA as an additive at a flow rate of 1mL/min, unless otherwise stated. Infrared spectroscopy was recorded on a Perkin Elmer Precisely, Spectrum 100 FT-IR Spectrometer. Fluorescence spectroscopy was performed on a Cary Eclipse single-beam Perkin-Elmer LS55 fluorometer. Mass spectroscopy was carried out using a Bruker Esquire 2000, electrspray (ESI) instrument. Elemental analysis was carried out in Warwick's analytical services.

4.5.2 Particles characterisation

For the statistical length analysis, a minimum of 100 individual cylinders were carefully traced by hand to determine the contour length. Each TEM micrograph was analysed completely, which means that every cylindrical micelle in each image was counted in order to reduce subjectivity. In addition only particles with cylindrical morphology were taken in account and spherical particles or other non 1-dimensional particles were not measured. From these data L_n and L_w of each sample of cylindrical micelles was calculated by the equations shown below (L = length of cylinder, N = number).

$$\overline{L_n} = \sum_{i=1}^{n} N_i L_i \Big/ \sum_{i=1}^{n} N_i$$

$$\overline{L}_w = \sum_{i=1}^{n} N_i L_i^2 \Big/ \sum_{i=1}^{n} N_i L_i$$

4.5.3 General considerations

Many of the unstained images illustrated in this chapter demonstrate particles that have a non-uniform contrast along their width, this is a contrast effect that could indicate that these particles are hollow and will be thoroughly discussed in Chapter 6.

4.5.4 Dynamic light scattering (DLS)

Hydrodynamic diameters of the nanostructures formed were determined by dynamic light scattering. Interparticle interactions should be screened as they will introduce a structure factor in the results, therefore, each micelle solution was diluted to 0.5 g/L and allowed to equilibrate before the measurements. The DLS instrumentation consisted of a Malvern Zetasizer NanoS instrument operating at 25 °C with a 4 mW He-Ne 633-nm laser module. Measurements were made at a detection angle of 173° (back scattering), and Malvern DTS 5.02 software was used to analyse the data. It should be noted that the the hydrodynamic radii (R_h) were calculated by fitting the apparent self-diffusion coefficients (D_{app}) measured, in the known Stokes-Einstein equation $R_h = kT/(6\pi\eta D_{app})$ where k is the Boltzmann constant, T is the temperature, and η is the viscosity of the solvent. R_h coincides to the real hydrodynamic diameter only for monodispersed spherical micelles where the apparent diffusion coefficient measured equals the translational diffusion (D_t) of the particles. In the case of cylinders where an amount of anisotropy is contained the contribution of the rotational diffusion (D_{rot}) is not negligible and contributes to the D_{app}. Therefore the hydrodynamic

diameters measured have only a relative value. However, CONTIN analysis, which is based on the inverse Laplace transform of the autocorrelation function, gives us the ability to detect multiple populations in solution and get information about their polydispersity. In this respect DLS provides valuable information even when the morphology is not spherical.

4.5.5 Transmission electron microscopy (TEM)

The samples were analysed on graphene oxide grids that provide a very thin support which is almost electron transparent. Therefore we could image our samples without the need of staining retaining excellent contrast.[64] The GO grids preparation method is the following: GO solutions (0.10 - 0.15 mg mL^{-1}) were sonicated for 30 s prior to use. Lacey carbon grids (400 Mesh, Cu) (Agar Scientific) were cleaned using air plasma from a glow-discharge system (2 min, 20 mA): this step is not essential but increases the hydrophilicity of the lacey carbon improving the coverage of GO to typically > 70%. One drop (~ 0.08 mL) of the sonicated GO solution was deposited onto each grid and left to air-dry for ~ 30 min. Once dry, the grids could be stored for several weeks before sample deposition. To deposit aqueous micellar assemblies, a small drop (~ 2-10 μL) of sample was pipetted onto a pre-prepared GO grid and freeze dried. Bright- field TEM images were captured with a transmission electron microscope (JEOL TEM-2011), operating at 200 kV. Average sizes of the micelles were determined from counting the sizes of at least 100 particles for 3 different images.

Alternatively, Solutions of micellar assemblies (2 μL) were drop-cast onto a formvar carbon grid. The grid was then left to air dry for 30 min in a desiccator. Phosphotungstic acid (PTA) stain (2 μL) was applied to the sample on the grid,

blotting after 1 min to give stained grids for additional TEM analysis. Importantly, the GO grids were developed at the same period with the present project and this is the main reason a lot of the experiments were performed with 'traditional' heavy metal staining.

4.5.6 Wide angle X-ray diffraction (WAXD)

X-ray diffraction scans (WAXD) were performed on a Panalytical X'Pert Pro MPD equipped with a curved Ge Johansson monocromator on the incident beam optics giving pure focussed Cu $K_{\alpha 1}$ radiation. The solid-state PiXcel detector has an active length of ~3.2° 2θ enabling fast data collection with excellent signal to noise. Standard "powder" 2θ-θ diffraction scans were made in the angular range from 10^{o} to 35^{o} 2θ. It has to be noted that the WAXD data provide semi-quantitative information regarding the relative degree of crystallinity among the samples. In all cases the exact same amount of material was weighted and fitted in the same sample holder. In addition the samples were scanned in consecutive experiments using the same scanning method.

4.5.7 SANS data collection

SANS experiments were conducted by Dr Sarah Rogers at the ISIS neutron facility, Rutherford Appleton Laboratories, on the time-of-flight SANS 2D diffractometer. Absolute intensities for I(Q) (cm^{-1}) were determined within 5% by measuring the scattering from a partially deuterated polymer standard. Measurements were made at 25 °C and the sample was made up in D_2O and run in a 2 mm quartz cell. The FISH analysis program was used for data modeling. The model used for data fitting employed a core shell solid sphere or a core shell rigid rod form factor depending on the sample. For the rod form factor the scale factor (SF) is proportional to the

different in scattering length densities and the particle volume fraction. To obtain good agreement of the SFs it was found that the polymer aggregates were fully hydrated and a volume fraction of 0.001 (so this is around 1 mg/mL) was required. Further detail on the model used can be found in the FISH manual which can be downloaded from http://www.small-angle.ac.uk/smallangle/ Software.html.

4.5.8 PTHPA hydrolysis reaction to afford PAA followed by the CDSA with constant conditions.

In a representative procedure P(*L*-LA)-*b*-PTHPA (50 mg) was weigh in a 20 mL screw cap vial equipped with a stirring bar. Subsequently a stock solution containing the desired mixture of solvent was added (for example deionised H_2O (2.0 mL), THF (0.5 mL)). The vial was sealed and heated at 65 ^oC with a stirring rate of 500 rpm. When the self-assembly was completed the solution was freeze dried to produce a white solid which was stored at 4 ^oC. FT-IR and XRD characterisation was performed directly on the freeze dried solid. ^1H NMR spectroscopy was used to confirm the full hydrolysis of the PTHPA units. For further analysis by dynamic light scattering the freeze dried material was dissolved in a 0.25 or 0.5 $g \cdot L^{-1}$ nanopure water solution and stabilised overnight in the dark, this solution was also used for further TEM analysis. For small angle neutron scattering (SANS) the freeze dried solid was dissolved in D_2O at a concentration of $1 g \cdot L^{-1}$ and stabilised at least for 24 hours. Alternatively when the self-assembly was complete, instead of freeze drying, dilution down to 0.5 $g \cdot L^{-1}$ was performed followed by dialysis to remove the organics. The DLS and TEM analysis carried out on this solution demonstrated virtually no differences compared to the freeze dried samples.

4.5.9 PTHPA hydrolysis reaction to afford PAA followed by the CDSA with synchronous solvent evaporation.

In a representative experiment P(*L*-LA)-*b*-PTHPA (50 mg) was weigh in a 20 mL vial equipped with a stirring bar. Subsequently a stock solution containing the desired mixture of solvent was added (for example H_2O (2.0 mL), THF (0.5 mL)). A septum was placed on top of the vial with a syringe needle fitted so that the volatiles could escape during the process. The mixture was heated at 65 ^oC under stirring at a rate of 500 rpm. When the self-assembly was completed the solution was freeze dried to produce a white solid and then it was stored at 4^oC. XRD characterisation was performed directly on the freeze dried solid. For further analysis by dynamic light scattering the freeze dried material was dissolved in a 0.25 or 0.5 $g \cdot L^{-1}$ nanopure water solution and stabilised overnight in the dark, this solution was also used for further TEM analysis.

4.6 References

(1) Zhang, L. F.; Eisenberg, A. *Macromolecules* **1999**, *32*, 2239.

(2) Zhang, L. F.; Eisenberg, A. *Polym Advan Technol* **1998**, *9*, 677.

(3) Cui, H. G.; Chen, Z. Y.; Zhong, S.; Wooley, K. L.; Pochan, D. J. *Science* **2007**, *317*, 647.

(4) Lund, R.; Willner, L.; Pipich, V.; Grillo, I.; Lindner, P.; Colmenero, J.; Richter, D. *Macromolecules* **2011**, *44*, 6145.

(5) Nicolai, T.; Colombani, O.; Chassenieux, C. *Soft Matter* **2010**, *6*, 3111.

(6) Bhargava, P.; Zheng, J. X.; Li, P.; Quirk, R. P.; Harris, F. W.; Cheng, S. Z. D. *Macromolecules* **2006**, *39*, 4880.

(7) Chen, C. K.; Lin, S. C.; Ho, R. M.; Chiang, Y. W.; Lotz, B. *Macromolecules* **2010**, *43*, 7752.

(8) Shen, L.; Wang, H.; Guerin, G.; Wu, C.; Manners, I.; Winnik, M. A. *Macromolecules* **2008**, *41*, 4380.

(9) Zhang, L. F.; Eisenberg, A. *Science* **1995**, *268*, 1728.

(10) Hayward, R. C.; Pochan, D. J. *Macromolecules* **2010**, *43*, 3577.

(11) Zhu, J.; Hayward, R. C. *J. Am. Chem. Soc.* **2008**, *130*, 7496.

(12) Terreau, O.; Luo, L. B.; Eisenberg, A. *Langmuir* **2003**, *19*, 5601.

(13) Lu, A.; Smart, T. P.; Epps, T. H.; Longbottom, D. A.; O'Reilly, R. K. *Macromolecules* **2011**, *44*, 7233.

(14) Cotanda, P.; Lu, A.; Patterson, J. P.; Petzetakis, N.; O'Reilly, R. K. *Macromolecules* **2012**, *45*, 2377.

(15) Bang, J.; Jeong, U.; Ryu, D. Y.; Russell, T. P.; Hawker, C. J. *Adv. Mat.* **2009**, *21*, 4769.

(16) Discher, D. E.; Ortiz, V.; Srinivas, G.; Klein, M. L.; Kim, Y.; David, C. A.; Cai, S. S.; Photos, P.; Ahmed, F. *Prog Polym Sci* **2007**, *32*, 838.

(17) Geng, Y.; Dalhaimer, P.; Cai, S. S.; Tsai, R.; Tewari, M.; Minko, T.; Discher, D. E. *Nat Nanotechnol* **2007**, *2*, 249.

(18) Liu, J.; Thompson, Z. J.; Sue, H. J.; Bates, F. S.; Hillmyer, M. A.; Dettloff, M.; Jacob, G.; Verghese, N.; Pham, H. *Macromolecules* **2010**, *43*, 7238.

(19) Israelachvili, J. N. *Intermolecular and Surface Forces*; McGraw-Hill Publishing Co. Japan, Ltd., 1991.

(20) Burke, S. E.; Eisenberg, A. *Langmuir* **2001**, *17*, 6705.

(21) LaRue, I.; Adam, M.; Pitsikalis, M.; Hadjichristidis, N.; Rubinstein, M.; Sheiko, S. S. *Macromolecules* **2006**, *39*, 309.

(22) Moughton, A. O.; O'Reilly, R. K. *Chem Commun* **2010**, *46*, 1091.

(23) Moughton, A. O.; Patterson, J. P.; O'Reilly, R. K. *Chem Commun* **2011**, *47*, 355.

(24) Liu, S. Y.; Armes, S. P. *Angew Chem Int Edit* **2002**, *41*, 1413.

(25) Blanazs, A.; Madsen, J.; Battaglia, G.; Ryan, A. J.; Armes, S. P. *J. Am. Chem. Soc.* **2011**, *133*, 16581.

(26) Spatz, J. P.; Mossmer, S.; Moller, M. *Angew. Chem., Int. Ed.* **1996**, *35*, 1510.

(27) Kim, S. H.; Nederberg, F.; Jakobs, R.; Tan, J. P. K.; Fukushima, K.; Nelson, A.; Meijer, E. W.; Yang, Y. Y.; Hedrick, J. L. *Angew. Chem., Int. Ed.* **2009**, *48*, 4508.

(28) Muellner, M.; Lunkenbein, T.; Breu, J.; Caruso, F.; Mueller, A. H. E. *Chem. Mater.* **2012**, *24*, 1802.

(29) Muellner, M.; Yuan, J.-Y.; Weiss, S.; Walther, A.; Foertsch, M.; Drechsler, M.; Mueller, A. H. E. *J. Am. Chem. Soc.* **2010**, *132*, 16587.

(30) Xu, Y.; Bolisetty, S.; Ballauff, M.; Mueller, A. H. E. *J. Am. Chem. Soc.* **2009**, *131*, 1640.

(31) Xu, Y.; Plamper, F.; Ballauff, M.; Mueller, A. H. E. *Adv. Polym. Sci.* **2010**, *228*, 1.

(32) Bolton, J.; Bailey, T. S.; Rzayev, J. *Nano Lett.* **2011**, *11*, 998.

(33) Johnson, J. A.; Lu, Y.-Y.; Burts, A. O.; Lim, Y.-H.; Finn, M. G.; Koberstein, J. T.; Turro, N. J.; Tirrell, D. A.; Grubbs, R. H. *J. Am. Chem. Soc.* **2011**, *133*, 559.

(34) Hartgerink, J. D.; Beniash, E.; Stupp, S. I. *Science* **2001**, *294*, 1684.

(35) Lee, O.-S.; Stupp, S. I.; Schatz, G. C. *J. Am. Chem. Soc.* **2011**, *133*, 3677.

(36) Soukasene, S.; Toft, D. J.; Moyer, T. J.; Lu, H.; Lee, H.-K.; Standley, S. M.; Cryns, V. L.; Stupp, S. I. *ACS Nano* **2011**, *5*, 9113.

(37) Seyler, H.; Kilbinger, A. F. M. *Macromolecules* **2010**, *43*, 5659.

(38) Schleuss, T. W.; Berger, R.; Kilbinger, A. F. M. *PMSE Prepr.* **2006**, *95*, 807.

(39) Koenig, H. M.; Kilbinger, A. F. M. *Angew. Chem., Int. Ed.* **2007**, *46*, 8334.

(40) Bohle, A.; Brunklaus, G.; Hansen, M. R.; Schleuss, T. W.; Kilbinger, A. F. M.; Seltmann, J.; Spiess, H. W. *Macromolecules* **2010**, *43*, 4978.

(41) König, H. M.; Gorelik, T.; Kolb, U.; Kilbinger, A. F. M. *J. Am. Chem. Soc.* **2006**, *129*, 704.

(42) Hentschel, J.; Börner, H. G. *J. Am. Chem. Soc.* **2006**, *128*, 14142.

(43) Hentschel, J.; Krause, E.; Börner, H. G. *J. Am. Chem. Soc.* **2006**, *128*, 7722.

(44) Lotz, B.; Kovacs, A. J.; Bassett, G. A.; Keller, A. *Colloid & Polymer Science* **1966**, *209*, 115.

(45) Vilgis, T.; Halperin, A. *Macromolecules* **1991**, *24*, 2090.

(46) Massey, J.; Power, K. N.; Manners, I.; Winnik, M. A. *J. Am. Chem. Soc.* **1998**, *120*, 9533.

(47) Massey, J. A.; Power, K. N.; Winnik, M. A.; Manners, I. *Adv. Mater.* **1998**, *10*, 1559.

(48) Massey, J. A.; Temple, K.; Cao, L.; Rharbi, Y.; Raez, J.; Winnik, M. A.; Manners, I. *J. Am. Chem. Soc.* **2000**, *122*, 11577.

(49) Wang, X.-S.; Winnik, M. A.; Manners, I. *Macromol. Rapid Commun.* **2002**, *23*, 210.

(50) Wang, X. S.; Winnik, M. A.; Manners, I. *Macromolecules* **2002**, *35*, 9146.

(51) Wang, X.-S.; Arsenault, A.; Ozin, G. A.; Winnik, M. A.; Manners, I. *J. Am. Chem. Soc.* **2003**, *125*, 12686.

(52) Gohy, J.-F.; Lohmeijer, B. G. G.; Alexeev, A.; Wang, X.-S.; Manners, I.; Winnik, M. A.; Schubert, U. S. *Chem.--Eur. J.* **2004**, *10*, 4315.

(53) Wang, H.; Winnik, M. A.; Manners, I. *Macromolecules* **2007**, *40*, 3784.

(54) Shen, L.; Wang, H.; Guerin, G.; Wu, C.; Manners, I.; Winnik, M. A. *Macromolecules* **2008**, *41*, 4380.

(55) Wang, X.; Guerin, G.; Wang, H.; Wang, Y.; Manners, I.; Winnik, M. A. *Science* **2007**, *317*, 644.

(56) Lazzari, M.; Scalarone, D.; Vazquez-Vazquez, C.; Lopez-Quintela, M. A. *Macromol Rapid Comm* **2008**, *29*, 352.

(57) Zhang, J.; Wang, L. Q.; Wang, H. J.; Tu, K. H. *Biomacromolecules* **2006**, *7*, 2492.

(58) Fujiwara, T.; Miyamoto, M.; Kimura, Y.; Iwata, T.; Doi, Y. *Macromolecules* **2001**, *34*, 4043.

(59) Portinha, D.; Boué, F.; Bouteiller, L.; Carrot, G.; Chassenieux, C.; Pensec, S.; Reiter, G. *Macromolecules* **2007**, *40*, 4037.

(60) Bahar, I.; Erman, B.; Fytas, G.; Steffen, W. *Macromolecules* **1994**, *27*, 5200.

(61) Gilroy, J. B.; Lunn, D. J.; Patra, S. K.; Whittell, G. R.; Winnik, M. A.; Manners, I. *Macromolecules* **2012**, *45*, 5806.

(62) Kamps, A. C.; Fryd, M.; Park, S.-J. *ACS Nano* **2012**, *6*, 2844.

(63) Wilhelm, M.; Zhao, C. L.; Wang, Y.; Xu, R.; Winnik, M. A.; Mura, J. L.; Riess, G.; Croucher, M. D. *Macromolecules* **1991**, *24*, 1033.

(64) Patterson, J. P.; Sanchez, A. M.; Petzetakis, N.; Smart, T. P.; Epps, I. I. I. T. H.; Portman, I.; Wilson, N. R.; O'Reilly, R. K. *Soft Matter* **2012**.

Chapter 5: Living crystallisation driven self-assembly of polylactide-b-poly(acrylic acid) block copolymers towards the synthesis of cylinders of controlled length and dispersity

5.1 Abstract

In Chapter 4 a route towards the formation of cylindrical micelles based on a crystallisation driven methodology was explored. The particles obtained were well defined, however, the polydispersity of the resultant cylinders was relatively broad and the length of the products could not be controlled. The micelle dynamics had a key role in our system and provided means to control the concentration of unimers in solution but also the ability to block or facilitate nucleation and growth of the PLA core.

Herein, we take advantage of this feature to manipulate the assembly conditions and hence the micelle dynamics in order to gain control over the nucleation and growth steps of the self-assembly process. The Goal of this study is to demonstrate better control over the size and dispersity characteristics of the produced cylinders. The self-assembly in more dilute solutions was performed while the efficacy of the system at different self-assembly temperatures was explored. These studies were primarily based on TEM and DLS.

5.2 Introduction

5.2.1 Living crystallisation driven self-assembly (CDSA)

Work published in 2007 by Wang *et al* reinvented the field of crystallisation driven self-assembly.[1] In this work the authors introduced for the first time the idea of a living self-assembly process. Notably, the authors demonstrated the ability of their system to produce the so called co-micelles. In this case already formed micelles based on poly(ferrocenyldimethylsilane)-*b*-polyisoprene (PFS-*b*-PI) block copolymers were 'chain-extended' with a PFS-*b*-P(methylvinylsiloxane) (PFS-*b*-PMVS) block copolymer. They demonstrated in this manner the ability to control the chemical composition along the cylinders. In addition dark field TEM was utilised to demonstrate that the epitaxial growth was occurring in bidirectional fashion as both ends of the cylinders were remaining active for further deposition of unimers (Figure 5.1).[1]

Importantly the authors demonstrated that the micelle growth could not occur if the ferrocenylsilane block had a different chemical structure that prevented crystallisation. Poly(ferrocenylmethylethylsilane) (PFMES) is an amorphous polymer, and PFMES-*b*-PMVS forms spherical micelles in hexane. When a THF solution of PFMES-*b*-PMVS was added to a hexane solution of performed PFS-*b*-PI cylindrical micelles, the product appeared by TEM to be a mixture of PFMES-*b*-PMVS spherical micelles and unchanged PFS_{53}-*b*-PI_{320} cylindrical micelles illustrating that the crystallisation of PFS in the core is the major driving force in these assemblies and therefore cylinder growth cannot be realised with amorphous polymers.

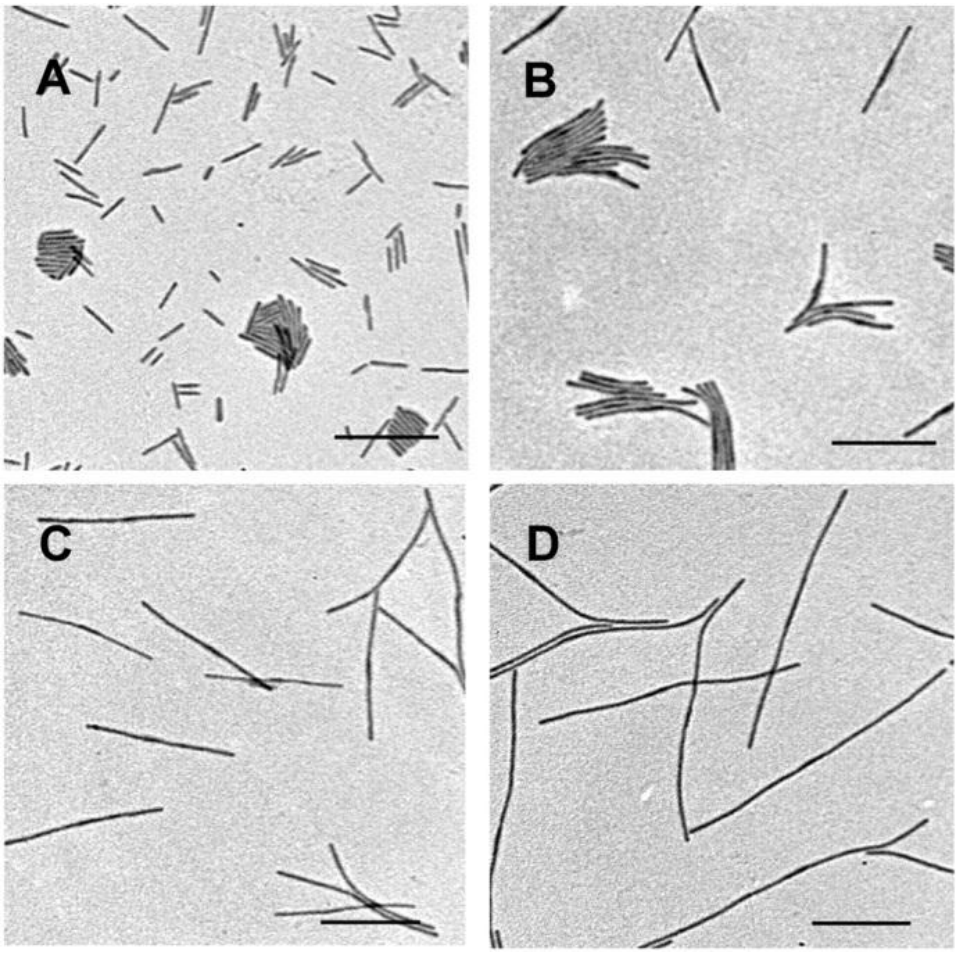

Figure 5.1 TEM images for (*A*) sonicated PFS_{53}-PI_{320} micelles in hexane (0.5 mg/mL); (*B* to *D*) elongated micelles after adding 0.5 mg (B), 1 mg (C), and 2 mg (D) of PFS_{53}-PI_{320} in THF (0.1 mL - 1.0 mL) solutions of (A). Scale bars, 500 nm.[1]

In 2009, Gadt *et al*. reported the use of living crystallisation driven self-assembly to produce complex and hierarchical micelle architectures. In this paper the authors demonstrated that they could achieve heteroepitaxial crystal growth. More specifically, PFS-PI based cylindrical micelles were 'chain extended' with block copolymers (BCPs) that were based on a poly(ferrocenyldimethylgermane), PFG core block. Pentablock micelles of alternating core composition were synthesised in this means. Cylinders were also grown from PFS based platelets forming scarf-like micelles (Figure 5.2).[2]

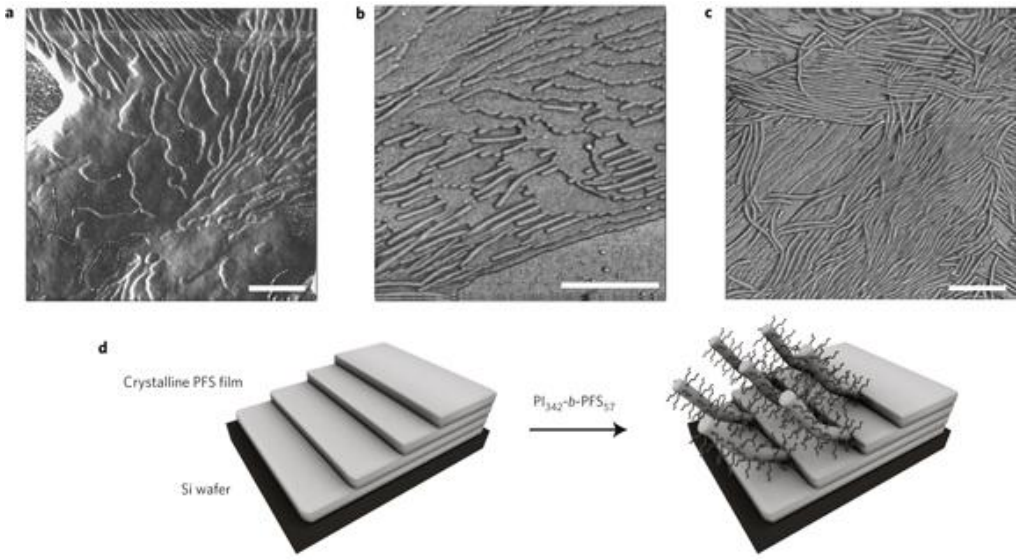

Figure 5.2 PI_{342}-*b*-PFS_{57} cylinders growing from the steps of the crystalline PFS_{129} substrate after immersing the crystalline PFS film in 4 mL of *n*-hexane and subsequently adding 4 μL of a 0.1 $mg \cdot mL^{-1}$ THF solution of PI_{342}-*b*-PFS_{57}.[2]

The same group also demonstrated a facile and efficient route to the fabrication of a range of metal oxide/polymer nanowires *via* a template-directed sol–gel process using PFS_{17}-*b*-$P2VP_{170}$ based cylindrical micelles. In their approach simply mixing the micelles with metal alkoxide precursors in a mixture of 2-PrOH and H_2O produced well-defined inorganic coatings with smooth and continuous textures. In the case of titania, introduction of a positively charged corona by partial quaternisation of the coronal P2VP block was a key factor in producing hybrid nanostructures with well adhered, smooth coatings that were embedded in the micelle corona (Figure 5.3).[3]

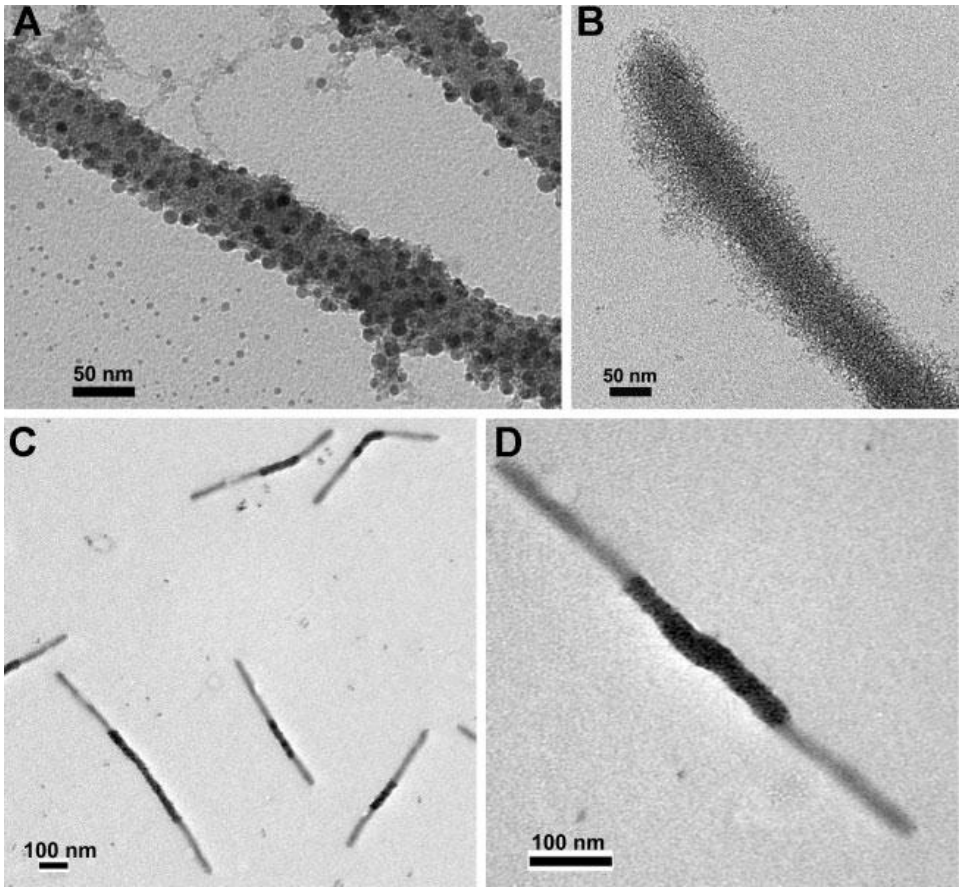

Figure 5.3 TEM images of PFS based co-micelles and the selective coating with titania at different magnifications.[3]

Manners and coworkers continued in 2010 when they reported the formation of highly monodispersed cylindrical micelles utilising a living self-assembly process. In this case preformed semicrystalline cylindrical micelles were sonicated in order to form highly monodispersed and very small semicrystalline micelles that could act as 'initiators' for further micelle elongation. By adding this simple but yet very effective feature to their system they achieved the formation of cylindrical micelles of unprecedentedly narrow length polydisperisty. Cylinders with lengths between ~200 nm and 2 μm with dispersities in length $L_w/L_n \leq 1.03$ were realised through variation of the seed-to-unimer ratio. They highlighted the analogy between this nanoscale living polymerisation and angstrom-scale living polymerisations in which

molecular monomers are polymerised to form monodisperse polymers by using small, well-defined initiators. The ability to prepare different nanocylinder samples with narrow dispersities in length allowed length-dependent, field-responsive liquid-crystalline behaviour of monodisperse cylindrical nanostructures in their products (Figure 5.4).[4]

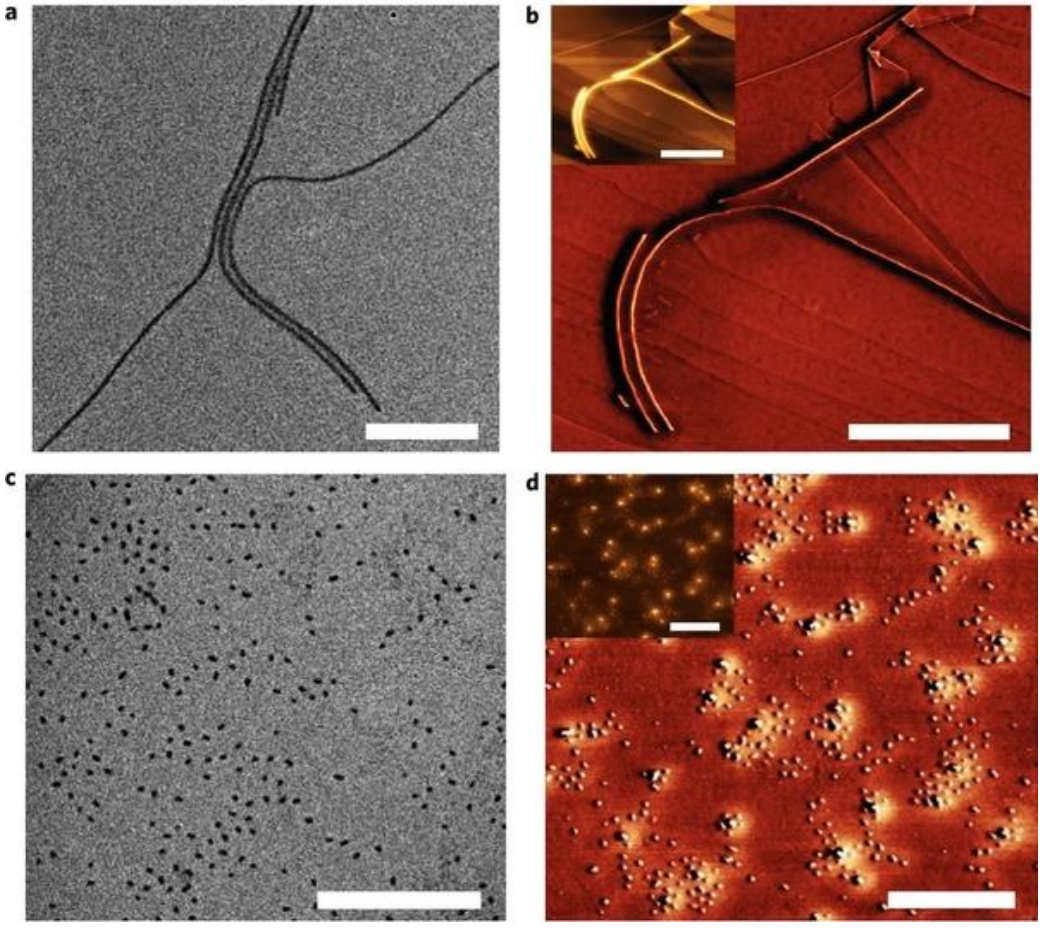

Figure 5.4 TEM and AFM images demonstrating cylindrical micelles based on PFS by 'conventional' CDSA (a and b) and highly monodispersed semicrystalline initiators fabricated by sonication (c and d).[4]

Notably, the Manners group applied the same methodology in other semi crystalline block copolymer systems. In 2011 they reported the living crystallisation driven self-assembly of poly(3-hexylthiophene)-*b*-poly(dimethylsiloxane) (P3HT-*b*-PDMS)

diblock copolymer. The micelles in this case contained a P3HT core. They yielded cylindrical micelles with average lengths (L_n) of 72, 133, 215, and 320 nm by tuning the seed/unimers ratio as revealed by TEM. The polydisperisty of these micelles was also very narrow (Figure 5.5).[5]

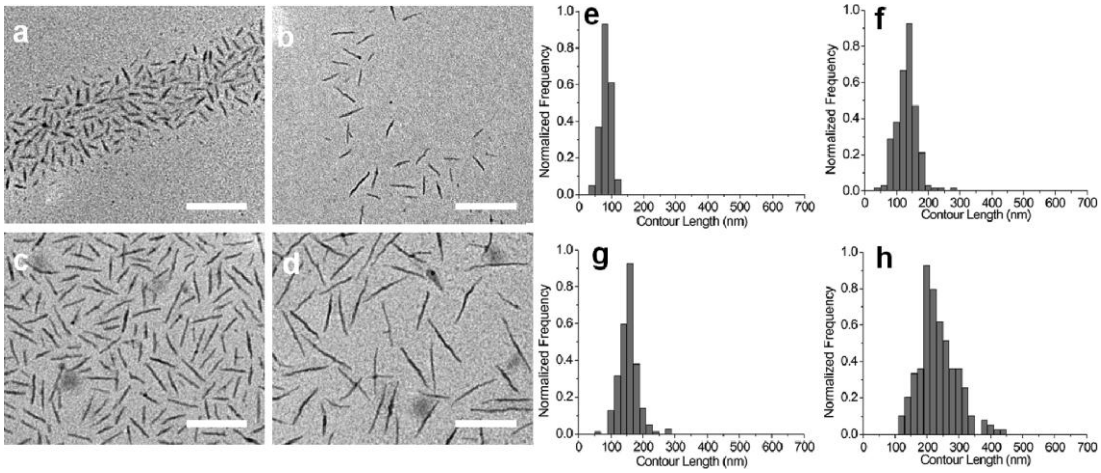

Figure 5.5 (a-d) Bright-field TEMmicrographs of monodisperse cylindrical micelles of P3HT-*b*-PDMS obtained by adding (a) 700, (b) 1400, (c) 2100, and (d) 2800 μg of unimers (as 7 mg/mL solution in toluene) to 33 μg of seed micelles (L_n = 38 nm) in 100 μL of an 85% (v/v) Et_2O/toluene mixture diluted by further addition of 1.5 mL of Et_2O. Scale bars: 200 nm. (e-h) Contour length distributions of samples (a)-(d), respectively.[5]

Very recently, Schmalz and coworkers applied the crystallisation driven living self-assembly to triblock copolymers based on polyethylene cores. Impressively, the authors managed to form co-micelles (for the first time in a non-PFS based system) by extending poly(styrene)-*b*-poly(ethylene)-*b*-poly(styrene) (PS-*b*-PE-*b*-PS) triblock copolymer based seed micelles with poly(styrene)-*b*-poly(ethylene)-*b*-poly(methyl methacrylate) (PS-*b*-PE-*b*-PMMA) unimer addition. The resultant micelles had a patchy-like PS/PMMA corona and a uniform polyethylene core (Figure 5.6).[6]

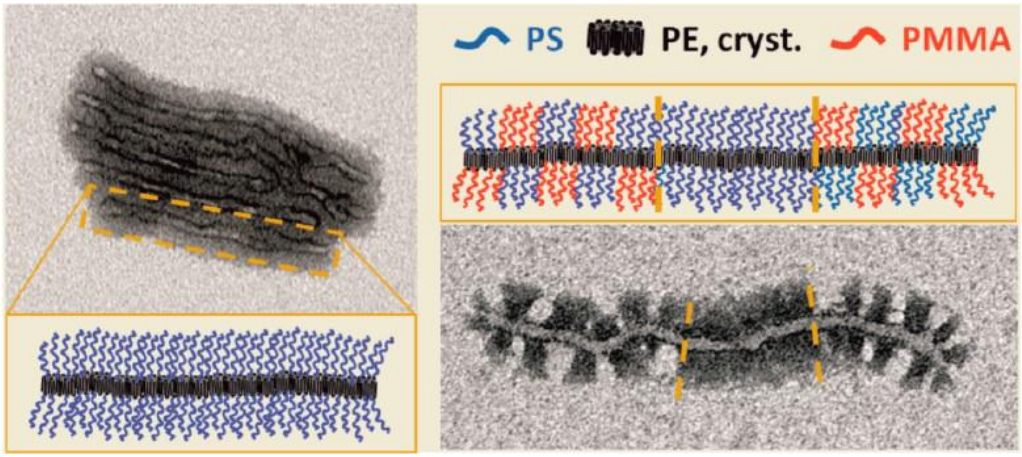

Figure 5.6 Co-micelles based on polyethylene cores demonstrated by Schmalz and coworkers.[6]

Key feature of the conditions they used to achieve the co-micelle formation was that further polyethylene nucleation was neglected while the cylinder growth was still promoted. That was achieved by conducting the seeded growth at 30 ^{o}C, a temperature above the T_c (crystallisation temperature) of the polyethylene core but lower than its $T_{m.}$ (melting temperature).

The latest report from Manners and Winnik demonstrated an unprecedented approach to the controlled formation of non-centrosymmetric colloidally stable core-shell nanoparticles with shape anisotropy from BCPs. Impressively, the supramolecular copolymer (co-micelle) was then further self-assembled into super micelles (Figure 5.7). [7]

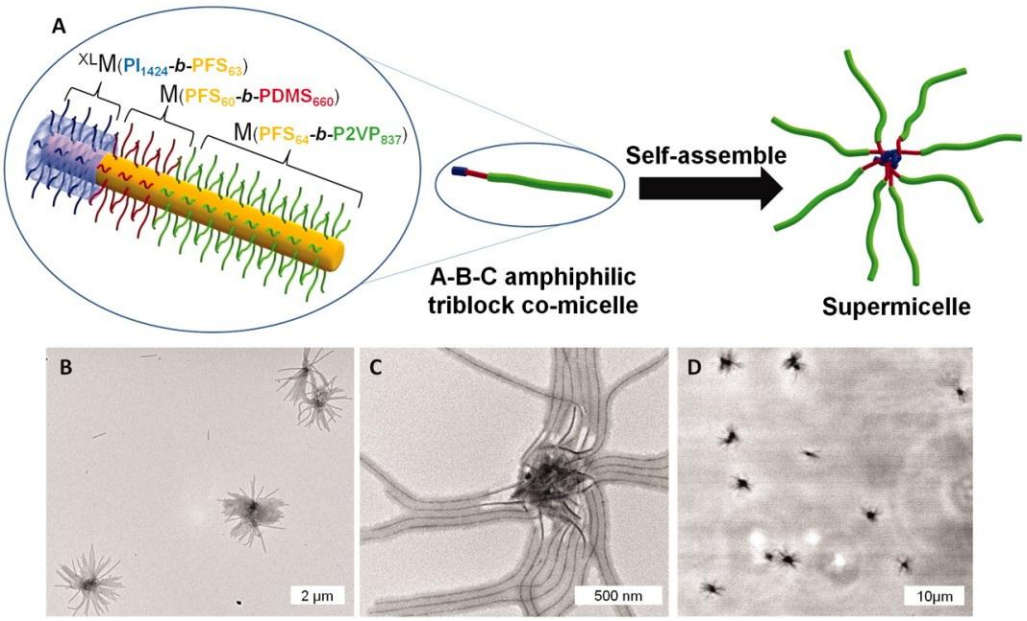

Figure 5.7 TEM images showing the formation of super micelles as a product of the multiple elegant features developed by Manners, Winnik and coworkers during the last 14 years.[7]

5.3 Results and discussion

In the previous chapter we described the formation of cylindrical particles through a crystallisation driven process. Importantly, quantitative sphere-to-cylinder transitions were observed by polymers even with 10 times longer (in terms of DP) hydrophilic than hydrophobic segments. This process demonstrated unprecedented versatility on the formation of cylindrical particles based on polylactides in wide range of conditions. However, the process suffered from the slow nucleation that was present through the whole transition. As it was mentioned earlier this self-assembly could be parallelised to a supramolecular polymerisation where the initiation step (*i.e* nucleation) is slow compared to the propagation (*i.e* crystal growth), exhibiting similarities to a free radical polymerisation. As a consequence of that the length of the cylinders could not be controlled while the polydispersity of the resultant micelles was relatively broad. Obviously, to gain control over the products we had to apply conditions in which the system would afford semicrystalline micelle nuclei much faster than the cylinder growth occurs. As it was demonstrated in the previous chapter the micelle dynamics play a central role on the nucleation/growth ability of the system. In turn the micelle dynamics depend on the conditions (*i.e* self-assembly temperature, concentration of the polymer, quality of the solvent). Micelles with a semicrystalline core are expected to have different (more restricted) dynamics than the micelles with an amorphous core. Importantly, in the previous chapter we showed that in concentrations lower than 1 $g \cdot L^{-1}$ at 65 ^{o}C cylinders were not formed and the products were found to be completely amorphous (perhaps indicative of the increased dynamics disrupting the nucleation step).

To further explore the self-assembly behaviour and take advantage of the aforementioned features of our system, we performed experiments in which mixtures of crystalline cylinders and amorphous spherical micelles (as produced from the early stages of the sphere-to-cylinder transition studied in the previous chapter) were diluted between 0.25 $g \cdot L^{-1}$ to 0.5 $g \cdot L^{-1}$ and heated at 65 ^{o}C. The aim of these experiments was to increase the self-assembly temperature above the T_g of the PLA block in order to facilitate core mobility and aid the micelle dynamics, generating unimers in solution. In addition, under these dilute conditions we have shown that further nucleation cannot take place and therefore cylinder growth can only happen at the ends of the preformed cylindrical species that could act as crystallisation seeds providing this way means for better control of the cylinder length and polydispersity.

5.3.1 Preparation of seed micelles solution based on P(*L*-LA)$_{32}$-*b*-PAA$_{265}$

P(*L*-LA)$_{32}$-*b*-PTHPA$_{265}$ (**3.9**) was treated under conditions that afforded the PTHPA hydrolysis followed by the *in situ* self-assembly of P(*L*-LA)$_{32}$-*b*-PAA$_{265}$ (**5.1**) (65 ^{o}C, 20 $g \cdot L^{-1}$, THF/H_2O, 0.5/9.5 v/v). The solution was exposed to these conditions for 10 hours in order to facilitate nucleation and enable the formation of cylindrical micelles with a semicrystalline core. The final solution was freeze dried and the product dispersed in nanopure water at 0.25 $g \cdot L^{-1}$ and stirred at room temperature. Subsequently, the sample was characterised by DLS and TEM. By DLS analysis two populations were present (Figure 5.8), and TEM illustrated the presence of spheres and short cylinders with an average length of $\overline{L}_n = 76\,\text{nm}$ and $\overline{L}_w / \overline{L}_n = 1.11$ (Figure 5.9), indicating an incomplete sphere-to-cylinder transition which was in agreement with what was expected according to the results obtained in Chapter 4.

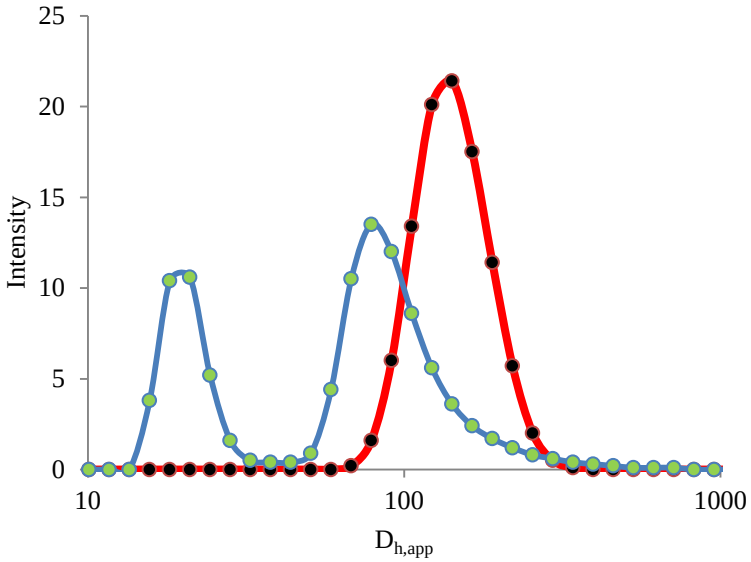

Figure 5.8 DLS traces of the solution of polymer **5.1** before (blue trace) and after heating the solution for 60 minutes at 65 ^{o}C (red line)

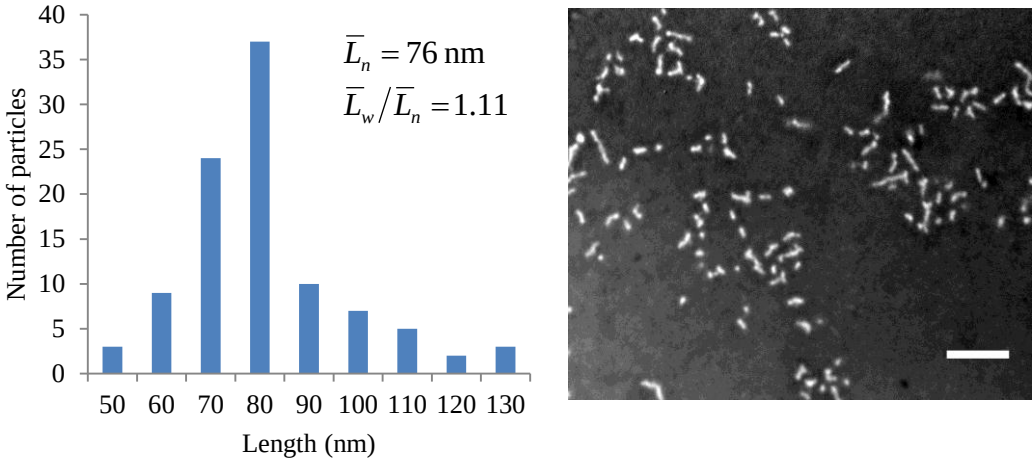

Figure 5.9 Representative TEM image of the cylinders present in solution of polymer **5.1** (PTA stained) and the cooresponding histogram straight after dissolution in nanopure water at 0.25 g·L^{-1} (Scale bar 200 nm).

5.3.2 Living crystallisation driven self-assembly (CDSA) under dilute, thermal conditions

Following dissolution of the block copolymer at 0.25 $g \cdot L^{-1}$, the solution was heated at 65 ^{o}C for 80 minutes Removing aliquots from the solution in regular time intervals (10, 20, 40, 60, 80 minutes) and characterise by TEM provided valuable information regarding the cylinder length and polydispersity evolution. Notably, the cylinder length appeared to increase with time reaching a final length of $\bar{L}_n = 212\,\text{nm}$ whilst the dispersity decreased to a $\bar{L}_w / \bar{L}_n$ value of 1.08 (Figure 5.10). Furthermore, a plot of the average length of the cylinders against the self-assembly time had a linear relationship (Figure 5.11). These data suggested a linear growth of the cylindrical micelles such that the length of the cylinders can be kinetically controlled. These observations mirror the living epitaxial micelle growth observed by Manners, Winnik and coworkers, showing that these principles of CDSA are applicable to organic polymer cores thus expanding the scope of possible polymer systems with which to synthesise cylindrical micelles of highly controlled size and functionality. In addition, the cryo-TEM data for the solution heated for 80 minutes were consistent with the presence of cylindrical particles in solution (Figure 5.12). These observations are entirely consistent with an epitaxial growth process of the cylinders by the addition of remaining unimers on the already existing cylinders/seeds. The presence of crystallinity on the final product was confirmed by WAXD analysis (Figure 5.13).

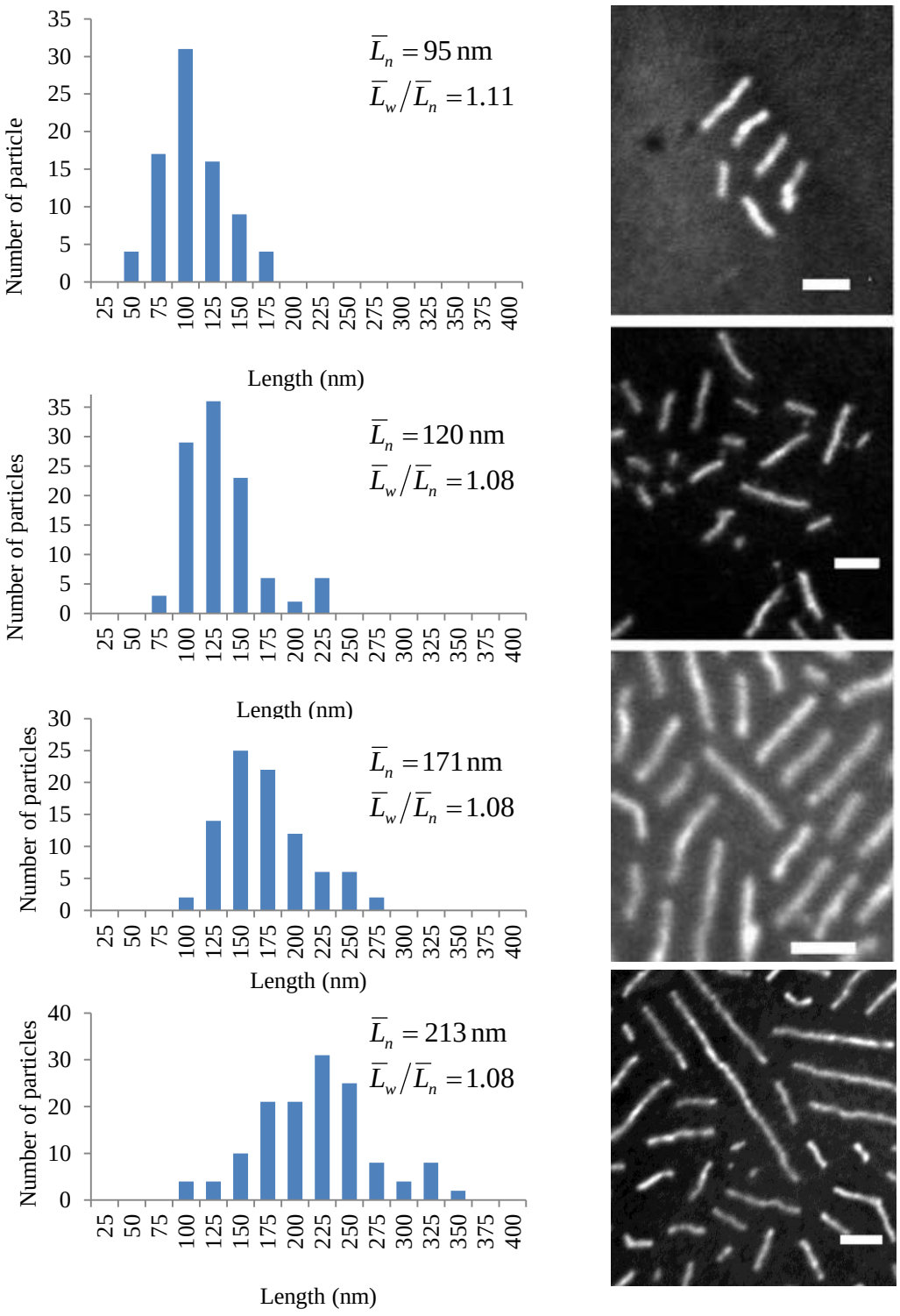

Figure 5.10 From top to bottom : Representative TEM images and corresponding length histograms of the cylinders in solution (**5.2**) at 0.25 g·L^{-1} after heating at 65 ^{o}C for 10 minutes; 20 minutes; 40 minutes; 60 minutes; all samples stained with PTA (Scale bars 100 nm).

Clearly, the quality (size and polydispersity) of the micelle seeds but also the seed:unimer ratio are critical to both the final dimensions but also the dispersity of the resultant micellar assemblies.

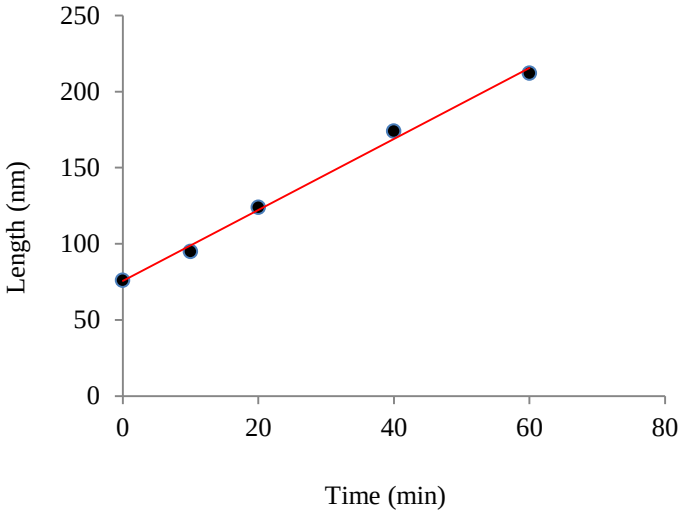

Figure 5.11 Graph indicating the linear relationship between cylinder length versus time when the self-assembly carried out at 65 ^{o}C, 0.25 g·L^{-1} aqueous solution.

Further investigations indicated that the cooling rate does not affect the size or dispersity of the resultant structures. It should be noted that the micelles formed from all polymers utilised in this study were stable for extended periods of time (up to 4 weeks) under normal benchtop conditions at room temperature.

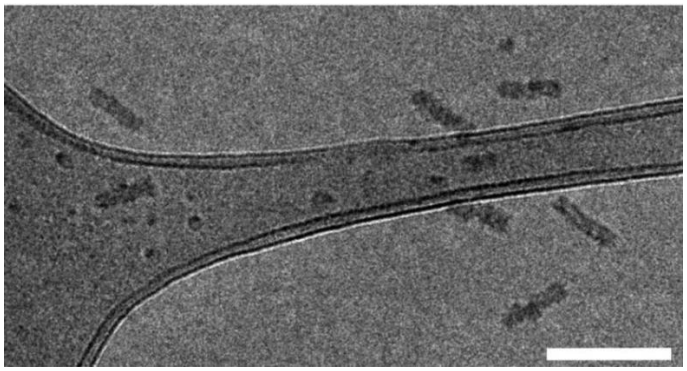

Figure 5.12 Cryo-TEM of the cylindrical particles generated by polymer **5.1 (**Scale bar = 200 nm)

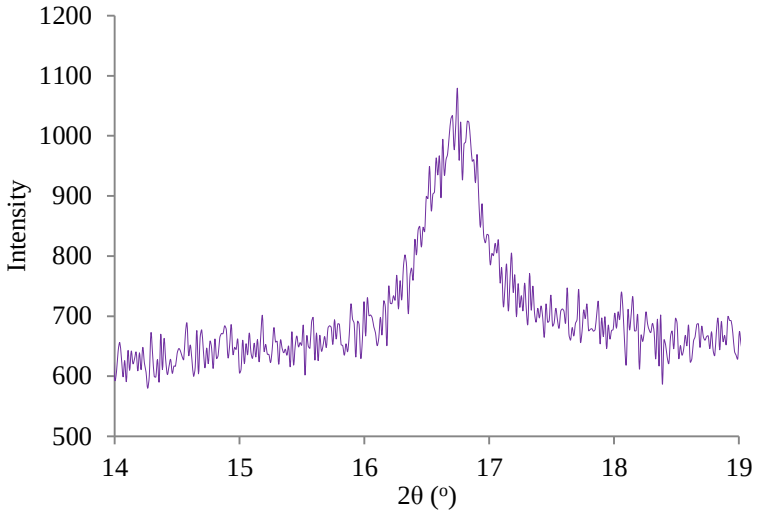

Figure 5.13 WAXD pattern of semicrystalline cylinders after heating at 65°C for 80 minutes.

5.3.3 Solvent switch of P(*L*-LA)$_{32}$-*b*-PTHPA$_{265}$ to afford spherical micelles

To further investigate the assembly and once more confirm the importance of the crystallisation process, the self-assembly of the P(*L*-LA)$_{32}$-*b*-PAA$_{265}$ block copolymer (**5.1**) was further examined under a range of conditions. In order to confirm that the presence of the already crystallised seed micelles had a key role in the transition, polymer **5.1** was also assembled using a conventional solvent switch method (acetone/water) as reported by LeRoux and coworkers.[8] By using this method, we ensured the self-assembly and crystallisation history was erased before introducing the selective solvent and let the self-assembly process commence. Under these conditions relatively well defined spherical particles were observed by DLS (R_h=48nm, PD=0.127) and TEM (R_h=17 nm) analysis, indicating that nucleation and growth in order to afford cylinders cannot take place under these conventional conditions (Figure 5.14).

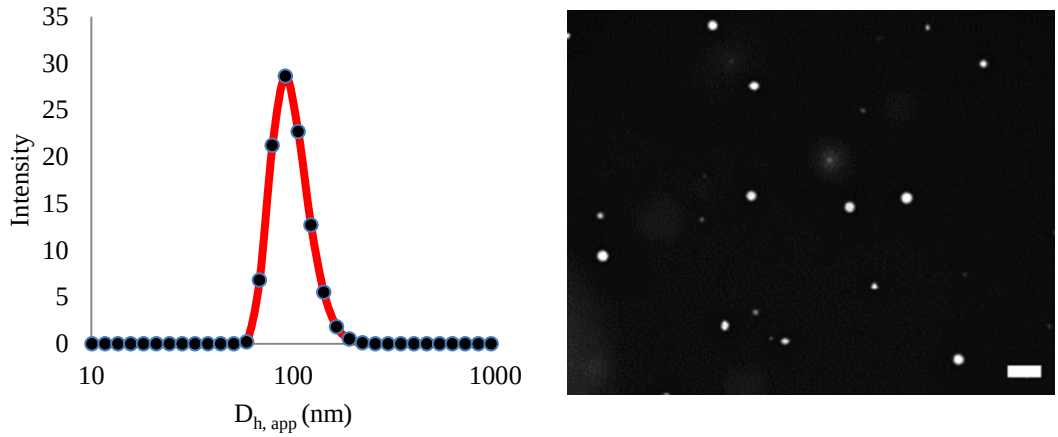

Figure 5.14 On the left : DLS data of solution following the solvent switch; On the right : TEM of the spherical micelles obtained by solvent switch methodology; sample stained with PTA (Scale bar 100 nm)

5.3.4 Study of temperature and assembly time on the living CDSA of P(*L*-LA)$_{32}$-*b*-PAA$_{265}$

With the requirement for conditions that promote effective crystal growth while neglecting further nucleation established, we further investigated the effect of temperature on the micelles formed. Heating the solution of polymer **5.1** at 95 ^{o}C for 20 minutes resulted in a 'messy' appearance by TEM in which we could observe that spherical micelles were coexisting with non-epitaxially (side to side) aggregated cylinders. Heating for 60 minutes at 95 ^{o}C led to complete 'consumption' of the spherical aggergates and transition to large aggregated cylinders (Figure 5.15).

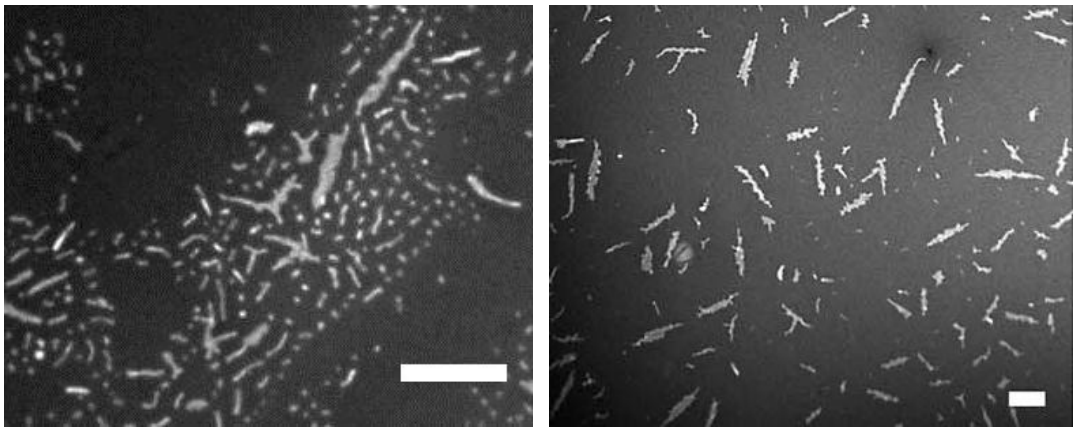

Figure 5.15 On the left : Aggregated cylinders observed when polymer **5.1** was heated at 95 ^{o}C for 20 minutes; On the right : aggregated cylinders observed when heated at 95 ^{o}C for 60 minutes; samples stained with PTA (Scale bar = 300 nm)

These studies strongly suggest that the observed cylindrical structures are kinetically trapped stable intermediates that can only be accessed through core-crystallisation above the T_g of the PLA block. In addition, it is evident that an elegant balance should be achieved through the living CDSA conditions in order to get on the desired kinetic pathway by facilitating crystallisation and neglecting nucleation but also by promoting the epitaxial cylinder growth without allowing any non-epitaxial (side to side) aggregation to occur. Investigation of the effect of heating times on the formation of the cylindrical micelles revealed that, in common with the preparation of micelles at higher temperatures, large and non-epitaxially aggregated structures were observed at extended periods.

5.4 Conclusions

This work demonstrates the living crystallisation-driven self-assembly of readily accessible PLA-containing block copolymers through a thermally controlled crystallisation under dilute aqueous conditions that promotes crystal growth but neglects further nucleation. The simple assembly procedures reported herein, in combination with the application of accessible RAFT and ROP synthetic methodologies, enables significant versatility in the preparation of well-defined cylindrical micelles based on polylactide. Furthermore it was found that the evolution of cylinder length with time was linear suggesting the living character of the process. Importantly, studies at higher temperatures illustrated that fine tuning of the conditions is required in order to achieve control over the kinetic pathway followed. Upon conditions that destroyed the preformed micelle initiators (seeds) the whole process was completely inhibited and spherical micelles were observed in agreement to what the conventional self-assembly rules would dictate. Finally, it is important to highlight, that our work in Chapters 4 and 5 provides comprehensive understanding regarding the behaviour we observed in Chapter 2 with the DA containing polymers, which was what initiated this research.

5.5 Experimental Section

5.5.1 General considerations for this work

The conclusions of this work were primarily based on TEM characterisation. As TEM is not a quantitative method subjectivity is always an issue when trying to interpret the data. For this reason a large amount of particles was always measured to produce the corresponding histograms and therefore come to as reliable conclusions as possible. Furthermore, the WAXD analysis demonstrated in this chapter was carried out with a different experimental set up and conditions than the one we used in Chapter 4 and hence quantitative comparisons are meaningless.

5.5.2 Materials and instrumentation

The nanostructures in aqueous solutions were determined by dynamic light scattering (DLS). The DLS instrumentation consisted of a Malvern Zetasizer NanoS instrument operating at 25 °C with a 4 mW He-Ne 633-nm laser module. Measurements were made at a detection angle of 173° (back scattering), and Malvern DTS 5.02 software was used to analyse the data. All samples were then examined with a transmission electron microscope (JEOL TEM-1200), operating at 120 kV. Average sizes of the micelles were determined from counting the sizes of at least 100 particles for 3 different images.

X-ray diffraction scans (WAXD) were performed on a Panalytical X'Pert Pro MPD equipped with a curved Ge Johansson monochromator on the incident beam optics giving pure focussed Cu $K\alpha_1$ radiation. The solid-state PiXcel detector has an active length of ~3.2° 2θ enabling fast data collection with excellent signal to noise. The samples were mounted on a piece of offcut Si, and aligned to the direct beam to

ensure that the effect of height error in the scans was minimised. Standard "powder" 2θ-θ diffraction scans were made.

5.5.3 Preparation of samples for TEM analysis

Solutions of micellar assemblies (2 μL) were drop-cast onto a formvar carbon TEM grid. The grid was then left to air dry for 30 min in a desiccator. Phosphotungstic acid (PTA) stain (2 μL) was applied to the sample on the grid, blotting after 1 min to give stained grids for additional TEM analysis.

5.5.4 Living crystallisation driven self-assembly of (5.1) to obtain cylinders of different lengths

10 mg of polymer **5.1** were added to a round-bottom flask equipped with a stirrer bar followed by deionised (nanopure) water (40 mL). The mixture was allowed to stir at 65 °C for 80 minutes. Aliquots were removed in regular time interval (after 10, 20, 40, 60 and 80 minutes of heating) and analysed by TEM and DLS.

5.5.5 Solvent switch self-assembly of (5.1) to obtain spherical micelles

15 mg of polymer **5.1**were dissolved in 10 mL of acetone before being subsequently added dropwise to filtered nanopure water (30 mL). The solution was left overnight in the fume hood with an open top to remove acetone. The resultant particles were characterised by DLS and TEM analysis.

5.5.6 Self-assembly of (5.1) in different temperatures

10 mg of this polymer **5.1** were added to a round-bottom flask equipped with a stirrer bar followed by deionised (nanopure) water (40 mL). The mixture was allowed to stir at 95 °C for 60 minutes. Aliquots were after 20 and 60 minutes of heating and analysed by TEM and DLS.

5.6 References

(1) Wang, X.; Guerin, G.; Wang, H.; Wang, Y.; Manners, I.; Winnik, M. A. *Science* **2007**, *317*, 644.

(2) Gaedt, T.; Ieong, N. S.; Cambridge, G.; Winnik, M. A.; Manners, I. *Nat. Mater.* **2009**, *8*, 144.

(3) Wang, H.; Patil, A. J.; Liu, K.; Petrov, S.; Mann, S.; Winnik, M. A.; Manners, I. *Adv. Mater.* **2009**, *21*, 1805.

(4) Gilroy, J. B.; Gadt, T.; Whittell, G. R.; Chabanne, L.; Mitchels, J. M.; Richardson, R. M.; Winnik, M. A.; Manners, I. *Nat. Chem.* **2010**, *2*, 566.

(5) Patra, S. K.; Ahmed, R.; Whittell, G. R.; Lunn, D. J.; Dunphy, E. L.; Winnik, M. A.; Manners, I. *J. Am. Chem. Soc.* **2011**, *133*, 8842.

(6) Schmelz, J.; Schedl, A. E.; Steinlein, C.; Manners, I.; Schmalz, H. *J. Am. Chem. Soc.*, Ahead of Print.

(7) Rupar, P. A.; Chabanne, L.; Winnik, M. A.; Manners, I. *Science* **2012**, *337*, 559.

(8) Kang, N.; Perron, M.-E.; Prud'homme, R. E.; Zhang, Y.; Gaucher, G.; Leroux, J.-C. *Nano Lett.* **2005**, *5*, 315.

Chapter 6: Hollow block copolymer nanoparticles through a spontaneous one-step structural reorganisation

6.1 Abstract

Interestingly, visualisation of our spherical and cylindrical particles by TEM (without staining on a graphene oxide support) revealed that the particles had a non-uniform contrast along their width. This finding was of fundamental importance as it could indicate that the particles have a hollow interior. Herein, we perform a thorough characterisation study with main objective the clarification of the origins of this effect. Recently, it has been demonstrated that dry state TEM can be performed on a graphene oxide (GO) surface. This allows organic polymer based particles (low–z materials) to be imaged without the need of heavy metal stains. Thus, all the structural information of the dried particles is retained and directly imaged. In the present work we take advantage of this multi-technique method in order to fully understand and resolve the morphology of the particles on the dried state. The role of crystallinity in the core of the cylindrical particles has been studied as well as the effect of different drying protocols on the resultant morphology.

The work presented herein is the result of collaboration. In particular the SANS data were collected and analysed by E. G. Kelley and T. H. Epps III. The cryo-TEM images were collected by P. H.H. Boman and N. A. J. M. Sommerdijk. The SEM images were collected by P.Cotanda. The AFM imaging was carried out by J.P. Patterson, some of the TEM imaging was performed by N. Hondow and M. Brydson, while the P(D,L-LA)$_{4k}$-b-PEO$_{5k}$ self-assembly experiments were carried out by M. Robin.

6.2 Introduction

Hollow nanoparticles of either spherical or cylindrical morphologies (nanocages and nanotubes) are highly desirable due to their potential utility as nanoreactors,[1] nanocontainers,[2] purification agents,[3] delivery vehicles[4] and nanofluidic materials.[5] Several synthetic approaches have been developed for their fabrication in solution and in bulk; including layer-by-layer deposition,[6] templated synthesis,[7] and block copolymer (BCP) self-assembly.[8,9] The latter is of particular importance due to the great versatility of BCPs in generating nanoparticles of controlled size and shape (spheres,[10] cylinders,[11,12] and bilayers).[13,14] In the following sections a brief discussion regarding the self-assembly methodology for the preparation of hollow particles is presented. In addition, some examples of unusual contrast effects by electron microscopy are demonstrated.

6.2.1 Hollow particles from BCP self-assembly

Work by Wooley *et al*. utilised poly(acrylic acid)-*b*-polyisoprene (P(AA)-*b*-PI) spherical micelles as scaffolds for the synthesis of nanocages by sequential shell cross-linking and core degradation.[8] In summary, the cross-linked shell of the particles created a stable hydrophilic membrane that expands after removal of the core to give hollow particles (nanocages). The authors highlighted the comparison with uncrosslinked polymeric micelles, where the organised particles are destroyed upon removal of the nucleating core domain. Additionally, they claimed that the unique method they used for the production of their particles should provide for remarkable control over the composition of the nanocages from the outer surface, through the shell, and the inner surface (Figure 6.1).

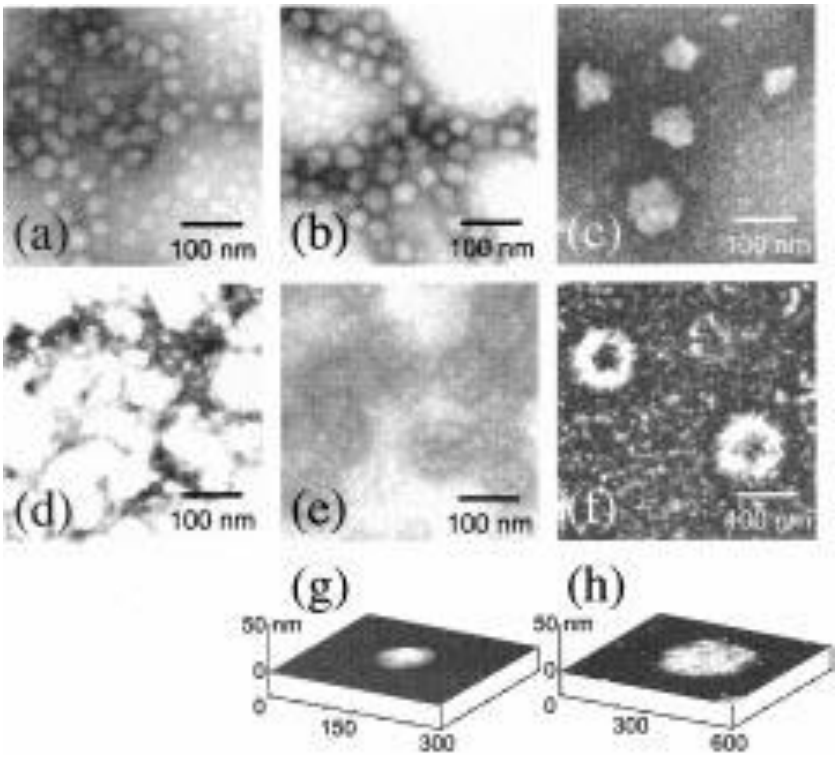

Figure 6.1 Nanocages prepared by Wooley *et al.* using BCP self assembly, shell cross linking followed by core degradation.[8]

This approach was subsequently extended to other BCP systems.[15-17] Shell cross-linked particles possessing an amphiphilic core-shell morphology consisting of a cross-linked shell and a hydrolytically degradable, crystalline core domain were synthesised from poly(ε-caprolactone)-*b*-poly(acrylic acid) (PCL-*b*-PAA) amphiphilic diblock copolymers (Figure 6.2). The PCL core domains exhibited interesting crystallisation and melting behaviors, in which the PCL melting transition temperature increased as the shell cross linked (SCK) core volume increased. According to the authors, this suggested that the lamellar thicknesses of PCL cores in larger SCKs were greater. They utilised ^{1}H NMR spectroscopy and AFM to confirm the successful synthesis of the nanocages.[15]

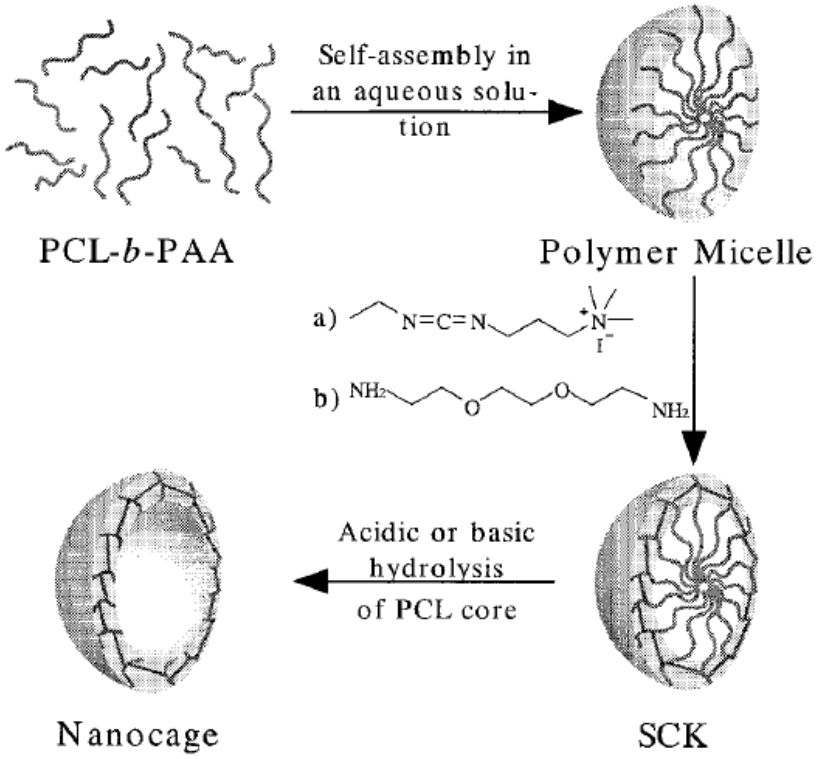

Figure 6.2 Expanded Wooley methodology to other BCP systems.[15]

The same group recently used a different polymer to prepare hollow particles (Figure 6.3). Namely, a P(NAS$_{0.24}$-*co*-NAM$_{0.76}$)$_{210}$-*b*-PLLA$_{43}$ diblock copolymer was utilised. The overall methodology was very similar to the previous one, however in this case enzymatic degradation of the polylactide core was employed by the addition of proteinase k. Interestingly, a faster degradation rate of the polylactide core was observed compared to the degradation rate of the free polylactide in solution. The authors noted that these data were not fully understood and warranted further investigations. [17]

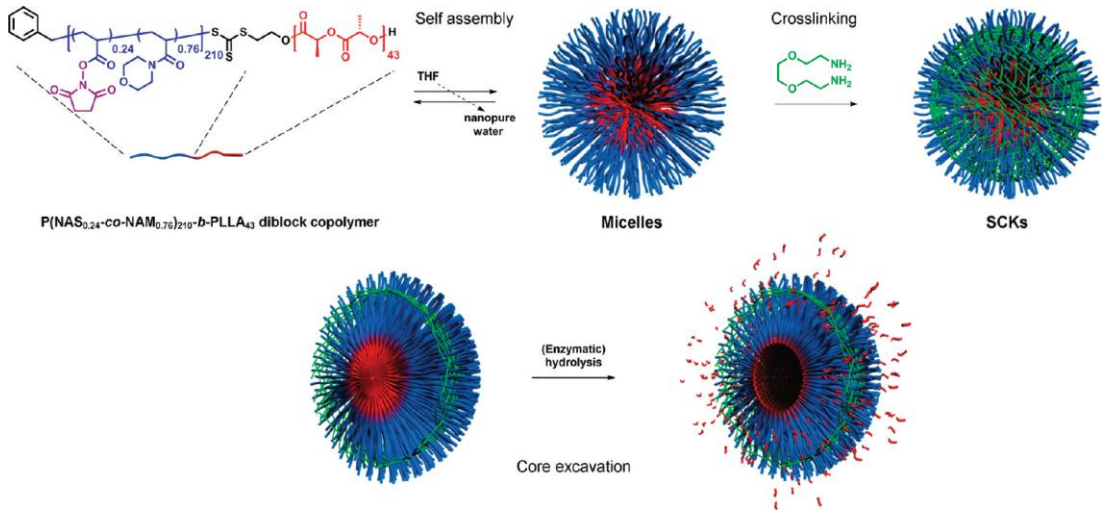

Figure 6.3 Preparation of SCK nanoparticles by self-assembly of amphiphilic diblock copolymer P($NAS_{0.24}$-*co*-$NAM_{0.76}$)$_{210}$-b-$PLLA_{43}$ followed by crosslinking and production of a nanocage-like structure from selective hydrolysis of the PLA core of the SCK template.[17]

Liu and coworkers applied a similar methodology to spherical and cylindrical reverse micelles to fabricate nanocages and nanotubes in organic solvents.[18,19] In summary, they demonstrated cylindrical micelle formation in methanol from polyisoprene-*b*-poly(2-cinnamoylethyl methacrylate)-*b*-poly(*tert*-butyl acrylate), PI-*b*-PCEMA-*b*-PtBA. The cylindrical micelles consisted of a PtBA corona, PCEMA shell, and PI core. Nanotubes were obtained after PCEMA crosslinking and PI core degradation *via* ozonolysis (Figure 6.4).

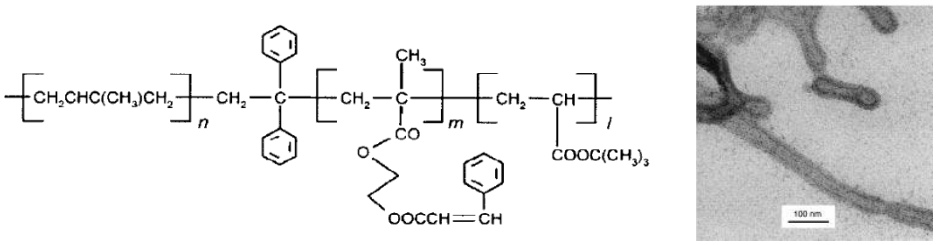

Figure 6.4 Chemical structure of the PI-*b*-PCEMA-*b*-PtBA block copolymer Liu and coworkers utilised and TEM image of organic nanotubes synthesised by a shell cross linking followed by core-degradation of reverse micelles methodology.[18]

Recently, Ho *et al.* utilised the bulk phase separation of polystyrene-*b*-polylactide (PS-*b*-P(LA)) block copolymers to form hexagonally ordered cylinders as it was confirmed by TEM analysis and small angle x-ray scattering (SAXS). With subsequent P(LA) hydrolysis they afforded PS nanotubes that were characterised by TEM analysis (Figure 6.5).[20]

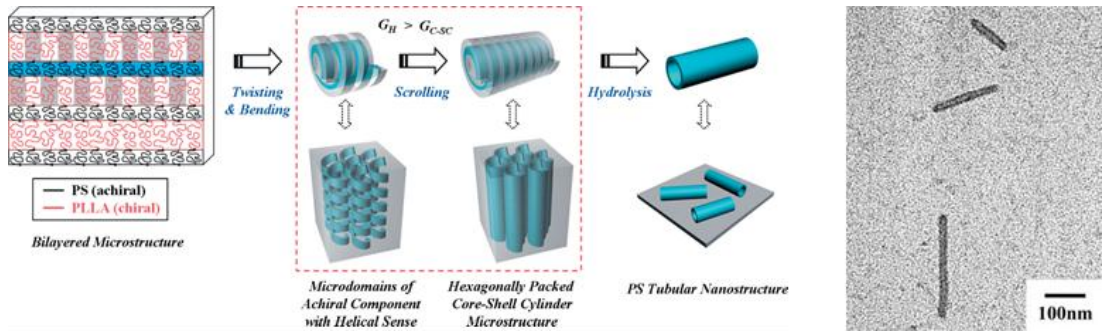

Figure 6.5 PS tubular particles generated by hydrolysis of the PLA compartments and TEM image of the hollow particles generated after hydrolysis.[20]

While these reports illustrated the potential of BCP self-assembly for the synthesis of hollow nanoparticles, they all involved additional synthetic and characterisation steps. Efficient, reliable, and scalable processing methods are still needed to match the experimental simplicity of BCP self-assembly.

Winnik and Manners demonstrated in 2003 a reversible tube-to-rod transition in a block copolymer micelle. In this report the authors described a morphology switch induced by an alteration in temperature for a PFS_{40}-*b*-$PDMS_{480}$. A sample which formed nanotubes at 23 °C, was found to reorganise to form short dense rods when was heated at 50 °C (Figure 6.6). Furthermore, they found the morphological transition to be reversible when more cooling and heating cycles were applied in the solution, all self-assemblies were thoroughly characterised by TEM and static light scattering (SLS).[9]

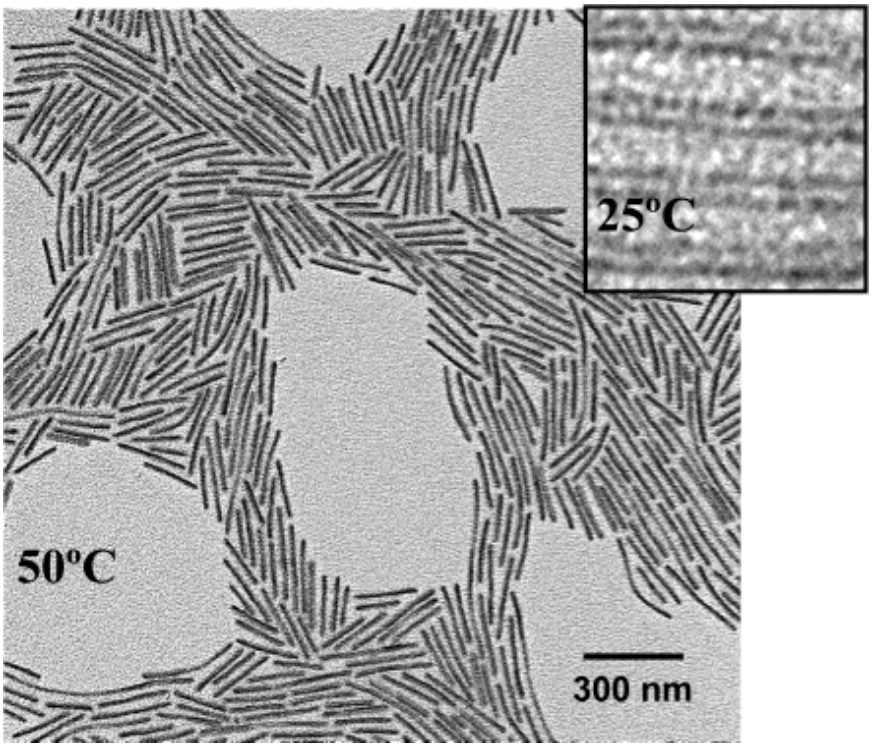

Figure 6.6 Nanotubes and nanorods observed by Winnik and Manners upon heating and cooling cycles.[9]

6.2.2 Microscopy in block copolymer (BCP) self-assembly

BCP self-assembly analysis is typically performed by conventional transmission electron microscopy (TEM) and cryo-TEM and often these data are complemented by solution based characterisation techniques like light, neutron and X-ray scattering. In many cases of microscopy characterisation, samples are imaged in the presence of heavy metal staining agents that are essential to enhance the otherwise poor electron density contrast between copolymer domains, and between the polymer nanostructures and the support.[21] We note that there are cases where low voltage TEM,[22] and energy filtered-TEM (EF-TEM),[23,24] for example, also can be used to overcome these contrast limitations. Though there have been a limited number of studies examining the effects of drying and staining procedures on the examination of BCP solution assemblies,[25,26] these effects have not been explored in systematic detail. This has not only led to misinterpretation of some TEM-based analyses of

solution-based assemblies,[27] but it is also a significant barrier for discovering new phenomena that spontaneously occur upon drying of polymer specimens. This is of particular importance as electron microscopy in principle has the potential to provide highly specific data without the need of independent information regarding the sample analysed.

6.2.3 Microscopy on graphene oxide (GO) supports

A significant advancement towards high contrast, stain free but yet cheap and efficient characterisation of soft matter self-assembled structures was achieved with the application of graphene oxide as a support for electron microscopy (Figure 6.7).[28] In 2009 Wilson *et al.* reported the structural analysis of graphene oxide (GO) by transmission electron microscopy (TEM). Electron diffraction patterns showed that on average the underlying carbon lattice maintained the order and lattice spacings of normal graphene. These results also revealed that single GO sheets were highly electron transparent and stable in the electron beam, and hence ideal support films for the study of nanoparticles and macromolecules by TEM. This was demonstrated through the structural analysis of physiological ferritin, an iron-storage protein.

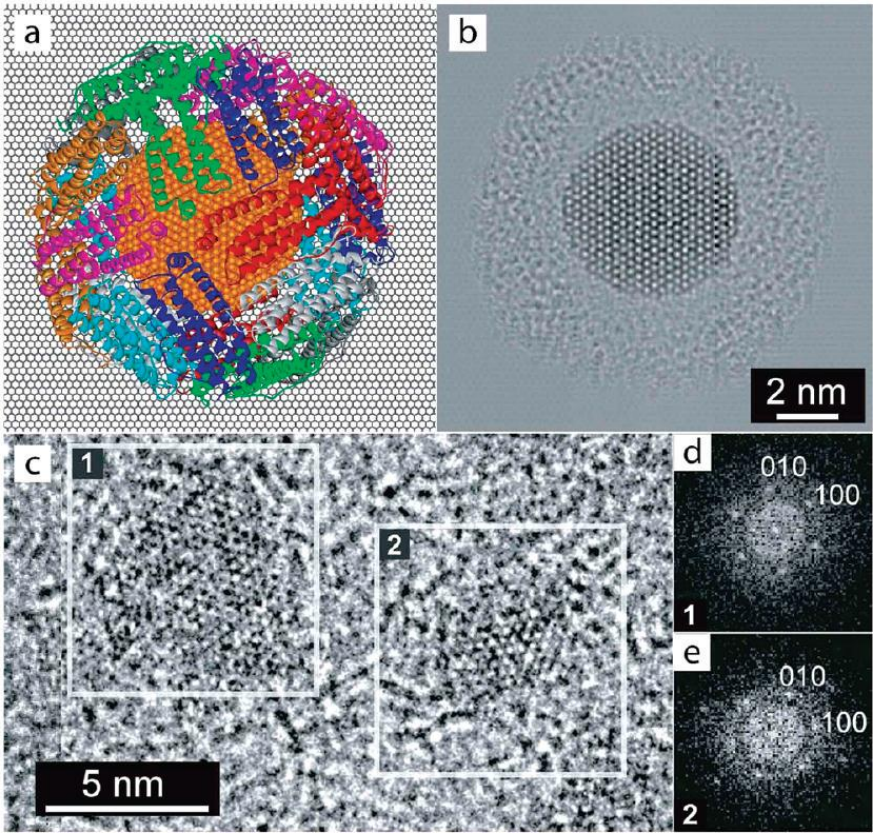

Figure 6.7 (a) Schematic model of ferritin on a graphene sheet. Ferritin consists of a protein shell (multicolored ribbons) containing a ferrihydrite core which here is oriented along [001] relative to the bulk crystal structure. (b) HRTEM image simulation of the structure in panel a. (c) 300 kV HRTEM image of ferritin on a single sheet graphene oxide support; (d,e) FFTs obtained from the marked regions 1 and 2, respectively, in panel c.

A further advancement was carried out in our research group. We showed for the first time the utility of graphene oxide as a support for multi-technique imaging of BCP assemblies. Amongst others, GO supports were utilised in this work to image BCP cylindrical micelles and vesicles without the addition of staining agents, furthermore the exact same nanoparticles were analysed by TEM, SEM and AFM, giving simple means to get more information from the image-based characterisation analysis performed routinely in BCP assemblies.

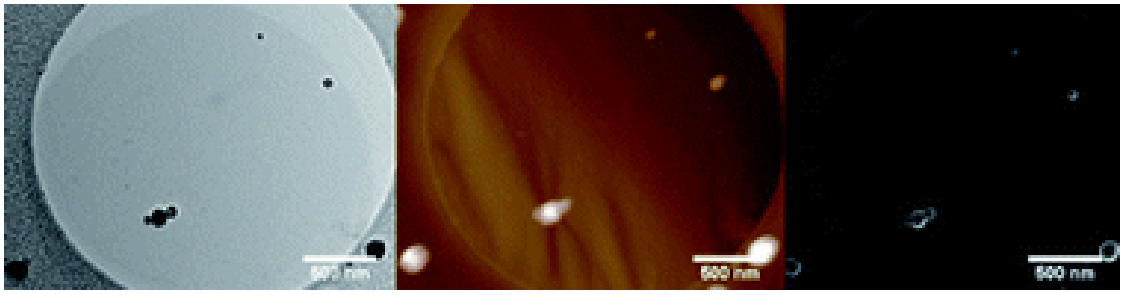

Figure 6.8 (a) Bright field TEM, (b) SEM, and (c) AFM images of exactly the same area of a GO grid.[29]

Imaging on GO supports cannot substitute cryogenic (cryo) microscopy techniques, which although are still not accessible by many research group (perhaps the majority) in the soft matter society; are very powerful by offering a better representation of the morphology and structure of the nanoparticles in their natural state. In the GO method the particles are dried on the thin substrate and drying effects will still be present as they would in conventional imaging. However, the fact that we can now image the sample without the need for additional staining agents maintaining outstanding contrast gives us the ability to observe, systematically study and therefore fully understand them.

In the present chapter we analysed samples of cylinders dried on a GO substrate and we attempt to understand the drying and visual effects observed by utilising the multi-technique imaging methodology. It is noted that although the present work is a bright example of how the GO multi technique imaging method can contribute to BCP self-assembly characterisation, we focus on the actual reorganisation that the drying process induces.

6.3 Results and discussion

6.3.1 Solution state characterisation

The cylindrical polymeric micelles were obtained from P(*L*-LA)$_{37}$-*b*-PAA$_{333}$ (**4.1**) that was prepared as described in Chapter 4. Solution-state characterisation confirmed the expected core-shell structure of these cylindrical micelles. Cryo-TEM gave valuable information regarding the morphological identity of the particles in their solution state. This was particularly useful for these cylindrical particles, whose light and neutron scattering data analysis was challenging due to the particle length scales and anisotropy. Analysis of the cryo-TEM data confirmed the presence of a solid core, with no core-shell contrast observed (Figure 6.9a). The lack of core-shell contrast is attributed to solvation of the corona. From the cryo-TEM images, the average core radius of the cylindrical particles was estimated to be 16 ± 1.5 nm. Small angle neutron scattering (SANS) experiments were performed on samples of cylindrical micelles prepared in D_2O. Analysis of the pair distance distribution function [P(r)] of the P(*L*-LA)$_{37}$-*b*-PAA$_{333}$ solution suggested that the micelles were solid cylinders with a radius of approximately 28 nm (Figure 6.9b).[30,31]

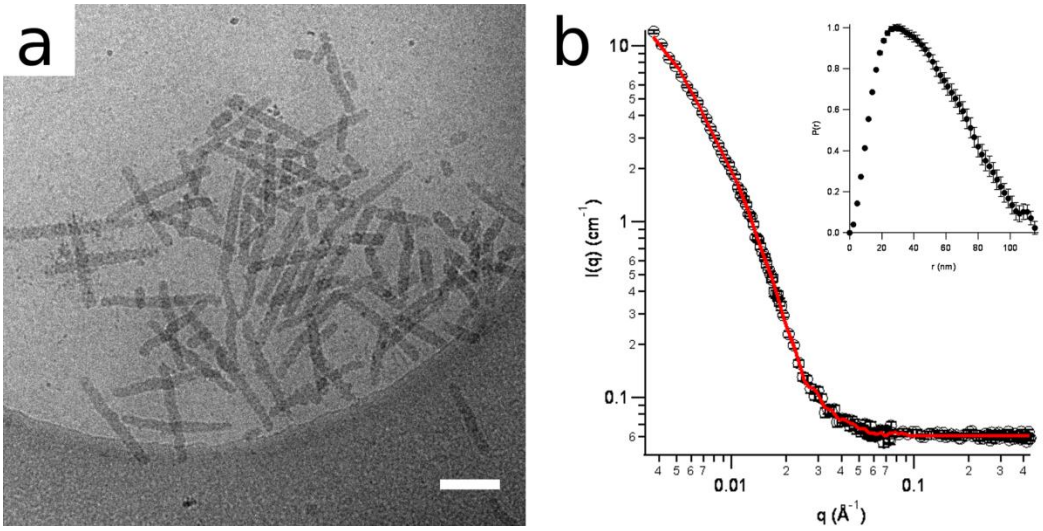

Figure 6.9 a) Cryo-TEM image of P(*L*-LA)$_{37}$-*b*-PAA$_{333}$ cylindrical micelles (scale bar = 200 nm); b) SANS data (points) and approximation for the indirect Fourier transform (line) for P(*L*-LA)$_{37}$-*b*-PAA$_{333}$ cylindrical micelles in D_2O; inset: pair distance distribution function [P(r)].

6.3.2 Hollow nanoparticle synthesis and characterisation

Aqueous solutions of cylindrical micelles were drop cast onto GO TEM grids and imaged directly. First, to prepare the grid a drop of GO dispersed in nanopure water was deposited on a lacey carbon support to give a virtually electron transparent substrate, then 2 μL of a 0.5 g·L^{-1} micelle solution was slowly air dried to the grid in a desiccator, with full evaporation of the solvent taking 30 mins.[29] The resultant images showed that the cylindrical micelles had appeared to undergo a spontaneous cavitation upon drying onto the surface (Figure 6.10a). These hollow cylinders were observed uniformly across the GO TEM grids, and were found to have an average core diameter (D_{core}) of 19.1 ± 1.9 nm. The cylinders were found to have lower electron density at the two ends strongly suggesting the formation of nanotubes. The formation of nanotubes relates to the crystallisation driven methodology that was used, which is known to produce cylinders containing uncapped ends that remain 'active' for further unimer addition.[11]

To further examine the particles and confirm that the noted electron density contrast was not the result of phase contrast; the same GO grids were also characterised by high angle annular dark field scanning TEM (HADDF-STEM). In this method, the collected electrons are scattered in wide angles where incoherent scattering dominates and therefore exclusively z-contrast dependent images are created. Again, the particles appeared hollow and the contrast effects were similar to conventional TEM, likely ruling out phase contrast as a source of this observed effect (Figure 6.10b). Further analysis by energy filtered TEM (EF-TEM) also supported that the observed core-shell contrast was due to a decreased density of carbon and oxygen (and therefore polymer) at the centre of the cylinders, revealing that the micelles had dried to form truly hollow structures on the GO surface (Figure 6.10c). One of the previously noted advantages of GO is the ability to use it for multi-technique imaging of the same sample preparation.[29] Atomic force microscopy (AFM) analysis of the hollow particles dried to a GO grid revealed that the cylindrical nanoparticles had not collapsed, but rather had retained their circular cross-section (Figure 6.10d and Figure 6.11). AFM height measurements (32 ± 2.1 nm) were in good agreement with the width values obtained by TEM (28 ± 1.8 nm), indicating the structures could be described as nanotubes consisting of 1-dimensional nano-channels with an internal diameter of 19 nm and a wall thickness of ~6 nm. Traditional dry-state TEM using the negative stain phosphotungstic acid (PTA) revealed cylindrical with the dimensions D_{core} = 27 nm (Figure 6.12), in agreement with unstained images. However the staining process obscured the hollow nature of the particles, with a uniform electron density observed across all nanoparticles.

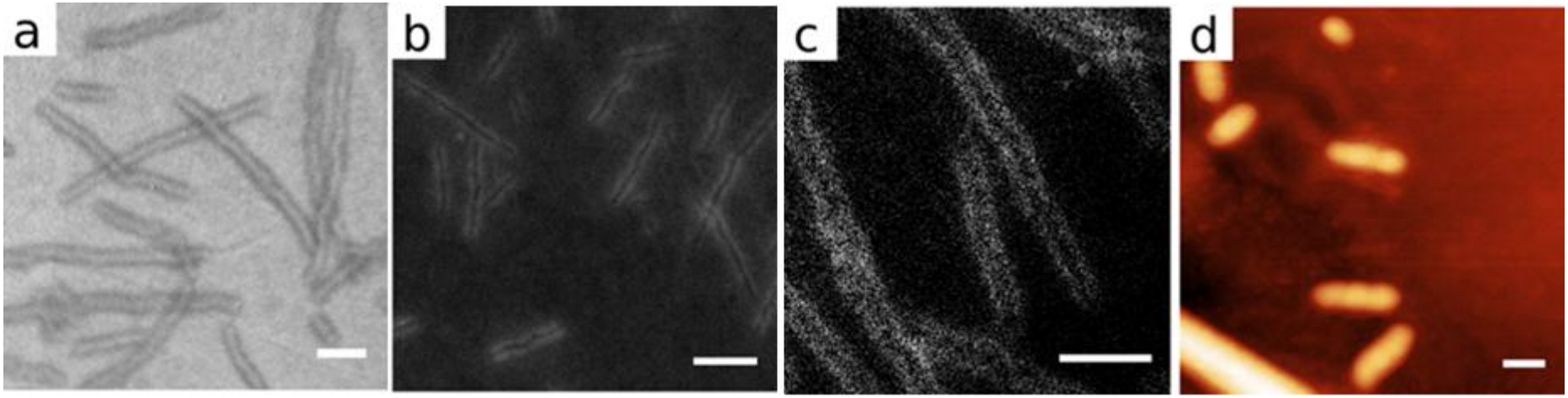

Figure 6.10 a) TEM image of hollow P(*L*-LA)$_{37}$-*b*-PAA$_{333}$ cylinders; b) HADDF-STEM image of hollow P(*L*-LA)$_{37}$-*b*-PAA$_{333}$ cylinders; c) EF-TEM carbon map of hollow P(*L*-LA)$_{37}$-*b*-PAA$_{333}$ cylinders; d) AFM image of hollow P(*L*-LA)$_{37}$-*b*-PAA$_{333}$ cylinders. All scale bars = 100 nm.

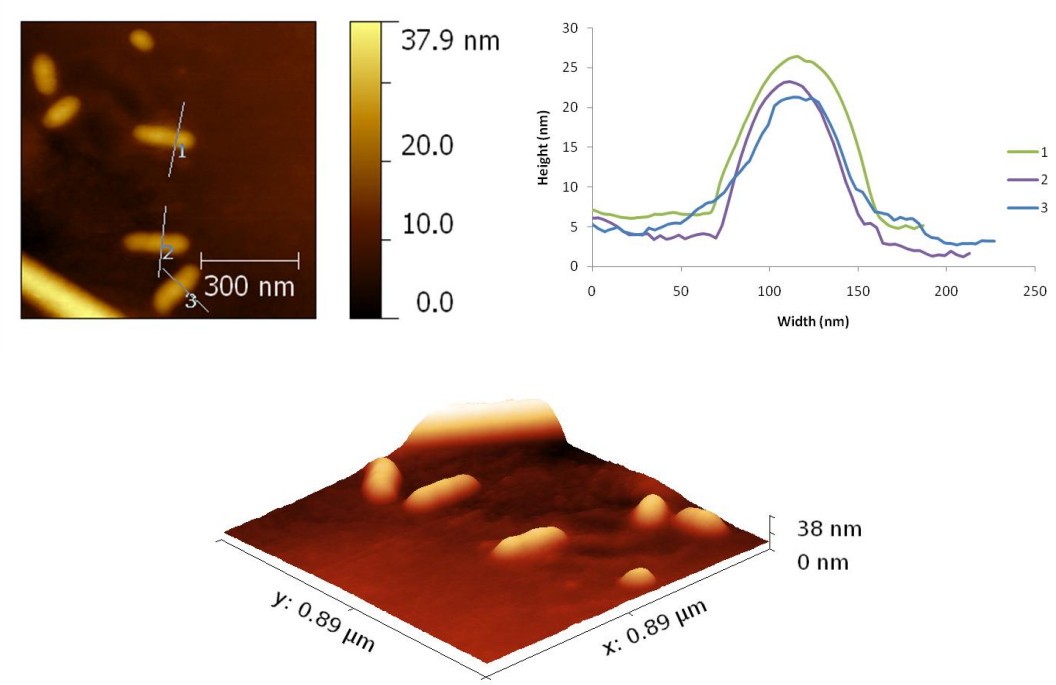

Figure 6.11 AFM height images of hollow P(*L*-LA)$_{37}$-*b*-PAA$_{333}$ cylinders prepared by slow evaporation and the corresponding height profiles.

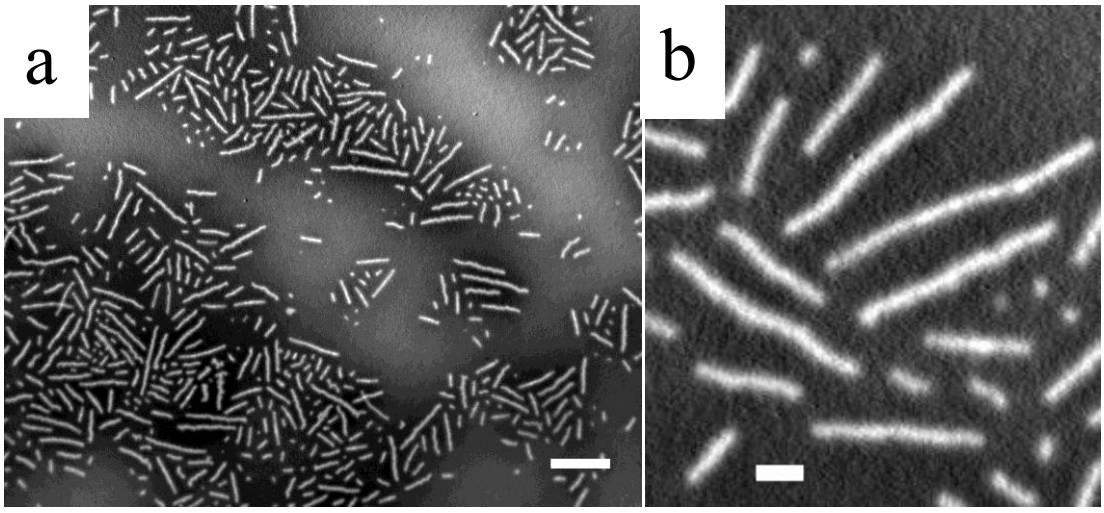

Figure 6.12 a) TEM image of P(*L*-LA)$_{37}$-*b*-PAA$_{333}$ cylinders on GO prepared by slow evaporation, and stained with PTA. Scale bar = 200 nm b) the same sample in different magnification scale bar = 50 nm.

6.3.3 Control over the structural reorganisation

The extent of the structural reconstruction that the particles undergo can be controlled, by altering the drying method applied to the particles. In contrast to the slow evaporation method (Figure 6.10), drop casting of the cylindrical micelles on a GO grid followed by blotting after 1 min (fast-drying) produced dried particles that had undergone a reformation to form necklace-like structures (Figure 6.13) In this case the compartments have an average length of 23 ± 3.1 nm and are separated by PLA layers which are as thin as 4 nm. This effect is related to the non-uniform degree of crystallinity along the core of the cylinders. We hypothesise that the fast-drying method provides less time for morphological rearrangement.

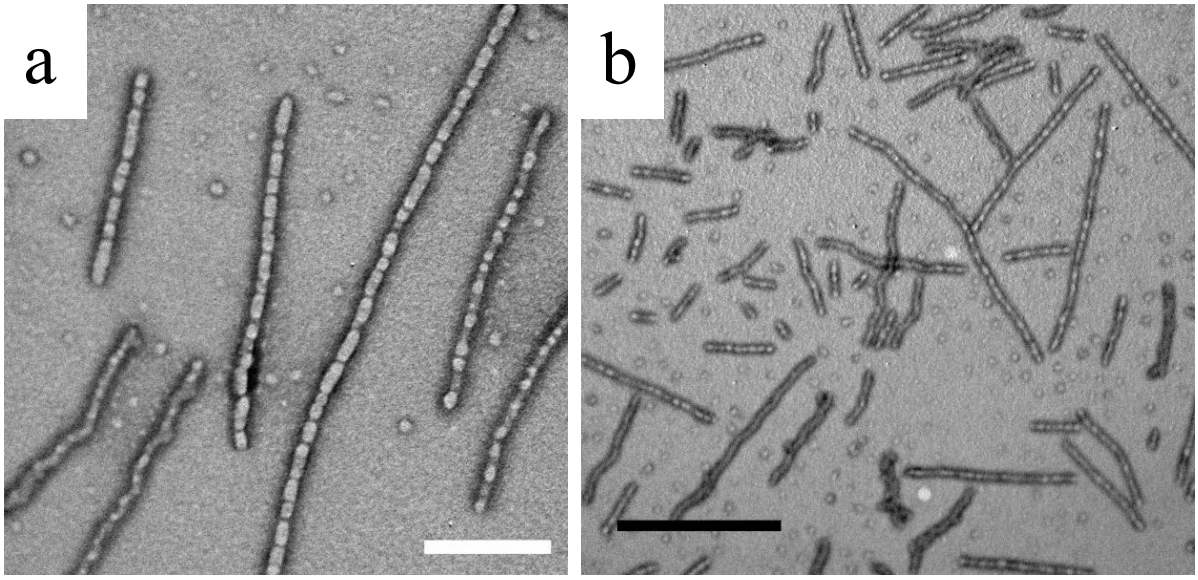

Figure 6.13 TEM images of necklace-like P(*L*-LA)$_{37}$-*b*-PAA$_{333}$ cylindrical micelles prepared by blotting; a) Scale bar 200 nm; b) Scale bar 200 nm.

As a consequence, the "hollowing" of the cylinders does not occur uniformly along the cylinder core, likely resulting from the fact that the PLA regions that contain higher crystallinity are more stable. Furthermore, structural reconstructions can be eliminated entirely by using a freeze drying preparation method. After drop casting the sample, the GO grid was immediately plunged into liquid nitrogen and freeze-dried to remove water.[32] The

resulting SEM (Figure 6.14) and TEM images (Figure 6.15) of the cylindrical micelles revealed solid particles with a uniform density across their diameter in agreement with their solution-state nanostructures, as determined by cryo-TEM.

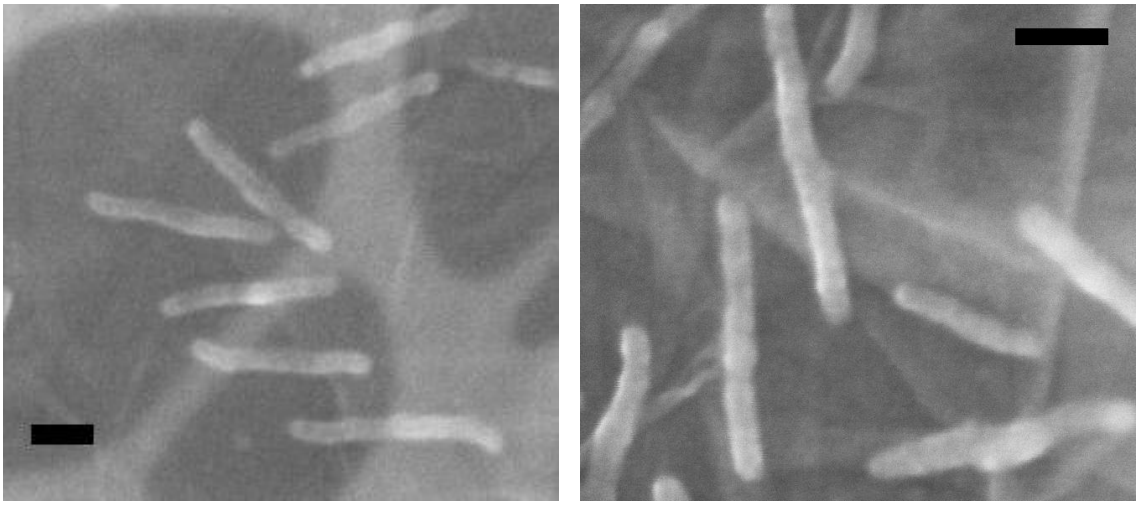

Figure 6.14 SEM images of solid P(*L*-LA)$_{37}$-*b*-PAA$_{333}$ cylinders prepared by freeze-drying. Scale bar = 100 nm.

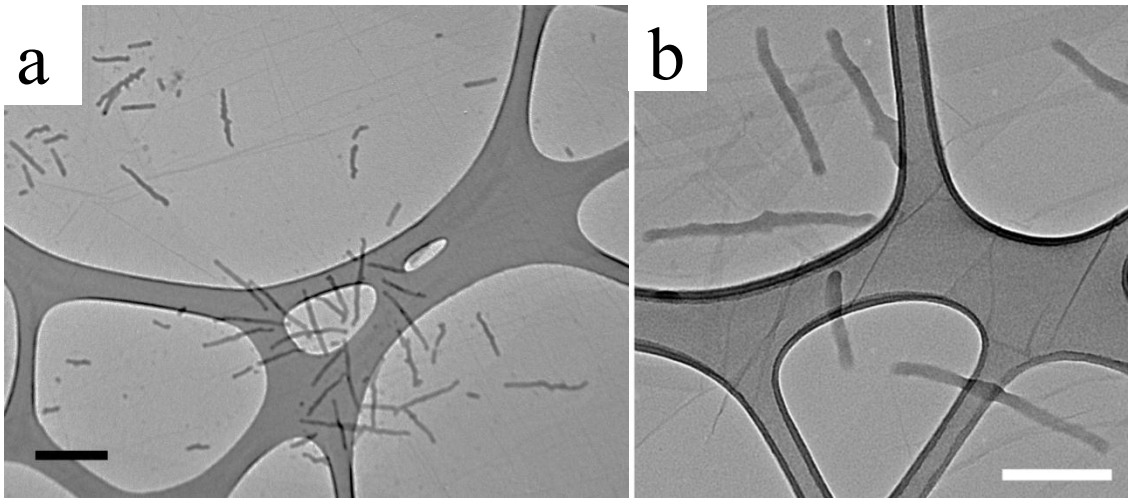

Figure 6.15 TEM images of solid P(*L*-LA)$_{37}$-*b*-PAA$_{333}$ cylindrical micelles prepared by freeze drying; a) Scale bar = 200 nm; and b) Scale bar = 200 nm.

6.3.4 Proposed driving force and mechanism

We propose that the spontaneous cavitation of the PLA-*b*-PAA nanoparticles when slowly dried to a substrate is due to hydrogen-bonding between the polylactide core and poly(acrylic

acid) corona. During the slow evaporation drying preparation, a contraction of the core to the corona occurs leaving a hollow centre perhaps also co-assisted by the shear stress applied on the particles during the drying process. Hydrogen-bonding driven contraction of polymers has been widely reported and investigated especially in the field of layer-by-layer (LbL) self-assembly.[33,34] In order to test this theory, poly(ethylene oxide) was utilised as an alternative, non-hydrogen-bond donor corona block. Spherical micelles with number average R_h of 8.0 nm (as measured by DLS) were obtained from commercially available P(*D,L*-LA)$_{4k}$-*b*-PEO$_{5k}$ as previously demonstrated.[35,36] Then, these particles were dried on GO TEM grids using the same slow evaporation preparation as with PLA-*b*-PAA. The resulting TEM images revealed a uniform electron density across the surface of the particles, with the complete absence of hollow structures, indicating that no structural reconstruction had occurred (Figure 6.16).

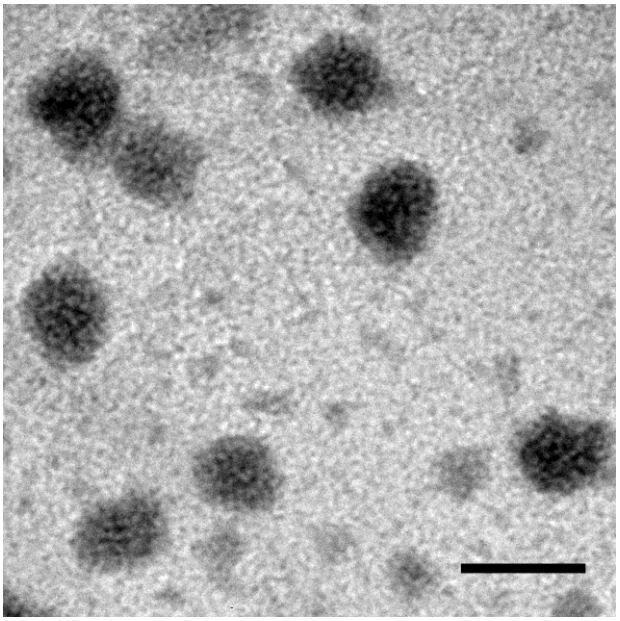

Figure 6.16 TEM image of solid P(*D,L*-LA)$_{4k}$-*b*-PEO$_{5K}$ spheres on GO prepared by slow evaporation. Scale bar = 50 nm.

6.4 Conclusions

The spontaneous one-step synthesis of hollow nanotubes from cylindrical micelles based on PLA-*b*-PAA block copolymers (BCPs) has been achieved. This structural reorganisation which occurs simply upon drying of the samples was elucidated by transmission electron microscopy (TEM) and atomic force microscopy (AFM). We show that it was necessary to use stain-free imaging to examine these nanoscale assemblies, as the hollow nature of the particles was obscured by application of a heavy metal stain. Additionally, the internal topology of the PLA-*b*-PAA particles could be tuned by manipulating the drying conditions to give solid or compartmentalised structures. The spontaneous structural reconstruction method presented herein should have wide-ranging potential for the synthesis of a broad range of hollow particles.

6.5 Experimental Section

6.5.1 Materials

Chemicals were used as received from Aldrich, Fluka and Acros. P(*D,L*-LA)$_{4k}$-*b*-PEO$_{5k}$ was purchased from Polymer Source (Montreal) and used as received. P(*L*-LA)$_{37}$-*b*-PAA$_{333}$ was prepared as described previously. *L*-lactide was donated by Purac and further purified/dried over 4 Å molecular sieves in dichloromethane solution before being dried under vacuum and sublimed. Lactides were stored in a nitrogen-filled glove box. Tetrahydropyran acrylate (THPA) was prepared as described previously and stored below 4 °C.[37] AIBN (2,2'-azo-bis(isobutyronitrile)) was recrystallised twice from methanol and stored in the dark at 4 °C. Dry dichloromethane was obtained by passing over a column of activated alumina using an Innovative Technologies solvent purification system. (-)-Sparteine was dried over CaH_2 and distilled prior to use and 1-(3,5-bis(trifluoromethyl)phenyl)-3-cyclohexyl-thiourea was prepared and dried as previously reported.[38] Copper TEM grids were purchased from Agar.

6.5.2 Instrumentation

^{1}H NMR and ^{13}C NMR spectra were recorded on a Bruker DPX-400 spectrometer in $CDCl_3$ unless otherwise stated. Chemical shifts are given in ppm downfield from TMS. Size exclusion chromatography (SEC) measurements were conducted using a Varian 390-LC-Multi detector suite fitted with differential refractive index (DRI) and photodiode array (PDA) detectors equipped with a guard column (Varian Polymer Laboratories PLGel 5 μm, 50×7.5 mm) and two mixed D columns (Varian Polymer Laboratories PLGel 5 μm, 300×7.5 mm). The mobile phase was tetrahydrofuran with 2% triethylamine eluent at a flow rate of 1.0 mLmin^{-1} and samples were calibrated against Varian Polymer laboratories Easi-Vials linear poly(styrene) standards (162 - 2.4 × 10^5 g.mol^{-1}) using Cirrus v3.3. Infrared spectroscopy was recorded on a Perkin Elmer, Spectrum 100 FT-IR Spectrometer. High

Resolution Mass Spectrometry (HR-MS) was conducted on a Bruker UHR-Q-TOF MaXis with electrospray ionisation. Formation of hollow P(*L*-LA)$_{37}$-*b*-PAA$_{333}$ nanotubes by slow evaporation

Solutions of micellar assemblies (2 μL) were drop-cast onto a pre-prepared GO TEM grid. The grid was then left to air dry for 30 min in a desiccator. The dried grid could be directly imaged by TEM, AFM, or SEM. Alternatively, phosphotungstic acid (PTA) stain (2 μL) was applied to the sample on the grid, blotting after 1 min to give stained grids for additional TEM analysis.

6.5.3 Formation of compartmentalised necklace like P(*L*-LA)$_{37}$-*b*-PAA$_{333}$ cylindrical nanoparticles by blotting

Solutions of P(*L*-LA)$_{37}$-*b*-PAA$_{333}$ cylindrical micelles (2 μL) were drop-cast onto a pre-prepared GO TEM grid. The grid was then left to air dry for 1 min, before excess solution was removed by blotting. The dried grid could be directly imaged by TEM.

6.5.4 Formation of solid P(*L*-LA)$_{37}$-*b*-PAA$_{333}$ cylindrical nanoparticles by freeze-drying

Solutions of micellar assemblies (2 μL) were drop-cast onto a pre-prepared GO TEM grid. The grid was then immediately plunged into liquid nitrogen, and water removed by freeze-drying the grid inside a glass ampoule. The dried grid could be directly imaged by TEM, AFM, or SEM.

6.5.5 Self-assembly of P(EO)$_{5k}$-*b*-P(*D,L*-LA)$_{4k}$ to give spherical micelles, and subsequent formation of solid nanoparticles

P(*D,L*-LA)$_{4k}$-b-PEO$_{5k}$ (10 mg) was dissolved in THF (5 mL) by sonicating for 2 h. Nanopure water (5 mL) was added dropwise to the polymer solution using a metering pump, and the mixture stirred overnight at room temperature. The mixture was then exhaustively dialysed

(MWCO 3.5 kDa dialysis tubing) against nanopure water. The resulting solution was drop-cast onto a pre-prepared GO TEM grid. The grid was left to air dry for 30 min in a desiccator. The dried grid could be directly imaged by TEM, AFM, or SEM.

6.5.6 Transmission electron microscopy (TEM)

Dry-stained images were obtained on 300 mesh formvar/carbon grids, GO imaging was performed on 400 mesh lacy carbon films, with deposited GO films. GO solutions[28] (0.10–0.15 $g.L^{-1}$) were sonicated for 30 s prior to use. Lacey carbon grids (400 Mesh, Cu) (Agar Scientific) were cleaned using air plasma from a glow-discharge system (2 min, 20 mA): this step is not essential but increases the hydrophilicity of the lacy carbon improving the coverage of GO to typically >70%. One drop (~ 0.08 mL) of the sonicated GO solution was deposited onto each grid and left to air-dry for 30 min. Once dry, the grids could be stored for several weeks before sample deposition. A video abstract is also available on how to prepare the GO grids.[39] Average sizes of the micelles were determined from counting the sizes of at least 100 particles for 3 different images.

The cryo-TEM experiments were performed on an FEI Tecnai 20 (type Sphera) TEM equipped with a LaB_6 filament operating at 200 kV. A Gatan cryo-holder operating at ~ -170°C was used. The images were recorded using a bottom-mounted 1024 × 1024 Gatan CCD camera. The sample vitrification procedure was carried out using an automated vitrification robot (FEI Vitro-bot™ Mark III). Cryo-TEM R2/2 Quantifoil Jena grids were purchased from Quantifoil Micro Tools GmbH. Prior to the vitrification procedure the grids were surface plasma treated using a Cressington 208 carbon coater.

6.5.7 Atomic force microscopy (AFM)

AFM images were taken in tapping mode on a Multimode AFM with Nanoscope IIIA controller with Quadrex, or an Asylum Research MFP3D-SA. Silicon AFM tips were used

with nominal spring constant and resonance frequency of 3.5 Nm-1 and 75 kHz (MikroMasch NSC18). A Zeiss Supra55VP was used to acquire the SEM images, operated at an accelerating voltage of 2 kV.

6.5.8 Small angle neutron scattering (SANS)

SANS data for P(*L*-LA)$_{37}$-*b*-PAA$_{333}$ in D_2O were collected at the National Institute of Standard and Technology Centre for Neutron Research (NCNR). Experiments were performed on the NG-7 30 m SANS instrument using an incident wavelength of 6.0 Å with a wavelength spread ($\Delta\lambda\backslash\lambda$) of 0.12 and sample to detector distances of 1.0 m, 4.0 m, and 13.5 m to cover a scattering vector range from 0.004 $Å^{-1}$ < q < 0.4 $Å^{-1}$. Absolute intensities were determined using the direct beam flux method.[40] The data were reduced using standard procedures provided by NIST.[40]

The pair distance distribution functions [P(r)] were determined from the indirect Fourier Transform of the measured SANS intensity using the SansView Program developed by the University of Tennessee as part of the Distributed Data Analysis of Neutron Scattering Experiments (DANSE) project. The P(r) for P P(*L*-LA)$_{37}$-*b*-PAA$_{333}$ is shown in (Figure 6.9b). The tail at higher values of r supports that the micelles are cylindrical, with a radius of approximately 28 nm.[31] Fitting the data with a form factor model for cylinders using procedures provided by NIST,[40] suggested that the cylinders were greater than 100 nm in length; however, the fit values were not sensitive to values greater than 100 nm.

6.6 References

(1) Moughton, A. O.; O'Reilly, R. K. *J. Am. Chem. Soc.* **2008**, *130*, 8714.

(2) Dergunov, S. A.; Kesterson, K.; Li, W.; Wang, Z.; Pinkhassik, E. *Macromolecules* **2010**, *43*, 7785.

(3) Bolton, J.; Bailey, T. S.; Rzayev, J. *Nano Letters* **2011**, *11*, 998.

(4) Wakasugi, A.; Asakawa, M.; Kogiso, M.; Shimizu, T.; Sato, M.; Maitani, Y. *International Journal of Pharmaceutics* **2011**, *413*, 271.

(5) Kameta, N.; Masuda, M.; Minamikawa, H.; Mishima, Y.; Yamashita, I.; Shimizu, T. *Chemistry of Materials* **2007**, *19*, 3553.

(6) Donath, E.; Sukhorukov, G. B.; Caruso, F.; Davis, S. A.; Möhwald, H. *Angew. Chem. Int. Ed.* **1998**, *37*, 2201.

(7) Marinakos, S. M.; Novak, J. P.; Brousseau, L. C.; House, A. B.; Edeki, E. M.; Feldhaus, J. C.; Feldheim, D. L. *J. Am. Chem. Soc.* **1999**, *121*, 8518.

(8) Huang, H.; Remsen, E. E.; Kowalewski, T.; Wooley, K. L. *J. Am. Chem. Soc.* **1999**, *121*, 3805.

(9) Raez, J.; Tomba, J. P.; Manners, I.; Winnik, M. A. *J. Am. Chem. Soc.* **2003**, *125*, 9546.

(10) Zhang, L. F.; Eisenberg, A. *Polym Advan Technol* **1998**, *9*, 677.

(11) Wang, X.; Guerin, G.; Wang, H.; Wang, Y.; Manners, I.; Winnik, M. A. *Science* **2007**, *317*, 644.

(12) Petzetakis, N.; Dove, A. P.; O'Reilly, R. K. *Chem. Sci.* **2011**, *2*, 955.

(13) Discher, D. E.; Eisenberg, A. *Science* **2002**, *297*, 967.

(14) Zhang, L.; Eisenberg, A. *Science* **1995**, *268*, 1728.

(15) Zhang, Q.; Remsen, E. E.; Wooley, K. L. *J. Am. Chem. Soc.* **2000**, *122*, 3642.

(16) Turner, J. L.; Wooley, K. L. *Nano Letters* **2004**, *4*, 683.

(17) Samarajeewa, S.; Shrestha, R.; Li, Y.; Wooley, K. L. *J. Am. Chem. Soc.* **2012**, *134*, 1235.

(18) Stewart, S.; Liu, G. *Angew. Chem., Int. Ed.* **2000**, *39*, 340.

(19) Stewart, S.; Liu, G. *Chemistry of Materials* **1999**, *11*, 1048.

(20) Ho, R. M.; Chen, C. K.; Chiang, Y. W.; Ko, B. T.; Lin, C. C. *Adv. Mater.* **2006**, *18*, 2355.

(21) Sawyer, L. C. a. G., D.T. *Polymer Micrscopy*; 2 nd ed.; Chapman & Hall: London, UK, 1996.

(22) Drummy, L. F.; Yang, J.; Martin, D. C. *Ultramicroscopy* **2004**, *99*, 247.

(23) Allen, F. I.; Watanabe, M.; Lee, Z.; Balsara, N. P.; Minor, A. M. *Ultramicroscopy* **2011**, *111*, 239.

(24) Gomez, E. D.; Panday, A.; Feng, E. H.; Chen, V.; Stone, G. M.; Minor, A. M.; Kisielowski, C.; Downing, K. H.; Borodin, O.; Smith, G. D.; Balsara, N. P. *Nano Lett.* **2009**, *9*, 1212.

(25) Zhao, H.; Chen, Q.; Hong, L.; Zhao, L.; Wang, J.; Wu, C. *Macromolecular Chemistry and Physics* **2011**, *212*, 663.

(26) Wang, Y.; Coombs, N.; Manners, I.; Winnik, M. A. *Macromolecular Chemistry and Physics* **2008**, *209*, 1432.

(27) Talmon, Y. *Journal of Colloid and Interface Science* **1983**, *93*, 366.

(28) Wilson, N. R.; Pandey, P. A.; Beanland, R.; Young, R. J.; Kinloch, I. A.; Gong, L.; Liu, Z.; Suenaga, K.; Rourke, J. P.; York, S. J.; Sloan, J. *ACS Nano* **2009**, *3*, 2547.

(29) Patterson, J. P.; Sanchez, A. M.; Petzetakis, N.; Smart, T. P.; Epps, I. I. I. T. H.; Portman, I.; Wilson, N. R.; O'Reilly, R. K. *Soft Matter* **2012**, *8*, 3322.

(30) Moore, P. B. *Jour. of App. Crystallog.* **1980**, *13*, 168.

(31) Svergun, D. I.; Koch, M. H. J. *Rep Prog Phys* **2003**, *66*, 1735.

(32) Friedrich, H.; Frederik, P. M.; de With, G.; Sommerdijk, N. A. J. M. *Angew. Chem., Int. Ed.* **2010**, *49*, 7850.

(33) Kim, B.-S.; Park, S. W.; Hammond, P. T. *ACS Nano* **2008**, *2*, 386.

(34) Nguyen, C. A.; Argun, A. A.; Hammond, P. T.; Lu, X.; Lee, P. S. *Chem. Mater.* **2011**, *23*, 2142.

(35) Riley, T.; Heald, C. R.; Stolnik, S.; Garnett, M. C.; Illum, L.; Davis, S. S.; King, S. M.; Heenan, R. K.; Purkiss, S. C.; Barlow, R. J.; Gellert, P. R.; Washington, C. *Langmuir* **2003**, *19*, 8428.

(36) Riley, T.; Stolnik, S.; Garnett, M. C.; Illum, L.; Davis, S. S.; Taylor, P.; Tadros, T. F. *Langmuir* **2002**, *18*, 7663.

(37) Wooley, K. L.; O'Reilly, R. K.; Joralemon, M. J.; Hawker, C. J. *Chem-Eur J* **2006**, *12*, 6776.

(38) Pratt, R. C.; Lohmeijer, B. G. G.; Long, D. A.; Lundberg, P. N. P.; Dove, A. P.; Li, H.; Wade, C. G.; Waymouth, R. M.; Hedrick, J. L. *Macromolecules* **2006**, *39*, 7863.

(39) Wilson, N. R.; Pandey, P. A.; Beanland, R.; Rourke, J. P.; Lupo, U.; Rowlands, G.; Römer, R. A. *New Journal of Physics* **2010**, *12*, 125010.

(40) Kline, S. *Journal of Applied Crystallography* **2006**, *39*, 895.